AD-771 166

PRINCIPLES OF THE RADIATION OF GLASS AND CERAMIC MATERIALS

S. M. Brekhovskikh, et al

Army Foreign Science and Technology Center
Charlottesville, Virginia

5 July 1973

DISCLAIMER NOTICE

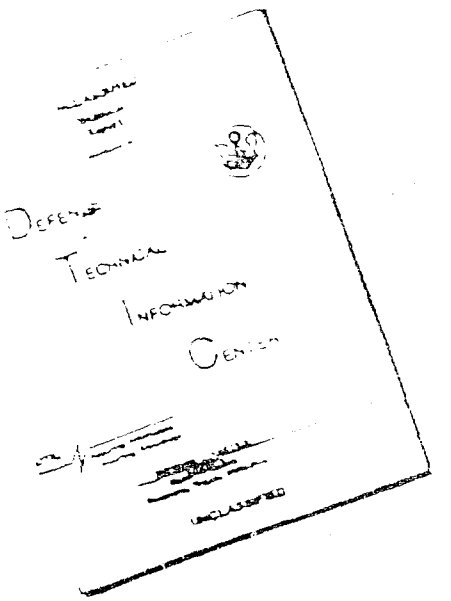

THIS DOCUMENT IS BEST QUALITY AVAILABLE. THE COPY FURNISHED TO DTIC CONTAINED A SIGNIFICANT NUMBER OF PAGES WHICH DO NOT REPRODUCE LEGIBLY.

TECHNICAL TRANSLATION

FSTC-HT-23-1744-73

ENGLISH TITLE: PRINCIPLES OF THE RADIATION STUDY OF GLASS AND CERAMIC MATERIALS

FOREIGN TITLE: OSNOVY RADIATSIONNOGO MATERIALOVEDENIYA STEKLA I KERAMIKI

AUTHOR: S. M. Brekhovskikh, Yu. N. Viktorova, Yu. L. Grinshteyn, and L. M. Landa

SOURCE: Lit. po Stroitel'stvu, Moscow, 1971, pp. 1-256

Translated for FSTC by Leo Kanner Associates, Redwood City, CA

NOTICE

UNCLASSIFIED
Security Classification

AD 771166

DOCUMENT CONTROL DATA - R & D

(Security classification of title, body of abstract and indexing annotation must be entered when the overall report is classified)

1 ORIGINATING ACTIVITY (Corporate author)
Foreign Science and Technology Center
US Army Materiel Command
Department of the Army

2a. REPORT SECURITY CLASSIFICATION
Unclassified

2b. GROUP

3 REPORT TITLE
PRINCIPLES OF THE RADIATION STUDY OF GLASS AND CERAMIC MATERIALS

4 DESCRIPTIVE NOTES (Type of report and inclusive dates)
Translation

5 AUTHOR(S) (First name, middle initial, last name)
S. M. Brekhovskikh, Yu. N Viktorova, Yu. L. Grinshteyn, and L. M. Landa

6 REPORT DATE
15 October 1973

7a. TOTAL NO. OF PAGES
236

7b. NO. OF REFS
N/A

8a. CONTRACT OR GRANT NO

b. PROJECT NO

c. T702301 2301

d. Requester AMXST-SD Mr. Bryant

9a. ORIGINATOR'S REPORT NUMBER(S)
FSTC-HT-23-1744-73

9b. OTHER REPORT NO(S) (Any other numbers that may be assigned this report)

10 DISTRIBUTION STATEMENT
Approved for public release; distribution unlimited.

11 SUPPLEMENTARY NOTES

12 SPONSORING MILITARY ACTIVITY
US Army Foreign Science and Technology Center

13 ABSTRACT
This book examines the effects of kinds, dose intensity, and regimes of irradiation on optical, mechanical, electrical, and heat-physical and other properties of glasses and ceramics. It also explores the dependence of the radiation stability of these materials on their composition and their processing technology. Existing radiation-stable materials based on glasses and ceramics and their possible applications are described. The book is intended for scientific specialists in radiation physics and solid-state physics, designers building objects that operate in ionizing radiation fields, engineering-technologists on glasses and ceramics, and also for students and graduate students at higher educational institutions. Materials intended for service in radiation conditions are classified into the following three groups: 1) radiation-resistant materials; 2) radiation-sensitive materials; and 3) materials for absorption of radiation.

DD FORM 1 NOV 68 1473 REPLACES DD FORM 1473, 1 JAN 64, WHICH IS OBSOLETE FOR ARMY USE.

UNCLASSIFIED
Security Classification

14. KEY WORDS	LINK A		LINK B		LINK C	
	ROLE	WT	ROLE	WT	ROLE	WT
Radiation Effect						
Irradiation						
Ceramic Material						
Glass Property						
Nuclear Physics						
Optic Radiation Stability						
Nuclear Radiation						
Solid State Physics						
Irradiation Resistance						
Radiation Dosimetry						
COSATI SUBJECT CODE: 18; 20; 14; 11; 06						
COUNTRY CODE: UR						

TABLE OF CONTENTS

AUTHORS' ABSTRACT

This book examines the effect of various kinds, doses, intensities, and conditions of irradiation on optical, mechanical, electrical, heat-physical, and other properties of glasses and ceramics, and also the dependence of the radiation stability of these materials on composition and processing. Existing radiation-stable materials based on glasses and ceramics and their possible applications are described.

The book is intended for scientific specialists in radiation physics and solid-state physics, designers building objects that function in a field of ionizing radiation, engineer-technologists on glasses and ceramics, and also students and graduate students at higher educational institutions.

INTRODUCTION

Prominent among synthetic products are materials based on glass and ceramics widely used in all industries. Of particular interest is the use of glasses and ceramics in instruments and equipment intended to explore outer space and for research in nuclear physics, atomic power engineering, and solid-state physics. In objects and equipment intended for these purposes, during service articles and materials are subject to corpuscular and electromagnetic nuclear radiations. Nuclear radiation acting on glasses and ceramics modifies their properties so strongly that these changes take on no little technical importance and in several cases make the further use of the articles impossible.

The first information on radiation-caused changes and glass properties, in particular, darkening and coloring, pertains to the time of the discovery of radioactivity and did not have great practical value. Vigorous progress of research into the effect of nuclear radiation on materials began as part of the discovery of the possible use of atomic energy for peaceful purposes, and especially after the breakdown of various materials in nuclear reactors was discovered in 1947.

In the past two and half decades much information has accumulated, enabling us to state with certainty that there are practically no properties of a solid which are unaffected by nuclear radiation. Exposure to nuclear radiation usually adversely affects optical, thermal, mechanical, chemical, electrical, and other properties of materials. However, in several cases the positive effect of radiation on certain properties of materials has been noted. In addition, nuclear radiation, being a controllable method of introducing defects into solids, permits a more profound study of the structure of materials and its relationship with their properties.

One feature of radiation exposure is the complexity of the processes occurring in a solid being irradiated. Often it does not appear possible to predict the radiation breakdown, therefore in each case one must set up an experiment. Thus, it is altogether necessary to make a detailed study of the maximum number of properties for the largest number of materials of diverse chemical and phase composition in order to attempt to establish

certain correlations in property changes of glasses and ceramic materials that have been irradiated.

In studies made on the radiation resistance of glasses and ceramic materials, one often encounters incompatible and even contradictory data, therefore their interpretation and generalization poses difficulties, which are aggravated by the lack of well-grounded theoretical ideas on the structure of materials studied and the relationship of radiation resistance with composition and structure.

The authors of this present book set out not only to systematize literature data, but -- by supplementing them with the results of their own experiments -- to attempt to generalize all available information in order to reach conclusions on how radiation damage depends on the structure and chemical and phase composition of materials.

Since light transmission is one of the most radiation-sensitive characteristics of glasses, it is natural that the greatest wealth of material has been accumulated precisely on radiation coloration of glasses at the present time, enabling the authors to begin work on elucidating the kinetics of color center formation and breakdown and establishing quantitative correlations relating radiation-optical stability with the composition of a glass.

Problems of the effect radiation has on materials take on growing importance for the most diverse fields of science and technology, and radiation stability will become one of the essential characteristics of material, with knowledge of which the material cannot be used in structures functioning under irradiation.

Considering the requirements imposed by conditions of service under irradiation, a large number of materials with special radiation properties have been and continue to be formulated. However, thus far there is no scientifically based classification of materials intended for service under irradiation. An attempt at this classification undertaken in 1963 was fruitful to some extent, which also spurred the authors to further efforts in this direction.

Based on the classification proposed in this book, materials intended to serve under conditions of irradiation are combined into three groups:

1) radiation-resistant materials;
2) radiation-sensitive materials; and
3) materials for absorption of radiation.

The first group includes materials that interact least with the radiation flux and which have stable characteristics when serving for extended periods under irradiation.

The second group includes materials also weakly affected by the radiation flux, however upon irradiation some of their properties undergo changes

in the desired direction, while other characteristics remain fairly stable.

The third group embraces materials that interact most with radiation flux, that is, absorbing, scattering, and attenuating radiation. Materials in this group, in spite of their intense absorption of radiation energy, must also have adequate radiation resistance.

In the view of the authors, this classification affords not only the systematization of known materials, but also guides efforts of researchers in seeking new materials with special radiation properties.

In contrast to certain monographs and surveys dealing with the effect radiation has on solids and of interest above all for physicists and scientific workers studying radiation effects, the book offered to readers is intended for a wide range of engineers, designers, and technologists formulating and using materials intended to serve under conditions of exposure to nuclear radiation of different kinds and energies.

This first attempt at presenting the essentials of a growing science — radiation materials science on glasses and ceramics — is unquestionably not free of shortcomings, and the authors gratefully welcome readers' comments.

CHAPTER ONE

PASSAGE OF NUCLEAR RADIATION THROUGH GLASSES AND CERAMICS

1. Kinds of Radiation

Among the main kinds of radiation capable of substantially affecting the physical properties of materials are α-, β-, and γ-rays, protons and neutrons, comprising nuclear radiation, and also x- and hard ultraviolet rays combined with α-, β-, and γ-rays and protons as ionizing radiation. Characteristics of the various kinds of ionizing radiation and their dosimetry methods are presented in numerous works [1-5].

Alpha-particles are doubly-charged nuclei of helium atoms and are produced in the α-decay of the nuclei of radioactive isotopes of heavy elements. The energy of α-particles emitted in radioactive decay fluctuates in the range 9-20 Mev. Higher-energy α-particles can be produced in accelerators.

Either radioactive isotopes or various accelerators (linear, betatrons, and so on) are a source of β-radiation (electron flux). Electron energy depends on the accelerator parameters or on the kind of radioactive isotope. Particles emitted in β-decay have a continuous energy spectrum in the limits from zero to the maximum value, which for various isotopes lies in the range from several kilo-electron-volts to several mega-electron-volts. The energy of electrons attained in betatron type accelerators is tens and even hundreds of mega-electron-volts.

γ-Rays are emitted by the nuclei of radioactive isotopes or else are produced in the deceleration of electrons when a target is bombarded.

Energy spectra of γ-rays produced during radioactive decay represent a set of monochromatic lines, each of which characterizes the possible transition between discrete energy levels of excited nuclei. The value of these energies usually lies in the range from several kilo-electron-volts to several mega-electron-volts.

In electron deceleration, a continuous spectrum of γ-rays is produced, on which are imposed individual lines determining the possible transitions between discrete enegy levels characteristic of the target material. The maximum energy of bremsstrahlung γ-quanta is as high as the energy of incident bombarding electrons. The effect of energy of bremsstrahlung γ-quanta is usually about 30 percent of the maximum energy.

Protons are the nuclei of hydrogen atoms. They have considerably less penetrating depth than electrons or γ-rays. In materials-science investigations, linear or circular-orbit accelerators, for example, cyclotrons, are the proton source. Proton energies achieved in cyclotrons amount to several and tens of mega-electron-volts. In synchrotron, phasotron, and synchrophasotron type accelerators, proton beams with energies of as much as tens of billions of electron-volts can be produced.

Neutrons are elementary particles present in the composition of atomic nuclei that bear no electrical charge. Energywise, they are classified as fast (with energies from 0.1 to 50 Mev) and thermal neutrons (from 0.005 to 0.5 ev).

In nuclear reactors the chain reaction of the fission of heavy nuclei is the neutron source. In various accelerators neutrons can be produced as the result of secondary radiation formed by the bombardment of a target with protons and α-particles.

Radioactive preparations mixed with a substance that on exposure to α- or γ-rays emits neutrons, for example, a mixture of radium with beryllium, can also serve as a neutron source.

As a rule, neutron emission is accompanied by other ionizing radiation. Strong γ-radiation exists along with neutron radiation in the channels of atomic reactors.

2. Problems of Dosimetry

The concepts of exposure dose and absorbed dose are used in characterizing the conditions of irradiation and to determine the effect of radiation on a solid.

The exposure dose characterizes the radiation field or the radiation energy emitted by a source, that is, the external conditions in which a material is situated within the range of action of the radiation source. The absorbed dose characterizes the energy obtained by the sample due to radiation exposure. In addition, the concepts of dose rate and radiation intensity are used.

Dose rate (exposure dose or absorbed dose) is characterized by the amount of energy emitted by a source or absorbed by a sample per unit time. By definition, dose rate is

$$P = D/t,$$

where D is the dose and t is time.

The radiation intensity refers to the energy of radiation per second per cm^2 of surface perpendicular to the direction in which the radiation is propagated.

GOST [State Standard] 8848-63 establishes the units most typical of indicated fields of use, with allowance for the specific details of physical processes occurrring. By this GOST, the density of a flux of ionizing particles of quanta is measured in particles (quanta)/sec · m^2, radiation intensity is measured in w/m^2, absorbed dose -- in j/kg, and rate of absorbed dose -- in w/kg.

A supplement to the GOST gives the definition of a unit of absorbed dose, according to which j/kg is the absorbed dose for which 1 j of energy is transmitted to a mass of 1 kg of the radiated substance independently of the kind of radiation.

The exposure dose of x- and γ-radiation is measured in k/kg. And k/kg is also the exposure dose of x- and γ-radiation in which the combined corpuscular emission per kilogram of dry atmospheric air produces in the air ions bearing charge equal to 1 coulomb of electricity of each sign.

GOST 8848-63 also permits the use of certain extra-system units and their derivatives. These units include the unit of exposure dose for x- and γ-radiations -- the roentgen (1 r = 2.57976×10^{-4} k/kg) and the unit absorbed dose is a rad (1 rad = 10^{-2} j/kg). We must bear in mind that according to the standard it is allowed to use the exposure dose units k/kg and r (roentgen) for radiation with quanta energy not exceeding 3 Mev.

For irradiation with charged particles, usually the current in the beam I is determined experimentally and the energy of the particle flux is calculated from these data:

$$I = nze \text{ particles/sec},$$

where n is the number of particles passing through the beam cross-section per second and z and e are the charges on the particle.

In many investigations, for example, in radiation chemistry and solid-state physics, the absorbed dose plays the decisive role [5]. In materials-science investigations it is the exposure dose that is central, since the researcher is interested primarily in the change or lack of change of properties for a specific external exposure. However, determination of the absorbed dose is also important in materials-science investigations since only in this way can one compare the effect of different kinds and energies of radiation. The exposure dose is determined experimentally in different ways [1, 6]. The absorbed dose is either calculated by a method presented below, or measured, for example, by chemical dosimetry [5].

3. Attenuation of Radiation

When radiative flux passes through any medium, its attenuation is observed, described by Lambert's law (for parallel rays):

$$I = I_0 e^{-\mu\delta}, \qquad (1)$$

where I_0 is the incident flux intensity; I is the transmitted flux intensity; δ is the thickness of the attenuating layer; and μ is the total linear coefficient of attenuation.

The value of the coefficient μ is determined both by the attenuating medium and the kind and energy of radiation. Depending on the kind and energy of irradiation, flux attenuation takes place due to several processes, each of which contributes to the value of the coefficient μ. In the general case these processes can be divided into scattering and absorption.

Scattering can be elastic, that is, a process in which only the direction of travel of the particle is modified, without energy loss, for scattering may be inelastic, when the change in the direction of travel is accompanied by a change in the kinetic energy of the particle. Some of the particle's energy in the latter case is expended in displacing atoms from lattice sites, exciting nuclei and electrons, and ionizing atoms.

Major losses in energy resulting from numerous inelastic collisions for adequate material thickness can lead to the total deceleration of a moving particle, which is analogous to the absorption of radiation. However, by true absorption we mean the elementary act of interaction of radiation with a medium that leads, in jumplike fashion, to the total loss of kinetic energy of the bombarding particle. Nuclear reactions and the formation of photoelectrons and electron-positron pairs are examples of this kind of process.

The coefficient of attenuation μ serves as a characteristic of the properties of a medium, which in the case of a glass or ceramic generally speaking is a multicomponent system. Therefore it is comprised of partial coefficients μ_i relating to individual components of the material.

To calculate the linear coefficient of attenuation of a material based on its chemical composition, we must use partial values of the mass coefficients of attenuation, that is, coefficients relating to the density of the component material μ_i/ρ_i, calculated for a number of substances (Tables 1-3). In this case

$$\mu = \rho \sum a_i \frac{\mu_i}{\rho_i}, \qquad (2)$$

TABLE 1. MASS COEFFICIENTS OF ATTENUATION OF GAMMA-RAYS BY OXIDES OF CERTAIN ELEMENTS

A Окисел	B Коэффициент ослабления в см²/г при энергии фотона в Мэв			
	0,5	1	3	6
Al_2O_3	0,0857	0,0626	0,0356	0,0261
BaO	0,0967	0,0579	0,0362	0,0354
BeO	0,0936	0,0610	0,0341	0,0236
B_2O_3	0,0814	0,0622	0,0345	0,0262
V_2O_3	0,0856	0,0595	0,0347	0,0274
V_2O_5	0,0833	0,0603	0,0349	0,0270
Bi_2O_3	0,1487	0,0706	0,0410	0,0428
W_2O_3	0,1218	0,0650	0,0392	0,0390
Gd_2O_3	0,1095	0,0619	0,0379	0,0377
Ga_2O_3	0,0833	0,0590	0,0352	0,0294
HfO_2	0,1200	0,0640	0,0390	0,0394
GeO_2	0,0835	0,0592	0,0350	0,0291
Ho_2O_3	0,1130	0,0623	0,0385	0,0386
Dy_2O_3	0,1123	0,0620	0,0383	0,0384
Eu_2O_3	0,1153	0,0616	0,0383	0,0380
EuO	0,1167	0,0615	0,0384	0,0386
FeO	0,0847	0,0607	0,0361	0,0293
Fe_2O_3	0,0859	0,0610	0,0360	0,0289
Fe_3O_4	0,0849	0,0610	0,0359	0,0290
In_2O_3	0,0913	0,0578	0,0363	0,0339
Yb_2O_3	0,1186	0,0732	0,0389	0,0396
Y_2O_3	0,0861	0,0590	0,0358	0,0318
CdO	0,0907	0,0583	0,0363	0,0342
K_2O	0,0862	0,0623	0,0365	0,0283
CaO	0,0863	0,0635	0,0372	0,0288
CoO	0,0834	0,0596	0,0354	0,0290
NiO	0,0867	0,0618	0,0367	0,0305
Nb_2O_5	0,0867	0,0600	0,0362	0,0315
SnO_2	0,0811	0,0587	0,0360	0,0334
SnO	0,0917	0,0592	0,0361	0,0334
Pr_2O_3	0,1032	0,0606	0,0377	0,0369
HgO	0,1425	0,0689	0,0407	0,0427
RbO	0,0838	0,0572	0,0341	0,0316
Sm_2O_3	0,1069	0,0611	0,0380	0,0375
SmO	0,1078	0,0603	0,0381	0,0380
PbO	0,1473	0,0698	0,0409	0,0431

[KEY on following page]

TABLE 1. [Continued]

A Окисел	B Коэффициент ослабления в $см^2/г$ при энергии фотона в *Мэв*			
	0,5	1	3	6
PbO_2	0,1432	0,0693	0,0405	0,0419
Ag_2O	0,0917	0,0590	0,0359	0,0342
AgO	0,0913	0,0593	0,0367	0,0348
Sc_2O_3	0,0841	0,0607	0,0353	0,0274
Sb_2O_3	0,0919	0,0583	0,0361	0,0332
Sb_2O_5	0,0914	0,0589	0,0361	0,0332
Tl_2O	0,1475	0,0693	0,0409	0,0434
Tl_2O_3	0,1425	0,0689	0,0405	0,0347
Ta_2O_5	0,1205	0,0646	0,0392	0,0393
Tb_2O_3	0,1114	0,0616	0,0382	0,0382
TiO_2	0,0842	0,0610	0,0353	0,0271
Ti_2O_3	0,0835	0,0604	0,0351	0,0275
ThC	0,1619	0,0747	0,0420	0,0439
Th_2O_3	0,1177	0,0635	0,0390	0,0398
UO_3	0,1678	0,0754	0,0462	0,0434
U_3O_8	0,1700	0,0757	0,0424	0,0428
P_2O_5	0,0863	0,0627	0,0359	0,0263
Cr_2O_3	0,0841	0,0603	0,0364	0,0282
CrO_3	0,0848	0,0606	0,0354	0,0267
Cs_2O	0,0975	0,0589	0,0367	0,0366
CeO_2	0,1001	0,0579	0,0370	0,0357
Ce_2O_3	0,0910	0,0597	0,0371	0,0363
ZnO	0,0847	0,0595	0,0357	0,0302
ZrO_2	0,0865	0,0592	0,0360	0,0317
Er_2O_3	0,1159	0,0628	0,0387	0,0392
SiO_2	0,0870	0,0634	0,0362	0,0266
La_2O_3	0,0981	0,0589	0,0367	0,0355
Li_2O	0,0817	0,0591	0,0326	0,0236
Lu_2O_3	0,1203	0,0640	0,0391	0,0401
MgO	0,0865	0,0628	0,0360	0,0262
MnO	0,0829	0,0594	0,0360	0,0284
MnO_2	0,0838	0,0603	0,0353	0,0279
CuO	0,0840	0,0597	0,0356	0,0298
Mo_2O_3	0,877	0,0600	0,0361	0,0314
As_2O_3	0,0838	0,0592	0,0363	0,0294
As_2O_5	0,0840	0,0595	0,0353	0,0292
Na_2O	0,0845	0,0616	0,0351	0,0255
Nd_2O_3	0,1041	0,0606	0,0376	0,0369

KEY: A -- Oxide
B -- Coefficient of attenuation in cm^2/g for listed proton energy in Mev

TABLE 2. MASS COEFFICIENTS OF ABSORPTION OF GAMMA-RAYS BY GLASSES WITH COMPOSITIONS $4SiO_2 \cdot Na_2O \cdot 0.5M_xO_y$

A Молярный состав стекла	B Коэффициент поглощения в $см^2/г$ при энергии фотона в *Мэв*			
	0,5	1	3	6
$4SiO_2 \cdot Na_2O \cdot 0,25Li_2O$	0,0843	0,0632	0,0358	0,0254
$4SiO_2 \cdot 1,25Na_2O$	0,0864	0,0630	0,0360	0,0263
$4SiO_2 \cdot Na_2O \cdot 0,25K_2O$	0,0865	0,0629	0,0360	0,0265
$4SiO_2 \cdot Na_2O \cdot 0,25Rb_2O$	0,0862	0,0622	0,0357	0,0270
$4SiO_2 \cdot Na_2O \cdot 0,25Cs_2O$	0,0886	0,0622	0,0361	0,0282
$4SiO_2 \cdot Na_2O \cdot 0,5BeO$	0,0867	0,0629	0,0359	0,0262
$4SiO_2 \cdot Na_2O \cdot 0,5MgO$	0,0864	0,0629	0,0359	0,0263
$4SiO_2 \cdot Na_2O \cdot 0,5CaO$	0,0864	0,0631	0,0360	0,0266
$4SiO_2 \cdot Na_2O \cdot 0,5BaO$	0,0886	0,0629	0,0354	0,0283
$4SiO_2 \cdot Na_2O \cdot 0,5ZnO$	0,0862	0,0625	0,0358	0,0218
$4SiO_2 \cdot Na_2O \cdot 0,5CdO$	0,0871	0,0635	0,0360	0,0277
$4SiO_2 \cdot Na_2O \cdot 0,25B_2O_3$	0,0862	0,0630	0,0359	0,0263
$4SiO_2 \cdot Na_2O \cdot 0,25Al_2O_3$	0,0864	0,0630	0,0359	0,0263
$4SiO_2 \cdot Na_2O \cdot 0,25Ga_2O_3$	0,0860	0,0624	0,0360	0,0268
$4SiO_2 \cdot Na_2O \cdot 0,25In_2O_3$	0,0869	0,0620	0,0359	0,0274
$4SiO_2 \cdot Na_2O \cdot 0,5TiO_2$	0,0860	0,0627	0,0358	0,0264
$4SiO_2 \cdot Na_2O \cdot 0,5ZrO_2$	0,0864	0,0622	0,0359	0,0273
$4SiO_2 \cdot Na_2O \cdot 0,5HfO_2$	0,0953	0,0633	0,0357	0,0298
$4SiO_2 \cdot Na_2O \cdot 0,5GeO_2$	0,0861	0,0625	0,0351	0,0268
$4SiO_2 \cdot Na_2O \cdot 0,5SnO_2$	0,0853	0,0622	0,0354	0,0278
$4SiO_2 \cdot Na_2O \cdot 0,5SnO$	0,0874	0,0622	0,0356	0,0272
$4SiO_2 \cdot Na_2O \cdot 0,5PbO$	0,0934	0,0647	0,0367	0,0308
$4SiO_2 \cdot Na_2O \cdot 0,25V_2O_5$	0,0859	0,0625	0,0358	0,0265
$4SiO_2 \cdot Na_2O \cdot 0,25Ta_2O_5$	0,0947	0,0630	0,0360	0,0295
$4SiO_2 \cdot Na_2O \cdot 0,25P_2O_5$	0,0863	0,0629	0,0359	0,0265
$4SiO_2 \cdot Na_2O \cdot 0,25As_2O_3$	0,0861	0,0624	0,0357	0,0268
$4SiO_2 \cdot Na_2O \cdot 0,25Sb_2O_5$	0,0875	0,0622	0,0359	0,0277
$4SiO_2 \cdot Na_2O \cdot 0,25Bi_2O_3$	0,1039	0,0649	0,0374	0,0311
$4SiO_2 \cdot Na_2O \cdot 0,5MoO_3$	0,0867	0,0625	0,0360	0,0276
$4SiO_2 \cdot Na_2O \cdot 0,5WO_4$	0,0964	0,0636	0,0369	0,0301
$4SiO_2 \cdot Na_2O \cdot 0,25Nb_2O_5$	0,0865	0,0623	0,0360	0,0251
$4SiO_2 \cdot Na_2O \cdot 0,25La_2O_3$	0,0889	0,0616	0,0361	0,0283

KEY: A -- Molar composition of glass
B -- Coefficient of absorption in cm^2/g for listed proton energy in Mev

TABLE 5. VALUES OF LINEAR COEFFICIENTS OF ABSORPTION OF GAMMA-RAYS FOR CERTAIN COMMERCIAL MATERIALS

A Материал	B Линейный коэффициент поглощения в $см^{-1}$ γ-квантов с энергией в Мэв		
	0,5	1	3
C Кварцевое стекло	0,19	0,14	0,08
D Непрерывный прокат E	0,21	0,15	0,08
Оптическое термостойкое стекло ЛК-5	0,21	0,16	0,09
Оптическое стекло К-8 F	0,21	0,16	0,08
Баритовый крон G	0,22	0,15	0,09
Термостойкое стекло 13в H	0,21	0,15	0,09
Тяжелый флинт I	0,80	0,41	0,24

KEY: A — Material
B — Linear coefficient of absorption in cm^{-1} of gamma-quanta with listed energy, in Mev
C — Quartz glass
D — Continuous rolled stock
E — LK-5 optical heat-resistant glass
F — K-8 optical glass
G — Barite crown
H — 13v heat-resistant glass
I — Heavy flint

where ρ is the density of the material; a_i is the weight fraction of the component; and μ_i/ρ_i is the partial mass coefficient of attenuation.

In turn

$$\frac{\mu_i}{\rho_i} = \frac{N}{A_i}\sigma_i, \qquad (3)$$

where N is Avogadro's number; A_i is the gram-atomic weight of the component; and σ_i is the integral cross-section of interaction of the component atom with radiation.

The integral cross-section is the sum of differential sections, each of which is the probability that some single elementary process will take place when the nucleus is bombarded with a flux of one particle per cm^2 per sec. The section has the value of the order of the nucleus' area and is measured in barns (1 barn = 10^{-24} cm^2).

For the case of γ-irradiation

$$\sigma_i = \sigma_{c.s} + \sigma_{c.s} + \sigma_p + \sigma_{pa} + \sigma_n, \qquad (4)$$

TABLE 4. VALUES OF CONSTANTS CHARACTERIZING THE ABSORPTION OF THERMAL NEUTRONS OF OXIDES (WITH ENERGY OF 0.025 ev)[7]

A Оксиды	$\sigma_{M_xO_y}$	$\rho_{M_xO_y}$	$\mu_{M_xO_y}$	$\delta_{1/2}$	$W_{M_xO_y}$
Li_2O	148,2	2,01	5,99	0,116	2,99
Ag_2O	134,2	7,15	2,49	0,279	0,349
BeO	7,55	3	0,546	1,27	0,182
MgO	7,2	3,48	0,385	1,8	0,108
ZnO	3,5	5,66	0,356	1,94	0,0629
CdO	2354	8,15	90	0,0077	11
HgO	414	11,2	12,9	0,0537	1,15
MnO	20,5	5,4	0,942	0,736	0,174
FeO	17,5	5,75	0,848	0,822	0,147
NiO	23,2	6,8	1,27	0,545	0,187
CuO	25,4	6,0	1,15	0,6	0,192
SnO	8,7	6,25	0,243	2,85	0,037
PbO	12,8	9,49	0,328	2,11	0,0316
B_2O_3	1452,6	1,81	22,8	0,0304	12,6
Al_2O_3	45,8	3,8	0,355	1,95	0,0935
In_2O_3	392,6	7,04	5,98	0,116	0,853
La_2O_3	142,6	6,51	1,72	0,403	0,264
Eu_2O_3	9212,6	7,42	116,9	0,0065	15,8
Gd_2O_3	92012,6	7,41	1130	0,00061	153
Dy_2O_3	2312,6	7,81	29,2	0,0237	3,74
Fe_2O_3	36	9,65	0,458	1,51	0,0475
Cr_2O_3	27	5,21	0,558	1,24	0,107
Mn_2O_3	45,2	4,65	0,8	0,867	0,173
Bi_2O_3	26,6	8,5	0,292	2,37	0,0344
SiO_2	10,7	2,2	0,238	2,91	0,108
CeO_2	14,4	3,63	0,301	2,3	0,083
ZrO_2	18,4	6	0,538	1,29	0,09
SnO_2	12,9	7	0,362	1,92	0,051
PbO_2	17	9,6	0,41	1,69	0,042
MnO_2	24,7	5	0,855	0,811	0,171
Nb_2O_5	47,5	2,05	0,555	1,25	0,271
P_2O_5	29,9	2,74	0,348	1,99	0,127
Sb_2O_5	37,6	7,86	0,551	1,26	0,07
Ta_2O_5	74	8,02	0,809	0,858	0,101
Bi_2O_5	35	5,1	0,216	3,21	0,0423
CrO_3	19,8	2,81	0,336	2,06	0,119
WO_3	35,6	7,16	0,662	1,05	0,0926

KEY: A -- Oxides

Remark. $\sigma_{M_xO_y}$ is the effective cross-section of absorption by the oxide in barns; $\rho_{M_xO_y}$ is the density in g/cm^3; $\mu_{M_xO_y}$ is the linear coefficient of attenuation for oxides in cm^{-1}; $\delta_{\frac{1}{2}}$ is the thickness of a layer of the material in cm, corresponding to half-attenuation; and $W_{M_xO_y}$ is the mass coefficient of absorption in cm^2/g.

where $\sigma_{e.s}$ and $\sigma_{c.s}$ are the differential cross-sections of elastic and Compton scattering; σ_p, σ_{pa}, and σ_n are the differential photon absorption cross-sections for the photoeffects, formation of electron-positron pairs, and nuclear reactions, respectively.

The last term in equation (4) is significant only at very high photon energies when nuclear processes become possible, but for ordinary energies obtained in reactors and from radioactive isotopes it can be neglected.

For neutron irradiation,

$$\sigma_i = \sigma_{e.s} + \sigma_{i.s} + \sigma_{abs}, \qquad (5)$$

where $\sigma_{e.s}$ and $\sigma_{i.s}$ are the cross-sections of elastic and inelastic scattering; σ_{abs} refers to absorption processes.

For irradiation with thermal neutrons, the last term in equation (5) characterizing nuclear reactions takes on decisive importance. Absorption cross-sections of thermal neutrons by certain oxides are given in Table 4.

In all cases of the irradiation of materials, the absorbed dose is defined as the fraction of the radiation energy transmitted to the target material and, therefore, depends on the coefficient of attenuation of the radiation of the materials. More exactly, the components of the coefficient μ not associated with elastic scattering play the decisive role, therefore in this process energy is not transmitted.

4. Passage of Charged Particles Through Material

Processes of the interaction of charged particles with material have certain specific features compared with the interaction of electromagnetic radiation. They are detailed in several studies by Soviet and foreign authors [8-12]. In this book the authors do not set out to present their detailed examination, but limit themselves only to general principles necessary for a rough estimation of absorbed dose when charged particles act on material.

Let us consider two cases.

1. The thickness of the sample is less than the length of the particle's free path. The absorbed dose can be estimated by the formula

$$D = \frac{\Delta Ent \cdot 1{,}6 \cdot 10^{-8}}{\delta \rho} = \frac{\Delta Ent \cdot 1{,}6 \cdot 10^{-8}}{\varkappa} \text{ rad}, \qquad (6)$$

where ΔE is the energy lost by the particle on passing through the sample, in Mev; n is the flux intensity in particles/cm^2 · sec; t is the time of irradiation in sec; δ is the linear thickness of the sample in cm; ρ is the density of the material in g/cm^3; and $\delta\rho = \kappa$ is the mass thickness of the specimen in g/cm^2.

In irradiation, usually the current in the beam of charged particles is measured to determine the dose. If the current is measured in microamperes, then for protons

$$D = \frac{\Delta E It}{\delta\rho} 10^6 = \frac{\Delta E It}{\gamma} 10^6 \quad \text{rad.}$$

For α-particles, the absorbed dose will be determined by the formula

$$D = \frac{\Delta E It}{2\kappa} 10^6 \quad \text{rad,}$$

since the particle charge is twice as large as the proton charge.

If a particle gives all of its energy to the sample, the absorbed dose can be estimated by the formula

$$D = \frac{Ent \cdot 1.6 \cdot 10^{-6}}{R\rho} = \frac{EIt}{zR\rho} 10^{-6} \quad \text{rad,} \qquad (7)$$

where E is the energy of the incident particle in Mev; z is the charge on the particle; and R is the length of the particle's path in the material, in cm.

To calculate the absorbed dose, we must know the energy lost by the particle in the sample (formula (6)) or the path length (formula (7)). Generally, these quantities depend on the energy of the particle, its charge, and also on the composition of the material.

A rigorous theory enabling us to calculate these quantities is overly complex. However, for many practical purposes it is sufficient to estimate these quantities even though within limits of an order of magnitude. The quantity ΔE appearing in formula (6) can be calculated to the first approximation as proportional to the mass thickness of sample κ:

$$\Delta E = \kappa\left(-\frac{dE}{dx}\right), \qquad (8)$$

where dE/dx is the stopping power of the material.

Heavy particles lose their energy practically continuously; their trajectory is nearly linear; and the path length in the material corresponds to the depth of penetration. At energies usually employed in materials science investigation (for example, not more than 100 mega-electron-volts

for protons), the main losses are ionizational (expenditure of energy in exciting atoms and molecules) and losses in the elastic interaction of a particle with nuclei of the material or with atoms as a whole, leading to the displacement phenomenon. Losses caused by elastic collisions with electrons and inelastic collisions with nuclei can be neglected. Therefore, practically all the energy lost by a particle goes to determine the absorbed dose of the sample.

When electrons pass through a material, in addition to ionizational losses making the principal contribution to the absorbed dose, radiational losses associated with the initiation of secondary radiation, and also scattering of electrons, their reflection from the surface of the sample, and so on begin to play a considerable role.

Ionizational losses appearing in formula (8) and therefore, ΔE are proportional to the expression

$$\frac{\delta\rho}{v^2} \cdot \frac{Z}{A}, \qquad (9)$$

where ρ, Z, and A are the density, atomic number, and atomic weight of the absorber, respectively; and v is the particle velocity.

Since for most elements $Z/A \approx 0.38$-0.5, that is, practically the same, ionizational losses of energy in a material are determined mainly by the particle energy and by the mass thickness of the sample $\varkappa = \delta\rho$. Below are indicated the specific ionizational losses of electrons with different energies in aluminum [8].

A E, Мэв . .	0,5	1	2	3	4	5	6	7	8	9	10
$\frac{dE}{dx}$, Мэв·см²/г B	1,75	0,5	0,5	0,5	0,6	0,6	0,7	0,75	0,8	0,85	0,9

KEY: A -- Mev
B — Mev · cm^2/g

Values of the mass stopping power of protons, expressed in Mev · cm^2/g, for aluminum are given in Table 5 and can be used for glasses and ceramics.

2. The particle loses all its energy in the sample. With the complete absorption of a particle in a sample, to calculate the absorbed dose we must know the length of the particle's path in the test material. This case is encountered most often in practice when a material is irradiated with heavy particles.

TABLE 5. THEORETICAL VALUES OF THE MASS STOPPING POWER AND PATH LENGTH OF PROTONS IN ALUMINUM [1]

E	$\frac{1}{\rho}\left(\frac{dE}{dx}\right)$, Mev·cm²/g A	R, mg/cm² B	E	$\frac{1}{\rho}\left(\frac{dE}{dx}\right)$, Mev·cm²/g A	R, mg/cm² B
0,1	371	—	6	50	70,42
0,2	345	—	7	44,5	91,64
0,4	279	—	8	40,2	115,3
0,6	230	—	9	36,8	141,3
0,8	197	—	10	33,9	169,6
1	173	4,15	12	29,5	233,1
2	111	11,6	14	26,1	305,3
3	83,2	22,15	16	23,5	386
4	67,6	35,56	18	21,5	475,1
5	57,3	51,7	20	19,8	572,3

KEY: A -- Mev · cm^2/g
B -- mg/cm^2

For the approximate estimation of the length of the path of protons in air, we can use the formula

$$R_{air} = (E/9.3)^{1.8}, \tag{10}$$

where E is the proton energy in Mev.

This formula is suitable for energies to 200 Mev.

For a rough estimate of the path length in other media, it can be regarded as inversely proportional to the density of the medium, that is

$$R = (\rho_{air}/\rho_m)R_{air}, \tag{11}$$

where ρ is the density and R is the path length in meters.

The length of the path of protons with different energies in aluminum, whose density is close to the density of many glasses, is given in Table 5.

Half-values calculated for aluminum based on formulas (10) and (11) agree with those given in Table 5, with an accuracy to 10 percent. The path length of electrons for light materials like aluminum and glasses is determined with the formula

$$R = 0.2E \text{ cm}, \tag{12}$$

where E is the electron energy [5].

Formula (12) is valid when $E > 0.5$ Mev. For energies below 0.5 Mev,

$$R = 0.1E \text{ cm}. \tag{13}$$

We must remember that due to multiple scattering, the depth of particle penetration in the material proves to be less than the maximum possible path length, which naturally also introduces an error into the estimation of the absorbed dose.

CHAPTER TWO

RADIATION EFFECTS IN SOLIDS

When nuclear radiation acts on a solid, several effects are produced, dependent both on the kind and energy of radiation, and on the nature and properties of the irradiated material.

The action of radiation on matter is a complex process since the same kind of radiation can cause different effects. The process is complicated still further by the fact that radiation exposure only in rare cases reduces to the collision of an incident particle or quantum with a target atom. Most often, this collision is only the beginning of a chain of subsequent acts, the primary stage causing various secondary phenomena, often more severe and ultimately determining the nature of the effect of a given radiation on the material (cf. scheme).

Of all the kinds of radiation effects, we can single out three large groups:

1) effects of the interaction of radiation with the nuclei of elements;

2) electronic effects (ionization and excitation) caused by the interaction of radiation with the electron shells of atoms; and

3) displacement effects in which the normal positions of the atoms (or ions) at lattice sites undergo changes.

1. Interaction of Radiation With Nuclei of Elements

The collision of a bombarding particle with a target nucleus can lead to various consequences. Firstly, there may be an interaction in which the particle and the nucleus behave as elastic spheres flying apart after collisions in accordance with the laws of elastic impact (elastic scattering). Secondly, interaction is possible which results in the production of a particle of the same kind as the bombarding particle, but the terminal nucleus remains in the excited state (inelastic scattering). Finally, interaction leading

to changes in the composition of the target nucleus and thus to the flight of a particle distinct from the bombarding particle (nuclear transformation) is possible.

Neutrons, not possessing a charge, interact very little with the electrons of atoms, therefore the decisive role in the determination of the fate of neutrons on passing through a material is played by their interaction with the nuclei of atoms.

The absorption of a neutron leads to an increase in the nuclear energy for most elements, except the lightest, by about 8 Mev [1] (neglecting the kinetic energy of the incident neutron). So in the capture of even a thermal neutron the composite nucleus passes over to the highly excited state.

A nucleus in an excited state exists only for some time interval and then decays and passes into a state with lower energy or into the ground state. This transition is accompanied by the emission of nuclear particles or gamma quanta.

It has been established for nuclei with a mass number in the medium range ($\sim$ 50) that in the region of low neutron energies the largest cross-sections are observed for the reaction (n,γ) -- radiation capture, and in the transition to high energies scattering begins to predominate. Reactions with the emission of charged particles, for example, the following, are observed for some light nuclei at low energies: $Li^6(n,\alpha)H^3$; $B^{10}(n,\alpha)Li^7$; $B^{10}(n,p)Be^{10}$; $N^{14}(n,p)C^{14}$; and $C^{35}(n,p)S^{35}$, where the cross-sections of these reactions are much larger than those for radiation capture. The cross-section of the reaction (n,α) at the isotopes B^{10} and Li^6 is particularly large.

When the mass number of target nuclei is greater than 40, processes of the (n,α) type occur infrequently. Processes of the (n,2n) type are more probable for elements with higher mass number. While the dependence of the capture cross-section of slow neutrons on their energy in the low-energy region is of the form 1/v (v is the neutron velocity), the cross-sections of scattering processes (n,n) and (n,2n) increase with neutron velocity. A certain so-called threshold neutron energy is needed for these processes to occur, below which they are not observed at all. For the process (n,n) the threshold lies in the region of hundreds of kilo-electron-volts, depending on the target element. The threshold of the reaction (n,2n) for these elements is in the region of several mega-electron-volts, where after the attainment of an energy of about 20 Mev, the cross-section of this process changes but little.

When gamma-rays pass through a material, nuclear reactions of the (γ,n) and (γ,p) types can have an attenuating effect. However, as already noted, these photonuclear reactions are excited only for a high enough radiation energy.

PROCESSES OCCURING IN A SOLID WHEN EXPOSED TO NUCLEAR RADIATION

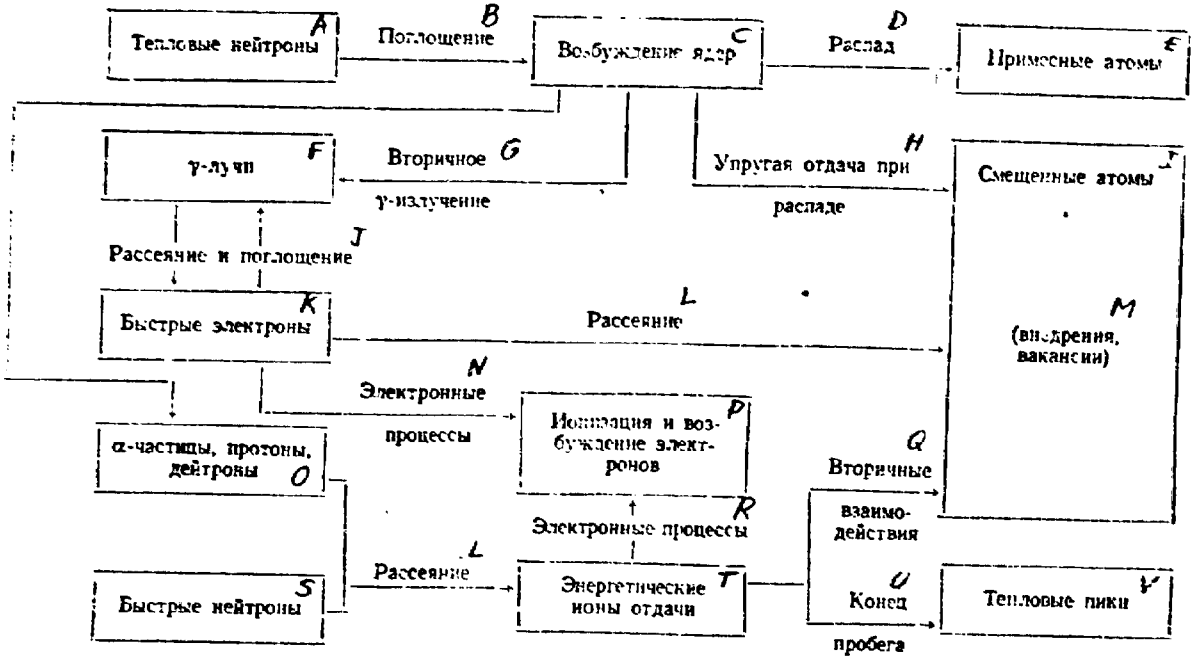

/KEY on following page/

/KEY to scheme on preceding page/

A -- Thermal neutrons
B -- Absorption
C -- Excitation of nuclei
D -- Decay
E -- Impurity atoms
F -- Gamma-rays
G -- Secondary gamma-radiation
H -- Elastic recoil in decay
I -- Displaced atoms
J -- Scattering and absorption
K -- Fast electrons
L -- Scattering
M -- (interstitials, vacancies)
N -- Electronic processes
O -- Alpha-particles, protons, and deutrons
P -- Ionization and excitation of electrons
Q -- Secondary interactions
R -- Electronic processes
S -- Fast neutrons
T -- Energetic recoil ions
U -- End of path
V -- Thermal spikes

Nuclear reactions caused by electrons require a very high electron energy. The effective cross-section of electron splitting of nuclei is about 400 times smaller than the corresponding cross-section of photosplitting, but the energy thresholds of these processes are the same. Nuclear reactions caused by electrons remain practically without significance.

In cases when bombardment is carried out with positively charged particles, each particle -- before combining with a target nucleus -- must surmount the potential barrier produced by the electrostatic forces of repulsion. To overcome this barrier and to approach the nucleus at a distance for which nuclear forces begin to come into play, the charged particle must have a high enough energy.

Nuclear reactions can affect the properties of solids directly owing to the formation of impurity atoms; however, this requires that a sufficient number of nuclei undergo transformations. Of greatest importance are the secondary processes accompanying nuclear reactions: ionization under the effect of secondary gamma-radiation, displacements of recoil nuclei, and a good many processes arising in internal bombardment of a material with the high-energy products of nuclear reactions.

2. Electronic Effects (Ionization and Excitation)

These effects arise virtually for exposure to all kinds of nuclear radiation, however their relative magnitude compared with other processes fluctuates widely. Atoms are ionized in all cases when the scattering of bombarding particles or quanta occurs at electrons, independently of the atomic nucleus. Electrons receiving a high enough energy upon interacting can leave their orbits and thus become free electrons. But if the energy imparted to electrons is inadequate for ionization, they enter orbits farther removed from the nucleus, causing the atom to become excited.

Thermal neutrons, owing to their low energy, cannot directly cause the atoms of a medium to become ionized. However, if the capture of neutrons is accompanied by the emission of quanta and particles, ionization now takes place as a secondary phenomenon under the effect of the products of nuclear reactions.

Fast neutrons produce ionization indirectly, since the energy acquired from neutrons is expended by an atom in ionization during secondary processes. Ionization will proceed more effectively, the smaller the mass of the atoms undergoing collisions, so the nature and magnitude of effects depend on the position of the target element in the periodic system and on the neutron energy.

Processes of ionization and excitation are the main types of radiation effects arising in a solid when irradiation by gamma-rays and electrons. The ionization mechanism may vary. The main kinds of ionization processes are the following.

1. Photoionization. In this case a photon is absorbed when it interacts with an orbital electron. The energy of the gamma-quantum is completely expended in the work of ionization and in the kinetic energy of the expelled electron. For small gamma-quantum energy, the photo-effect is predominant for materials with a high atomic number.

2. Compton effect. This phenomenon consists of the scattering of photons by free electrons, that is, by the electrons for which the work of ionization is small compared with the photon energy. Since nearly all electrons have this value for their work of ionization, the Compton effect may occur very frequently. The scattering quantum loses energy and the electrons participating in scattering acquire it. Compton electrons then gradually lose their energy through excitation and ionization of surrounding atoms.

3. Formation of electron-positron pairs. Near heavy nuclei when the photon energy is more than 1 Mev, photon absorption and formation of an electron-positron pair may occur. The excess photon energy above the energy of the particles formed is carried away by them as kinetic energy. The positron has a short lifetime and ultimately recombines with an electron, whence two

has a short lifetime and ultimately recombines with an electron, whence two photons are formed, which together with the electrons in turn cause excitation in the ambient medium.

In electron irradiation, ionization and excitation play the main role. If the electron energy is less than the ionization energy, radiation effects consist of the excitation of target atoms. Ionization processes begin with an increase in electron energy, resulting in the formation of secondary electrons, and ionization is extended to deeper-lying orbits.

For exposure with heavy charged particles exhibiting high energies, the main proportion of this energy is expended in interaction with the electron shells of atoms, where the remainder of energy used in other radiation effects is small up to 10 percent). So the ionization density for bombardment with charged particles is high. Only at the end of a flight when the particle energy has been sufficiently reduced will the particle be capable of elastic collisions.

Electrons expelled from their orbits, traveling through the lattice, lose their energy by coloumbic interaction with the electrons of other atoms. The site from which the electron is expelled, the so-called "hole" in the electronic shell, also travels through the lattice, as long as it is not captured by an atom with the least affinity for an electron. On being captured, a hole can migrate in the lattice until it meets an electron, with which it recombines. Also, the capture of electrons and holes can occur at impurity atoms present in the material or other structural defects, causing the formation of color centers. Holes in the valency zone initiated in ions with high affinity for electrons are replenished by means of atoms and ions with lesser affinity, that is, the hole migrates to the least deep-lying electronic levels.

Formation of excited electronic states, color centers, free electrons, and free holes substantially modifies the electronic characteristics of the material -- paramagnetism, optical absorption, dielectric losses, and electroconductivity -- and causes photoconductivity, luminescence, and so on.

3. Displacement Effects

In solids with molecular, ionic, metal, and covalent bonds for irradiation with electrons, neutrons, and charged particles, and in some conditions -- also with gamma-quanta, displacement occurs; with this phenomenon are associated disturbances in the geometry of the arrangement of atoms and energy changes leading to property changes of the material.

Damage to a lattice caused by the displacement of atoms from their normal positions can be divided into the following simple types [2-6]:

a) point structural defects; and
b) local damage (spikes).

Point defects. Point radiation defects can include vacancies, that is, lattice sites from which ions or atoms have been expelled; knock-ons, that is, atoms or ions expelled from lattice sites lodge at interstices in the nonequilibrium state; displacements arising when a collision of a moving atom or of a particle with an atom at a lattice site leads to the atom being expelled, and the kinetic energy of the interstitial atom is insufficient to remove it from the vacancy formed by it, whence the bombarding atom can lodge in the vacant site, and its residual energy will be converted into thermal oscillations of the lattice.

Vacancies and knock-ons do not remain at the points of inception, but due to the thermal motion of atoms they can migrate. If the temperature ensures the mobility of defects in the crystal lattice, as a rule they undergo several transformations: first of all, vacancies and knock-ons can become annihilated upon direct collisions; secondly, they can emerge at the surface, that is, they can cease to exist as internal defects; and thirdly, they can cluster at impurities and other defects present in the solid, in particular, at dislocations.

Irradiation with gamma-rays always leads to the internal bombardment of a material by electrons with high enough energy, which can cause the displacement of atoms. The recoil of nuclei when emitting secondary gamma-quanta can also lead to displacement.

In addition to the effect of internal bombardment with electrons and the direct recoil of nuclei, two more possible mechanisms for the initiation of displacement in gamma-irradiation have been proposed. According to Seitz [2], local regions of electronic excitation are formed -- excitons, which on transferring energy to the lattice promote the pinning of point defects.

A mechanism proposed by Varli [7] is applicable to materials with ionic bonds. It reduces to the fact that in irradiation some negative ions as the result of multiple ionization can change their charge sign and exist in an unstable position, from which as the result of thermal oscillations they can be knocked into interstitial sites by the action of surrounding positive ions. A vacancy in the lattice is capable of capturing an electron and being converted into a color center.

For atom displacements to take place, electrons -- owing to their low mass -- must travel at relativistic velocities. In this case, coulombic interaction of an electron with a target nucleus leads to displacement.

Local damage (spikes) are produced when a solid is bombarded with fast neutrons or with high-energy heavy particles, in particular, particles emitted in nuclear reactions. In this case, an atom receiving a high enough momentum in its primary collision and traveling through the lattice causes other nearest atoms to be displaced. A cascade of displacements is formed, resulting in the initiation of a region with a very high density of displacements -- a displacement spike.

Since in irradiation it is not the individual atoms but the crystal lattice as a whole that undergoes exposure, the atom receiving a sufficient impact in order to begin vibrating with the large amplitude will rapidly transfer energy and excite neighboring atoms. Local excitation arises in the lattice, similar to rapid heating of a bounded region to high temperature -- thermal spike. If the excitation of atoms in a spike is sufficient to displace large number of atoms, a displacement spike is formed. Since the temperature in the spike region rises extremely rapidly, and also owing to the effect of surrounding material, this region is close to the state of a superheated solid, and melting of the material is possible in the very center of the spike. The danger of heating can never arise in gamma-irradiation owing to its high penetrating power.

Zones of microheating can also arise along the initial sections of charged particle trajectories, and the probability that initiation is the greater, the higher the ionization density. Heating results from nonradiative transformation of the energy of excited atoms, that is, its transfer to the crystal lattice. This applies mainly to the case of bombardment with heavy charged particles.

Obviously, properties of any solid change markedly if an appreciable fraction of its atoms are displaced from their normal positions and if the diffusion rate is not high enough to eliminate the effect of displacements.

The presence of any specific type of radiation effects in the pure form is possible only in rare cases. Usually different types of effects (primary or secondary) coexist, sometimes causing contrary consequences. The external manifestation of radiation effect can proceed as follows:

1) changes in the material's properties related to structural damage. These include not only changes in "geometrical" structure, that is, the relative arrangement of atoms (ions) of the material, but also disruption of force interaction between individual structural elements (the formation of stresses between the defect region, change in depth of potential wells, in frequencies of oscillations, and so on);

2) changes in properties associated with the state of electrons in the material, so-called electronic or hole properties; and

3) changes in the rates of individual processes ongoing in the solid.

CHAPTER THREE

INDUCED OPTICAL ABSORPTION OF SIMPLE-COMPOSITION GLASSES

Two kinds of absorption in crystals and glasses are differentiated: intrinsic and supplementary. Intrinsic absorption generally lies in the ultraviolet spectral region and is caused by the excitation of electrons in the material's atoms. Bands of intrinsic absorption have a sharp long-wave edge and a sizeable coefficient of absorption at the maximum. Supplementary or induced optical absorption is produced by color centers: by electrons or holes localized at lattice defects.

The structure of color centers cannot be regarded as established. Several models of electron and hole centers have been proposed in the studies [1-6]. Essentially, models of F-centers amount to the following:

the center is an electron captured by an anionic vacancy (de Bour model);

the center is an interstitial cation capturing an electron (Gil'sh-Polya-Frenkel' model); and

the center has two modifications (Varly model) -- the first of these is the de Bour model, and the second is an electron localized at a vacant anionic site captured by the metal atom. At present the de Bour model is widely accepted.

A V-center is a negative of a F-center. The role of electron is played by the hole. In addition to these simple centers, there may be various combinations of them.

The complex absorption spectrum observed for irradiated glasses is due to the complex nature of color centers. Each color center is responsible for its specific band, however owing to the complexity of glass composition bands induced by different color centers often overlap, therefore it is difficult to interpret bands and to ascribe their formation to particular centers. However, investigation of absorption bands of simple-composition

glasses can yield interesting data for our understanding of what color centers are and for the directed synthesis of radiation-resistant glasses.

1. Glasses of the System SiO_2-R_xO_y

Kats and Stevels [7, 8], in studying alkali-silicate glasses containing 30 mole percent alkali oxide detected three absorption bands after irradiation. The 310 nm (4 ev) band was ascribed to the hole near a non-immobilized oxygen atom and is independent of the type of alkali metal. The position of the 610 nm long-wave band ($\sim$ 2 ev) is quite stable, though its intensity depends on the glass composition and increases from lithium to rubidium glass, but is the smallest for cesium glass. The band in the 415-490 nm region (3-2.5 ev) is shifted toward the long-wave spectral region when the alkali oxide is added in the following order: $Li_2O < Na_2O < K_2O < Rb_2O < Cs_2O$ (Fig. 1). The nature of this band is dictated by the electron near the alkali ion.

Danilov and Berbash [9] showed that absorption bands with maximas of 320, 450, and 600-620 nm (3.9, 2.8, and 2.1-2 ev) are induced in silicate glasses of the composition $Na_2O \cdot 2SiO_2$ when exposed to gamma-rays. Investigation of the absorption of irradiated glasses with the composition $Na_2O \cdot 2SiO_2$, where the amount of Na_2O varied within the limits 26-46 mole percent shows that an increase in the Na_2O content leads to a change in the nature of the absorption spectrum, and also to an increase in absorption in the ultraviolet, visible, and near infrared spectral regions. Glasses containing more than 35 mole percent Na_2O have an absorption spectrum with bands in the regions 310 and 520 nm (4 and 2.4 ev).

Absorption spectra of two-component potassium-containing glasses with variable composition (Fig. 2) are characterized by a stable band in the 475 nm (2.6 ev) region [10]. The ultraviolet band [310 nm (4 ev)] is shifted toward the short-wave spectral region with decrease in K_2O concentration. The absorption maximum of glasses containing 30, 15, and 1 mole percent K_2O will be, respectively, 310, 300, and 280 nm (4, 4.1, and 4.4 ev). The intensity of the long-wave 620 nm (2 ev) band is proportional to the K_2O content. If we express the intensity ratio of the 475 nm and 620 nm absorption bands (2.6 and 2 ev) as a function of the potassium oxide concentration, we get a curve with two maxima when the K_2O content is 12.5 and 20 mole percent.

We must note that the intensities of all bands depend on the potassium oxide concentration. As a rule, the absorbing ability of a glass rises as the K_2O content is raised. The only exception is the band with a maximum at 475 nm (2.6 ev) and the glass containing 15 percent K_2O.

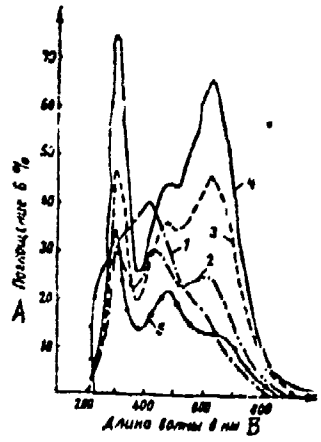

Fig. 1. Spectral absorption curves of glasses with compositions 70 % SiO_2 and 30 % R_2O containing the following oxides
1 -- of lithium
2 -- of sodium
3 -- of potassium
4 -- of rubidium
5 -- of cesium
KEY: A -- Absorption in %
B -- Wavelength in nm

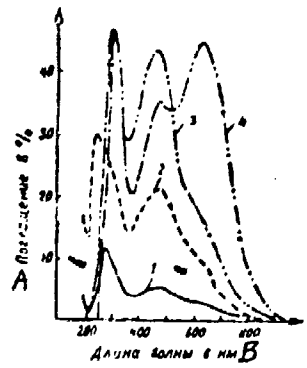

Fig. 2. Spectral absorption curves of glasses containing the following compounds, after irradiation with x-rays
1 -- 99 % SiO_2, 1 % K_2O
2 -- 95 % SiO_2, 5 % K_2O
3 -- 85 % SiO_2, 15 % K_2O
4 -- 70 % SiO_2, 30 % K_2O
KEY: A -- Absorption in %
B -- Wavelength in nm

Kats [8] proposed the existence of three following possible disruptions in the SiO_2 lattice: 1) oxygen vacancies; 2) unbound oxygen ions; and 3) intermediate cations (lattice modifiers).

Irradiated lead-silicate glasses (PbO-80 percent, SiO_2 - 20 percent) yield three absorption bands: 730, 540, and 375 nm (1.7, 2.3, and 3.3 ev) [11, 12]. It is suggested that during the radiation two processes are occurring: capture of electrons at defects existing in the glass before irradiation, and the initiation during irradiation of defects of the same type, which behave similarly to the previously existing defects, that is, they capture electrons and produce the same color centers.

2. Glasses of the System SiO_2-R_2O-R_xO_y

When aluminum oxide is added to a glass with the composition $Na_2O \cdot 4SiO_2$, a change is observed in the intensities of the 340, 480, and 620 nm bands (3.6, 2.6, and 2 ev).

As the content of alkali metal oxides is increased in a glass with composition 80 percent by weight (SiO_2 + R_2O) and 20 percent by weight B_2O_3 (R_2O - Li_2O, Na_2O, K_2O), induced absorption rises systematically, and this function is linear for potassium glasses when the K_2O content is about 15 percent [13].

When oxides of alkali or alkaline-earth metals in silicate glasses are replaced with PbO in equal molar ratios [14], the absorption spectrum undergoes appreciable alteration: a well-defined maximum appears in the region of 700 nm (1.8 ev) and bands of the visible spectral region disappear.

The nature of absorption centers was studied in relation to their structure in glasses of the system Na_2O-Al_2O_3-SiO_2 [15]. It was found that when there is excess Al_2O_3, the Al^{3+} ion appears in sixfold coordination, which lacks an oxygen for construction of the tetrahedron.

The 365 nm absorption band (3.4 ev) owes its appearance to the presence of a nonbridging oxygen. As the Al_2O_3 content is varied, qualitative and quantitative changes occur in the spectra, which is accounted for by the tendency of Al^{3+} to be incorporated in the network of $[SiO_4]$ tetrahedron; here the deficient oxygen atom is introduced by Na_2O. When the Na_2O:Al_2O_3 ratio is 1, all of the nonbridging oxygen is bound into the $[AlO_4]$ tetrahedron and thereby a network consisting of $[SiO_4]$ and $[AlO_4]$ is formed.

Typical of gamma-ray irradiated borosilicate glasses [16] containing PbO is an absorption band when the photon energy is 825 nm (1.5 ev). This absorption band is attributed to Pb^{2+} and increases with a rise in the glass content of boron as well as lead.

Our investigations of the spectra of induced optical absorption of glasses of the system SiO_2-Na_2O-R_xO_y (R_xO_y represents oxides of group I, II, III, IV, and V elements) enables us to find several dependences of the change in supplementary absorption on the particular variable component involved.

Absorption spectra of glasses containing oxides of tin, antimony, arsenic, germanium, cadmium, indium, and ruthenium as the variable components are shown in Fig. 3. Absorption spectra of these glasses have no well-defined maxima. The pattern of the curves is quite smooth. After irradiation a marked increase in optical density is observed in the ultraviolet spectral region from 300 to 400 nm (4.1-3.1 ev). In the near infrared spectral region the optical density remains practically unchanged. An exception is the glass with the composition $4SiO_2 \cdot Na_2O \cdot 0.25As_2O_5$ (Fig. 3 c),

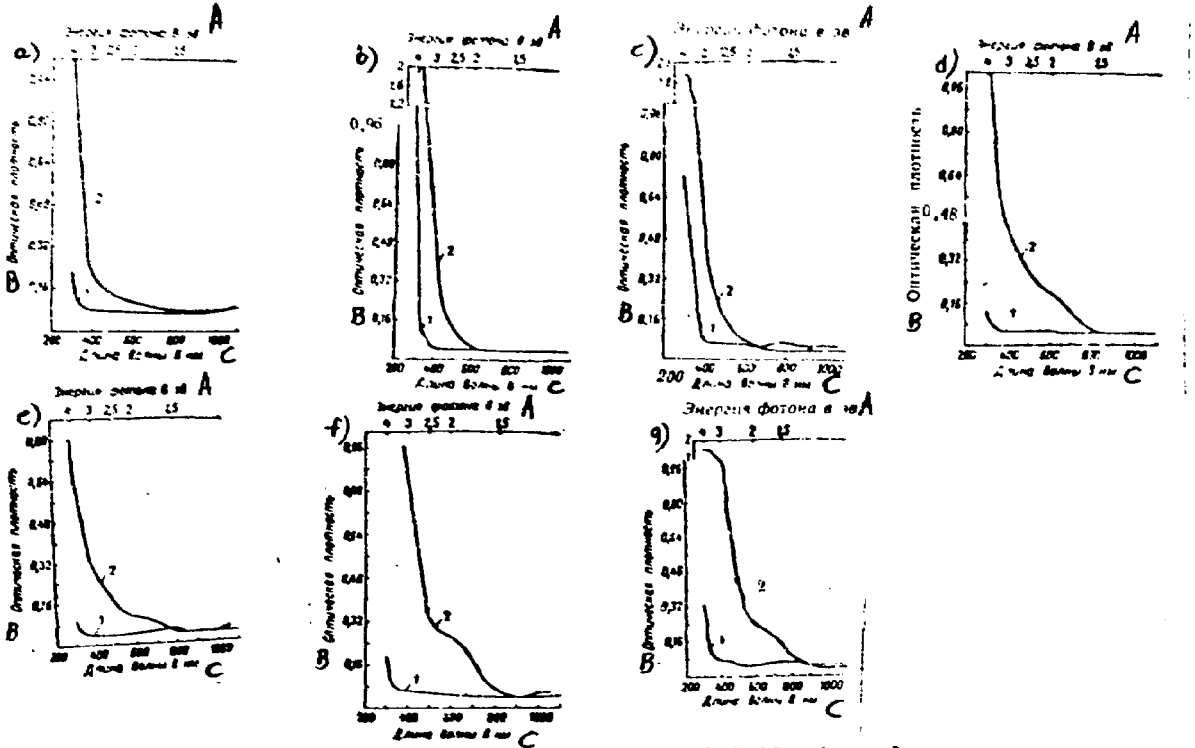

Fig. 3. Optical density of following glasses
a — $4SiO_2 \cdot Na_2O \cdot 0.5SnO_2$
b — $4SiO_2 \cdot Na_2O \cdot 0.25Sb_2O_3$
c — $4SiO_2 \cdot Na_2O \cdot 0.25As_2O_3$
d — $4SiO_2 \cdot Na_2O \cdot 0.5GeO_2$
e — $4SiO_2 \cdot Na_2O \cdot 0.25In_2O_3$
f — $4SiO_2 \cdot Na_2O \cdot 0.5CdO$
g — $4SiO_2 \cdot Na_2O \cdot 0.25La_2O_3$
1 — before irradiation
2 — after irradiation (10^7 r dose)
KEY: A — Photon energy in ev
B — Optical density
C — Wavelength in nm

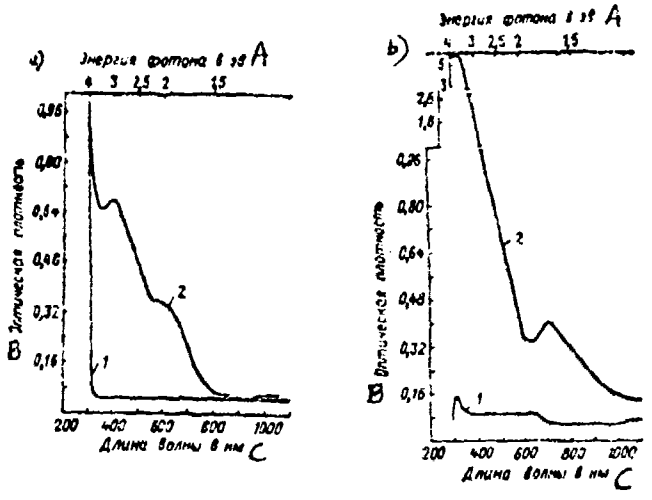

Fig. 4. Optical density of following glasses
a -- $4SiO_2 \cdot Na_2O \cdot 0.5ZnO$
b -- $4SiO_2 \cdot Na_2O \cdot 0.5PbO$
1 -- before irradiation
2 -- after irradiation (10^7 r dose)
KEY: A -- Photon energy in ev
B -- Optical density
C -- Wavelength in nm

for which the optical density in the infrared region examined decreases following irradiation. In the wavelength range from 400 to 760 nm (3.1-1.6 ev), a rise in optical density was observed for all glasses of this group after irradiation. Irradiated glass with a composition $4SiO_2 \cdot Na_2O \cdot 0.5SnO_2$ (Fig. 3 a) has the lowest optical density in the visible spectral region. This glass markedly surpasses the glasses of all listed compositions in terms of its resistance to irradiation.

We must separately consider the absorption spectra of glasses with the composition $4SiO_2 \cdot Na_2O \cdot 0.5ZnO$ and the composition $4SiO_2 \cdot Na_2O \cdot 0.5PbO$ (Fig. 4). The optical density curve of the unirradiated glass with the composition $4SiO_2 \cdot Na_2O \cdot 0.5ZnO$ has a weak maximum in the 380 nm region (3.3 ev), which on exposure to gamma-rays is shifted toward the visible spectral region -- 400 nm (3.1 ev). Typical of the glass with a composition $4SiO_2 \cdot Na_2O \cdot 0.5PbO$ after irradiation is intense absorption in the ultraviolet spectral region. The absorption maximum is observed at 300-400 nm (4.1-3.1 ev), and a second, less intense, maximum lies at 700 nm (1.7 ev). A rise in optical density is noticeable in the near infrared spectral region after irradiation.

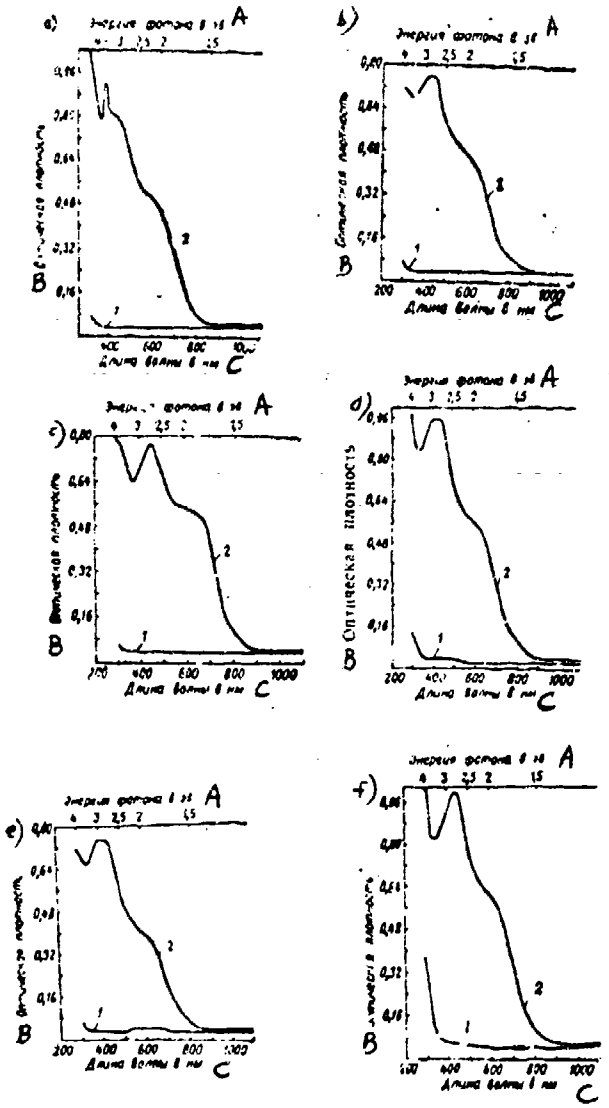

Fig. 5. Optical density of following glasses
a — $4SiO_2 \cdot Na_2O \cdot 0.25Al_2O_3$
b — $4SiO_2 \cdot Na_2O \cdot 0.5CaO$
c — $4SiO_2 \cdot Na_2O \cdot 0.5BaO$
d — $4SiO_2 \cdot Na_2O \cdot 0.25Li_2O$
e — $4SiO_2 \cdot Na_2O \cdot 0.5MgO$
f — $4SiO_2 \cdot Na_2O \cdot 0.5SrO$
1 — before irradiation
2 — after irradiation (107 r dose)
KEY: A — Photon energy in ev
B — Optical density
C — Wavelength in nm

Absorption spectra of glasses containing oxides of boron, magnesium, aluminum, calcium, barium, lithium, magnesium [sic], and strontium are shown in Fig. 5. Spectra of the induced absorption of these glasses have more complicated structures compared with the above-considered compositions. A supplementary absorption band with its maximum in the 400-450 nm region (3.1-2.8 ev) is induced in these glasses after irradiation. Thus, adding Al_2O_3 to a glass composition leads to the appearance of an absorption band with its maximum at 380 nm (3.3 ev) (Fig. 5 a).

Glasses containing BaO and SrO as the third component (Fig. 5 c and f) have a maximum in the 650 nm region (1.9 ev) on the optical density curve.

The optical density remains virtually unchanged in the near infrared spectral region for glasses of all listed compositions after irradiation.

All unirradiated glasses are practically transparent in the visible spectral region given the condition that they do not contain cations of transition elements, for which transitions between multiplet levels are permitted.

Upon irradiation, the picture changes markedly. Secondly electrons formed after exposure to gamma-rays migrate through the system and become localized at the ions whose atoms have the smallest electroconductivity. First of all, this applies to alkali and alkaline-earth elements. Actually, all glasses containing Li^+, Mg^{2+}, Ca^{2+}, Si^{2+}, and Ba^{2+} as the third component have virtually identical spectra after irradiation. A well-pronounced band in the 400-450 nm region (3.1-2.8 ev) in all probability is due to the group $[Me^{2+} + e^-]$. The highest intensity of this band is observed for glasses containing Li^+, Sr^{2+}, and Ba^{2+}, and the smallest -- in glasses containing Mg^{2+} and Ca^{2+}. But this then indicates some displacement of the band in the 400 nm region toward the long-wave region in glasses containing Li^+, Sr^{2+}, and Ba^{2+} compared to glasses containing Ca^{2+} and Mg^{2+}. The highest intensity of this band in a glass with composition $4SiO_2 \cdot Na_2O \cdot 0.5SrO$ can be explained by the imposition of the intrinsic resonance absorption of the Sr atom.

With time the nature of spectra of these glasses remains unchanged, and only integral absorption is reduced, to differing degrees in different glasses. The inflection on the curve in the 600 nm region (2.1 ev) in all probability indicates the presence in the glass of oxygen vacancies or the formation of free oxygen atoms arising when electrons are transferred to the alkali or alkaline-earth ion. This then explains the fact that glasses containing large amounts of ions with low electronegativity capable of producing ionic bonding have lower radiation resistance under otherwise equal conditions.

It is highly interesting to estimate the radiation-optical stability (ROS) of glasses as a function of the ionic radii of elements being varied (Table 6). If we arrange elements in the order of increasing atomic number,

TABLE 6. DEPENDENCE OF RADIATION-OPTICAL STABILITY ON IONIC RADIUS

A Стекло	B Состав	C Период	D Номер элемента	E Ионный радиус R в нм	F Показатель РОУ
C-3 G	$4SiO_2 \cdot Na_2O \cdot 0{,}25Li_2O$	2	3	0,068	0,17
C-5 H	$4SiO_2 \cdot Na_2O \cdot 0{,}25B_2O_3$		5	0,02	0,39
C-11 I	$4SiO_2 \cdot Na_2O$		11	0,098	0,32
C-12 J	$4SiO_2 \cdot Na_2O \cdot 0{,}5MgO$	3	12	0,074	0,32
C-13 K	$4SiO_2 \cdot Na_2O \cdot 0{,}25Al_2O_3$		13	0,057	0,3
C-20 L	$4SiO_2 \cdot Na_2O \cdot 0{,}5CaO$		20	0,104	0,24
C-30 M	$4SiO_2 \cdot Na_2O \cdot 0{,}5ZnO$		30	0,083	0,4
C-32 N	$4SiO_2 \cdot Na_2O \cdot 0{,}5GeO_2$	4	32	0,044	0,63
C-33 O	$4SiO_2 \cdot Na_2O \cdot 0{,}25As_2O_3$ (As_2O_5)		33	0,069 (0,047)	0,85
C-38 P	$4SiO_2 \cdot Na_2O \cdot 0{,}5SrO$		38	0,12	0,21
C-40 Q	$4SiO_2 \cdot Na_2O \cdot 0{,}5ZrO_2$		40	0,082	0,7
C-41 R	$4SiO_2 \cdot Na_2O \cdot 0{,}25Nb_2O_5$		41	0,066	0,74
C-48 S	$4SiO_2 \cdot Na_2O \cdot 0{,}5CdO$	5	48	0,099	0,54
C-49 T	$4SiO_2 \cdot Na_2O \cdot 0{,}25In_2O_3$		49	0,092	0,7
C-50 U	$4SiO_2 \cdot Na_2O \cdot 0{,}5SnO_2$		50	0,067	0,92
C-51 V	$4SiO_2 \cdot Na_2O \cdot 0{,}25Sb_2O_3$		51	0,09	0,68
C-56 W	$4SiO_2 \cdot Na_2O \cdot 0{,}5BaO$		56	0,138	0,2
C-57 X	$4SiO_2 \cdot Na_2O \cdot 0{,}25La_2O_3$	6	57	0,104	0,59
C-82 Y	$4SiO_2 \cdot Na_2O \cdot 0{,}5PbO$		82	0,126	0,28

KEY:
A — Glass
B — Composition
C — Period
D — Atomic number of element
E — Ionic radius, R, in nm
F — ROS indicator
G — S-3
H — S-5
I — S-11
J — S-12
K — S-13
L — S-20
M — S-30
N — S-32
O — S-33
P — S-38
Q — S-40
R — S-41
S — S-48
T — S-49
U — S-50
V — S-51
W — S-56
X — S-57
Y — S-82

then within the limits of the same period we observe a quite specific agreement between the ion sizes and the radiation stability of glasses. However, in glasses containing third-period elements the ROS is practically independent of the ionic radii of the element. A possible explanation of this

fact can be the assumption that a considerable proportion of aluminum oxide is a glass forming agent and only a lesser fraction is a modifier. Therefore introducing aluminum into the silicon-oxygen framework, owing to the relatively large dimensions of the $[AlO_4]$ tetrahedron compared with the $[SiO_4]$ tetrahedron, leads to a drop in ROS even with a reduction in the sizes of the ionic radii, all the more so since here we must allow for the covalent radius, which is larger than the ionic.

An increase in radiation resistance with decrease in ionic radius is observed for fourth-period elements only for the first three elements. For arsenic, the radius of both As^{3+} (0.047 nm) as well as As^{5+} (0.067 nm) is larger than for germanium (0.044 nm), however the tendency to a transition to one valency state to another is greater in arsenic, and this has a stronger effect on a rise in ROS than the relatively small increase in ionic radius.

For glasses containing fifth-period elements ROS increases by a factor of 3.5 when SrO ($4\ d^0$) is replaced by ZrO_2 ($4d^2$) and Nb_2O_5 ($4d^3$). This is related to the much smaller energy of the 4d-orbital in Zr and Nb atoms compared with the Sr atom, primarily, and to the reduction in the ionic radius from Sr to Nb, in the second place. Filling of the 4d-orbital, completed at the Cd atom, leads to rise in the radius and a reduction in ROS. Beginning with cadmium, we again observed a decrease in radius, which is accompanied by a strong increase in ROS. As we move from Sn (R = 0.069 nm) to Sb (R = 0.09 nm), the ROS decreases somewhat, but proves to be considerably above the ROS of indium glass, since antimony is more prone to a valency change than is indium.

Glass whose composition includes sixth-period elements (Ba, La, and Pb) are also governed by this rule. Their stability in general is low, since the radii and polarizability of these elements is quite high. Lanthanum glass proves to be most resistant, which is due to the smaller radius, increase in charge, and thus, to the appreciable drop in polarizability.

The study [17] dealt with silicate glass containing 15 mole percent K_2O and 15 mole percent BaO, SrO, CaO, MgO, or BeO. The 450 nm absorption band (2.8 ev) is somewhat shifted toward the long-wave region of the spectrum as the change is made from magnesium to barium. Barium glass violates this correlation.

A comparison of individual characteristics of variable elements enables us to derive a certain dependence of the radiation-optical stability of glass on electronegativity (EN), ionic radius, polarizability, oxidation-reduction capacity, acidity, or basicity of an oxide and the tendency to vitrification:

1) a general trend of a decrease in ROS with a decrease in the EN of the introduced ion is observed;

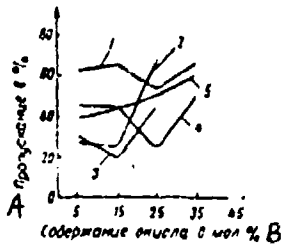

Fig. 6. Dependence of radiation-optical stability of glass in the system SiO_2-Na_2O-RO on the concentration of the RO component being varied

1 -- CdO
2 -- CaO
3 -- BaO
4 -- SrO
5 -- ZnO

KEY: A -- Transmission in %
B -- Content of oxide in mole %

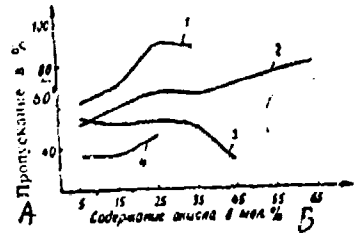

Fig. 7. Dependence of radiation-optical stability of glass in the system SiO_2-Na_2O-RO_x on the concentration of the following component being varied

1 -- SnO_2
2 -- GeO_2
3 -- PbO
4 -- ZrO_2

KEY: A -- Transmission in %
B -- Content of oxide in mole %

2) adding oxides of the elements of the main subgroups leads to a smaller ROS;

3) the more strongly the principal properties of the oxide are pronounced, the lower is their ROS values;

4) ROS decreases with increase in the polarizability of ions of the main subgroups;

5) adding elements of secondary subgroups as a rule promotes a higher glass ROS value;

6) elements capable of a facile transition to another valency under otherwise equal conditions (EN and ionic radius) increase the ROS;

7) for the same principal quantum number, a rise in ROS increases in concert with a decrease in ionic radius; and

8) the ROS of a glass is a periodic function of the charge on the nucleus of the element being varied.

The ROS of glasses depend heavily on the molar proportion of the components being varied. For example, when the content of barium in a

glass of the system SiO_2-Na_2O-BaO is increased by reducing the molar percentage of silicon dioxide, the ROS initially drops, but then rises steeply. The minimum ROS corresponds to roughly 10-15 mole percent BaO (Fig. 6). Interestingly, a content of 10-15 mole percent in glass is the threshold beyond which a sharp change in all kinds of properties of the glass sets in -- electroconductivity, magnetic properties, and so on. The nature of this phenomenon is not wholly clear and requires special investigation.

A similar pattern is observed with variation in the CaO content in glass -- a sharp drop in light transmission for a concentration of 10-15 mole percent and an increase in light transmission for 25 mole percent (cf. Fig. 6). Nearly all glasses studied containing group 2 elements have a minimum ROS at certain concentrations. An exception is represented by glasses containing zinc oxide as the component being varied.

The effect of concentration on the radiation-optical stability of glasses containing certain oxides of group IV and V elements as the component being varied are shown in Figs. 7 and 8.

3. Borate Glasses

Obviously, as B_2O_3 is introduced into a glass composition instead of SiO_2 new chemical bonds are induced. The probability that color centers typical of silicate glass of the initial composition will form decreases. The absorption spectrum loses its well-defined structure [9].

The absorption spectrum of irradiated sodium-silicate glass (initial composition $Na_2O \cdot 3SiO_2$), represented by curve 1 in Fig. 9, consists of three absorption bands with maxima corresponding to the wavelength 320, 450, and 600 nm (3.9, 2.8, and 2.1 ev). The spectral absorption curve (curve 2) corresponds to a glass with the other extreme composition $Na_2O \cdot 3B_2O_3$.

In terms of the effects on an increase in optical density of glasses with the composition $Al_2O_3 \cdot 2.5B_2O_3 \cdot 1.5MeO$ when irradiated, Me^{2+} cations lie in the series Ba-Sr-Ca-Mg (Fig. 10 a), and the Me^+ cations in glasses with the composition $Al_2O_3 \cdot 2.5B_2O_3 \cdot 1.5Me_2O$ formed the series K-Na-Li (Fig. 10 b) [18].

Bishay [18] noted that glasses with the composition $Al_2O_3 \cdot 4.5B_2O_3 \cdot R_2O$, fused in a reducing medium, have prior to irradiation a much higher transmission in the ultraviolet region and glasses fused under normal conditions. It was also noted that the absorption band with wavelength 250 nm (5 ev) is possibly associated with oxygen vacancies, since it is very strongly pronounced in glasses fused in reducing conditions.

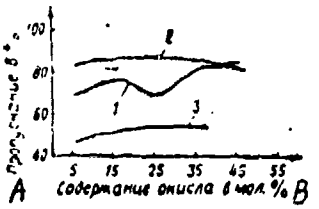

Fig. 8. Dependence of radiation-optical stability of a glass in the system SiO_2-Na_2O-R_2O_x as a function of the concentration of the R_2O_x component being varied

1 -- Nb_2O_5

2 -- Sb_2O_3

3 -- Ta_2O_5

KEY: A -- Transmission in %
B -- Content of oxide in mole %

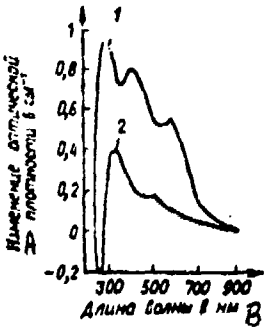

Fig. 9. Spectral absorption of glasses (radiation dose $5 \cdot 10^6$ r)

1 -- $Na_2O_3 \cdot 3SiO_2$

2 -- $Na_2O \cdot 3B_2O_3$

KEY: A -- Change in optical density in cm^{-1}
B -- Wavelength in nm

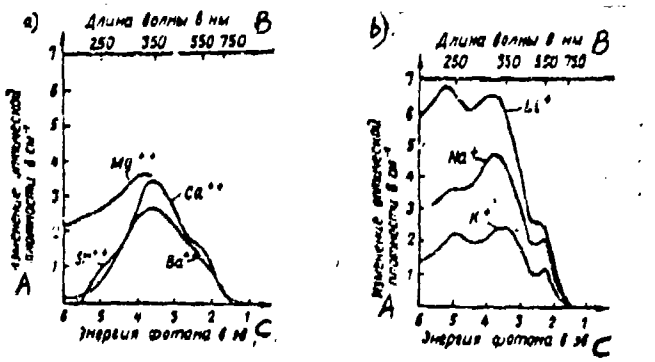

Fig. 10. Effect on induced absorption at a dose of $1.2 \cdot 10^7$ r by the following replacement

a -- Ca^{2+} replaced by Mg^{2+}, Sr^{2+} or Ba^{2+}

b -- Li^+ replaced by Na^+ or K^+

KEY: A -- Change in optical density in cm^{-1}
B -- Wavelength in nm
C -- Photon energy in ev

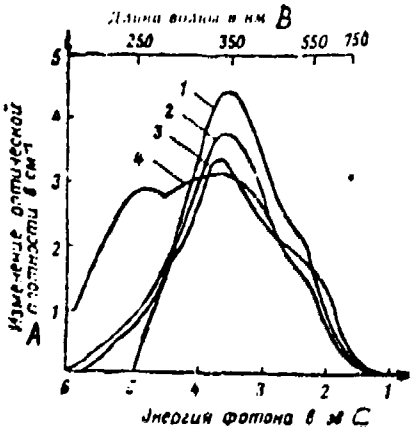

Fig. 11. Effect of replacing CaO with oxides on the radiation stability of a glass (radiation dose $1.15 \cdot 10^7$ r) of different compositions, in mole %

1 — $10Al_2O_3 \cdot 25B_2O_3 \cdot 0.75CaO$

2 — $10Al_2O_3 \cdot 25B_2O_3 \cdot 1.25CaO$

3 — $10Al_2O_3 \cdot 25B_2O_3 \cdot 1.75CaO$

4 — $10Al_2O_3 \cdot 25B_2O_3 \cdot 2.26CaO$

KEY: A — Change in optical density in cm^{-1}
B — Wavelength in nm
C — Photon energy in ev

A study [18] was made of the effect that CaO content has on the intensity of glass darkening. The spectrum (Fig. 11) has three absorption bands with maxima 550, 350, and 250 nm (2.3, 3.5, and 5 ev). The intensity of the 550 nm band (2.3 ev) decreases with increase in CaO content, reaches a minimum, and then increases again. The intensity of the 350 nm band (3.5 ev) gradually decreases with increase in CaO content. For a CaO content more than 1.75 mole, there is an abrupt change in the intensity of the 250 nm absorption band (5 ev). A decrease in the Al_2O_3 content in glass also leads to a weaker intensity of the 350 nm band (3.5 ev). The reduced intensity of this band as most of the boron passes from the three-coordinated to the four-coordinated state can be a consequence of the tendency of three-coordinated boron to capture electrons and to completely fill its shell.

Starting at glass 1 (cf Fig. 11) where all the boron is in threefold coordination, the intensity of the 250 nm band (5 ev) increases as far as glass 4, which has an adequate amount of free oxygen compared with four-coordinated aluminum and boron.

When lead oxide is replaced with titanium oxide in borate glass, two absorption bands appear: one at 825 nm (1.5 ev) (as in the case of lead borate glass) and the second at 1235 nm (1 ev). It is assumed that this is associated with the changed coordination of boron.

In borate glasses [19] with the following composition in percent by weight: 52 Bi_2O_3, 24 B_2O_3, 17 PbO, 4.5 SiO_2, and 2.4 Al_2O_3 receiving doses of 10^4 - 10^9 r, absorption bands are induced at 350 and 510 nm (3.5 and 2.4 ev). The appearance of the 360 nm band (3.4 ev) is attributed to a reduction reaction:

4. Germanate Glasses

Pure GeO_2 was studied in detail by Cohen [20, 21, 22]. When prepared in mildly reducing conditions, prior to irradiation this glass has an absorption band in the region of 245 nm (5.1 ev), which is due to the reduced germanium dioxide. Irradiation with gamma- or ultraviolet rays decolorizes this band and simultaneously shifts the edge of the absorption band toward the short-wavelength side. Germanate glasses are less affected by irradiation than their silicate analogs. When subject to ultraviolet rays, sodium germanate glass is only slightly colored even when it is exposed to high radiation doses. An increase in coloration is observed when calcium or aluminum is added to the glass [23]. The induced absorption spectrum of sodium-calcium germanate glass irradiated with a dose of 10^7 r consists of two bands in the 450 and 640 nm regions (2.8 and 1.9 ev).

5. Phosphate Glasses

Characteristic of irradiated phosphate glasses are two absorption bands: 525 and 425 nm (2.3 and 3.8 ev) [23-29]. Resolution of the absorption spectra of phosphate glass [30] made it possible to determine the maxima of three bands -- 540, 430, and 225 nm (2.3, 3.8, and 5.5 ev) in glass with the composition $Al_2O_3 \cdot 2CaO \cdot 3Na_2O \cdot 7P_2O_5$. An absorption band with its maximum at 520 nm (2.4 ev) is observed for glass with the composition $Al_2O_3 \cdot 2BaO \cdot 2K_2O \cdot 2P_2O_5$ [31]. When BaO in this glass is replaced with PbO, the 520 nm absorption band (2.4 ev) is weakened and a new band appears with its maximum near 750 nm (1.7 ev). A glass with the composition in mole percent: 40 $Al_2(PO_3)_3$, 17 $Ba(PO_3)_2$, 43 KPO_3, when irradiated, yields absorption bands with their maxima in the regions 375 and 530 nm (3.3 and 2.3 ev).

CHAPTER FOUR

RADIATION-OPTICAL STABILITY OF COMMERCIAL-COMPOSITION GLASSES

Investigation of radiation-optical ability of commercial-composition glasses is of great practical importance, determining their possible use in radiation fields.

1. Quartz Glass

Several studies deal with the effect radiation has on quartz glass [1-12]. However, most studies relate to optical properties of quartz glass when irradiated with x- and gamma-rays, much less often -- with neutrons, and there is very little data on the irradiation of quartz glasses with protons and electrons.

Exposure of crystalline and fused quartz to ionizing radiation produces additional absorption bands in the visible and ultraviolet spectral regions. The arrangement of these bands, from the data in the study [1] is given in Table 7, from what it is clear that C-, A-, or A_1- and A_2-bands can be initiated in crystalline quartz, depending on the nature of the sample.

Noteworthy are two facts: first of all, no B-bands ever are produced in crystalline quartz; secondly, absorption bands of quartz glass are wider than in crystalline quartz, which is accounted for [2] by the change in the interatomic Si-O distances. A similar point of view underlies the elaboration of the interstitial theory of glass structure, by which the distortion of the silicon-oxygen tetrahedron absorbed in crystalline quartz [3, 4] becomes so appreciable in glass that one can speak of interstitial oxygen ions [5].

The irradiation of quartz glass with fast neutrons, high-energy electrons (0.2-2 Mev), x-, and gamma-rays from a Co^{60} source produced identical band distribution [1]. High-energy electrons are extremely effective in forming ultraviolet absorption bands both in terms of the rate of their formation as well as the absorption coefficient, which depends on the energy of the bombarding particles [2].

TABLE 7. ABSORPTION BANDS IN CRYSTALLINE AND FUSED QUARTZ

Материал [1]	Энергия полосы в эв [2]	Длина волны в нм [3]	Обозначение полосы [4]
Кристаллический кварц: [5]			
природный [6]	2	620	A_1
	2,6—2,75	450—480	A_2
	5,9—5,6	210—220	C
синтетический [7]	2,3	540	A
	5,9—5,6	210—220	C
Кварцевое стекло [8]	2,3	540	A
	4,1	300	B_1
	5,6—5,2	220—240	B_2
	5,9—5,6	210—220	C

KEY: 1 -- Material
2 -- Band energy, in ev
3 -- Wavelength in nm
4 -- Band symbol
5 -- Crystalline quartz
6 -- natural
7 -- artificial
8 -- Quartz glass

The initiation of absorption bands is determined not only by the radiation acting on the glass, but also depends very strongly on the material's method of preparation and its purity. Quartz glasses can be divided into three groups by the induced absorption spectra [6]:

1) glasses that have three absorption groups after irradiation: 210-240, 300, 540 nm (5.9-5.2, 4.1, and 2.3 ev), that is, C-, B-, and A-bands;

2) glasses that have two absorption bands after irradiation with doses up to 10^8 r: 210-240 and 300 nm (5.9-5.2 and 4.1 ev), that is, C- and B-bands; and

3) glasses with a C-band in the 210-220 nm region (5.9-5.6 ev).

Absorption bands in quartz glass become wider up to a certain radiation dose, and then breakdown of the color centers during irradiation takes place. This is observed for the B_1-band [1], as well as for the A-band at doses of $5 \cdot 10^{16}$ neutrons/cm^2 [7]. Absorption bands are decolorized also upon light exposure (for example, resulting from flashes of a xenon lamp), and thermally [7-8]. And thermal and optical de-excitation first of all breaks down the 300 nm band (4.1 ev) and the remaining bands, much more slowly. When radiation-

resistant quartz glasses are irradiated, initially lightening is observed in the region of the B_2-band, while this effect is not detected in quartz glasses, which darken when irradiated [9]. Besides these bands, an absorption band (7.6 ev) is found for neutron irradiation of crystalline and fused quartz, which is not produced for other kinds of irradiation [9-11].

The intensity of the 450 nm absorption band (2.7 ev) detected in crystalline quartz [12] was found to be dependent on the amount of aluminum present [13]. A similar dependence was also found for the 540 nm band (2.3 ev) in fused quartz. The role of aluminum in the coloring of quartz is examined in several studies [15-19]; possible color centers associated with aluminum have been proposed. However, it is shown in the work [14] that variation in the lithium concentration present in quartz glass also affects absorption bands, as does variation in aluminum concentration.

The studies [20-21] indicate the relationship of color centers with structure of defects (oxygen vacancies). To illustrate, it is noted in [21] that coloring is observed mainly when glass produced in vacuum furnaces is irradiated; it was found that if glass not producing coloring in the visible spectral region when irradiated is treated under conditions promoting the formation of oxygen vacancies (at 1620° K in silicon vapor, and at 2270° K in air), this treatment leads to coloring after subsequent irradiation.

The above experimental data have received varying interpretations. We return to some of them in Section 3, but here we will examine the experimental data as such.

We systematically investigated the effect of gamma-rays, electrons, protons, and electrons in high vacuum on grade KI and KV quartz glasses.

Effect of gamma-rays

Irradiation of KI and KV glasses with gamma-rays shows that doses of 10^4 - 10^7 r, only KI glass changes its light transmission in the visible spectral region [22]. Fig. 12 shows the change in the integral light transmission of these glasses as a function of radiation dose. In the figure it is clear that KI glass, when irradiated with a dose 10^4 r, retains 87 percent of its light transmission, 40 percent -- for a dose 10^5 r, 2 percent -- at a dose 10^6 r, but at a dose of 10^7 r the specimen becomes opaque. The change in the light transmission of KV glass could not be recorded. However, as the invariability of light transmission is intrinsic to these glasses only in the visible spectral region.

At the same doses interesting alterations are observed in the ultraviolet spectral region for KV glass [22] (Fig. 13). At radiation doses of 10^4 and 10^5 r, two facts are striking. First of all, light transmission of glasses in this case remains unchanged not only in the visible spectral

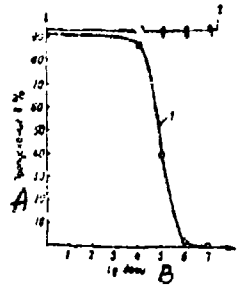

Fig. 12. Dependence of light transmission of quartz glasses (10 mm thick samples) on dose of gamma-ray irradiation
1 -- KI glass
2 -- KV glass
KEY: A -- Transmission in percent
B -- Lg dose

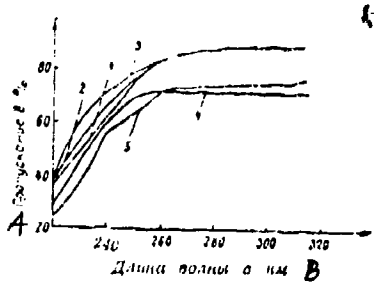

Fig. 13. Spectral light transmission of KV glass (5 mm thick samples) in the ultraviolet spectral region at different gamma-ray radiation doses
1 -- unirradiated glass
2 -- 10^4 r radiation dose
3 -- 10^5 r
4 -- 10^6 r
5 -- 10^7 r
KEY: A -- Transmission in percent
B -- Wavelength in nm

region, but also in the near ultraviolet region all the way up to 260 nm (4.8 ev); secondly, irradiation leads to increased light transmission in the range 220-260 nm (5.6-4.8 ev).

At a wavelength of 240 nm (5.2 ev), transmission of an irradiated specimen amounts to 63 percent, when irradiated with a dose of 10^4 r -- 66 percent, and when irradiated with a dose of 10^5 r -- 71 percent. Confirming that this difference is not the result of experimental error was a differential measurement of light transmission of irradiated specimens compared with unirradiated. A light transmission value of about 105 percent was obtained for a sample irradiated with a dose 104 r, and 110 percent for a sample irradiated with a dose of 10^5 r. The literature [9] includes data on the increase in light transmission in the 240 nm region (5.2 ev), for irradiation with a dose of 10^6 r. The author of [9] assumed that in the glass there exist hole color centers, which capture electrons freed when glass interacts with gamma-rays. The breakdown of the centers thereby accounts for the increased light transmission.

However, even at a dose 10^6 r, we did not observe this phenomenon, that is, electrons localized at hole centers. The presence of these centers is determined probably by impurities present in the glass. The fact that this effect was observed by us for doses smaller than those in the study [16] is evidently accounted for by the different purity of glasses used in the investigation.

Fig. 14. Dependence of additional optical density of KI glass on radiation dose with 4.8 Mev protons (depth of penetrations ~ 0.25 mm)
KEY: A -- Change in optical density in cm^{-1}
B -- Dose in protons/cm^2

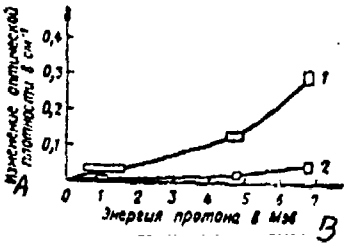

Fig. 15. Dependence of supplementary optical density of glass on proton energy for a radiation dose of 10^{15} protons/cm^2
1 -- KI glass
2 -- KV glass
KEY: A -- Change in optical density in cm^{-1}
B -- Proton energy in Mev

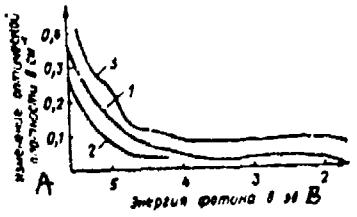

Fig. 16. Supplementary optical density of KV glass when irradiated with 4.8 Mev protons (depth of penetration ~ 0.25 mm)
1 and 3 -- a dose of 10^{16} protons/cm^2
2 -- 10^{15} protons/cm^2
KEY: A -- Change in optical density in cm^{-1}
B -- Proton energy in ev

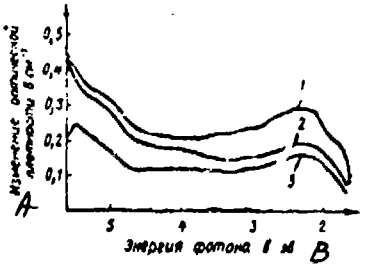

Fig. 17. Supplementary optical density of KI glass when irradiated with protons
1 -- at a dose of 10^{15} protons/cm^2; 6.8 Mev energy
2 -- 10^{16} protons/cm^2, 4.8 Mev
3 -- 10^{14} protons/cm^2, 4.8 Mev
KEY: A -- Change in optical density in cm^{-1}
B -- Proton energy in ev

Effect of protons

Irrediating quartz glasses with high-energy protons shows a slight change in the light transmission of KV glass for a radiation dose up to 10^{16} protons/cm^2. KI glass becomes colored even at doses of 10^{13} protons/cm^2 [22]. The fact that KV glass does not become darkened for gamma-irradiation and darkens when irradiated with protons is accounted for by the fact in proton irradiation in a cyclotron the absorbed dose for an exposure dose of 10^{14} protons/cm^2 was estimated by us to be $1.4 \cdot 10^8$ rad, while when irradiation with gamma-rays at a dose of 10^7 r was used, the absorbed dose was $8.8 \cdot 10^6$ rad. The radiation dose dependence of change in optical density proved to be linear within the limits of measurement error (Fig. 14). Here we must bear in mind that the change in optical density is determined only by the absorbing layer.

Irradiation of specimens with different thicknesses using identical doses shows that within the limits of measurement error induced absorption remains constant. The proton energy dependence of optical density was investigated with KI glass for a dose of 10^{15} protons/cm^2 (Fig. 15). This function is not linear. Optical density increases at high energies more rapidly than at small energies, which is evidently caused by the increase in path length and, therefore, in the thickness of the coloring layer.

Spectral curves of the increment in optical density of KV and KI glasses at different proton radiation doses and energies are given in Figs. 16 and 17. The specific details of coloring upon proton irradiation include the absence of the 300 nm (4.1 ev) B_1-band and the appearance of A- and C-bands. In only one case -- for the irradiation of KV glass with a dose up to 10^{14} protons/cm^2 -- was absorption corresponding to the B_1-band detected in the region of 300-320 nm (4.1-3.9 ev).

Effect of electrons

High-energy electron irradiation of quartz glasses shows that at doses to 10^6 r inclusively, only KI glass shows a change in light transmission in the visible spectral region. For this glass the integral induced optical absorption within the limits of measurement error is independent of the kind of irradiation (with protons, electrons, or gamma-rays) and is determined to the first approximation only by the absorbed radiation dose (Fig. 18).

The spectral increment in the optical density of KI and KV glasses is shown in Fig. 19. All three groups of bands familiar in the literature are present in the absorption spectrum of KI glass. Only two band groups are observed in the absorption spectrum of KV glass: B and C.

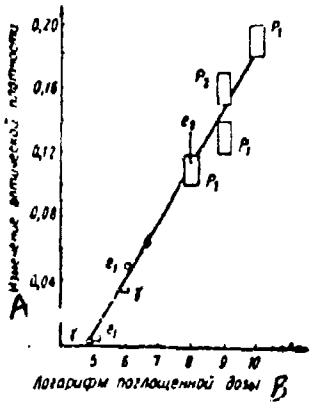

Fig. 18. Dependence of change in optical density of KI glasses as a function of absorbed does (in rad) of radiation of different kinds and energy (0.25 mm thick samples)
-- gamma-rays of Co^{60}
e_1 -- 10 Mev electrons
e_2 -- 0.2 Mev electrons
p_1 -- 4.8 Mev protons
p_2 -- 6.8 Mev protons
KEY: A -- Change in optical density
B -- Logarithm of absorbed dose

Irradiation with protons and electrons in high vacuum

Irradiation of quartz glass with a mixed beam of protons and electrons at an integral dose of 10^{16} particles/cm^2 and with 180-185 kev particle energy under high-vacuum conditions ($1.3 \cdot 10^{-6} - 6.5 \cdot 10^{-7}$ n/m^2) showed reduced light transmission. Composite data on the effect that electron, proton, and combined irradiation has on the light transmission of glasses are given in Table 8, from which we see that protons with these energies do not cause coloring in quartz glasses. This situation is examined more closely in Section 3 of this chapter.

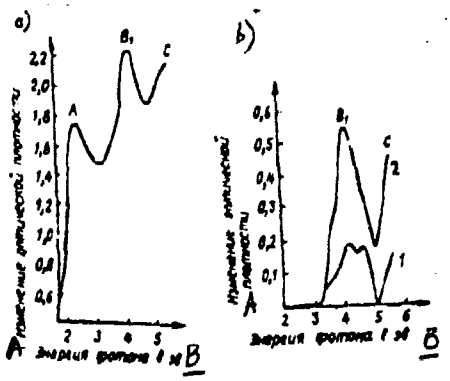

Fig. 19. Change in optical density of quartz glasses (5 mm thick samples) when irradiated with electrons at energy up to 10 Mev

a -- KI glass, 10^6 r dose

b -- KV glass:

1 -- 10^5 r dose

2 -- 10^6 r dose

KEY: A -- Change in optical density

B -- Photon energy in ev

TABLE 8 CHANGE IN LIGHT TRANSMISSION OF QUARTZ GLASSES WHEN IRRADIATED WITH PROTONS AND ELECTRONS

1 Марка стекла	2 Интегральное светопропускание стекла в %			
	3 исходного	4 облученного протонами	5 облученного электронами	6 совместное облучение
7 КВ	92	92	87	90
8 КИ	92	92	69	67

KEY: 1 -- Glass grade

2 -- Integral light transmission of glass in percent

3 -- initial

4 -- irradiated with protons

5 -- irradiated with electrons

6 -- combined irradiation

7 -- KV

8 -- KI

2. Silicate Glasses

Colorless glasses

Most commercial glasses suffer a large drop in light transmission when irradiated with gamma-rays, neutrons, and alpha- and beta-particles [23-25]. Commercial glasses as a rule readily transmit gamma-rays and have neutrons. Exposure to this kind of radiation causes coloring of a glass throughout its thickness. The depth of alpha-particle penetration in the glass is very slight, therefore coloring of glass occurs to a shallow depth ($\sim$ 0.04 mm). Data we secured on the change in integral light transmission upon exposure of certain commercial-composition glasses to gamma-rays are given in Table 9.

From Table 9 we see that the concentration of color centers reaches a saturation level for all glasses studied at a radiation dose of 10^8 r. The optical absorption spectra of irradiated commercial-composition glasses had no well-defined bands; reduced light transmission is observed throughout the full wavelength range.

Colored signaling glasses

Most color glasses modify their optical properties when irradiated. Induced absorption spectra of color glasses do not have well-defined absorption bands. Just as in colorless glasses, there is a drop in light transmission throughout the wavelength range. Table 10 gives the light characteristics of "copper ruby" type red glasses before and after irradiation with a dose of 10^6 r.

From Table 10 we see that though the integral light transmission of glasses of this type drops off somewhat, color characteristics of the glasses remain practically unchanged.

Table 11 gives data on the change in light transmission of certain color glasses produced by all industry.

Data on the radiation-optical stability of light filters produced by foreign companies are given in the study [26].

3. Effect of Thermal Prehistory of Glass on Induced Optical Absorption

Above we stated that radiation-optical stability of a glass is determined both by glass chemical composition and structure. The thermal prehistory of the glass can affect a number of factors responsible for the intensity of induced optical absorption: first of all, the glassmaking conditions can be reflected in the valency state of certain elements incorporated in the glass, and also on its chemical composition; secondly, the regime of annealing or heat treatment of finished glass can affect the

TABLE 9. CHANGE IN LIGHT TRANSMISSION OF GLASSES AFTER IRRADIATION

Марка стекла 1	Интегральное светопропускание 2							
	до облучения 3	после облучения дозами в р 4						
		10^4	10^5	10^6	10^7	10^8	10^9	$2 \cdot 10^9$
К-8	92	90	80	37	10	7	6	6
5 ВВ	89	87	80	43	18	15	15	15
6 ЛК-5	92	91	87	65	44	37	37	37
7 13В	88	87	84	78	65	—	—	—

KEY: 1 — Glass grade
2 — Integral light transmission
3 — prior to irradiation
4 — after irradiation with listed doses in r
5 — VV
6 — LK-5
7 — 13V

TABLE 10. EFFECT OF GAMMA-IRRADIATION ON COLOR CHARACTERISTICS OF GLASSES

Стекло 1	Толщина стекла в мм 2	Длина волны λ в нм 3	Интегральное светопропускание 4	Цветовые координаты 5		Насыщенность цвета в % 6
				x	y	
7 Медный рубин № 13 без наводки; завод «Красный луч»:						
8 до облучения	5	620	2,2	0,695	0,305	100
9 после облучения . . .	5	620	0,9	0,700	0,295	100
10 Медный рубин СКСГ; Чертинский завод:						
8 до облучения	5,1	638	2,6	0,715	0,284	100
9 после облучения . . .	5,1	638	0,8	0,705	0,285	100

KEY: 1 — Glass
2 — Thickness of glass in mm
3 — Wavelength in nm
4 — Integral light transmission
5 — Correct coordinates
6 — Color saturation in percent
7 — No 13 copper ruby without finishing: Krasnyy Luch Plant
8 — prior to irradiation
9 — after irradiation
10 — SKSG copper ruby; Chertinsk Plant

TABLE 11. EFFECT OF GAMMA-IRRADIATION ON LIGHT TRANSMISSION OF COLORED GLASSES

1 Стекло	2 Интегральное светопропускание					
	3 до об-лучения	4 после облучения дозами в р				
		10^6	10^8	10^7	10^8	$5\cdot10^{10}$
5 Селеновый рубин К3/2	2,15	2,6	2	3,8	5,7	0
6 Селеновый рубин К4/2	2,8	4,6	4,6	5	1,7	0,3
7 Селеновый рубин КС1	4,5	4,2	3,7	—	5,7	0
8 Медный рубин СКСГ	2,2	2,2	1,1	—	0,6	0
9 Оранжевое без наводки ОС-6	81,8	78,8	53,6	—	22,5	0
10 Оранжевое после наводки ОС-6	37	46,7	37,8	—	9	0
12 Зеленое 5П3	18,6	21,3	17,9	13,6	9,6	0
13 Зеленое 18	13,8	15,7	13,1	12,5	7,9	1,4
14 Кобальтовое 17	3,46	0,8	1	1,1	1,1	0
15 Опаловое 14	47,5	39,6	11,2	—	0	0
16 Опаловое ОПЛС	35,6	34,6	9	—	0	0

KEY: 1 -- Glass
2 -- Integral light transmission
3 -- prior to irradiation
4 -- after irradiation with listed doses in r
5 -- K3/2 selenium ruby
6 -- K4/2 selenium ruby
7 -- KS1 selenium ruby
8 -- SKST copper ruby
9 -- OS-6 orange ruby without finishing
10 -- Orange ruby after finishing
11 -- OS-6
12 -- 5P3 green
13 -- Green 18
14 -- Cobalt 17
15 -- Opal 14
16 -- Opal OPLS

concentration of defects capable of capturing electrons or holes, which must also be reflected in the number of color centers following irradiation; and thirdly, the conditions in which the glasses heat-treated can promote diffusion from or into the glass of an element capable of affecting radiation-optical stability.

As examples confirming the validity of the first assertion, we can cite the effect that glassmaking conditions have on the radiation-optical stability of a glass containing cerium ion additives. We know well that adding cerium to a glass composition reduces the absorption of irradiated glasses in the visible spectral region [27-29]. Here it is not simply the concentration of the cerium ions that is critical, but also the valency state in which the ions exist, and this depends heavily on the glassmaking conditions. The question of the effect that heat treatment conditions

have on the radiation-optical stability of a glass has been studied much less than the effect of glassmaking conditions, therefore we will dwell on it more closely.

Radiation-optical stability of annealed and hardened glasses

Studies [30-31] were made of the radiation-optical stability (ROS) of the glasses K-8, K-108, and K-208, and also of the GP rolled glass produced by the Gusev Plant imeni F. E. Dzerzhinskiy.

K-108 and K-208 glasses correspond to K-8 glass in composition, but to increase the ROS cerium dioxide is added to their compositions, and the cerium ion concentration in K-208 glass is much higher than in K-108 glass.

The temperature at which extended heat treatment of a glass was conducted was determined by the upper and lower bounds of the annealing zones, namely 830 and 860° K. The heat treatment period was 25, 50, 100, and 200 hours. Additionally, these glasses were cooled in air under natural-convection conditions and with liquid hardening [30]. The extent of hardening for air cooling was 0.5 N/cm, and 2.2 N/cm, after cooling in liquid.

The initial 3 mm thick specimens and the 3 mm thick specimens subject to heat treatment were irradiated with gamma-rays from a Co^{60} source. The exposure radiation dose was 10^7 r. Samples of K-8 and GP glasses after irradiated acquired an intense brown color; the color of the K-108 glass varied only slight; K-208 glass remained virtually unchanged in color.

The spectral absorption curves of irradiated GP and K-8 glasses after heat treatment for different regimes are shown in Figs. 20 and 21. The pattern of the spectral absorption curves given in these figures is characterized by the absence of well-defined absorption bands in the visible spectral region, intrinsic to most complex-composition glasses. As the exposure time is extended at elevated temperatures, the optical density of irradiated glasses drops off throughout the wavelength range and increases with the extent of hardening. Table 12 gives data characterizing the change in the integral light transmission of irradiated glasses as a function of irradiation preceding heat treatment.

As follows from Table 12, integral light transmission of irradiated glasses not containing cerium ions (K-8 and GP) depends to a large extent on their thermal prehistory. Extended exposure of a glass at the annealing temperature leads to some increase in light transmission following gamma-irradiation. Hardened glasses, in contrast, are characterized by reduced light transmission.

The increase in ROS of glasses following extended annealing is due to the ordering of the glass structure resulting from heat treatment. Evidently, during long-term exposure of glasses at the annealing temperature

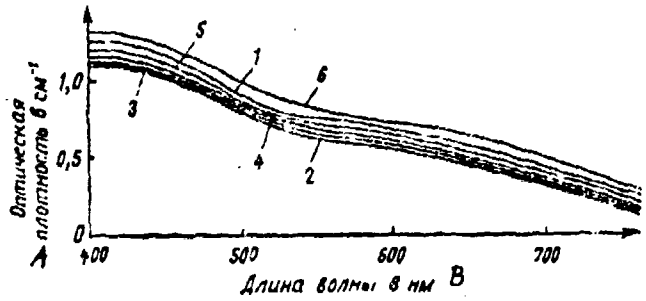

Fig. 20. Effect of heat treatment on induced optical absorption of GP glass

1 -- initial sample
2 -- heat treatment at 830° K, 50 hours
3 -- as above, 25 hours
4 -- heat treatment at 660° K, 200 hours
5 -- as above, 25, 50, and 100 hours
6 -- hardened sample (2.2 N/cm)

KEY: A -- Optical density in cm^{-1}
B -- Wavelength in nm

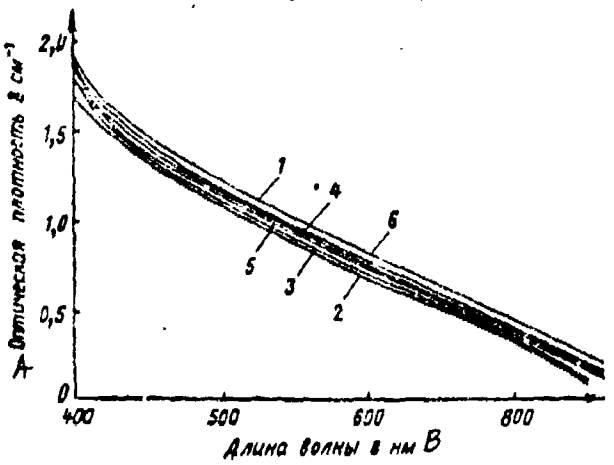

Fig. 21. Effect of heat treatment on induced optical absorption of K-8 glass

1 -- initial sample
2 -- heat treatment at 770° K, 50 hours
3 -- as above, 25 hours
4 -- heat treatment at 660° K, 25 and 50 hours
5 -- as above, 100 and 200 hours
6 -- hardened sample (2.2 N/cm)

KEY: A -- Optical density in cm^{-1}
B -- Wavelength in nm

TABLE 12. EFFECT OF GLASS HEAT TREATMENT ON GLASS ROS [30]

Образцы 1	Интегральное светопропускание в % стекла 2			
	К-8	ГП 3	К-108	К-208
4 Исходные	10	17	78	90
5 Выдержанные при 830° К:				
6 25 ч	13	23	80	90
7 50 »	14	24	80	90
8 Закаленные:				
9 0,5 Н/см	9	16	76	90
10 2,2 »	7	14	75	90

KEY: 1 -- Samples
2 -- Integral light transmission in percent of listed glass
3 -- GP glass
4 -- Initial
5 -- Exposed at 830° K
6 -- 25 hours
7 -- 50 hours
8 -- Hardened
9 -- 0.5 N/cm
10 -- 2.2 N/cm

the number of structure defects of the type of interstitial Me^+ and O^{2-} ions capable of localizing free electrons and hole formed upon irradiation is reduced. But upon hardening, the number of these defects in glasses increases, which then leads to their reduced ROS.

The spectral absorption curves of K-108 and K-208 glasses after different heat treatment conditions are virtually superimposed on each other, as to be expected. This is because the ROS of glasses with these compositions is determined by cerium ions, whose stabilizing action prevails over effects occurring in the structure of glass resulting from its heat treatment. Thus, this study established a relationship between thermal prehistory and the radiation-optical stability of glasses.

Effect of heat treatment conditions on radiation-optical stability of quartz glass

Yokota [12] showed that the heat treatment of glasses fused in the flame of an oxygen-hydrogen torch substantially affects their ROS. Thus, the treatment of glass in silicon vapor at 1620° K causes coloration to appear in the visible spectral region upon subsequent gamma-irradiation with doses that before treatment did not cause an increment in optical density. This was related by Yokota to the increased number of oxygen vacancies in glass after treatment, which also accounts for the reduced ROS. This explanation gave us doubts, since it is difficult to assume

that during melting glass is produced with so few a number of vacancy type point defects that coloring does not occur even at radiation doses of 10^7 - 10^8 r. We also cannot presume that treatment of glass in the vapor of high-purity silicon contaminates glass with metal cations, whose presence is responsible for the coloring of glass in the visible spectral region.

More probable appears the assumption that agents promoting the formation of color centers and increasing the ROS of a glass compared with glass obtained by the vacuum-compression method are present in quartz glass melted in the flame of a hydrogen torch. Considering the different technologies, it is natural to assume that the increased ROS of a glass melted in the flame of a hydrogen torch is accounted for by the presence in the glass of hydroxyl groups, as was advanced by Cohen [32], and also by Botvinkin and Zaporozhskiy [33]. Without denying the role of hydroxyl groups, nonetheless we do assume that a major contribution to the rise in ROS of quartz glass is made by free hydrogen, whose role from our point of view is more appreciable than that of hydroxyl groups. During heat treatment free hydrogen can diffuse from the glass, which accounts, as we see it, for the drop in ROS observed by Yokota.

To verify these statements, a series of experiments were conducted. First of all we thought it necessary to conduct heat treatment at much lower temperatures than Yokota used [12], since hydrogen quite readily diffuses through quartz glass at even lower temperatures than his. Therefore we selected temperature of about 1100° K*. Samples of KV quartz glass were heat-treated for different periods of time (up to 15-20 hours). The 2700 nm absorption band was monitored; no changes in it were recorded. The ROS was checked in two ways:

1) samples were cut from each piece of glass; each sample was heat-treated for a specific time and then irradiated with gamma-rays at a dose of 10^7, using a Co^{60} source; and

2) to cancel out the effect of data scatter from sample to sample, the kinetics of ROS change were observed as a function of the heat treatment time for the same specimens in sequence, for every 5 hours of heat treatment. In this case each sample underwent gamma-irradiation a number of times, and coloring was removed by subsequent heat treatment.

Both methods yield similar results in principle. Optical density was measured before and after irradiation with gamma-rays using a SV-50 spectrophotometer. The increment in optical density was reconverted to a thickness of 1 cm. Though the probability of the increase in the number

---

* Similar treatment conditions are described in the studies [35, 36].

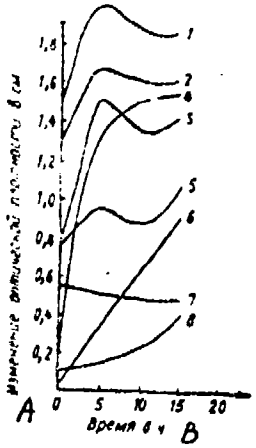

Fig. 22. Effect of heat treatment on supplementary optical absorption of quartz glasses

1 -- KV glass, 1.2 mm thick sample, 250 nm band (5.6 ev)
2 -- as above, 240 nm band (5.1 ev)
3 -- 300 nm band (4.1 ev)
4 -- 540 nm band (2.3 ev)
5 -- KV glass, 12 mm sample thickness, 300 nm band (4.1 ev)
6 -- as above, 540 nm band (2.3 ev)
7 -- KI glass, 540 mm band (2.3 ev)
8 -- KI glass, previously treated in hydrogen atmosphere

KEY: A -- Change in optical density in cm^{-1}
B -- Time in hours

of oxygen vacancy type defects resulted from each treatment at 1100° K is negligibly small, still for greater experimental rigor, KI glass also underwent heat treatment simultaneously with KV glass, since if it is assumed that oxygen volatilizes from the glass, then it must appear also when a glass prepared by the vacuum-compression method is heat treated.

The results of this study [34] are shown in Fig. 22. Heat treatment leads to a change in the increment in optical density after irradiation for all absorption bands observed in quartz glass: 220, 240, 300, and 340 nm (5.6, 5.1, 4.1, and 2.3 ev) (corresponding to curves 1-4). The fact that heat treatment alters all absorption bands is in agreement with the assertion that free oxygen volatilizes from the glass, for its presence in the glass can reduce the concentration of both electron and hole color centers. This is also confirmed by the fact that the increment in optical density calculated per 1 cm of thickness is much more effective after the heat treatment of thin samples than of thick, which can be seen by comparing curves 3 and 5, and also curves 4 and 6. Curves 3 and 4 were plotted after the results of irradiating and heat treating 1.2 mm samples were recalculated, and curves 5 and 6 — for a 12 mm sample thickness.

Heat treatment of KI glass, as to be expected, does not cause appreciable changes in its ROS (curve 7).

The extremal pattern of the change in intensity of supplementary of absorption in the regions 220, 240, and 300 nm (5.6, 5.1, and 4.1 ev) shows that besides hydrogen diffusing from glass, thus lowering its ROS, some other processes also take place, whose nature at present is unclear.

If the mechanism of decrease in ROS of quartz glass after heat treatment is properly understood, then we should have the opposite effect: treatment of quartz glass in hydrogen atmosphere must lead to a rise in its radiation-optical stability. This is confirmed by studies of Soviet [34] as well as foreign authors [35, 36]. Results of ROS change after a glass has been treated in hydrogen atmosphere are shown in Table 13.

From Table 13 it follows that the most intense rise in radiation-optical stability is observed in the visible spectral region, and its dependence on the treatment temperature is more strongly pronounced than its time dependence. This indicates that the process of the ROS increase is diffusional in nature. Naturally, treatment of a glass in hydrogen proved to be more effective at elevated pressures. Actually, glasses treated with hydrogen at high pressure [36] revealed resistance to certain kinds of irradiation. In some glasses paramagnetic effects and induced optical density associated with the irradiation of glasses are diminished by a factor of 20. Irradiation increases the concentration of hydroxyl ions, which is confirmed by the greater absorption in the infrared region (2700 nm) and indicates that treated quartz glass contains free hydrogen.

Hydrogen treatment of a glass was conducted as follows: the glass was heated to 1170° K in hydrogen atmosphere at 300 Mn [meganewtons]/m^2. Then with pressure held unchanged, the glass was cooled down to room temperature, and the pressure was decreased to normal. The resulting glass contained 8 mole percent of dissolved hydrogen. When glasses composed of SiO_2 and B_2O_3 underwent this treatment after being irradiated with neutrons or gamma-rays, the electron paramagnetic resonance signal and absorption in the ultraviolet and visible spectral regions ordinarily observed in glasses were markedly diminished.

TABLE 13. EFFECT OF TREATMENT IN HYDROGEN ATMOSPHERE ON COLORING OF KI GLASS WHEN GAMMA-IRRADIATED WITH A DOSE OF 10^6 r (2.5 mm THICK SAMPLES)

1 Режим обработки	2 Изменение оптической плотности стекла при длине волны в нм							
	210		240		300		550	
	3 необработанного	4 обработанного	3 необработанного	4 обработанного	3 необработанного	4 обработанного	3 необработанного	4 обработанного
5 2,5 ч при 1170 °K	0,92	1	0,48	0,4	0,39	0,16	0,29	0,05
6 2,5 ч при 870 °K	0,96	0,96	0,52	0,4	0,46	0,32	0,35	0,16
7 5 ч при 870 °K	0,92	1	0,48	0,42	0,39	0,28	0,29	0,18

KEY: 1 -- Treatment regime
2 -- Change in optical density of glass at listed wavelength, in nm
3 -- untreated
4 -- treated
5 -- 2.5 hours at 1170° K
6 -- 2.5 hours at 870° K
7 -- 5 hours at 870° K

As a result of the irradiation of quartz glasses with neutrons at a dose of $1.2 \cdot 10^{18}$ neutrons/cm^2, transmission was lowered down to 30 percent at 300 nm (4.1 ev), 2 percent at 265 nm (4.7 ev), and 1 percent at 240 nm (5.2 ev), while glass treated by the above-described method and containing 2 percent hydrogen had, following irradiation, about 80 percent transmission at 300 nm (4.1 ev), 55 percent at 265 nm (4.7 ev), and 35 percent at 240 nm (5.2 ev).

In order to eliminate the possible reaction between hydrogen and SiO_2, with hydroxyl groups forming, the effect of preliminary treatment of quartz glasses in hydrogen on the 2700 nm band in the infrared absorption spectrum was examined before and after the glasses were irradiated with neutrons. The irradiation of glasses containing hydrogen causes a reaction of hydrogen with SiO_2 and an increase in the formation of OH groups. We can conclude that the increase in the formation of hydroxyl during the irradiation period is directly proportional to the drop in the concentration of color centers formed [36].

Similar results were obtained in our own experiments [34]: glass samples were treated at 1120° K and at increased hydrogen pressure. As a result, we will be able to raise the radiation-optical stability of KI quartz glass up to doses of 10^7 r. The change in optical density in

the visible spectral region for a radiation dose of 10^7 r did not exceed 0.02 (7 mm thick samples), while the initial glass with this thickness virtually lost its transparency after irradiation. The rise in ROS was determined by diffusion parameters and increased with rise in temperature, exposure, and hydrogen pressure. However, we must remember that raising the treatment temperature to 1370° K can cause hydroxyl groups to form in the glass, which was detected in the 2700 nm absorption band. An increase in ROS was also observed in those cases when the 2700 nm band was not manifested.

The question arises: is the rise in ROS associated with the fact that during heat treatment the penetration of hydrogen into glass causes some structural or chemical changes, or that free hydrogen has an effect during the irradiation process? In the first case, the rise in ROS must be irreversible, and in the second -- reversible. Heat treatment in the air at 1120° K of KI quartz glass previously enriched with hydrogen showed that even after 15 hours of annealing the increment in optical density in the 540 nm region (2.3 ev) (for gamma-irradiation at a dose of 10^5 r: cf. Fig. 22, curve 8) reaches a value corresponding to that of the KI glass.

These studies show that the quartz glass ROS is determined by the presence in it of free hydrogen, which enters the glass either during melting or via diffusion. However, these two processes of enriching glass with hydrogen differ by the fact that in the first case hydroxyl groups responsible for absorption in the 2700 nm region are formed, and OH groups do not form in the second case.

The increment in the ROS of quartz glass can also be brought about by treating it in water vapor at temperatures of 575-920° K and elevated pressure. Here quartz glass is crystallized to a depth of several millimeters. To be able to measure transmission, the cristobalite crust must be removed. After gamma-irradiation with a dose of 10^6 r, an absorption band appeared in treated specimens in the region 3200-3500 nm; absorption in the 2700 nm region was absent. As we can see from Table 14, a rise in the treatment temperature increased the radiation resistance of the glass.

The appearance of hydroxyl groups bringing about absorption in the 3200-3500 nm region shows that water molecules break down and, therefore, in addition to hydroxyl groups free hydrogen can also exist in the glass, and its concentration is proportional to the number of hydroxyl groups present. A similar relationship between hydrogen and hydroxyl groups can also exist when glass is melted in the flame of an oxygen-hydrogen torch. Therefore, it is not precluded that the proportionality of ROS and the hydroxyl group concentration is brought about by the proportional content of hydroxyl groups and hydrogen.

Experiments showed that an increase in glass ROS when hydrogen is diffused into it takes place also when hydroxyl groups are not formed.

TABLE 14. EFFECT OF TREATMENT TEMPERATURE IN WATER VAPOR ON OPTICAL ABSORPTION OF QUARTZ GLASS WHEN GAMMA-IRRADIATED WITH A DOSE OF 10^7 r

1 Температура обработки в °К	2 Изменение оптической плотности в $см^{-1}$ при длине волны в нм			
	210	245	300	550
920	0,5	0,25	0,20	0,08
575	0,8	0,58	0,58	0,27

KEY: 1 -- Treatment temperature in ° K
2 -- Change in optical density in cm^{-1} at listed wavelength, in nm

But it has not been possible to demonstrate or refute the role of hydroxyl groups in enhancing the radiation-optical stability of quartz glass, at present. As for the role of free hydrogen in raising the ROS of glass, it becomes evident not only when glass is heated in hydrogen atmosphere. Irradiation with neutrons at energies up to 200 kev even at a dose of about 10^8 rad does not cause coloring of the glass in the visible spectral region. This evidently is caused by the fact that the low depth of penetration leads to a high proton concentration (up to 10^{19} protons/cm^3) in the layer being irradiated, which then prevents coloring from being initiated. All the foregoing allows us to assert that the penetration of hydrogen or protons into a glass increases its ROS, and this rise is reversible and evidently not associated with chemical reactions in the glass.

CHAPTER FIVE

KINETICS OF THE ACCUMULATION OF COLOR CENTERS IN GLASSES

The dependence of induced optical absorption on irradiation time and in general as a function of dose in any given form has been investigated by all researchers studying color centers in glasses. The main method of study is to plot curves describing the dependence of optical density (or its increment) on irradiation time or dose. Finding the time function of optical density has the same physical meaning as determining the concentration of color centers, since these quantities can be regarded as proportional. For practical purposes, it is sufficient to know the dependence of the optical density increment on radiation dose. Here by no means in every case must we resort to decomposing the absorption bands into elementary components, which is a very laborious process. In most cases curves of the rise in optical density are plotted without preliminary decomposition of the bands.

In the study [1] it is suggested that the rapid rise in the concentration of color centers in the first irradiation stage is associated with the formation of color centers at traps already present in the glass before its irradiation and the reduction in the rate is associated with filling of the traps formed during irradiation.

The studies [2,3] attempt to give theoretical methods of calculating the concentration of color centers in glass as a function of dose. It is assumed that the formation of color centers is associated with filling traps present in glass before irradiation while centers formed are thermally stable at room temperature. These theories are examined closely in the work [4], where the complexity of solving the proposed differential equations and the difficulty of their experimental verification are quite properly emphasized.

At the same time, the phenomenological approach to studying the kinetics of the accumulation of color centers has proven useful for alkali-halogen has proven useful for alkali-halogen crystals; in this

approach the parameters of the kinetic equation are determined from experiment [5]. The approach is promising also in studying the kinetics of the accumulation of color centers in glasses.

1. Phenomenological Equation of the Kinetics of the Accumulation of Color Centers

Ionizing radiation can produce radiation defects in a purely electron-hole process when the electrons freed by radiation and the holes are captured by intrinsic and impurity defects of the glass lattice; similar radiation defects can be thus produced also in an electron-ionic process when the energy of ionizing radiation is used in producing and exciting new defects in the glass lattice [2]. In the first case, the curve of the growth of absorption bands must tend to saturation, at which point the corresponding finished defects will be populated by electrons or holes.

Theoretical curves of the rise in absorption have been derived in the work [3] for electronic centers, but this process easily lends itself to the phenomenological description in the initiation of both electronic and hole centers [6]. If for a given irradiation intensity, a constant concentration of nonequilibrium electron-hole pairs is maintained in a glass, then we can introduce the probability of the initiation of color centers for capture of a charge carrier, p, and the probability that the color center will break down on being irradiated, q. In addition, there is a definite probability of the thermal breakdown of color centers at a given temperature, q_T. Then we can write the following equation for the rise in the color center concentration, n:

$$dn = [(N - n)p - n(q + q_T)]dt, \qquad (14)$$

where N is the concentration of defects at which color centers are produced; and t is the time elapsing from the onset of irradiation.

The solution of the equation is as follows:

$$n = n_0 + \left[N\frac{p}{(p + q + q_T)} - n_0\right]\left[1 - e^{-(p+q+q_T)t}\right], \qquad (15)$$

where n_0 is the concentration of color centers before beginning of irradiation, for example, the 5.2 ev band in quartz glass.

It follows from the solution of equation (15) that the increase in optical density must have a limit. The optical density on attainment of saturation must be characterized as the concentration of sites at which color centers are formed, as well as the ratio of the probabilities of their formation and breakdown. In practice, equation (15) can be used in finding the variation in the color center concentration ($n - n_0$) in the optical density scale as a function of the irradiation time:

$$\frac{n_{t_2} - n_0}{n_{t_1} - n_0} = \frac{1 - e^{-(p+q+q_T)t_2}}{1 - e^{-(p+q+q_T)t_1}}. \qquad (16)$$

From equation (16), we can determine the quantity $a = p + q + q_T$. To do this, we must know the increment in optical density for irradiation times t_2 and t_1 corresponding to the ratio $t_2 = 2t_1$. In this case the experimentally found quantity $K = (n_{t_2} - n_0)/(n_{t_1} - n_0)$ is associated with a by the simple relationship $K - 1 = e^{-at_1}$, knowing a, we can also determine the pre-exponential multiplier in optical density units.

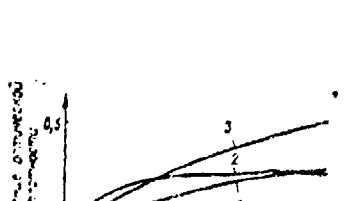

Fig. 23. Kinetics of variation in optical density of KI quartz glass (2 mm thick samples) for x-ray irradiation at the absorption band maxima
1 -- 540 nm (2.3 ev)
2 -- 300 nm (4.1 ev)
3 -- 215 nm (5.7 ev)
KEY: A -- Change in optical density
B -- Time in hours

The quantity q_T can be determined in approximate terms by studying the isothermal decolorization of glass after irradiation ceases (cf. Chapter Eight, Section 4). However, at constant temperature and radiation rate when no specific problems are posed, we cannot separate q_T and q and we can speak only of the overall probability of color center breakdown.

If we have been able experimentally to determine the ratio p/a, then it proves possible to establish the concentration of defects in glass responsible for the absorption in a given spectral region. Fig. 23 shows the kinetic curves obtained from x-ray irradiation of KI quartz glass (tungsten anticathode, U = 37 kv; I = 20 ma). These curves are characterized by the following values of parameters A and np/a when $N_0 = 0$ (Table 15).

Table 15 VALUES OF PARAMETERS A AND Np/a

A Номер кривой на рис. 23	a	$\frac{Np}{a}$
1	0,3	0,65
2	0,23	0,31
3	0,04	0,85

KEY: A -- Curve number in Fig. 23

The proposed approach to describing color center accumulation can be used in solving several theoretical and practical problems that are considered in this chapter.

2. Combined Exposure to Two Kinds of Radiation

Investigating the kinetics of color center accumulation for simultaneous and successive exposure to different types of radiation is of interest from two points of view. First of all, the correlations found will make it possible to predict the degree of glass coloring upon complex exposure to several kinds of radiation. Secondly, since from the experimental function $\Delta D(t)$ one can determine directly the product Np in general, studying the kinetics of color center accumulation for simultaneous and successive exposure to two types of radiation -- x-ray and ultraviolet rays at producing new defects in glasses -- became extremely important.

These studies revealed that the numerator of the preexponential multiplier actually consists of the products of two quantities Np, of which one quantity, p, characterizes the interaction of radiation with the glass, and the second -- N -- is a characteristic of only the glass. If the quantity Np/a found experimentally had characterized only the interaction of glass and radiation and did not depend on the concentration of defects in the glass, we would have observed the additivity of the concentrations of color centers produced by each type of radiation. But if we introduce into this product the cofactor characterizing a finite number of defects, then we must have additivity of the probabilities p and q.

Exposure to one kind of radiation (for example, x-rays) produces a concentration of color centers described by the following equation:

$$n = n_0 + \left(\frac{Np}{a} - n_0\right)(1 - e^{-at}),$$

where n_0 is the concentration of color centers produced upon irradiation by the first source.

Exposure to the other radiation source (for example, ultraviolet radiation) produces a concentration of color centers determined by the equation:

$$n = n_0 + \left(\frac{Np_1}{a_1} - n_0\right)\left(1 - e^{-a_1 t}\right).$$

The equation characterizing the concentration of color centers for combined exposure to two sources will be of the form:

$$n = n_0 + \left[\frac{N(p + p_1)}{a + a_1} - n_0\right]\left[1 - e^{-(a_1 + a)t}\right].$$

Successive irradiation by two kinds of radiation produces the following color center concentration:

$$n = n_0 + \left[\frac{Np_1}{a_1} - n_0\right]\left(1 - e^{-a_1 t}\right) = n_0 e^{-a_1 t} + \frac{Np_1}{a_1}\left(1 - e^{-a_1 t}\right). \quad (17)$$

From equation (17) it follows that the saturation level for exposure to the second source must be Np_1/a_1. Therefore, if the initial concentration n_0 were higher than this level, we would have observed the glass becoming decolorized, and if lower -- then we would have observed additional coloration.

Experimental verification of these equations was performed by the authors on a glass with the composition $Na_2O \cdot 4SiO_2$. The increment in the optical density of the glass when exposed to x-rays from a tube containing a tungsten anticathode (U = 37 kv, I = 20 ma) for $n_0 = 0$ is described by the equation $\Delta D = 1.14\ (1 - e^{-0.16t})$ (Fig. 24, curve number 1).

Simultaneous exposure to x- and ultraviolet rays at wavelength 250 nm from a UXL-500 xenon lamp leads to a variation in optical density obeying the law $\Delta D = 0.97\ (1 - e^{-9.23t})$ (Fig. 24, curve number 2). Hence it follows that $a_1 = 0.07$ and $Np_1/a_1 = 0.57$. The increment in optical density must be stabilized at the level 0.57 for exposure only to ultraviolet rays.

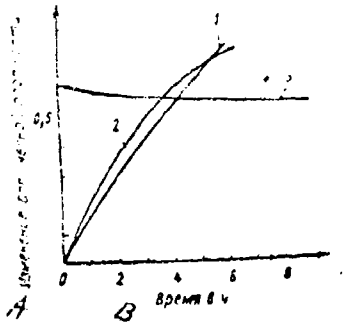

Fig. 24. Kinetics of change in optical density of glass with composition $Na_2O \cdot 4\ SiO_2$ at the 410 nm maximum of the absorption band (2.9 ev) for sample thickness 2 mm.
1 -- Irradiation with x-rays
2 -- Combined irradiation with x- and ultraviolet rays
3 -- Irradiation with ultraviolet rays
KEY: A -- Change in optical density
B -- Time in hours

Curve 3 shows the variation in the optical density of the glass with $n_0 = 0.61$ for exposure to ultraviolet rays. The stabilization level corresponds to 0.55, that is, differs from the predicted value by less than 4 percent, which fits in quite well within the error of radiation intensity.

This result demonstrates the principle that the probabilities of color center formation and breakdown are additive and shows that each kind of radiation cannot act independently of another kind. So the parameter N has an actual physical significance.

3. Kinetics of the Accumulation of Color Centers in Glasses with Additives Enhancing Radiation-optical Stability

Introducing a small amount of oxides of polyvalent ions leads to a decrease in the concentration of color centers absorbing in the visible spectral region, but produces new absorption bands in the ultraviolet spectral region.

According to the work [7], the decrease in color center formation can be caused by the fact that the additive competes with impurities at which color centers are formed, either in the absorption of energy, or else in the capture of electrons or holes. In either case, this is manifested phenomenologically in a reduction in absorption for the selected spectral region compared with the original glass. Since the glass structure does

not change and since the nature of the radiation-glass interaction is also the same, we can anticipate that the probability of color center breakdown in this spectral region (for example, in the visible region) after an additive has been introduced will remain unchanged, that is, the presence of the additive reduces the probability of center formation, but does not interfere with the probability of breakdown of centers formed. Below it will be shown that because of this circumstance it proves possible to determine the ratio p/a and thus, N.

In examining a sodium silicate glass (Na_2O -- 25%, SiO_2 -- 75%) containing cerium ion additives, the authors of the work [8] started from the premise that adding variable-valency ions does not markedly affect glass structure, that digestion conditions are manifested in the equilibrium level of oxidized and reduced variable-valency ions, and, finally, that the formatio of new traps during irradiation virtually does not take place at all. They proposed the following method of describing the optical density of silicate glasses irradiated by x- or γ-rays.

$$n = n_0(1 - e^{-VC}); \quad N = n_0 e^{-VC},$$

where N is the number of holes captured by traps; n_0 is the total number of electron-hole pairs produced by radiation; n is the number of holes captured by Ce^{3+} ions; C is the concentration of Ce^{3+} ions; and V is the volume of charge capture by the Ce^{3+} ion.

The proposed equations completely ignore the kinetics of the process. But C changes its value during irradiation, which must be borne in mind.

Suppose that a polyvalent additive is added to the glass, and its concentration is $C_0 = C_0' + C_0''$ (where C_0' and C_0'' are the additive concentrations in two different valency states). During irradiation the additive makes a transition from state C'' to the state C', which leads to a smaller rise in optical density in the particular spectral region in question compared with the original glass, that is, the concentration of the corresponding centers $n_p < n$, where n_p and n characterize the concentration of color centers in glass containing the additive and in the original glass, respectively. The variation in concentration n_p is described by the equation

$$dn_p = [(N - n)p - qn - (C_0 - C')p_1]dt.$$

If we consider that the concentration C' varies according to a law similar to expression (15) then

$$\frac{dn_p}{dt} = N_p - C_0 p_1 + \frac{C_0 p_1^2}{a_1}(1 - e^{-a_1 t}) + C_0' p_1 - an, \quad (18)$$

where p_1 and a_1 are parameters characterizing the accumulation of centers C'. Hence

$$n_p = n - \left(\frac{C_0 p_1}{a} - \frac{C_0 p_1^2}{a_1 a}\right)(1 - e^{-at}) - \left(\frac{C_0 p_1^2}{a_1 (a - a_1)} - \frac{C_0' p_1}{a - a_1}\right)(e^{-a_1 t} - e^{-at}) = n - b(1 - e^{-at}) - m(e^{-a_1 t} - e^{-at}). \quad (19)$$

Equation (19) is best represented in a somewhat different form, by rearranging the terms:

$$n_p = n - b + (b + m) e^{-at} - m e^{-a_1 t}; \quad (19a)$$

$$n - n_p = b - (b + m) e^{-at} + m e^{-a_1 t}. \quad (19b)$$

At the same time, the kinetics of color center accumulation in a glass containing an additive must be described by an equation of the form (15):

$$n_p = \frac{NP}{A}(1 - e^{-At})^*.$$

Therefore,

$$n - n_p = \frac{Np}{a}(1 - e^{-at}) - \frac{NP}{A}(1 - e^{-At}) = \left(\frac{Np}{a} - \frac{NP}{A}\right) - \frac{Np}{a} e^{-at} + \frac{NP}{A} e^{-At}. \quad (20)$$

The right terms of equations (19b) and (20) must be identical, hence it follows that

$$\frac{Np}{a} - \frac{NP}{A} = b = \frac{C_0 p_1}{a}\left(1 - \frac{p_1}{a_1}\right) = \frac{C_0 p_1 q_1}{a a_1}; \quad (21)$$

$$\frac{Np}{a} = b + m = \frac{C_0 p_1 q_1}{a a_1} + \frac{p_1}{a - a_1}\left(\frac{p_1}{a_1} C_0 - C_0'\right); \quad (22)$$

---

* Parameters A and B mean the same as a and p, but characterize the additive-containing glass.

$$\frac{NP}{A} = m = \frac{p_1}{a - a_1}\left(\frac{p_1}{a_1}C_0 - C_0^*\right); \tag{23}$$

$$a_1 = A \tag{24}$$

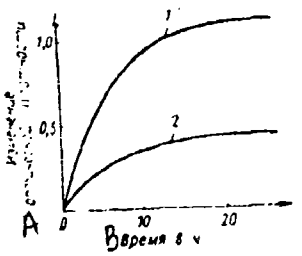

Fig. 25 Kinetics of variation in optical density of glass at the 420 nm absorption band maximum (2.9 ev) for 2 mm thick samples
1 -- Original glass
2 -- Glass containing 0.3 percent Ce_2O_3
KEY: A -- Change in optical density
B -- Time in hours

Based on equalities (21) --(24), we can write

$$n_p = m\left(1 - e^{-a_1 t}\right). \tag{25}$$

As noted above, when a glass with composition $Na_2O \cdot 4SiO_2$ is irradiated with x-rays, the kinetics of color center accumulation in optical density units for λ = 2.9 ev is described by the equation

$$\Delta D = \frac{Np}{a}\left(1 - e^{-at}\right) = 1{,}14\left(1 - e^{-0{,}16t}\right).$$

Adding 0.3 percent Ce_2O_3 to this glass under reducing digestion conditions increases the relative optical density of the glass (Fig. 25) and

$\Delta D = 0.43\ (1 - e^{0,10t})$, that is, b = 0.71; m = 0.43; A = a_1 = 0.1. Assuming Q = q = q_1, and N remaining unchanged, we have

$$\frac{Np_1}{Np} = \frac{p_1}{p} = \frac{0,043}{0,182} \approx 0,24.$$

With the system of equations $p_1/p = 0.24$; $p_1 + q = 0.1$; $p + q = 0.16$, we find the values $p_1 = 0.02$; $p = 0.08$, $q_1 = q = 0.08$. Therefore, $Np/a = N/2$ when cerium is not added, and $Np_1/a_1 = N/5$ when cerium is added.

The presupposition that $q_1 = q$ is an assumption. This compels us to verify whether or not it is contradicted by equations (21) and (23), according to which

$$\frac{m}{b} \approx \frac{p_1 a}{q_1 (a - a_1)} - \frac{\frac{C_0'}{C_0} a a_1}{(a - a_1) p_1 q_1}.$$

If we consider that the increase in the relative optical density is due to the presence of trivalent cerium ions, then considering the digestion conditions, we can take C_0'/C_0 to be a very small quantity, since cerium is present mainly in the trivalent state, $m/b \approx p_1/q_1 \cdot a/(a-a_1)$, and $p_1/q_1 \approx (a-a_1)/a \cdot m/b = 0.06/0.16 \cdot 0.43/0.71 \approx 0.23$, which agrees well with the resulting value $p_1/q_1 = 0.02/0.08 = 0.25$. Therefore, N/2 and N/5 can be regarded as close to actual values.

This makes it possible, after determining the conversion factor, to estimate the maximum concentration of defects as well as color centers not in the optical density scale, but in percentages of the total number of structural elements of the glass -- $Na_2O \cdot 4SiO_2$ groups.

Adding 0.3 percent Ce_2O_3 reduces the optical density at saturation by the amount b = 0.71. By formula (21), b is 0.03 percent, that is, one unit of optical density is caused by a center concentration of 0.04 percent, therefore, Nt/a = 0.046 percent, and N = 0.092 percent, that is N < 0.1 percent which gives a value close to $5 \cdot 10^{18}$ cm^{-3}. The same result can be obtained from formula (23), assuming C_0' to be a small quantity.

Let us consider the system of equations (21) - (24), which enables us to trace the relationships of parameters p, p_1, and P for different C_0 and C_0' values. The main assumption made above is that introducing the

additive reduces the probability that the centers under study will be formed ($P < p$), but does not affect their breakdown probability ($Q = q$). Then equation (24) can be written as:

$$p_1 + q_1 = P + q \qquad (24a)$$

In our above example, we have the equality $q = q_1$, therefore, $p_1 = P$. However, these equalities are valid only when $C_0' = 0$ since in the general case with the assumption $p_1 = p$ and $q_1 = q$ equations (21) and (23) are not compatible. Therefore, p_1 and q_1, just as P, are functions of C_o and C_0', and only when $C_0' = 0$ does $p_1 = P$. In the general case the values of $P_1(C_0, C_0')$, and $P(C_o, C_0')$ satisfying equations (21) and (23), are expressed very awkwardly, therefore we will limit ourselves to considering particular cases.

1. Suppose $C_0' = 0$, that is, the additive is introduced in a valency state, where the transition from this state to the state C' competes with the formation of color centers n. In this case equations (21) and (23) become:

$$\frac{Np}{a} - \frac{NP}{A} = \frac{Np}{a} - \frac{NP}{a_1} = \frac{C_0 p_1 q_1}{a a_1};$$

$$\frac{NP}{A} = \frac{NP}{a_1} = \frac{p_1^2 C_0}{(a - a_1)\, a_1}.$$

These equations are valid when

$$p_1 = \frac{Np^2 + Npq - Npq_1}{Np + aC_0 - C_0 q_1};$$

$$P = \frac{Np^2}{Np + aC_0 - C_0 q_1}.$$

From the experimentally confirmed assumption that $q = q_1$, it follows that

$$p_1 = P = \frac{Np}{N + C_0}.$$

Hence

$$A = a_1 = \frac{Na + qC_0}{N + C_0};$$

$$n_p = \frac{N^2 p}{Na + qC_0}\left(1 - e^{-\frac{Na_1 qC_0}{N + C_0} t}\right).$$

For small t values, we have

$$n_p = \frac{N^2 p}{Na + qC_0} \cdot \frac{Na + qC_0}{N + C_0} t = \frac{N^2 p}{N + C_0} t.$$

2. Suppose $C_0' = C_0$. In this case equations (21) and (23) will become:

$$\frac{Np}{a} - \frac{NP}{A} = \frac{Np}{a} - \frac{NP}{a_1} = \frac{C_0 p_1 q_1}{aa_1};$$
$$\frac{NP}{A} = \frac{NP}{a_1} = \frac{p_1 q_1 C_0}{(a - a_1) a_1}.$$

Equations are compatible when $p_1 =$ $\frac{Np(a - q_1)}{Np - C_0 q_1}$; ; P = p.

However, when P = p, we have $A = a_1 = a$, that is, $\frac{NP}{A} = \frac{Np}{a}$ and, therefore, $\frac{C_0 p_1 q_1}{aa_1} = 0.$. The latter is satisfied only when $p_1 = 0$ and $q_1 = a$, or when $p_1 = a$ and $q = 0$.

It also must be noted that in principle the decrease in the induced absorption in a glass with an additive introduced is possible, compared with the original glass ($a > A$), also as a result of the additive not reducing the probability of color center formation, but increasing the probability of color center breakdown. In this case, evidently, $A > a$, therefore, it is experimentally easy to determine which of these two mechanisms is at work.

4. Effect of Irradiation Rate on Induced Optical Absorption

To allow for the effect of the intensity of irradiation on the induced optical absorption, in equation (14) we must introduce the irradiation dose dD = Idt in place of t:

$$dn = \left[(N - n) p' - nq' - nq_T\right] \frac{dD}{I},$$

where p' and q' are the probabilities of color center formation and breakdown after irradiation with a unit dose.

Hence it follows that

$$\frac{dn}{dD} = \frac{(N-n)\,p'}{I} - n\frac{(q'+q_T)}{I} = N\frac{p'}{I} - n\frac{p'+q'+q_T}{I}.$$

In equation (14) p and q are defined for a unit of time and must be proportional to the intensity of irradiation. Hence it follows that the ratios P'/I and q'/I are constants for a given kind of irradiation and for a selected glass. The quantity q_T does not depend on irradiation intensity, since it is determined only the the temperature of irradiation and by the selected glass.

The differential equation taking account of the effect that irradiation intensity has on the kinetics of color center accumulation will be of the form:

$$\frac{dn}{dD} = Np - \left(p + q + \frac{q_T}{I}\right)n. \qquad (26)$$

The following function is the solution of this equation:

$$n_t = n_0 + \left(\frac{Np}{p+q+\frac{q_T}{I}} - n_0\right)\left[1 - e^{-(p+q)D - q_T\frac{D}{I}}\right] =$$
$$= n_0 + \left(\frac{Np}{p+q+\frac{q_T}{I}} - n_0\right)\left[1 - e^{-(p+q)D - q_T t}\right]. \qquad (27)$$

If equation (15) describes the process of color center accumulation after irradiation, whose intensity is taken as unity, equation (27) enables us to calculate the color center concentration at an irradiation intensity I, which is important for methods of testing glass for their radiation-optical stability, since it enables us to compare the change in optical density at different irradiation intensities.

Experimentally, equation (27) was verified for a glass with composition $Na_2O \cdot 4SiO_2$ for 2 mm thick samples. The dose obtained by the sample after being irradiated for one hour with x-rays on a URS-60 installation (U = 27 kv, I = 20 ma), was adopted as the unit. In this case for a glass with

composition $Na_2O \cdot 4SiO_2$ $p + q + q_T = 0.16\ hr^{-1}$, and $N_p = 0.182$. The increment in optical density is described by the equation $N_t = 1.14 (1 - e^{16D})$, where D is numerically equal to the irradiation time. The intensity of irradiation at a current of 10 ma is 0.6 - 0.7 of the intensity at 20 ma. The quantity a_T determined experimentally from the isothermal anealing of an irradiation sample is $0.02\ hr^{-1}$. Therefore, the dependence of the increment in the optical density must be described by the equation $n_p = 1.07 (1 - e^{-0.16t})$. Fig. 26 shows n_t values calculated based on this equation and those obtained experimentally. The differences do not exceed 10 percent of the measured quantity.

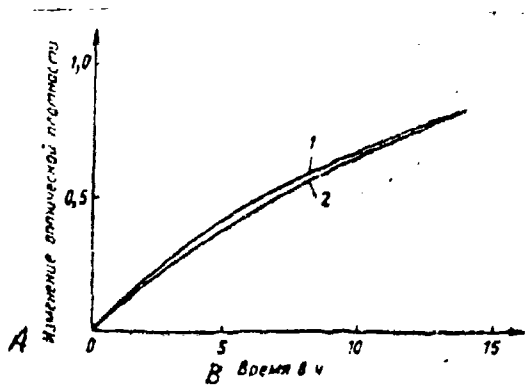

Fig. 26. Kinetics of variation in optical density of the glass $Na_2O \cdot 4SiO_2$ at the 420 nm absorption band maximum (2.9 ev) when irradiated with x-rays (sample thickness 2 mm)
1 -- Calculated curve
2 -- Experimental curve
KEY: A -- Change in optical density
B -- Time in hours

CHAPTER SIX

LUMINESCENCE OF GLASSES

The phenomenon of luminescence as applied to glasses can be viewed in two aspects — strongly luminescing glasses and glasses with reduced luminescence. Strongly luminescing glasses are widely used in laser equipment, luminescence analysis, and as glowing screens in instruments. However, in a large number of applications of glass, luminescence is an undesirable effect, since it reduces the quality of optical instruments, because it deteriorates the clarity of imaging on television screens and the quality of photographs. This chapter examines problems relating to luminescing glasses and the effect glass composition has on luminescence.

1. Problems in the Theory of Excitation and Quenching of Luminescence

More than 350 years have passed since the discovery of luminescence, however thus far there is no general theory of luminescence even for crystals. The reason lies in the extreme complexity of processes causing solids to luminesce.

By the definition of Vavilov [1, 2], luminesc[illegible] excess over the temperature emission of a body if this exces[illegible] a finite duration, much longer than the period of light vi[illegible]

Vavilov [2] evaluated all cases of luminescen[illegible] two three kinds: spontaneous, forced, and recombination.

Spontaneous and forced luminescence is caused by the presence in a material of discrete centers [3]. Luminescence of discrete centers is exhibited by phosphors, in which all electronic processes take place at individual "phosphorescing centers." Individual [illegible]s or molecules or their combinations can act as these "centers".

We know that luminescence of solid [illegible]rogen, [illegible]anyl salts [4, 5], boric and sugar phosphors [6, 7], and certain other solids is the phosphorescing

of discrete centers. Solid phosphors -- zinc sulfide, alkaline-earth, alkali-halogen, silicate, and others, with the recombination phosphorescing mechanism, comprise the group of typical crystal phosphors. The act of light absorption is accompanied in these phosphors by an internal photo effect, and the emission of the luminescence quantum results from the recombination of the photoelectron with an activator ion.

The laws of the transformation of excitation energy into luminescence energy are valid for all phosphors in any states of aggregation.

The law of the spectral transformation of light was first formulated by Stokes [8] as a statement of the necessary increase in wavelength during luminescence ($\lambda_{lum} \geqslant \lambda_{exc}$). The physical content of Stokes law was elucidated by Einstein [9] based on primitive ideas of the quantum theory of light. A reduction in the frequency of light evidently means that in the active luminescence only part of the energy absorbed by the phosphor is emitted ($h\nu_{lum} \leqslant h\nu_{exc}$).

However, Stokes' law is frequently violated [10, 11]. Violations of Stokes' law indicate the possibility of the reverse transition of internal (thermal) energy of a body into the energy of luminescence emission.

Lommel [12] gave a more expanded formulation to the law of the spectral transformation of light. According to Lommel, the luminescence band as a whole, and also its intensity maximum must always be shifted toward the long-wave side of the spectrum with respect to the absorption band and its maximum.

A modern formulation of the law of this spectral transformation of light has been given by Vavilov [1, 15-16] in the formula of the following principles.

1. The energy yield of luminescence cannot exceed unity.

2. In anti-Stokes excitation, that is, when $\nu_{exc} \leqslant \nu$ (when ν is the mean frequency in the emission band), the energy yield of photoluminescence must decay with increase in the frequency difference $\nu - \nu_{exc}$, and do so more rapidly the lower the temperature of the body.

Depending on in which form the energy is brought to the luminescing body, photo-cathodo-roentgeno-electro-and other kinds of luminescence are differentiated [17].

Luminescence excited by light quanta is called photoluminescence, luminescence excited by electrons is called cathodo-luminescence, and luminescence caused by x-rays is called roentgeno-luminescence, while when γ-rays are used -- it is called γ-luminescence. The spectrum of cathodo-luminescence is similar to the photoluminescence spectrum. The most important difference between cathodo-luminescence and photoluminescence is

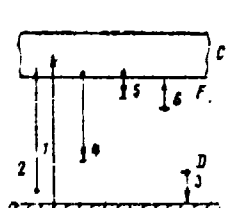

Fig. 27. Energy zone diagram of a crystal phosphor

the short lifetime of luminescence, not exceeding tenths of a second, and sometimes amounted to 10^{-5} - 10^{-6} sec.

Fast heavy particles -- ions, protons, neutrons, and mesons can also cause liquid and solids to luminesce. It is assumed that excitation caused by x- and -rays, and also by bombarding electrons or particles, causes phenomena similar to what is observed for exposure to ultraviolet light.

The theoretical bases of modern concepts of the luminescence mechanism of crystal phosphors is the zone theory of solids [18]. Under this theory, the energy spectrum of an electron in a nonideal crystal lattice consists of quasicontinuous energy zones and discrete local levels. Discrete levels are caused by the "defects" in the crystal structures -- foreign atoms impregnated in the crystal, vacancies and atoms at interstitial sites, mosaic structure, microcracks, crystal grain boundaries, external crystal boundaries, and so on. In these discrete states electrons prove to be localized either at the actual "defects" of the structure or near it.

Underlying the zone theory of the luminescence of crystal phosphors has been postulated a system of energy terms schematically shown in Fig. 27. This theory [19] associates levels b with an accelerator added to the crystal during preparation of this phosphor and associates level F with crystal structure defects. Absorption of light by a crystal leads to an internal photoeffect and to the transition of electrons from the ground zone B or from the level of activator D into the conductivity zone C. These transitions are noted by arrows 1 and 2, respectively.

Fundamental absorption of a crystal is associated with the first process, and supplementary absorption caused by introducing an activator and adjoining the long-wave boundary of fundamental absorption is associated with a second process.

When light is absorbed by the activator, ionization luminescence centers are created, or as is sometimes called, vacancy levels D in the energy diagram of the crystal. Absorption in the lattice leads to the formation of holes in the lower zone. These holes are filled with electrons from the activator level. This process is denoted with arrow 3. It is not

hard to see that it is energetically profitable, since it is associated with the transition of electrons to a lower level. As a result of this process, vacant levels D are also formed.

Some of the electrons falling into the conductivity zone C directly recombine with ionization luminescence centers, that is, pass into the vacancy levels of the activators (arrow 4). This process is responsible for short-term luminescence, or in the old terminology, the fluorescence of crystals. This component of crystal phosphor luminescence does not appear at any temperatures no matter how low. The remaining electrons, falling into zone C, are lodged at the trapping levels at the sites of crystal structure disruption (transition 5); here the possibility of their direct recombination with ionization luminescence centers is completely precluded. This recombination will require preliminary liberation of an electron, that is, its transition back to zone C (arrow 6). Energy required for this transition can be obtained in ordinary conditions only from the lattice, which means that the characteristic time of this process depends heavily on temperature.

Thermal fluctuations permit the gradual liberation of electrons localized at the trapping levels, that is, their transition back to the conductivity zone (arrow 6), from whence they immediately or after several retrappings recombine with the ionization centers of luminescence (curve 4). Emission accompanying the recombination of these electrons temporarily held at the trapping levels constitutes the afterglow or the phosphorescence of crystals.

Quenching of luminescence is associated with nonradiative transitions. In current literature the problem of nonradiative transitions in crystals is ordinarily associated with the theory of Moglich and Rompe [20]. The basis of this theory is the assumption of possible "multiple collisions," that is, the interaction of an electron simultaneously with a large number of elastic vibrations of the lattice. According to Moglich and Rompe, the simultaneous production of a large number of phonons takes place. By instantaneously exchanging its energy for the energy of the thermal vibrations of the lattice, the electron passes nonradiatively from the conductivity zone to the lower zone or to the local level. A reduction in the intensity of luminescence (quenching) can result from an overly high concentration of luminescing molecules (concentration quenching), a temperature rise (temperature quenching), or quenching by impurity atoms or molecules. There is no general theory of the quenching of luminescence processes. Work in this area applies mainly to solutions [21-26].

Authors of the papers [21-26] have noted the presence of an abrupt concentration quenching threshold for a large number of molecules. Concentration quenching begins at a quite specific concentration, that is, at a certain mean distance between molecules. Quenching is associated with the transfer of energy from excited molecules to unexcited molecules. This energy transfer can be carried out by different methods, depending on the mean distance between molecules. At distances much greater than a light

wavelength, the transfer of energy is executed with photons: excited molecules emit photons; unexcited molecules absorb them at very small distances, commensurable with the electron wavelength; now the energy carriers are no longer photons, but electrons, tunneling through potential barriers from molecule to molecule.

The addition of some impurities to a solution (for example, KI) leads to an abrupt attenuation of luminescence, a smaller quantum yield, and a shorter lifetime for the excited state. Similarly, the fluorescence of vapor is weakened or quenched completely when some foreign gases are added. Most often oxygen is a good quenching agent.

2. Luminescence of Quartz Glass

Quartz is a classical object of diverse physicochemical investigations, however, study of electronic processes in it has begun only in recent years [27-31].

Similar studies of alkali-halide crystals have been and are continuing to be conducted for an extended period, which in fact has led to appreciable advances [32-33].

The photoluminescence of quartz glass is caused by the presence of an absorption band in the 240 nm region (5.2 ev). The luminescence spectrum of quartz glasses consists of two bands: one is a short-wave band with its maximum in the 280 nm region (4.4 ev); the second has its maximum in the 296 nm region (3.1 ev) [34-37].

In the view of several workers [38-41], these two luminescence bands, with their maxima in the spectral regions 280 and 400 nm (4.4 and 3.1 ev) are caused by the same center. However, recently careful studies have been conducted on the luminescence of quartz glasses, showing that these ideas are in error [42, 43]. Investigations have also revealed some other correlations of the luminescence of quartz glasses. Unactivated quartz glasses of the following grades were studied:

KI -- contains random impurities of Ca, Al, Ba, Sb, Pb, Mn, B, Na, and Zn, about 10^{-1} - 10^{-3} percent by weight;

KV -- contains random impurities in about the same amount, and OH groups (at the wavelength λ = 2700 nm, the absorption coefficient d is 6.9 cm^{-1});

KS -- contains random impurities at one order of magnitude lower than the above values; and

KO -- a very pure material prepared by special procedures; contains large numbers of OH groups (at λ = 2700 nm, d is 10.5 cm^{-1}).

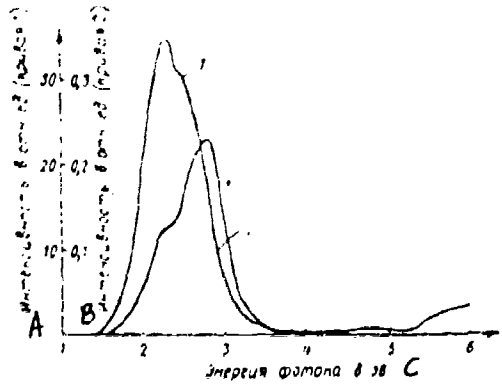

Fig. 28. X-ray luminescence spectra (BSV-2w tube, 50 kv, 10 ma) of KO glass at the following temperatures:
1 -- 100° K
2 -- 290° K
KEY: A -- Intensity in relative units (curve 1)
B -- Intensity in relative units (curve 2)
C -- Photon energy in ev

Quartz glass samples underwent external x-ray irradiation (to 50 kv, 20 ma), light irradiation (590-210 nm (2.1-6 ev)), and temperature exposure (from 77 to 420° K).

Nonequilibrium electrons and holes produced by x-ray irradiation are annihilated, by recombining with each other or via recombination centers (luminescence can be produced in this instance), or else are captured at impurity or intrinsic defects of the glass network (color centers are induced). Obviously, the fewer the capture centers (the purer the material), the higher will be its radiation-optical stability, but also the larger will be the proportion of nonequilibrium charge carriers that recombine with each other or via recombination centers. If this recombination is accompanied by emission, which is more probable at low temperatures, then as the purity of quartz glasses is increased for optical equipment operating under conditions of hard radiation, the problem of eliminating intense radioluminescence becomes primary.

The foregoing was experimentally confirmed on the test samples. In KO material the intensity of x-ray luminescence at 100° K in the principal emission band of 540 nm (2.3 ev) is higher than in KS or KI material; the spectrum has bands at 540-500 nm (2.3-2.5 ev) (Fig. 28). In the absorption

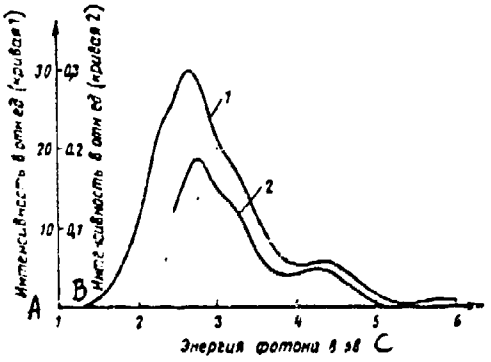

Fig. 29. Spectra of KS glass at 100° K

1 -- X-ray luminescence (50 kv, 10 ma)

2 -- Photo-stimulated luminescence on exposure to light at wavelength of 575 nm (2.15 ev)

KEY: A -- Intensity in relative units (curve 1)
B -- Intensity in relative units (curve 2)
C -- Photon energy in ev

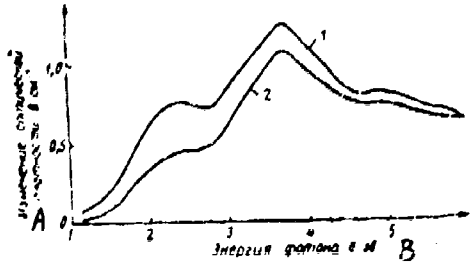

Fig. 30. Spectra of KS glass at 100° K

1 -- induced absorption of samples subject to x-ray irradiation (1 hour, 50 kv, 20 ma)

2 -- absorption after 30 minutes exposure of irradiated specimen to light at wavelength of 575 nm (2.15 ev)

KEY: A -- Change in optical density in cm^{-1}
B -- Photon energy in ev

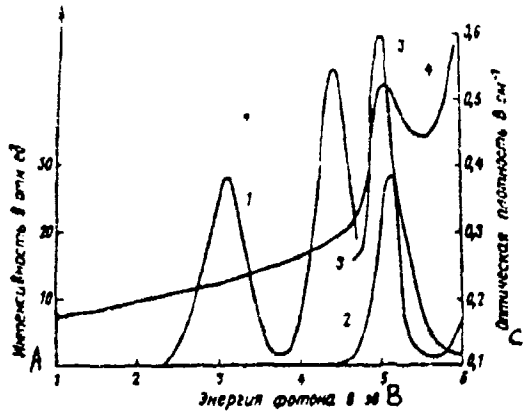

Fig. 31. Spectra of KS glass at 290° K
1, 2, 3 -- photoluminescence when excited with light at wavelength of 240 nm (5.1 ev), 400 nm (3.1 ev), and 280 nm (4.4 ev), respectively
4 -- absorption of unirradiated sample
KEY: A -- Intensity in relative units
B -- Photon energy in ev
C -- Optical density in cm^{-1}

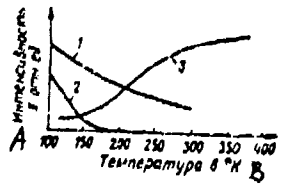

Fig. 32. Temperature dependence of the intensity of photoluminescence of quartz glasses
1 -- luminescence peak at 280 nm (4.4 ev), excitation energy 240 nm (5.1 ev)
2 -- 460 and 210 nm (2.6 and 5.9 ev)
3 -- 400 and 250 nm (3.1 and 5.2 ev)
KEY: A -- Intensity in relative units
B -- Temperature in ° K

spectrum of an unirradiated KO sample (T = 100° K), no band with a maximum at 240 nm (5.2 ev) is observed, but induced absorption consists of two weak bands with maxima at about 220 and 260 nm (5.7 and 4.8 ev).

In quartz glasses of grades KI, KV, and KS, the x-ray luminescence spectrum is richer — one can note bands with maxima at about 540, 500, 440, 400, and 275 nm (2.3, 2.5, 2.8, 3.1, and 4.5 ev) (Fig. 29). Data for KS glass are typical also for KI and KV glasses. Glasses of these grades are more strongly colored at 100° K than KO glass, and bands with maxima at about 540, 320, 240, and 220 nm (2.3, 3.9, 5.2, and 5.7 ev) appear in the induced absorption spectrum (Fig. 30).

At room temperatures x-ray luminescence is weakened by about one order. A band with maxima at 440 nm (2.8 ev) becomes stronger in the spectrum of KO material (cf. Fig. 28). In the x-ray luminescence spectrum of KI, KV, and KS materials, only one band with a maximum at 400 nm (3.1 ev) remains. Special verification showed that the excitation spectrum of this band has a maximum at about 240 nm (5.2 ev). Photoluminescence is excited in the region of 280 nm (4.4 ev), with a maximum at about 245 nm (5.05 ev) (Fig. 31). As the temperature is reduced, the intensity of the photoluminescence band in the region of 280 nm (4.4 ev) rises, but decreases in the 400 nm region (3.1 ev) (Fig. 32). Ten percent polarization of photoluminescence and the absence of a maximum in the 240 nm region (5.2 ev) in the excitation spectrum of photoconductivity indicates the intracenter nature of this luminescence. The difference in the maxima of the absorption spectra, the arbitrary ratio of intensities of the 400 and 280 nm (3.1 and 4.4 ev) photoluminescence bands for different samples at the same temperature, and the change in the position of the absorption band at about 240 nm (5.2 ev) in different initial samples indicate that a distinct center is responsible for each of the photoluminescence bands 400 and 280 nm (3.1 and 4.4 ev). Since these emission bands also appear in the x-ray luminescence spectrum, and with the same temperature dependence, we can conclude that the centers participate in the recombination annihilation of nonequilibrium carriers.

It was not possible to obtain photoluminescence bands 540, 500, and 440 nm (2.3, 2.5, and 2.8 ev) for excitation from 410 to 210 nm (from 3 to 6 ev). Since these bands are present in the x-ray luminescence spectra of all quartz glasses and have the same temperature pattern, we can assume that this luminescence arises via the annihilation of elementary electronic excitations in the glass network.

When quartz glass containing an impurity or lattice imperfections is irradiated, some of the nonequilibrium carriers are captured by deep traps (color centers can form), and some, especially at low temperatures, by shallow traps. Shallow traps can, with a reduction in the irradiation temperature, either increase or reduce the effectiveness of color center formation. If the traps begin to capture nonequilibrium carriers of the same size which on being captured by deep traps form color centers, the effectiveness of the formation of the centers is reduced, and in contrast, if the traps capture carriers of the opposite sign, that is, those that

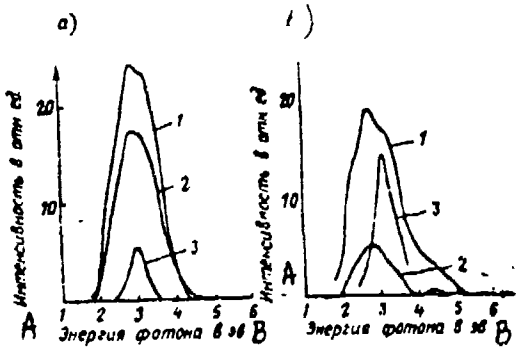

Fig. 33. Spectra of quartz glasses
a -- KV
b -- KI
1 -- x-ray luminescence (50 kv, 20 ma), T = 120° K
2 -- heat-stimulated luminescence, T = 140° K
3 -- photoluminescence (for KV glass, T = 115° K, for KI glass -- T = 183° K)
KEY: A -- Intensity in relative units
B -- Photon energy in ev

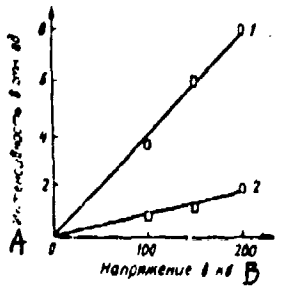

Fig. 34. Luminescence intensity of KV quartz glass
1 -- as a function of electron energy for a current of 2 μa
2 -- as a function of proton energy at a current of 0.4 μa

KEY: A -- Intensity in relative units
B -- Voltage in kv

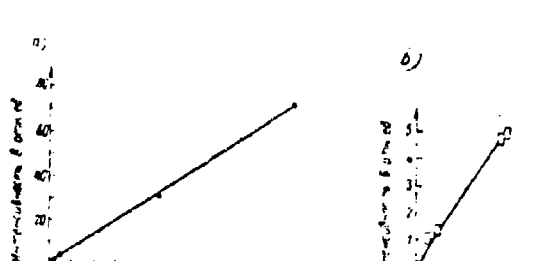

Fig. 35. Luminescence intensity of KV glass at a function of beam strength
a -- 195 kev electrons
b -- 185 kev protons
KEY: A -- Intensity in relative units
B -- Current in μa

break down the color centers formed, the effectiveness of the formation of these centers rises. In either case, the existence of shallow traps leads to the fact that at the appropriate temperature when traps begin to capture carriers the effectiveness of color center formation and breakdown will vary.

It was shown that thermal luminescence induced when charged carriers are free from shallow traps is recombinational in nature and its spectral composition coincides with the spectrum of x-ray luminescence at the corresponding temperature (Fig. 33). It is natural to anticipate a similar effect also for other methods of liberating carriers, for example, in the optical decolorizing of color centers.

Exposure of quartz glasses colored at 100° K to light at a wavelength of 575 nm (2.15 ev) causes decolorizing of the 540 and 320 nm absorption bands (2.3 and 3.9 ev) (cf. Fig. 30) and the luminescence bands in the 500-250 nm region (2.5-5 ev) (cf. Fig. 29). As to be expected, with increasing breakdown of color centers the intensity of recombination luminescence also falls off.

For practical purposes, the dependence of luminescence intensity on excitation conditions is of high interest. We studied the effect of energy as well as intensity of the exciting beam on the glow intensity of quartz glass (Figs. 34 and 35). Luminescence was excited by a beam of protons or electrons in the device shown in the study [46]. In both cases, a linear function was observed. When luminescence was excited with protons or electrons, the difference between the glow intensity of different types of quartz glasses is not substantial.

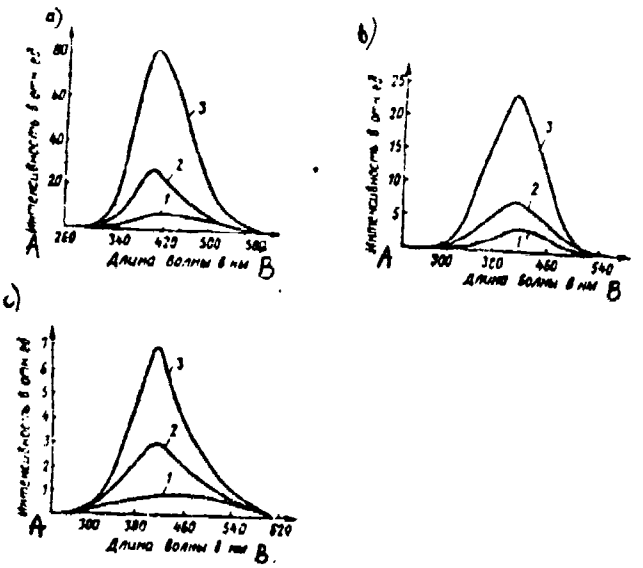

Fig. 36. Photoluminescence spectra of glasses at listed temperatures

а -- 96° K
б -- 293° K
в -- 395° K
1 -- K-8
2 -- K-208
3 -- K-108

KEY: A -- Intensity in relative units
B -- Wavelength in nm

3. Luminescence of Commercial-composition Glasses

Luminescence of commercial-composition glasses at different temperatures and therefore different kinds of excitation is of practical value, accounting for the possibility of using a given glass in particular optical systems.

Photoluminescence

Fig. 36 presents photoluminescence spectra of the optical glasses K-8, K-108, and K-208 excited by ultraviolet irradiation at 96, 293, and 395° K. As we can see, the glow intensity of the glasses K-108 and K-208 at all excitation temperatures is much higher than the glow intensity of K-8 glass. This can be explained by the fact that these glasses contain cerium ions which function as a luminescence activator. The glow intensity of K-208 glass at 96° K (Fig. 36 a) is about 3 times smaller than for K-108 glass.

A similar ratio of luminescence intensity is observed also at 295° K (Fig. 36 b) and 395° K (Fig. 36 c). The decrease in the glow intensity of K-208 glass containing CeO_2 is four times greater than for K-108 glass, which is due to the concentration quenching of luminescence caused by the increased cerium ion content in the glass. We know that at a CeO_2 concentration of about 1 percent by weight, an abrupt decrease in the luminescence yields sets in.

The luminescence color of glasses K-108 and K-208 is blue. A well-pronounced luminescence maximum at all excitation temperatures lies in the 400 nm region (3.1 ev).

The luminescence spectrum of K-8 glass characterized by a wide band. The luminescence maximum at 96° K is skewed somewhat to the short-wave spectral region. The low luminescence intensity of this glass when excited with light at wavelength of 310 nm (4 ev) is evidently accounted for the high purity of the materials used in optical glass-making, and by the presence of a large amount of alkalis and boron trioxide, which lead to an appreciable drop in the luminescence yield. Also, we must note that some of the long-wave decrease in the fundamental band of K-8 glass lies in the 260 nm region (4.8 ev). This glass transmits up to 50 percent of light at the 310 nm wavelength (4 ev), also leading to a reduced luminescence yield.

In glasses as well as in crystals, photoluminescence is much intensified as the temperature is lowered and decreases with temperature rise (cf. Fig. 36). The cause of this weakening of luminescence with temperature rise can be readily understood, since the stronger the thermal motion of surrounding atoms, the higher is probability of second-order collisions and energy dissipation.

X-ray luminescence

X-ray luminescence spectra of the glasses K-108 and K-208 (Fig. 37) at 96, 295, and 385° K are characterized by one broad band with a well-defined maximum in the 400 nm region (3.1 ev). Two blurred luminescence maxima are observed for K-8 glass in the regions of 400 and 480 nm (3.1 and 2.1 ev) at an excitation temperature of 295° K.

The intensity of x-ray luminescence of glasses, just as for photoluminescence, increases with temperature drop and decreases with temperature rise.

A comparison of the spectra of photo- and x-ray luminescence at the same temperatures is of unquestioned interest. Thus, the nature of the spectra of x-ray and photoluminescence of the radiation-resistant glasses K-108 and K-208 is practically the same, since it is mainly the cerium ions that are the source of luminescence for these glasses. The appearance

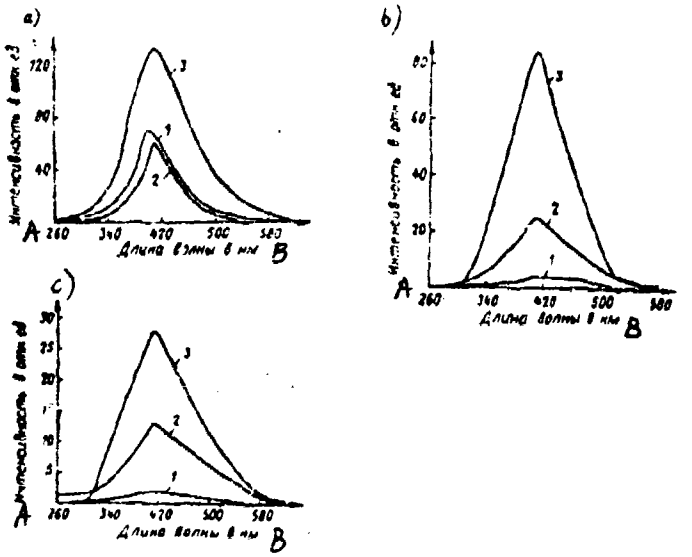

Fig. 37. X-ray luminescence spectra of glasses at listed temperatures

a -- 96° K
b -- 293° K
c -- 385° K
1 -- K-8
2 -- K-208
3 -- K-108

KEY: A -- Intensity in relative units
B -- Wavelength in nm

TABLE 16. INTEGRAL GAMMA-LUMINESCENCE

1 Марка стекла	2 Интегральная гамма-люминесценция в отн. ед. при температуре в °К	
	77	310
K-8	6	3,5
K-108	7	4
K-208	3	3
3 ЛК-5	3	3
4 ЛК-105	5	5

KEY: 1 -- Glass grade
2 -- Integral gamma-luminescence in relative units at listed temperature, in ° K
3 -- LK-5
4 -- LK-105

of a second maximum in the 480 nm region in the x-ray luminescence spectrum of K-8 glass can be attributed to centers formed in the glasses when they are irradiated with x-rays during luminescence excitation. Disappearance of this luminescence maximum at 385° K can be explained from the fact that with a temperature rise these centers either do not form or else are immediately broken down nonradiatively through thermal annealing.

Gamma-luminescence

The luminescence of glasses when exposed to gamma-rays is very slight. therefore no spectral distribution of gamma-luminescence has been recorded. Table 16 gives the data of integral gamma-luminescence at 77 and 310° K.

Investigation of the effect that gamma-ray irradiation time has on the luminescence intensity yielded the following general property for the glasses studied. The build-up of radioluminescence consists of two components: a rapid component with a rise time of less than 1 sec, followed by a relatively slowly increasing component.

The luminescence intensity of glasses as functions of the gamma-ray irradiation time is given in Fig. 38. As we see from Fig. 38 a-d, for the glasses K-8, K-108, K-208, and LK-105 initially a rapid rise in the intensity of gamma-luminescence is observed in the initial period of radiation, and then the rate of intensity increase slows down. This is particularly evident at 77° K.

Stabilization of the intensity of gamma-luminescence for glasses of different compositions is attained after different time periods. A climb in temperature to 310° K leads to lowered intensity of luminescence in the glasses K-8, K-108, and K-208 (Figs. 38 a, b, and c).

In glasses of grades LK-105 and LK-5, a variation in the irradiation temperature results in virtually no change in the intensity of radioluminescence (Fig. 38 d and e).

4. Effect of Heat Treatment on the Luminescence of Glasses

Investigation of the effect of the thermal prehistory of the glass on its photoluminescence is of interest in studying the extent of its defect status.

Owing to the limited study [47-49] of the heat-treatment dependence of the luminescence of glasses, investigations of the effect that stabilizing the structure of a glass during extended annealing and also fixation of high-temperature structure with intensive hardening have on photoluminescence takes on a certain significance. The authors of [50] K-8 commercial borosilicate glass (Fig. 39 a) and NP commercial silicate glass obtained by continuous rolling (Fig. 39 b). The long-term annealing regime

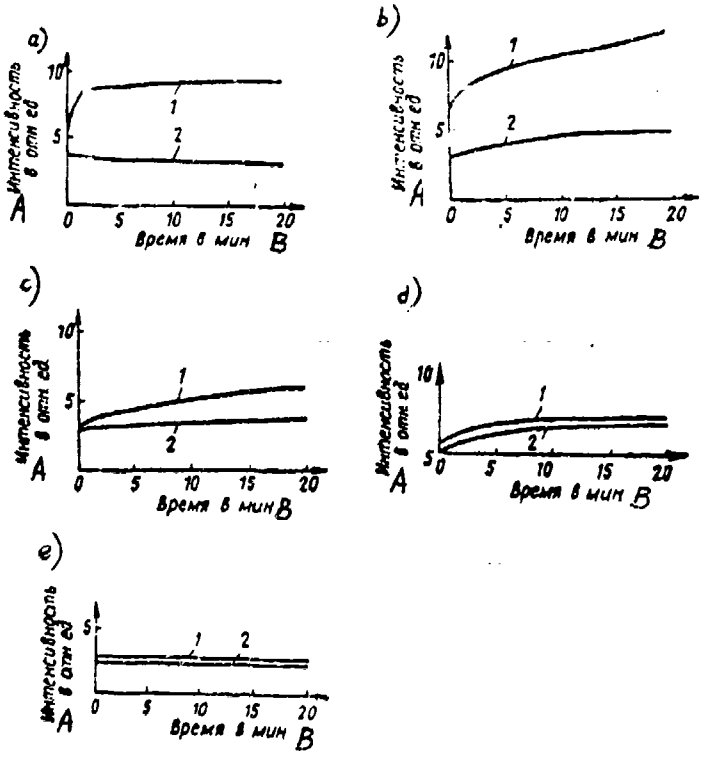

Fig. 38. Luminescence intensity as a function of irradiation time using gamma-rays of the following glasses

a -- K-8
b -- K-108
c -- K-208
d -- LK-105
e -- LK-5
1 -- 77° K
2 -- 310° K

KEY: A -- Intensity in relative units
B -- Time in minutes

is determined by the upper and lower boundaries of the annealing zones of the test glasses and is 830 and 660° K. The thermostatting time was 25, 50, 100, and 200 hours. The extent of air hardening was about 0.5 N/cm, and 2.2 N/cm -- for hardening in liquid. Photoluminescence was excited with glass at wavelength of 310 mm (4 ev).

Thus we can see from Fig. 39 b, the luminescence spectra of NP glass samples consist of two bands with maxima in the regions of 410-420 and 500 nm (3-2.95 and 2.5 ev). The position of the luminescence bands does not depend on the heat-treatment conditions, but their intensity changes

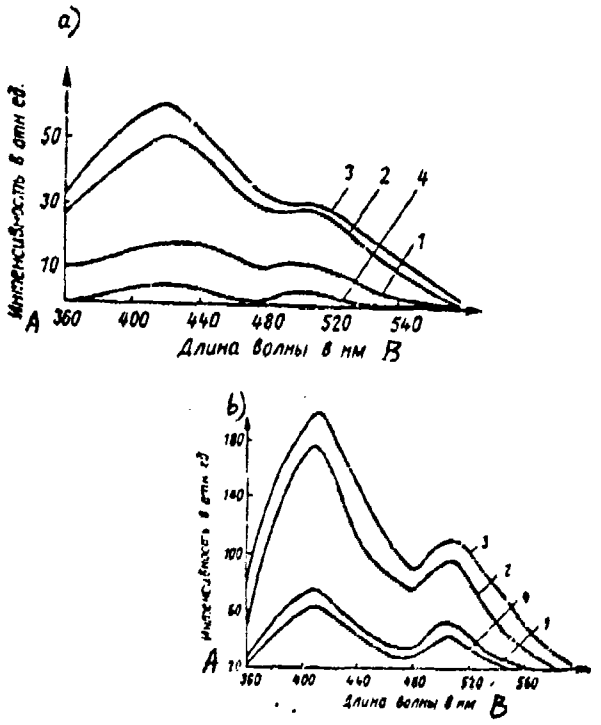

Fig. 39. Photoluminescence spectra.
a -- of K-8 glass
b -- of NP glass
1 -- initial sample
2 -- heat treatment at 830° K, 25 hours
3 -- heat treatment at 660° K, 100 hours
4 -- hardened sample (2.2 N/cm)
KEY: A -- Intensity in relative units
B -- Wavelength in nm

markedly. Samples subject to hardening (Fig. 39, curves 4) have the lowest luminescence intensity. Samples kept at 660° K for 100 hours (curves 3) have the strongest luminescence.

In comparing these data, we must note that the effect of increased luminescence intensity after long-term heat treatment is much less pronounced in K-8 glass than in NP glass. The effect of reduced luminescence level upon hardening is, conversely, expressed much more strongly in K-8 glass than in NP glass. This effect evidently can be accounted for by the effect that K-8 optical glass during production underwent mild annealing and its structure in the initial specimen was stabilized already to a large extent.

These glass thermal prehistory functions of the intensity of photoluminescence can be interpreted from the standpoint of ordering of the glass structure when it undergoes extended annealing [51], which leads to a rise in the intensity of luminescence in accordance with known data [47] on the strong luminescence of crystalline materials compared with glasses of the same composition. In hardened glasses with fixed high-temperature structure, the near-range order and the first coordination sphere is much more strongly violated than in annealed glasses, which evidently provides the major prerequisites for converting excitation energy into the energy of thermal oscillations, bringing about a strong drop in the luminescence level.

5. Luminescing Glasses

Luminescing glasses have found wide use as luminescent screens, in laser equipment, and so on.

Luminescing glasses containing uranium as an activator have been closely studied [52-55]. From a comparison of the emission spectra of uranium solutions and uranium glasses, it follows that glass spectra have a finer structure and greater intensity. This is due to the smaller polarizing influence of ions surrounding the luminescence centers in glass.

In most investigations of the luminescence of uranium-containing glasses, reference is made to the high intensity of their emission. However, a study [54] showed that in far from all compositions is uranium generally capable of luminescing, without even citing the fact that the luminescence brightness and yield fluctuate within very wide limits, depending on composition.

The main reason for this is that uranium is an element with variable valency. Of uranium compounds, only the hexavalent uranium ion, more exactly the uranyl group UO^{2+}, is capable of luminescing. Study of the luminescence of uranyl glasses made it possible to obtain under production conditions glasses with a luminescence yield of 50-60 percent.

A very interesting object of study has been manganese-containing glasses [56]. Manganese is one of the very widespread activators of crystal phosphors. On being added to a material with a different crystal structure, the manganese ion, depending on the position it occupies in the crystal lattice, is capable of producing luminescence in two colors, namely green and orange-red [57]. Thus, the luminescence of silicate glasses is green, while that of borate and phosphate glasses is red. Initially several investigators [58] were of the opinion that the different luminescence color was due to the different valency of the manganese ions. However, at present it can be regarded as established that either type of luminescence is accounted for only by ions of divalent manganese [59].

Copper is also a common luminescence activator in inorganic crystal phosphors [59-62]. Evidently, in glass copper can exist in three valency states: Cu^{2+}, Cu^{1+}, Cu^{0}. Glasses are known in which copper is present as the metal, for example, copper ruby. The luminescence of glasses and crystals activated with copper can vary from blue to orange [60-65]. In several cases glasses or crystals activated with copper have brief luminescence; sometimes, in contrast, the luminescence time is measured in hours [61, 62, 66]. To obtain glasses with bright luminescence upon exposure to x-ray and gamma-radiation, silicate glasses activated with copper are used, for example, BS-13 glass.

Luminescing glasses activated with trivalent chromium have not found practical use owing to the strong temperature dependence of luminescence. Only glasses containing trivalent chromium luminesce.

Among luminescing glasses, special prominence is shown by glasses activated by rare-earth elements [57]. The widest practical use has been found for glasses activated with neodymium, as being the most promising for laser construction. Their spectral, luminescent, and generating characteristics have been studied in several Soviet [59, 67-74] and foreign [75-96] works. At the present industry uses only neodymium as an activator in making glasses for lasers. The compositions of glasses and their characteristics are given in the work [57].

Glasses activated with neodymium are colored the characteristic lilac. The most intense bands are in the regions of 580, 740, 800, and 900 mm [57, 91, 97, 98]. Upon excitation, infrared luminescence is observed in any of these bands. Characteristic of these glasses is a luminescence quantum yield of about 40 percent.

Glasses activated with praseodymium [57] are colored green. The most intense luminescence is shown by silicate glasses. The luminescence intensity drops off in the transition to phosphate and borate glasses. Variation in the redox conditions of digestion has no appreciable effect on the luminescence of praseodymium-containing glasses. An increase in the praseodymium concentration in a glass leads to a higher intensity of luminescent bands.

Glasses activated with samarium [57, 69, 99, 100] are weakly yellow. Upon excitation with ultraviolet rays, orange luminescence is induced. Increasing the samarium concentration up to 10 percent leads to an increase in luminescence intensity without quenching.

The luminescence of glasses activated with cerium depends on the valency state of cerium [57, 97, 101, 102]. Only glasses containing ions of trivalent cerium luminesce. The absorption bands of trivalent cerium are in the region 310-320 nm (3.9-4 ev) [101, 103]. Upon excitation, blue luminescence in the form of a broad band is induced in these bands.

Europium can be present in glasses in two states of oxidation: in the di- and trivalent states. Glasses activated with trivalent europium are colorless. Ultraviolet irradiation causes red luminescence. Glasses activated with divalent europium exhibit blue luminescence in the region 420-440 nm (2.8-3.05 ev) [57, 69, 104-106].

Glasses containing gadolinium are colorless. Borate, phosphate, and silicate glasses containing 10 percent gadolinium, when excited with light at a wavelength of 303 nm (4.1 ev), have a luminescence maximum in the region 311 nm (4 ev) [57].

Glasses activated with terbium and erbium, when excited with ultraviolet rays, produce green luminescence. When special pumping methods are used, these glasses generate at room temperature [57].

Glasses containing dysprosium are colored weakly yellow. Ultraviolet radiation causes yellow luminescence. With increase in the dysprosium concentration from 0.1 to 10 percent by weight, the luminescence spectrum remains practically unchanged [57].

Glasses containing gallium and ytterbium exhibit luminescence in the infrared spectral region [57].

CHAPTER SEVEN

RESONANCE ABSORPTION OF GLASSES AND PYROCERAMICS

In most glasses the electron paramagnetic resonance (EPR) signal is absent if the glasses have not been exposed to ionizing radiation. An exception is found in certain glasses containing paramagnetic ions.

The EPR signal is detected virtually in all glasses after they have been irradiated, which is due to the appearance of unpaired electrons.

1. Problems in the Theory of Electron Paramagnetic Resonance

Owing to the exceptionally high sensitivity, well developed theory, and relative simplicity of interpreting results, the electron paramagnetic resonance method has found wide application in investigating material in the free-radical state or in detecting free radicals forming due to different exposure of a material. Most often the EPR method is employed to detect the free radical state in an irradiated substance. The irradiation of a material is accompanied by the manifestation of unpaired electrons. A system -- a molecule or part of a molecule with an unpaired electron in molecular orbit or in the outermost atomic orbit -- is called a free radical. It is precisely the presence of an unpaired electron that is responsible for the use of EPR method.

Underlying the EPR method is the Zeeman effect: this effect amounts to the following -- when an external constant magnetic field is applied on a paramagnetic particle with quantum number S, its ground level is split into 2S + 1 sublevels. The energy difference between these sublevels is

$$\Delta E = g\beta H,$$

where H is the intensity of the external field; β is Bohr's magneton; and g is the spectroscopic splitting factor [g-factor].

Since in the simplest case a free radical is characterized by a total spin $S_z = \frac{1}{2}$, two Zeeman levels are induced in the magnetic field (Fig. 40).

Obviously, in the case of a free electron the g-factor is roughly 2, more precisely, $g = 2.0023$.

If we assume that $H = 3000$ oersted, then $E = 0.3\ cm^{-1}$. The level populations differ and are governed by the Boltzmann distribution. At ordinary temperatures for our case, level populations differ only slightly (0.2 percent) and are in equilibrium. Therefore, there is a constant exchange of spins between levels, and the population of the lower level will be 0.2 percent larger.

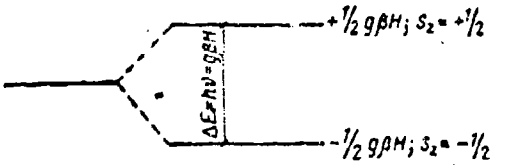

Fig. 40. Arrangement of energy levels of one unpaired electron

If a sample is placed in an alternating magnetic field with frequency ν, then given the condition $h\nu = g\beta H$, some of the electrons from the lower level pass into the upper. This transition is associated with the expenditure of energy. From the upper level some of the electrons move to the lower level, which is accompanied by the release of energy. However, owing to the Boltzmann distribution, the transition of electrons by energy levels from upper to lower is less probable than from lower to upper. The probability of this transition rises with decrease in temperature.

If a high-frequency electrical field with the orientation of the magnetic vector perpendicular to the constant field and with frequency $\nu = g\beta H/h$ is applied to the paramagnetic specimen placed in a constant magnetic field, the level populations tend to become equalized. However, complete equalizing of populations does not take place, since an electron can give off energy and pass from the upper level to the lower.

The EPR spectrum is characterized by the following main parameters: the g-factor, the splitting of electronic levels, ultrafine splitting, and resonance line width. Ultrafine splitting of the lines of electron spin resonance is due to the interaction of the magnetic moment of the unpaired electron and the magnetic moment of the nucleus. The width of the line is due to different interactions: dipole, spin-dipole, spin-lattice, and exchange.

The EPR method has proven highly effective in studying irradiated glasses, though as will be shown below, special conditions can arise in

which this method proves unsuitable. We must note that glass by virtue of its characteristics (high viscosity, isotropicity, and so on) is an exceptional object for study of paramagnetic resonance.

As we know, during irradiation paramagnetic centers of two types are induced: F-centers, that is, electrons localized at negative ion vacancies, and V-centers — holes localized at atoms with smallest affinity for the electron.

Experiment and theory show that even though the g-factor of irradiated material is determined by the free radical state, that is, it is close to 2, still for F-centers the g-factor is somewhat lower, and for V-centers — somewhat higher than 2.

A great deal of information on the nature of centers -- defects arising upon irradiation -- can be obtained by comparing the results of radiospectroscopic and spectroscopic studies of glasses, though a unique solution relative to identifying color centers and paramagnetic centers usually encounters a number of difficulties.

Numerous oxides usually included in glass compositions, and also certain systems of glasses and individual glasses and sometimes even unknown composition have been investigated by the EPR method.

2. Spectra of Electron Paramagnetic Resonance of Crystalline and Fused Quartz

The irradiation of quartz with gamma-rays leads to the initiation of EPR signals [1, 2], which correlate with the optical absorption bands. Thus, a signal with $g = 2.0006$ correlates with the band whose maximum lies in the 210 nm region (5.9 ev), and signals with $g = 2.0007$ and 2.0009 correlate with the 230 nm band (5.4 ev). The presence of a Si^{29} isotope leads to splitting of the signal with $g = 2.00$. A triplet is observed instead of a singlet. This indicates that the signal was produced by an electron localized at silicon [3]. Griffiths and O'Brien [4, 5], studying monocrystalline quartz irradiated with x-rays, detected two lines with $g = 2.06$ and $g = 2.00$. The ultrafine structure is due to the presence of an aluminum impurity. The intensity of the EPR signal causing splitting into six components is proportional to the amount of aluminum [4, 5]. The six-component structure of this signal disappears when the amount of sodium in the glass is increased.

Investigation of resonance absorption in grade KI and KV quartz glasses irradiated with electrons at a dose of 10^6 r showed that in addition to the common resonance line with $g = 2.00$, the EPR spectra also show an appreciable difference.

In a report by Sidorov and Tyul'kin [6], EPR spectra of fused quartz irradiated with gamma-rays at a dose of 10^7 r were studied. The fused

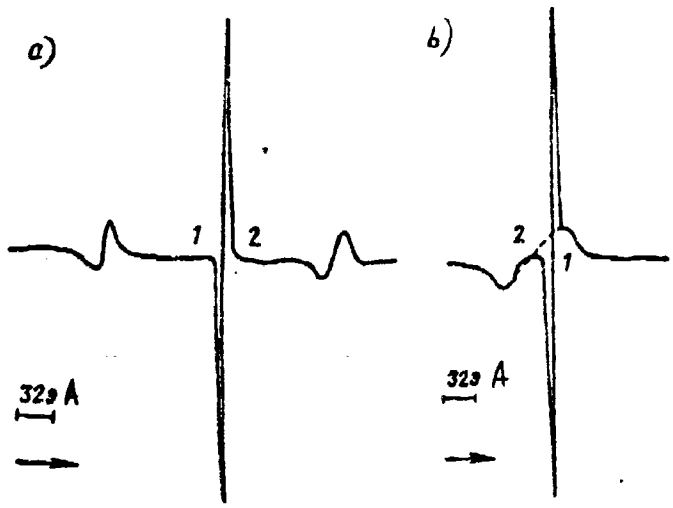

Fig. 41. EPR spectra of glasses irradiated with 10 Mev electrons at dose of 10^6 r
a — KV glass:
1 — g = 2.00
2 — g = 1.98
b — KI glass:
1 — g = 2.00
2 — g = 2.01
KEY: A — 32 oersteds

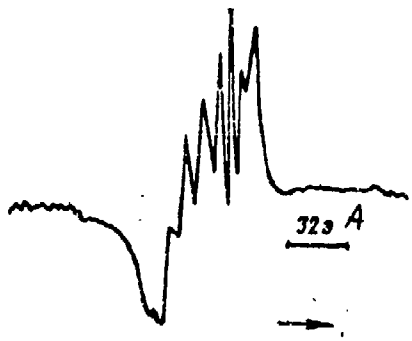

Fig. 42. EPR spectrum of KI glass irradiated with 10 Mev electrons at a dose of 106 r at the temperature of liquid nitrogen
KEY: A — 32 oersteds

quartz spectrum at a relative narrow asymmetric line, typical of the elastically oriented centers with axial symmetry. The well-resolved structure of this line enabled the authors to determine g_{II} and $g_{\perp}$ of this center, which were found to be $g_{II} = 2.002$, and $g_{\perp} = 2.000$, which agrees with $g_{II} = 2.0022 \pm 0.0001$ and $g_{\perp} = 2.0006 \pm 0.0001$ obtained for crystalline quartz [7]. This shows that centers initiated in fused and crystalline quartz after irradiation are of the same kind.

A previously unknown doublet with $g = 1.98$ and a splitting constant of 150 oersteds (Fig. 41 a) was detected in KV glass produced in hydrogen flame. KI glass which has coloring in the visible spectral region after irradiation has a broad signal with $g = 2.01$ (Fig. 41 b), which at liquid nitrogen temperature splits into six components (Fig. 42). This shows the interaction of the unpaired electron with the nucleus whose spin is 5/2 (properly, with the nucleus of aluminum).

The doublet found (cf. Fig. 41 a) can be caused by the paramagnetic center associated with hydroxyl, though the splitting constant differs from the value given in the work [8]. This difference can be explained by the effect of the matrix, just as we know in the case of the EPR spectra of nitrogen radicals [9]. Possibly, the signal is caused not by an OH group, but by a Si-OH group. In this case the reduction in splitting compared with atomic hydrogen (505 oersteds) can be counted for by the effect of OH bonding.

3. Spectra of Electron Paramagnetic Resonance of Silicate Glasses

Van Wieringen and Kats [sic] [10] detected two absorption lines in a simple glass with the composition $Na_2O \cdot 2SiO_2$. One line with $g \approx 1.96$--1.97 is ascribed to the electron captured at the alkali metal ion, and the other line with $g \approx 2.01$ -- to the presence in the system of a whole at the terminal, nonbridging, oxygen atom. This structure was obtained in sodium silicate glasses [11], and also in the work [12] when a study was made of a glass with composition $SiO_2 \cdot M_2O$ enriched with Si^{29} isotope, but was not detected in lithium silicate glasses [6].

The work [11] showed that if quartz glass after irradiation produces a very narrow EPR band with $g = 2$, then upon the transition to sodium silicate glasses one more band is produced with $g > 2$, and on attainment of composition corresponding to sodium disilicate, the band typical of quartz glass disappears totally and only the band with $g = 2.01$ typical of sodium silicate glass remains. By the authors' assertion, localization of an unpaired electron occurs at silicon. When the concentration of the alkali oxide is increased in the glass, the relative proportion of capture centers typical of quartz becomes less and disappears entirely at the composition $Na_2O \cdot 2SiO_2$, while the proportion of paramagnetic centers typical of the disilicate attains a large value in this case.

Glasses of the system Na_2O-B_2O_3-SiO_2 have a very complicated spectrum, therefore adding silicon oxide appreciably complicates the picture: paramagnetic centers typical of B_2O_3 appear. By comparing data from optical spectra and EPR spectra, the authors concluded that not all factors responsible for supplementary absorption bands can be detected by the EPR method.

Adding aluminum oxide to a glass leads to a very interesting pattern [12]. The authors studied sodium aluminum silicate glasses irradiated with x-rays and with neutrons and detected spectra of two types: the first type consists of six equidistant, partially resolved lines with spacings of 8.1 oersteds; the second type is an asymmetric line with $\Delta H = 18$ oersteds. The last spectrum appears after the specimen has been heated to 350° C; here the resonance line of the first type disappears. It is assumed that the first type of resonance curve is caused by a hole captured by a bridging oxygen which is bonded to an impurity aluminum ion. The second type is associated with a hole at a nonbridging oxygen. Measurement of the dependence of the EPR line intensity on the Al_2O_3 content in glass shows that impurity aluminum ions, forming the groups $[AlO_4]$ can cause nonbridging oxygen ions to appear. Only a broad line is observed in sodium aluminum silicate glasses. Nonbridging oxygen ions with holes localized at these ions are caused by the presence of Na_2O. Irradiating glasses with neutrons causes the additional narrow intense line produced by electrons captured by the silica framework to appear.

Investigations of lithium aluminum silicate glasses [13] showed the presence of two types of hole centers: the first type amounts to a hole localized at the terminal, nonbridging, oxygen atom bound to a silica atom, and the second consists of a hole localized at an oxygen atom bound to an aluminum atom. In glasses with $Li_2O:Al_2O_3 = 1$, only centers of the second type are present.

Glasses with composition $4SiO_2 \cdot Na_2O \cdot 0.5Me_xO_y$ or $0.25Me_xO_y$ have primarily an EPR spectrum of two types [14]. Glasses containing Li_2O and oxides of rare earth have spectra consisting of two components: narrow ($\Delta H = 10$ oersteds) with g 2.0087 $\pm$ 0.0005 and wide ($\Delta H = 56$ oersteds with $g = 1.9587$). Very similar to the spectra is the spectrum of glass containing La_2O_3. Glasses with composition $4SiO_2 \cdot Na_2O \cdot 0.25B_2O_3$ and $4SiO_2 \cdot Na_2O \cdot 0.25Al_2O_3$ have similar spectra, but with a narrower component at g 2.0023 ($\Delta H = 26$ oersteds). Even less absorption at g 2.002? is shown by glasses containing SnO, ZrO_2, and CdO (Table 17). We can classify in the second group glasses containing PbO, Nb_2O_5, GeO_2, SnO_2, and In_2O_3, and which have, for $g < 2.0023$, very limited absorption or none at all.

TABLE 17. EPR SPECTRA OF GLASSES WITH THE COMPOSITION $4SiO_2 \cdot Na_2O \cdot nM_xO_y$

Состав стекол 1	Линия поглощения 2			
	узкая 3		широкая 4	
	ΔH_1	g_1	ΔH_2	g_2
$4SiO_2 \cdot Na_2O \cdot 0{,}5MgO$	12,2	2,0110	61,5	1,9600
$4SiO_2 \cdot Na_2O \cdot 0{,}5CaO$	9,95	2,0082	58,2	1,9589
$4SiO_2 \cdot Na_2O \cdot 0{,}5SrO$	9,95	2,0082	53,5	1,9590
$4SiO_2 \cdot Na_2O \cdot 0{,}5BaO$	9,90	2,0092	50,5	1,9586
$4SiO_2 \cdot Na_2O \cdot 0{,}25Li_2O$	10,75	2,0082	58,1	1,9572
$4SiO_2 \cdot Na_2O \cdot 0{,}25La_2O_3$	15,30	2,0082	61,2	1,9610
$4SiO_2 \cdot Na_2O \cdot 0{,}25B_2O_3$	13,00	2,0073	26,0	1,9646
$4SiO_2 \cdot Na_2O \cdot 0{,}25Al_2O_3$	10,70	2,0082	26,0	1,9684
$4SiO_2 \cdot Na_2O \cdot 0{,}5ZrO_2$	13,8	2,0078	23,0	1,9720
$4SiO_2 \cdot Na_2O \cdot 0{,}5ZnO$	13,0	2,0082	22,9	1,9860
$4SiO_2 \cdot Na_2O \cdot 0{,}5CdO$	13,0	2,0073	12,25	1,9897
$4SiO_2 \cdot Na_2O \cdot 0{,}5GeO_2$	9,95	2,0082	7,65	1,9989
$4SiO_2 \cdot Na_2O \cdot 0{,}5SnO_2$	19,9	2,0140	10,70	1,9980
$4SiO_2 \cdot Na_2O \cdot 0{,}5PbO$	39,8	2,0120	—	—
$4SiO_2 \cdot Na_2O \cdot 0{,}25In_2O_3$	13,6	2,0073	—	—
$4SiO_2 \cdot Na_2O \cdot 0{,}25Nb_2O_5$	16,3	2,0082	—	—

KEY: 1 -- Glass composition
2 -- Absorption line
3 -- narrow
4 -- wide

A special place is occupied by glasses containing arsenic and antimony. Characteristic of the first is a highly complex EPR spectrum consisting of five absorption bands, with ΔH = 18.35 oersteds at g = 2.0188, ΔH_2 = 6.12 oersteds at g = 2.0054, ΔH_3 = 6.5 oersteds at g = 1.9888, ΔH_4 = 10.7 oersteds at g = 1.9851, and ΔH_5 = 7.65 oersteds at g = 1.9600. A glass with a composition $4SiO_2 \cdot Na_2O \cdot 0.25Sb_2O_3$ shows practically no resonance absorption in the g-factor region studied.

4. Spectra of Electron Paramagnetic Resonance of Borate and Phosphate Glasses

The spectrum of borate glass irradiated with gamma-rays has sharp resonance absorption lines at g = 2, calculating four components of ultrafine structure ΔH = [illegible] oersteds. The author attributes this ultrafine structure to the initial action of the electron removed from an oxygen atom with the nucleus of B^{11}, which has a nuclear spin I = 3/2 [15].

The work [11] studied two types of glasses prepared from boric anhydride. One was obtained from natural boron oxide; B_2O_3 enriched with

B^{10} isotope was used for the other. Both glasses had quite complex, but distinct spectra. As in the work [15], the spectrum was ascribed to an electron localized at boron and, therefore, the complexity of the spectrum is due to the fully resolved ultrafine structure.

Alkali-borate glasses irradiated with gamma-rays at a dose of $5 \cdot 10^6$ r [15] yield a signal somewhat distinct from the signal of pure fused boric anhydride and its occurrence is ascribed to the unpaired electron of the alkali metal. The difference is that the extreme maximum disappears, with simultaneous deterioration of the resolution of all the remaining components [11]. It is assumed that the electron in the glasses is localized at boron and that the spectrum is caused by the incompletely resolved ultrafine structure that results from the free electron interacting with the boron atom. Introducing an alkali oxide modifies the coordination of boron from ternary to quaternary or at least increases the proportion of BO_4 groups. Owing to the different spin-orbital interaction of electron with the nucleus of three- and four-coordinated boron, the EPR lines are somewhat displaced relative to $g = 2$.

Karapetyan and Yudin [16] investigated the system $Me_xO_y \cdot P_2O_5$, where Me_xO_y = 0.5 Na_2O, 0.5 ZnO, and 0.5 CaO. The spectrum of these glasses consists of two lines with an ultrafine structure resulting from the interaction of an unpaired electron with the P^{31} nucleus, which has a nuclear spin of $\frac{1}{2}$. The intensity of the EPR spectrum depends on the phosphate content and the gamma-irradiation dose. The g-factor is 2.01 ± 0.004, and the ultrafine splitting constant is 41 oersteds.

Based on a detailed examination of the models of phosphate glasses, the authors concluded that the electron capture centers in these glasses are $[PO_4]$ groups, and not oxygen vacancies near alkali ions, as was earlier assumed.

5. Kinetics of the Breakdown of Paramagnetic Centers

Ubersfeld [17], investigating a good many glasses (Pyrex, borosilicate crown, light flint, and so on) irradiated with neutrons and gamma-rays, detected an isolated resonance absorption line with $g = 2.002 \pm 0.005$ and $\Delta H = 45 \pm 7$ oersteds. One year after irradiation he did not find any change in the number of paramagnetic centers (PMC). Disappearance of PMC occurs only with heating to 200° C.

The PMC breakdown kinetics of glasses with the composition $4SiO_2 \cdot 2Na_2O \cdot 0.5Me_xO_y$ ($0.25Me_xO_y$) irradiated with gamma-rays was studied more closely. Based on EPR spectra recorded 1, 7, 30, and 110 days after irradiation, the paramagnetic center concentration was calculated (PMC/g).

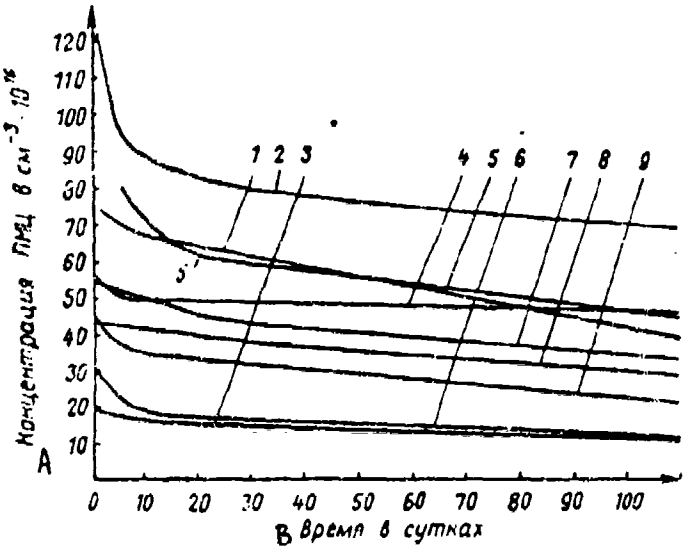

Fig. 43. Breakdown of paramagnetic centers with time for glasses with the following compositions

1 -- $4SiO_2 \cdot Na_2O \cdot 0.5CaO$

2 -- $4SiO_2 \cdot 0.5SrO$

3 -- $4SiO_2 \cdot Na_2O \cdot 0.5ZnO$

4 -- $4SiO_2 \cdot Na_2O \cdot 0.5MgO$

5 -- $4SiO_2 \cdot Na_2O \cdot 0.5BaO$

6 -- $4SiO_2 \cdot Na_2O \cdot 0.5SnO_2$

7 -- $4SiO_2 \cdot Na_2O \cdot 0.5CdO$

8 -- $4SiO_2 \cdot Na_2O \cdot 0.5PbO$

9 -- $4SiO_2 \cdot Na_2O \cdot 0.25As_2O_3$

KEY: A -- Concentration of PMC in $cm^{-3} \cdot 10^{16}$
B -- Time in days

The annealing curves (Fig. 43) show that as a rule the rate of annealing of paramagnetic centers during the first 7-10 days is much higher than in the subsequent annealing period. Naturally, for glasses containing maximum number of PMC the annealing rate during the first days is very high (glasses containing CeO_2, MgO, SrO, and Li_2O). However, the correlation is not observed for glasses containing CaO and BaO in which the PMC concentration falls off quite monotonely. In glasses containing arsenic, antimony, niobium, germanium, and zirconium, annealing of PMC also proceeds in two stages. The PMC annealing curves for glasses containing calcium,

Table 18. BREAKDOWN OF PMC WITH TIME

A Состав стекла	Константы ПМЦ при отжиге стекол B	
	быстром (менее 10 суток) C	медленном (более 10 суток) D
$4SiO_2 \cdot Na_2O \cdot 0{,}25Li_2O$	0,81	0,09
$4SiO_2 \cdot Na_2O \cdot 0{,}25B_2O_3$	—	0,058
$4SiO_2 \cdot Na_2O \cdot 0{,}5MgO$	0,69	0,05
$4SiO_2 \cdot Na_2O \cdot 0{,}25Al_2O_3$	—	0,0686
$4SiO_2 \cdot Na_2O \cdot 0{,}5CaO$	—	0,09
$4SiO_2 \cdot Na_2O \cdot 0{,}5ZnO$	0,3	0,05
$4SiO_2 \cdot Na_2O \cdot 0{,}5GeO_2$	0,6	0,033
$4SiO_2 \cdot Na_2O \cdot 0{,}5As_2O_3$	0,56	0,0778
$4SiO_2 \cdot Na_2O \cdot 0{,}5SrO$	0,81	0,0556
$4SiO_2 \cdot Na_2O \cdot 0{,}5ZrO_2$	0,33	0,04
$4SiO_2 \cdot Na_2O \cdot 0{,}25Nb_2O_5$	0,56	0,35
$4SiO_2 \cdot Na_2O \cdot 0{,}5CdO$	—	0,058
$4SiO_2 \cdot Na_2O \cdot 0{,}25In_2O_3$	—	0,067
$4SiO_2 \cdot Na_2O \cdot 0{,}5SnO_2$	0,49	0,053
$4SiO_2 \cdot Na_2O \cdot 0{,}25Sb_2O_3$	—	—
$4SiO_2 \cdot Na_2O \cdot 0{,}5SnO_2$	0,11	0,0556
$4SiO_2 \cdot Na_2O \cdot 0{,}25La_2O_3$	0,1	0,063
$4SiO_2 \cdot Na_2O \cdot 0{,}5PbO$	1,17	0,09

KEY: A -- Glass composition
B -- PMC constants when glass annealing is conducted as listed
C -- fast (less than 10 days)
D -- slow (more than 10 days)

aluminum, cadmium, and zinc, and to a less extent for glasses containing boron have no well-defined inflection.

The annealing constants of PMC calculated from experimental data are given in Table 18. From this table it is clear that the rate constants for so-called "rapid" annealing of PMC (less than 10 days) as a rule is 5-20 times greater than for "slow" annealing (more than 10 days). The constants of slow annealing of paramagnetic centers are approximately the same for glasses containing oxides of aluminum, lithium, cadmium, tin, and strontium.

6. Electron Paramagnetic Resonance Spectra of Pyroceramics

Pyroceramics exposed to ionizing radiation produce EPR spectra usually consisting of several signals. The most typical spectral lines are the lines with $g = 2.001 \pm 0.002$ and $\Delta H = 2 \pm 0.5$ oersteds, caused by an electron associated with the silicon atom, and a line with $g = 2.009 \pm 0.005$ and $\Delta H = 10.5 \pm 2$ oersteds caused by a hole localized at a non-bridging oxygen atom. In addition, depending on the chemical composition of the pyroceramic, a broad asymmetric line is observed, which in the presence of titanium has $g = 1.94 \pm 0.01$ and $\Delta H = 75 \pm 5$ oersteds.

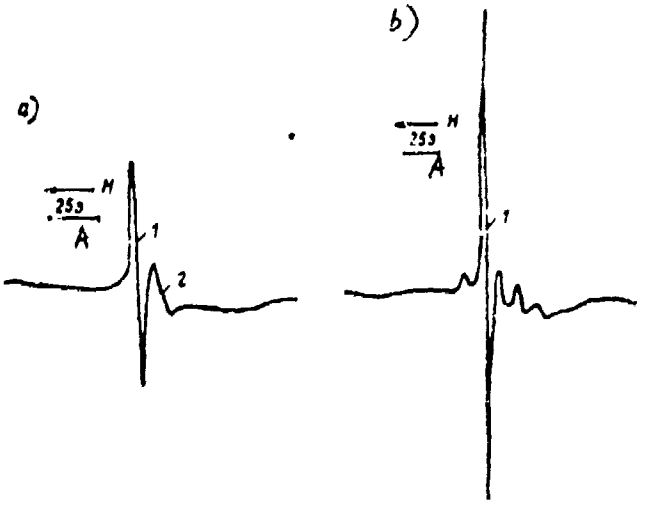

Fig. 44. EPR spectra recorded after irradiation with a dose of 10^{18} neutrons/cm^2
a -- glass IV-23
b -- pyroceramic IV-23
1 -- $g = 2.001$
2 -- $g = 2.009$
KEY: A -- 25 oersteds

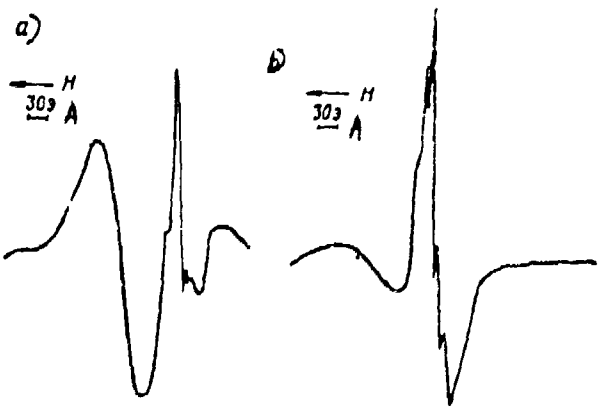

Fig. 45. EPR spectra of glass (a) and pyroceramic (b) with composition $Li_2O \cdot Al_2O_3 \cdot 4SiO_2 \cdot 2B_2O_3$ irradiated with a dose of 10^{18} neutrons/cm^2
KEY: A -- 30 oersteds

By comparing the EPR spectra of glasses and pyroceramics with identical chemical compositions irradiated with the same dose, we must above all refer to the intensified EPR signals for pyroceramics [18]. Crystallization of glass intensifies the components of the ultrafine spectral structure, so revealing the spectral structure of pyroceramics requires a lower radiation dose than for glasses (Fig. 44).

Beside this effect, certain changes in the spectral structure are observed in the transition from glasses to pyroceramics. For example, the signal produced by an electron center ($g = 2.001 \pm 0.0002$ and $\Delta H = 2 \pm 0.5$ oersteds), well-defined in the spectra of pyroceramics of lithium- and magnesium-aluminum silicate systems after reactor or gamma-ray irradiation, are absent in the initial uncrystallized glasses. At the same time the broad signal caused by the electron captured by the Ti^{4+} ion ($g = 1.94 \pm 0.01$ and $\Delta H = 75 \pm 5$ oersteds), observed in all titanium-containing glasses, is weakened in pyroceramics irradiated under the same conditions (Fig. 45).

Depending on the conditions and kind of irradiation, spectra are modified as follows: in the transition from reactor irradiation to irradiation with a Co^{60} source, splitting of the signal associated with the hole center is observed now at a radiation dose of 10^6 r, while neutron irradiation produces the same effect only at integral beams of the order of 10^{18} neutrons/cm^2 (which corresponds to a dose of 10^8 r).

The intensifying EPR signal of pyroceramics, as well as the increase in the increment of the optical density of transparent pyroceramics compared with the initial glasses after equal radiation doses, indicates diminished radiation resistance after pyroceramization.

CHAPTER EIGHT

EFFECT OF TEMPERATURE ON COLOR CENTER FORMATION AND BREAKDOWN

Investigating the kinetics of the accumulation of color centers at different temperatures, their thermal annealing (thermodecolorizing) and accompanying processes (thermal de-excitation, change in electroconductivity, and so on) is necessary for a proper understanding of the structure and mechanism of the formation of centers, to determine their energy parameters, and to establish the possible uses of glasses in different static and dynamic temperature conditions of service. Selecting test compositions must be determined above all by the task assigned.

Commercial multicomponent glasses can be investigated only to discover the possibilities of their service under specific conditions, since a complex chemical composition affords virtually no possibilities of reaching any conclusions on the mechanism of processes occurring in glasses at different temperatures. This purpose requires that we investigate glasses with simple chemical compositions in which the components are varied. We must particularly single out quartz glasses, whose study is of interest both from the standpoint of practical service as well as from the standpoint of understanding the mechanism of radiation processes.

1. Induced Optical Absorption at Different Irradiation Temperatures

In spite of the considerable interest posed by measuring induced optical absorption at different irradiation temperatures, the number of studies in this field is small, which is evidently accounted for by complexities of technique. The latter are particularly large when we are concerned with acquiring data at arbitrarily selected temperatures that are not reference boiling or melting points of any substance (nitrogen, carbon dioxide, and so on). Of the works dealing with a comparison of induced optical absorption of glasses irradiated at room temperatures and at temperatures close to the liquid nitrogen temperature, we must take note of studies [1-4]. They described several investigations of quartz glasses [1], boric anhydride glasses, and alkali-silicate and alkali-borosilicate glasses [3, 4]. When the studies are conducted, of interest

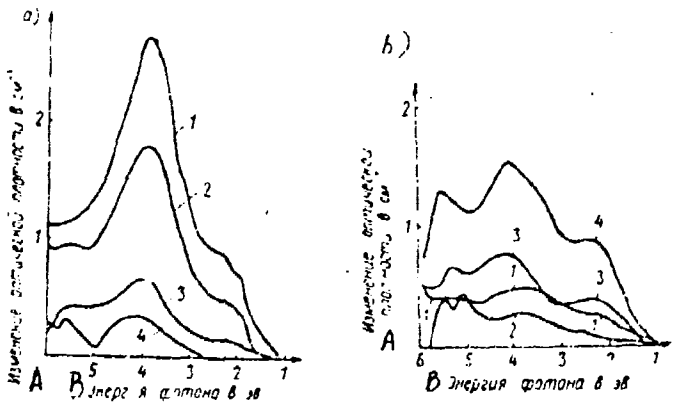

Fig. 46. Spectra of induced optical absorption of quartz glass at different irradiation temperatures

a -- KV glass
b -- KI glass
1 -- 120° K
2 -- 180° K
3 -- 240° K
4 -- 300° K

KEY: A -- Change in optical density in cm^{-1}
B -- Photon energy in ev

is the effect of temperature on the position of the spectral absorption bands as well as on their intensities.

Quartz glass

In quartz glass irradiation produces bands of supplementary optical absorption in the regions 220, 240, 500, and 540 nm (5.7, 5.2, 4.1, and 2.3 ev) (corresponding to the C-, B_2-, B_1-, and A-bands). At room irradiation temperatures, the 2.3 ev band in glasses melted in the flame of an oxygen-hydrogen torch is either observed at very large radiation doses or is not observed at all.

Changing the irradiation temperature fundamentally alters the pattern observed. KV and KI quartz glasses underwent x-ray irradiation on a URS-60 unit (tube containing constant anticathode U_{tu} = 50 kv, I = 10 ma) for 1 hour at an irradiation temperature of 120-300° K. Curves shown in Fig. 46 reveal several interesting correlations. In KI glass a reduction in the irradiation temperature causes reduced intensity of all absorption bands. The maximum of the B_1-band here is shifted toward the long-wave

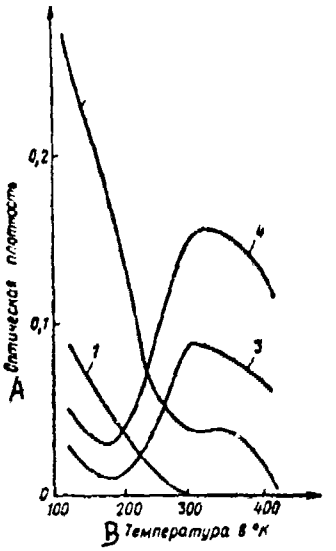

Fig. 47. Thermal de-excitation in the region of the following maxima
1 and 3 -- 2.3 ev
2 and 4 -- 4.1 ev
____ KV glass
_ _ _ _ KI glass
sample thickness 1 mm
KEY: A -- Optical density
B -- Temperature in ^{o} K

portion of the spectrum from 300 nm (4.1 ev) at 300° K to 330 nm (3.75 ev) at 120° K. The minimum intensities of the B_1- and A-bands are observed at an irradiation temperature of 180° K. A further drop in the temperature down to 120° K somewhat boosts the intensities of these bands.

A sharp intensifying of the induced optical absorption is observed for KV glass when the irradiation temperature is lowered. Even at 240° K the A-band absent in the case when irradiation is conducted at 300° K is observed. A further drop in the irradiation temperature intensifies this band, which becomes much more intense at 180 and 120° K than in KI glass at the same temperatures. The B_1-band behaves similarly: its intensity also is strongly increased with a reduction in the irradiation temperature. The maximum of this band is less distinctly displaced for the long-wave portion of the spectrum from 300 nm (4.1 ev) at 300° K to 315 nm (3.95 ev) at 120° K than in KI glass. The dependence of the intensities of the A- and B-bands in the KI and KV glasses on irradiation temperature is shown in Fig. 47.

Noteworthy is the similar course of the dependences of the intensity of supplementary absorption on the temperature of the A- and B_1-bands. This analogy is quite readily observable in KI glass owing to the presence of extrema (minimum in the area 180° K and maximum in the area 300° K). Of note is the fact that the radiation-optical stability of glass depends heavily on the irradiation temperature and that this function can be quite diverse.

Interestingly, the maximum of the B_1-absorption band is observed to be displaced not only with variation in temperature, but also with change in the impurity present in the quartz glass. Lell [6] showed that in quartz glass containing 0.2 percent aluminum the B_1-absorption band has the maxima 275, 300, 305, and 310 nm (4.5, 4.1, 4.05, and 4 ev), depending on whether the presence of aluminum is combined with that of hydrogen, lithium, sodium, and potassium, respectively. This factor lends added interest to studying induced optical absorption in simple-composition glasses where both the irradiation temperature and glass composition are changed.

Simple-composition Glasses

The most detailed investigations of oligocomponent glasses at liquid nitrogen temperatures were conducted in 1964 by Orlov and Leko [4] (Table 19).

The studies reveal several correlations relating the irradiation temperature, ionic radius of alkali ion, glass matrix, and the intensity of induced optical absorption. In alkali-silicate glasses reducing the irradiation temperature leads to stronger supplementary optical absorption mainly in the visible region of this spectrum.

The rise in optical density with the radiation temperature reduced (compared with glasses irradiated at room temperature) is roughly proportional to the alkali ion concentration. For the identical alkali ion concentrations, for example K^+ and Na^+, the intensity of induced optical absorption increases to a greater extent with a reduction in irradiation temperature than with a reduced cation radius. In alkali-borate glasses and in so-called leached alkali-porosilicate glasses, the change in optical density with decrease in irradiation temperature (compared with the radiation at room temperature) occurs mainly in the ultraviolet spectral region in the vicinity of 240 nm (5.2 ev).

The fact that a decrease in the ionic radius of an impurity ion leads to a much sharper rise in optical density with reduction in irradiation temperature afford. some analogy between KI quartz glass and the simple-composition glasses we have been discussing. A steep rise in the intensity of supplementary optical absorption in KV quartz glasses evidently

TABLE 19. COMPOSITIONS OF GLASSES STUDIED [4]

Номер стекла A	Состав стекла в мол. % B			
	SiO_2	B_2O_3	Na_2O	K_2O
1	80	—	20	—
2	60	—	40	—
3	80	—	—	20
4	—	80	20	—
5	60	32	8	—
6	57,1	14,3	28,6	—

KEY: A -- Glass number
B -- Glass composition in mole percent

TABLE 20. EFFECT OF IRRADIATION TEMPERATURE ON INDUCED OPTICAL ABSORPTION OF CERTAIN THREE-COMPONENT GLASSES

Состав стекла A	Наведенное оптическое поглощение при температуре в °K B		
	290	340	390
$4SiO_2 \cdot Na_2O \cdot 0{,}5SnO_2$	0,03	0,02	0,00
$4SiO_2 \cdot Na_2O \cdot 0{,}5GeO_2$	0,24	0,16	0,07
$4SiO_2 \cdot Na_2O \cdot 0{,}5ZnO$	0,32	0,23	0,20
$4SiO_2 \cdot Na_2O \cdot 0{,}25Li_2O$	0,75	0,41	0,31

KEY: A -- Glass composition
B -- Induced absorption at listed temperature in ° K

caused by the fact that the formation of color centers is associated with the hydrogen ion, not with the metal ion as in KI glass.

Several three-component glasses in which the third component was varied underwent irradiation with gamma-rays from a Co^{60} source at 290, 340, and 390° K with a dose of 10^7 r. The glass composition and the variation in glass optical density after irradiation are listed in Table 20.

From Table 20 we can see that the higher irradiation temperature reduced the coloring of the glass, probably caused by thermal annealing.

As for alkali-halide crystals, we know that there is an optimal irradiation temperature at which the formation of F-centers takes place most effectively, which indicates the participation of ionic processes in the formation of F-centers at a high enough temperature. The processes can include

breaking up of vacancy groups [7,8] and the displacement of ionized halides into cationic vacancies [9].

In silicate glasses we observed a decrease in coloring with increase in irradiation temperature. However, this fact does not yet mean that ionic processes do not play some role in the formation of color centers in glasses. Reducing the radiation temperature can lead to lower thermal annealing of centers during irradiation and have a more significant effect on the concentration than ionic processes. When thermal annealing is slight at room temperature (KI quartz glass), a reduction in the radiation temperature leads to less coloring.

Commercial-composition glasses

The radiation in the commercial-composition glasses K-8, K-108, K-208, LK-5, and LK-105 leads to a change in optical density, but individual absorption bands cannot be differentiated. In all cases irradiation with gamma-rays at 77, 300, and 400° K shows that optical density attained at low temperature is high. Even in K-208 glass which is resistant to radiation doses up to 10^7 r, irradiation at 77° K at a dose of $3 \cdot 10^6$ r enables coloring to be detected. However, centers formed at the low temperature can be unstable at room temperature, and heating glasses irradiated at 77° K up to 300° K leads to a significant decolorizing. In this case, the higher the irradiation temperature, the more stable are the centers formed (Fig. 48).

Effectiveness of accumulation of color centers at different temperatures

The effectiveness of color center formation at different temperatures is of high interest for the researchers on two counts. First of all, the same sample is investigated at different temperatures, which does away with the scatter of results from sample to sample. Secondly, investigations are conducted at low radiation temperatures, which permits to a large extent neglecting the radiation breakdown of color centers.

The effectiveness of color center formation is determined from the expression $\chi(\Delta n/\Delta q)$ (where Δn is the rise in the color center concentration upon irradiation with a dose of Δq). The quantity $(\Delta D/\Delta t) = (\Delta n/\Delta q) = \chi$ was found experimentally. These investigations were conducted on KI and KV quartz glasses. After irradiation with a dose of Δq and measurement of the spectra of optical absorption, the sample is annealed at 170° K in air for 20 minutes for the total breakdown of radiation color centers. The annealing conditions were selected in accordance with the work [10], and the effectiveness was verified by the extent of recovery of optical absorption. After annealing, the specimen was irradiated at the same dose, but now at different temperature in the range 120-420° K (Fig. 49).

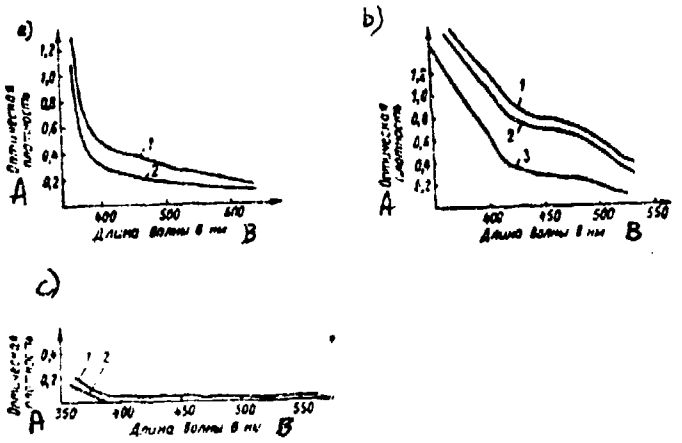

Fig. 48. Absorption spectra of irradiated glasses recorded at different temperatures with 3 mm thick samples

a -- K-108 glass, room temperature
b -- LK-105 glass, room temperature
c -- K-208 glass, 77° K
1 -- gamma-irradiation temperature 77° K
2 -- 300° K
3 -- 400° K

KEY: A -- Optical density
B -- Wavelength in nm

It must be remembered that heating a sample in air at 170° K does not restore optical density to its initial level. Still, the curves presented can be regarded as reliable, since the increment in optical density enters into the expression for χ. The fact that the change ΔD at different temperatures for a selected small dose $\Delta\Phi$ is linear is confirmed by the fact that after multiple irradiation and annealing, the value of χ for all bands except for the 540 nm band (2.3 ev) is easily reproduced. The effectiveness of formation of the color centers responsible for absorption in the region 540 nm (2.3 ev) falls off considerably, and evidently the corresponding curves are in need of correction.

2. Thermal De-excitation of Glasses

When glasses are irradiated, some of the absorbed energy can be released as light upon heating. The temperature dependence of the intensity of thermal de-excitation characterizes the level of traps at which electrons or holes are localized during irradiation. The spectral composition of the luminescence stimulated by heating affords conclusions on the nature of centers whose breakdown is responsible for thermal de-excitation.

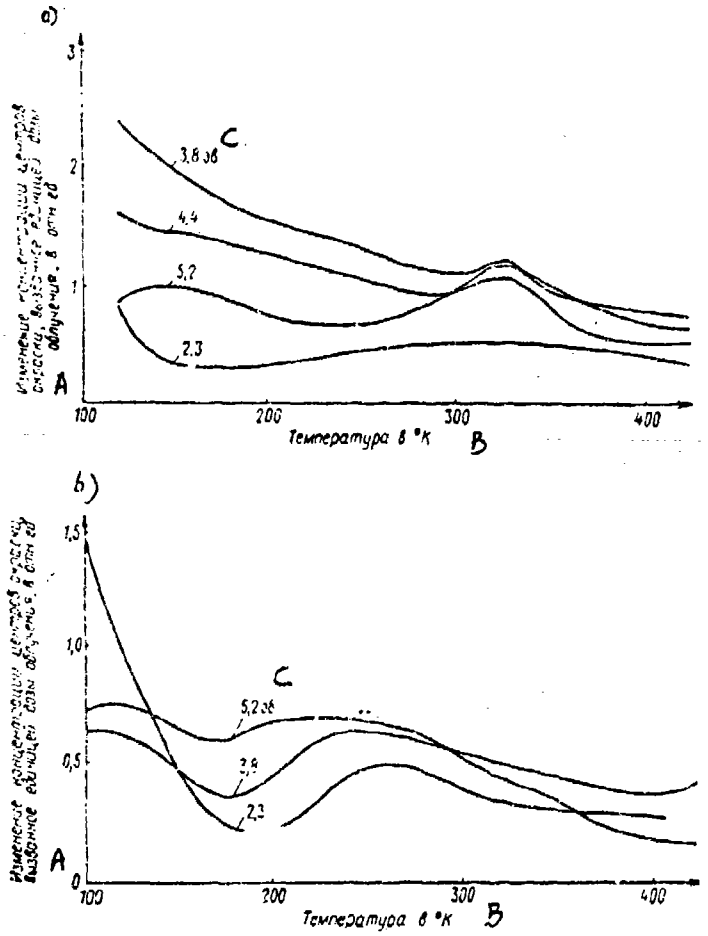

Fig. 49. Effectiveness of color formation in quartz glasses for the fundamental absorption bands (numbers next to curves) as a function of irradiation temperature

a -- KV glass
b -- KI glass
KEY: A -- Change in concentration of color centers produced per unit radiation dose, in relative units
B -- Temperature in ° K
C -- ev

Thermal de-excitation of glasses at low temperatures

The phenomenon of thermal de-excitation at low temperatures was observed by Kikuchi [11]. He detected spikes of thermal de-excitation of sodium silicate and quartz glasses irradiated with x-rays. Spikes were observed at 130° K, and in quartz glass the spike is much broader and has

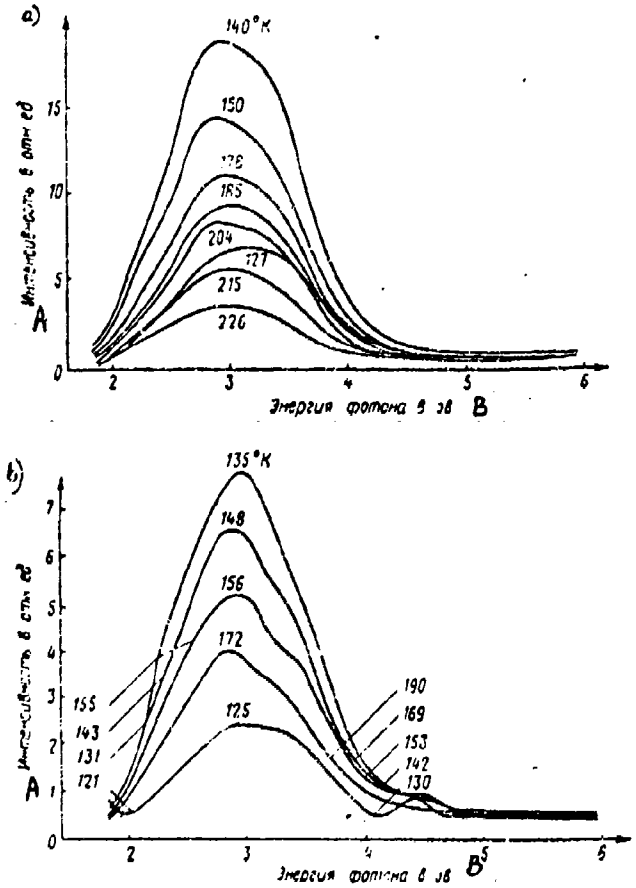

Fig. 50. Spectral composition of thermal de-excitation of quartz glass irradiation with x-rays at 120° K for 1 hour

a -- KV glass
b -- KI glass
KEY: A -- Intensity in relative units
B -- Photon energy in ev

a second maximum in the temperature range 180-190° K. The low-temperature thermal de-excitation spike was not detected after an investigation of crystal quartz, therefore Yokota [12] maintained that the broad low-temperature band of thermal de-excitation is a specific feature of the glassy state. In the spectrum of sodium silicate glass Kikuchi [13] observed two broad spikes, one of which also corresponds to increased temperature. These bands indicate the presence of two capture levels of electrons differing in depth, which agrees with concepts of the electronic structure of amorphous substances proposed by Froehlich [14].

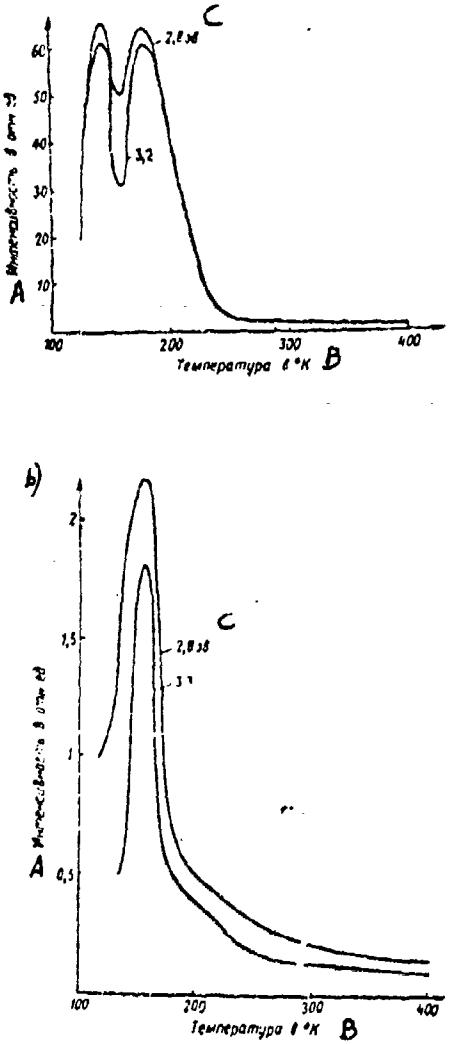

Fig. 51. Temperature dependence of the intensity of thermal de-excitation of glass for the quanta 2.8 and 3.2 ev

a -- KV glass

b -- KI glass

KEY: A -- Intensity of relative units

B -- Temperature in ° K

C -- ev

Low-temperature thermal de-excitation was observed by Starodubtsev et al. in crystalline quartz [15]. Irradiation of quartz at 96° K with 100 kev protons at a dose of $6.2 \cdot 10^{14}$ protons/cm^2 produces four thermal de-excitation spikes at temperatures of 120, 200, 237, and 256° K, which contradicts the viewpoint of Yokota [12]. Evidently, the problem is that upon irradiation with low-energy protons color centers are formed, but the localization of electrons liberated upon irradiation takes place at levels responsible for the thermal de-excitation effect. When irradiation is performed with x-rays, primarily centers responsible for optical absorption are formed. In this case thermal de-excitation in crystalline quartz is observed only at temperatures somewhat above room temperature [11]. The thermal de-excitation spike is also observed in quartz glass at a temperature of 80° K [16].

Studies of spectral composition and thermal de-excitation spikes at low temperatures were conducted by the authors on domestic KI and KV quartz glasses. Samples were irradiated with x-rays at 120° K. The heating rate was about 0.5 deg/sec. The spectral characteristics of thermal de-excitation are shown in Fig. 50. During the spectral recording period, the sample temperature was varied, therefore Fig. 50 b shows not only the temperatures at which the maximum in the spectral curve was recorded, but also the temperatures for certain other spectral points. The luminescence spectrum is characterized by maxima in the regions 440 and 390 nm (2.8 and 3.2 ev).

The temperature dependence of the luminescence intensity is shown in Fig. 51 for quanta of these energies. KV glass has two thermal de-excitation spikes in the regions 140 and 180° K. A maximum in the region 150° K is observed for KI glass. In addition, luminescence with its maximum in the region 280 nm (4.4 ev) is observed in the temperature region below 140° K. The thermal de-excitation spectra of these glasses agrees mainly with the spectra of x-ray luminescence, indicating the possible identity of the luminescent centers in these two cases. However, there are several differences. Thus, the x-ray luminescence spectrum of KI glass is marked by a maximum in the region 480 nm (2.6 ev), while the spectrum of thermal de-excitation has its maximum in the region 440 nm (2.8 ev).

Comparing the spikes of thermal de-excitation of quartz glasses with the spikes of heat-stimulated electroconductivity (cf. Chapter Nine) shows the spatial differentiation during irradiation of charge carriers and de-excitation centers.

Thermal de-excitation of glasses at elevated temperatures

Much more work has involved thermal de-excitation of glasses irradiated at room temperature than low-temperature thermal de-excitation. Both simple-composition glasses as well as commercial-composition glasses were investigated.

Thermal de-excitation of fused and quartz glass is described in the literature [7-19]. Three thermal de-excitation spikes were observed in crystalline quartz, and their intensity depends also on the location of the quartz, indicating a relationship between thermal de-excitation and impurities [17]. Thermal de-excitation of fused quartz has a maximum in the region 600° K, however often a second spike is observed near 380° K [19]. The spectral band is very wide and has a maximum in the region 436 nm (2.85 ev) [19]. Investigation of the thermal de-excitation of simple-composition glasses was made by Stepanov [20], who found two or three thermal de-excitation spikes, whose positions are shown in Table 21.

Virtually the same thermoluminescence spikes are observed in the spectra of silicate glasses as in crystalline quartz. The difference lies in the greater blurring of the spectra of thermal de-excitation of glasses compared with the quartz spectrum.

Vavilin and Stepanov maintained that the nature of the thermoluminescence spikes is determined only by the state of the SiO_4 tetrahedra (the presence of bridging and nonbridging oxygen ions). Hence it follows that the luminescent centers are near silicon atoms. The effect of different cations reduces to the appearance and disappearance, when they are introduced, of nonbridging oxygen ions in the glass structure. A presence of a large number of absorption bands and a relatively small number of thermal de-excitation spikes shows, in their view, that there is no direct relationship between individual absorption bands and individual thermal de-excitation spikes.

Small additions of a third component (Al_2O_3, ZnO, CaO, and K_2O) (approximately to 2.5 percent) has a very strong effect on absorption and thermal de-excitation spectra of irradiated glasses.

The change in the absorption and thermal de-excitation spectra when SiO_2 is replaced with K_2O and CaO in sodium silicate glasses is accounted for by the assumption that differentiated polar groups form in the glass. This is confirmed by a rise in the intensity of the 400 and 460° K spikes when K_2O and CaO are added to the extent of 10-12.5 mole percent, while their intensity drops off when Na_2O is added.

For an overall Na_2O and CaO content corresponding to the disilicate composition, there is a qualitative change in the absorption and thermoluminescence spectra. Qualitative changes are also observed in the thermal de-excitation spectrum -- the 460° K spike disappears and a spike appears near 420° K.

Investigation of the effect the composition of glasses has on their thermal de-excitation was conducted by the authors on the glasses whose composition was expressed by the general molar formula of $4SiO_2 \cdot Na_2O \cdot$

TABLE 21. POSITION OF THERMAL DE-EXCITATION SPIKES IN SEVERAL THREE-COMPONENT GLASSES

Состав стекла в мол. % A					Положение максимумов B	
Na_2O	Al_2O_3	CaO	ZnO	SiO_2	полос поглощения в эв C	пиков термовысвечивания в °K D
20	—	0—12,5	—	80—67,5	5,4—5,2; 4; 2,8—2,7; 2	340, 400, 460
20	—	12,5—20	—	67,5—60	5,2—5; 4; 2,7; 2	340, 400, 420
20	—	20—35	—	60—45	5; 4; 2,7; 2	340, 400, 460
20	0—17,5	—	—	80—62,5	5,6; 5; 4; 2,8; 2	340, 400, 460
20	20—25	—	—	60—65	5,6—5,5; 5; 4; 3,4; 2,3	340, 400, 460, 520
—	3	—	—	97	5,6; 5; 4; 3,1; 2,3	
35	0—5	—	—	65—60	4; 2,7; 2	340, 420
35	5—15	—	—	60—60	4; 2,7; 2	340, 400
20	—	—	0—35	80—45	5,6; 5; 4,6; 4; 2,8; 2	340, 400, 460
35	—	—	1,25—5	63,75—60	5; 4,6; 4; 2,7; 2	340, 370, 480
35	—	—	7,5—25	57,5—40	4,6; 2,7—2,8; 2	340, 400
—	15	—	30	55	4,6; 3,4; 4	340, 400, 460

KEY: A -- Glass composition in mole percent
B -- Position of maxima as listed
C -- of absorption bands in ev
D -- of thermal de-excitation spikes in ^{o} K

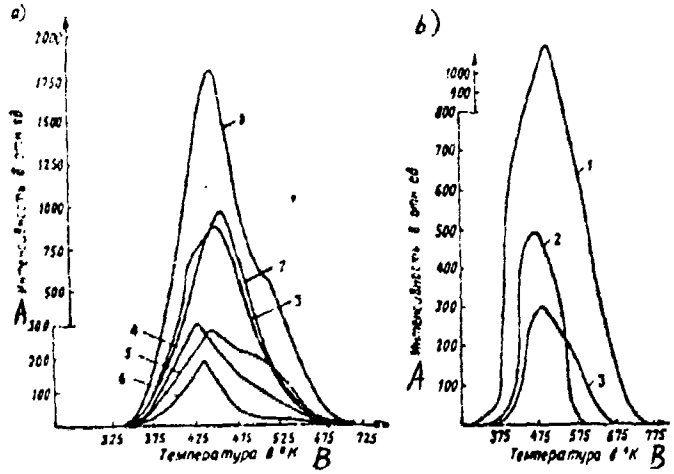

Fig. 52. Temperature dependence of integral intensity of thermal de-excitation for glasses with the composition $4SiO_2$, Na_2O, and $0.5\ M_xO_y$ containing the following as the third component:

a -- oxides of group I and group II elements
1 -- BaO
2 -- SrO
3 -- MgO
4 -- CaO
5 -- ZnO
6 -- Li_2O

b -- oxides of group III elements:
1 -- La_2O_3
2 -- Al_2O_3
3 -- B_2O_3

KEY: A -- Intensity in relative units
B -- Temperature in ° K

$0.5M_xO_y$. Oxides of group I-VI elements were added to the glass composition as the third variable component. The thermal de-excitation curves were recorded in the temperature range to 620° K after gamma-irradiation of the glasses with a dose of 10^7 r (Fig. 52).

The intensity of thermal de-excitation depends on the time elapsing from the moment of irradiation up to measurement. Table 22 presents data on the intensity of thermal de-excitation 10 and 30 days after irradiation.

In glasses containing group of I and group of II elements, within the limits of the same group a gain in radiation-optical stability leads to a reduced intensity of thermal de-excitation. However, in glasses containing

TABLE 22. EFFECT OF EXPOSURE OF GLASSES AFTER IRRADIATION ON INTENSITY OF THERMAL DE-EXCITATION

Варьируемый оксид A	B Интенсивность максимума термовысвечивания в отн. ед. при выдержке в сутках	
	10	30
BaO	1800	290
CaO	300	200
MgO	780	250
ZnO	280	175
SrO	960	600
Li_2O	185	180
B_2O_3	335	300
Al_2O_3	630	360
La_2O_3	2900	2100

KEY: A -- Oxide varied
B -- Intensity of maximum of thermal de-excitation in relative units when exposed for listed number of days

oxides of group III elements, for example Al_2O_3 and La_2O_3, the inverse dependence is observed. This shows that the centers of optical absorption and thermal de-excitation are not always identical.

During irradiation different kinds of traps can be initiated, differing both by their spatial location in the glass network, as well as by the depth at which the energy level lies. Some can be responsible for optical absorption, others -- for thermal de-excitation. Thermal de-excitation in glasses can be recombinational in origin, as well as be caused by the presence of discrete centers, which may be activating ions, for example, Ce^{3+}, Cr^{3+}, V^{6+}, and so on.

Besides the simple-composition glasses, the thermal de-excitation of commercial glasses K-8, K-108, ZhS-17, and VVS was investigated (Fig. 53, Table 23). These glasses are characterized by a broad thermal de-excitation spikes, whose position depends on the glass composition. Obviously, there is a number of capture levels which cannot be resolved. However, two maxima are observed on curves characterizing ZhS-17 glass: one at 420° K and the other at 530° K. Hence it follows that the energy levels of the traps can, in spite of their blurred state, be significantly differentiated. Studies of the structure of thermal de-excitation spikes are of interest and can be conducted by a method which was proposed in recent years and has come to be called the Gobrecht method.

3. Energy of Thermal Excitation of Capture Centers in Irradiated Glasses

In studying the spectrum of local levels in a solid, the main non-isothermal method is to investigate thermal de-excitation spectra. This

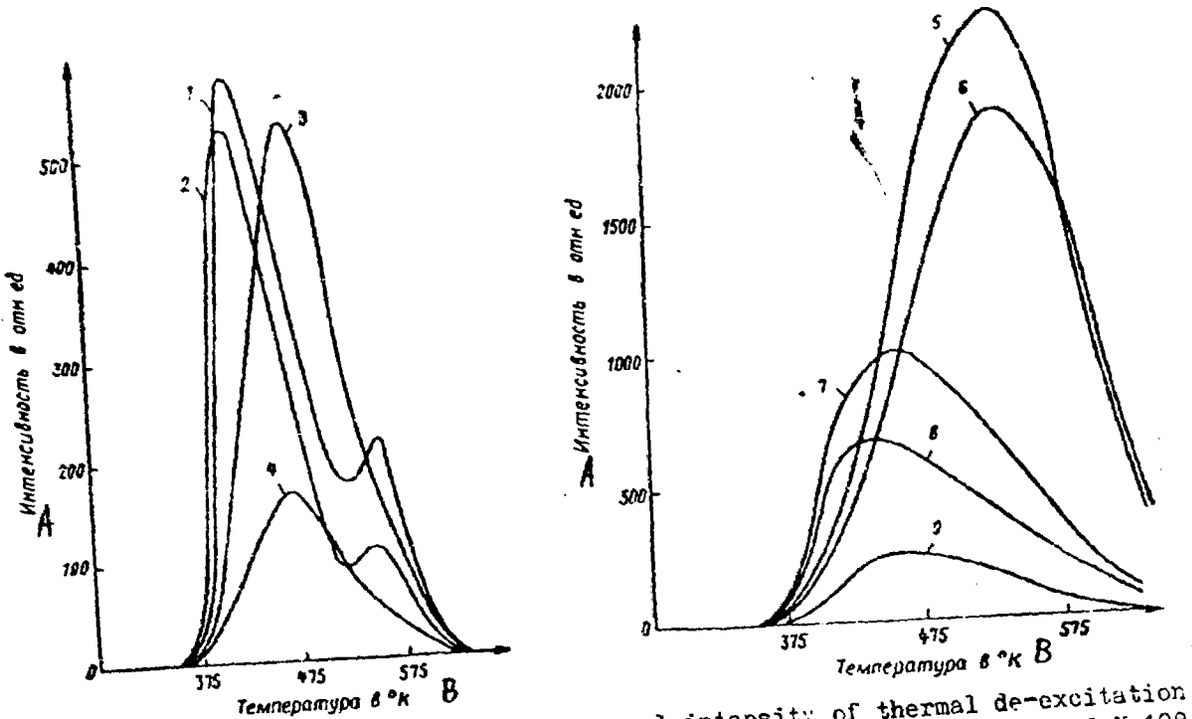

Fig. 53. Temperature dependence of integral intensity of thermal de-excitation for the commercial glasses Zhs-17 and VVS; and commercial glasses K-8 and K-108
KEY: A -- Intensity in relative units
B -- Temperature in ^{o} K

TABLE 23. RADIATION DOSE OF COMMERCIAL-COMPOSITION GLASSES

Номер кривой на рис. 53 A	Стекло B	Доза облучения в р C	Номер A кривой на рис. 53	Стекло B	Доза облучения в р C
1	D ЖС-17	$5\cdot10^6$	5	К-8	$1\cdot10^7$
2	ЖС-17	$1\cdot10^6$	6	К-8	$5\cdot10^6$
3	ВВС	$5\cdot10^6$	7	К-108	$1\cdot10^7$
4	ВВС	$1\cdot10^6$	8	К-108	$5\cdot10^6$
			9	К-108	$1\cdot10^6$

KEY: A -- Curve number in Fig. 53
B -- Glass
C -- Radiation dose in r
D -- ZhS-17
E -- VVS

method has several advantages: it is experimentally simple and provides qualitative data on the energy spectrum of traps, since the position of the thermoluminescence spike is directly associated with the depth at which the corresponding capture center lies. However, for a quantitative estimate of the depth of traps, in addition to the temperature of the luminescence maximum measured experimentally, we must know the probability of the re-capture of carriers and the frequency factors of centers. There are several methodological procedures for estimating these parameters [21, 22]. In spite of this, the quantitative calculation of the energy of thermal excitation based on the thermoluminescence curves is very approximate, and if a material has traps with several near-lying energies of activation or if the energies of activation are quasicontinuous, quantitative estimation becomes impossible. In this case one complex thermal de-excitation spike is formed, and based on the measurements of the half-width and symmetry of this complex spike one can no longer obtain information on the frequency factor and other parameters of the center.

To calculate the energy of thermal excitation, we can also adopt the analytic decomposition of the curve into its elementary components [23]. However, it is extremely difficult to apply this method, since the shape of the elementary components depends on constants, which can be determined only after decomposition.

The method of fractional heating was proposed by Gobrecht and Hoffman [24] for quantitative studies of the spectrum of thermal activation energies of capture centers. In the Soviet Union this method was mastered in the problem laboratory of semiconductor physics at the Latvian State University imeni P. Stuchka.

In the material studied, after excitation there are capture centers filled with charge carriers. According to [24], the probability of freeing a carrier from a trap is as follows:

$$P = S\exp(-E/kT). \tag{28}$$

Each capture centers characterized by its energy of thermal excitation E and by the frequency factor S. Therefore all capture centers can be described by the distribution function H_{ES}, which expresses the concentration of capture centers in the energy range $E \pm dE$ and the frequency factor range $S \pm dS$.

Each free electron recombines at an ionized activator or is again captured by a capture center. If the lifetime of the free charge carrier is much less than the time constant of the measuring equipment, the luminescence intensity measured experimentally is proportional to the rate at which free carriers are generated

$$I(t) = \eta Q \frac{dn}{dt}, \tag{29}$$

where η is the quantum yield of luminescence; Q is the probability that a carrier recombines at an activator; and dn/dt is the rate at which the carriers are freed.

If X is the coefficient at which the capture centers are filled with carriers, the intensity of luminescence is determined mainly by the capture centers for which the product PX is at a maximum.

Let us examine the contribution made by each of the terms of the product to the afterglow kinetics at constant temperature. Each type of capture center in isothermal conditions has a constant probability of freeing carriers, P, which depends on E_T and S. If the following ratio is set aside for two centers:

$$\ln\left(\frac{S_1}{S_2}\right) = \frac{1}{kT}(E_{T_1} - E_{T_2}), \tag{30}$$

and the centers have an identical probability of thermal excitation of carriers and they make the same contribution to the afterglow.

The population X of each type of center changes independently of each other type according to the exponential law:

$$X = X_0 e^{-Pt}. \tag{31}$$

The time constant of the luminescence decay $\tau = 1/P$ is inversely proportional to the probability of the thermal activation of capture centers. The afterglow curve consists of individual exponential sections with increasing decay time constants. The main contribution to the

afterglow intensity is afforded by emptying of the centers which in a given period have the highest probability of the thermal activation of carriers. The population of capture centers gradually diminishes. Calculation shows that centers for which the energy of thermal activation lies within the limits 2-3 kT become empty at the same time.

Let us consider how luminescence changes when a sample temperature is raised. According to expression (28), a temperature rise leads to the exponential growth in the probability that the capture centers will be ionized. As long as changes in the filling of capture centers X are slight (X = const), intensity of luminescence increases in proportion to the probability of ionization. This condition is satisfied over the low-temperature section of thermoluminescence curves. If monoenergetic capture centers are present in a specimen and if $I \approx P$, then we have

$$\frac{d \ln I}{d\left(\frac{1}{T}\right)} \approx \frac{d(\ln P)}{d\left(\frac{1}{T}\right)} = -\frac{E}{k}. \qquad (32)$$

Therefore, the depth of monoenergetic traps can be determined by the slope of the low-temperature section of the thermoluminescence curve in the coordinates ln I and 1/T. The condition X = const is not absolutely precisely satisfied in the experiment, but for practical purposes the unchanged population of capture centers can exist in the low-temperature section of the thermal de-excitation curve to a fairly good approximation. Actually, however, it is difficult to establish whether luminescence becomes stronger owing to the change P or if the slip of the curve becomes more gradual owing to the emptying of capture centers.

The oscillating heating regime was selected to monitor the changes in the population of capture levels. The sample temperature was raised a few degrees and then the sample was cooled to its initial temperature. If the luminescence intensity after the temperature cycle decreased only slightly, the population of levels changes quite little. Cycles of heating and cooling were repeated many times, while all carriers stored at capture centers recombined. From the slopes of the heating and cooling curves we can determine the mean depth of capture centers, which are mainly freed in the same temperature cycle.

Investigations by this method were conducted on KV quartz glass [25] (cf. Fig. 51 a). A complex low-temperature thermal de-excitation spike with its maximum near 140° K, and a higher-temperature thermal de-excitation spike -- at about 220° K -- are differentiated. The results of measuring the thermal de-excitation spectra showed that in KV type glasses there are at least two types of capture centers, but it is highly probable that the low-temperature spike is also caused by two types of capture centers. The depth at which the centers lie cannot be established based on thermal de-excitation spectra since we do not know the frequency factor of each center, and for the low-temperature spikes we do not know T_{max} of

each elementary subspike, owing to intense overlapping. The resultant spectrum of the energies of thermal excitation determined by the method of fractional heating is shown in Fig. 54 for the KV sample. The sample was excited at a temperature of 98° K with x-rays for 2 hours. The spectrum was averaged with respect to energies of excitation and light totals from 104 temperature cycles. The experiment was conducted so that the amplitude of the temperature cycle rose with a gradual increase in the mean cycle temperature and was $\Delta T = 0.1 T_{av}$.

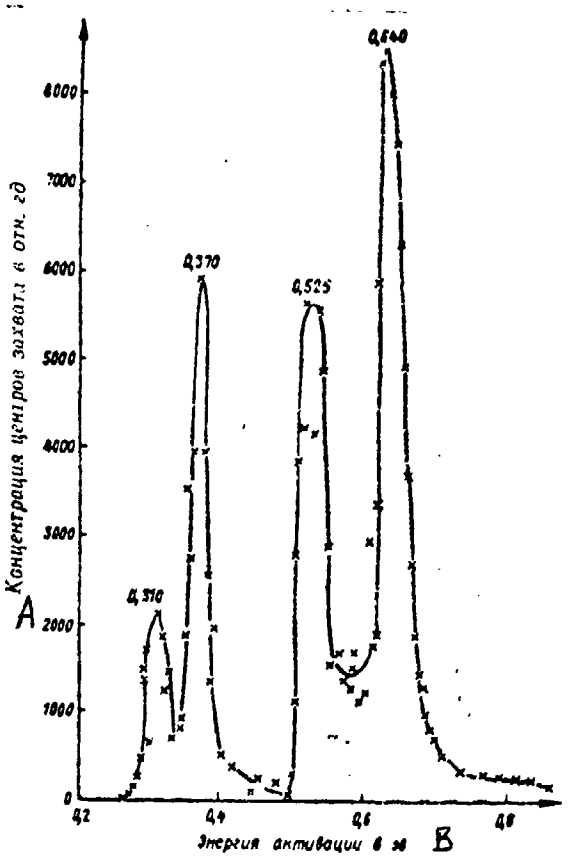

Fig. 54. Spectrum of energies of thermal activation of KV glass

KEY: A -- Concentration of capture centers in relative units
B -- Energy of activation in ev

Maxima on the curve are singled out for four energies of thermal activation: 0.31, 0.37, 0.525, and 0.64 ev. Therefore, samples of KV glasses have four types of local levels with corresponding energies of thermal activation. The area under the spikes shows the relative concentration of the corresponding filled local levels. Evidently, concentrations of three high-energy levels differ only slightly, while the population of the low-energy level is smaller by a factor of 4-6.

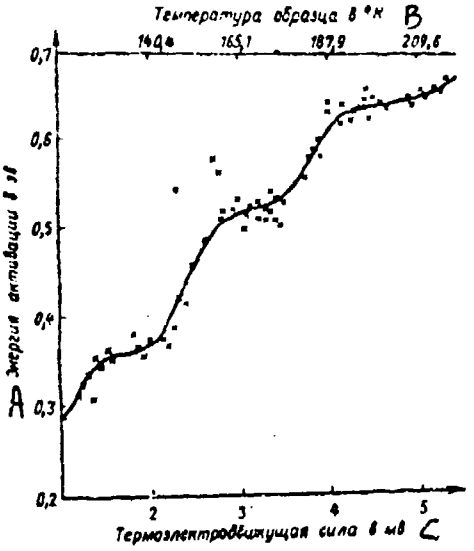

Fig. 55. Mean energy of activation as a function of mean cycle temperature for KV glass

KEY: A -- Energy of activation in ev
B -- Sample temperature in $^{\circ}$ K
C -- Thermoelectromotive force in mv

Fig. 55 shows the mean cycle energy as a function of the mean cycle temperature. Each point in this figure corresponds to one temperature cycle (approximately 60 of the 104 cycles are plotted on the graph). As we can see, from cycle to cycle the measured energy depth of the capture centers varies with increase in mean temperature. Here the measured temperature increases nearly monotonely during the first cycles (low-temperature points). At mean cycle temperatures (120-145° K) the measured mean cycle energy remains nearly unchanged, that is, it is predominantly the same type of trap that is emptied in the cycles. Corresponding to this plateau is the spike at E_{max} = 0.37 ev. In the next several cycles the measured mean cycle energy again increases smoothly to the next plateau, to which corresponds the spike at 0.525 ev. After the traps at this depth have been emptied, the cycle energy rises to the next plateau, which is formed by cycles de-exciting capture centers at a depth of 0.64 ev.

The temperature control regime in each cycle was selected as follows in measuring the spectra: the temperature was increased and then decreased linearly with time so that during a cycle the intensity of recombination luminescence, beginning from some level, increased and then decreased by a factor of 20, while the cycle time remains approximately constant. Therefore, in all cycles approximately the same light total was

obtained (that is, the number of recombined carriers was the same), which is reflected in the curve in Fig. 55. In the plateau region the mean temperature increases from cycle to cycle much more slowly than along the increasing sections, therefore the points lie more closely relative to the abscissa axis.

Fig. 55 has no plateau which would correspond to the first maximum in the curve of Fig. 54. A detailed analysis of the numerical results of measurements shows that this spike is formed by about five temperature cycles, whose mean energy does not increase from cycle to cycle, but fluctuates about the value 0.31 ev. Therefore the presence of capture centers at this depth cannot be regarded as demonstrated by the measurements made; additional study of this temperature region with a lower light sum de-excited in each cycle is required. A comparison of the thermal de-excitation curves and the fractional heating spectra shows the advantages of the latter method.

By measuring the energy spectra using the technique of fractional heating, one is able to resolve the energy levels of several thermal de-excitation spikes (spikes at E_T = 0.31, 0.37, and 0.525 ev, and the thermal luminescence spike at T_{max} = 413° K) and to prove that the others are elementary (E_T = 0.64 ev and the thermal de-excitation spike at T_{max} = 350° K). Based on the fractional-heating spectra, for the first time the energy of thermal activation of capture centers existing in KV glasses was established.

The half-width of spikes at the curve in Fig. 54 corresponds to 2 kT (where T is the temperature at which liberation of carriers occurs most effectively). Thus, the half-width of the spike and, therefore, the resolving power of the method corresponds to theoretical considerations. This fact shows that local states that are capture centers in KV type quartz glass are monoenergetic, that is, the thermal activation energies are discrete. Therefore it appears highly probable that formations serving as capture centers for carriers are formations with a stable physicochemical structure and, though the nature of these formations remains thus far unclear, the role of near order in determining their structure is dominant.

The depth of capture centers increases monotonely with mean temperature cycle (cf. Fig. 55). From this it follows that the frequency factor (pre-exponential cofactor of the probability that carriers will be liberated) is approximately the same for all capture centers.

After cessations of excitation at 100° K, intense afterglow of a sample is observed, decaying down to zero fairly rapidly. The first temperature cycles of fractional heating measured immediately after cessation of excitation show the following mean calculated energies: 0.18, 0.24, 0.28 ev, and so on. From this it follows that finer capture centers exist in appreciable concentration in samples, and their study necessitates lower temperatures. Therefore, to determine the complete energy

spectrum of capture centers in quartz glasses we must conduct measurements beginning with the liquid helium temperature. It can be anticipated that after these temperatures we will be able to observe details of the mechanism of recombination processes, recombination with the freeing of quasi-free carriers, tunneling recombination, and the manifestation of metastable levels.

4. Thermal Annealing of Color Centers

The breakdown of color centers during heating of an irradiated specimen is a widely known fact. As a rule, heating a sample to 700° K restores the optical absorption of a glass to its initial level. The temperature dependence of the rate of de-excitation of irradiated glasses has been studied in several works [26, 27], but correlations affording conclusions as to the nature of color centers have not been forthcoming. Isothermal and optical de-excitation of irradiated specimens was investigated more closely. A large number of well-executed studies are considered in detail in the review [28]. However, several aspects of this problem merit closer study.

The fundamental equation of the kinetics of color center accumulation (14) involves parameters characterizing radiation as well as thermal annealing of color centers. The work [29] examines the process of isothermal de-excitation of pre-irradiated glasses and proposes of formula for its description

$$-\frac{dn}{dt} = Ae^{-bt}, \tag{33}$$

where A and b are constants.

Actually, setting p = q = 0 in equation (14), we get

$$n = n_0 - n_0\left(1 - e^{-q_T t}\right) = n_0 e^{-q_T t},$$

whence

$$-\frac{dn}{dt} = n_0 q_T e^{-q_T t}. \tag{33a}$$

However, the results of our experimental studies and those of others [27] show that equation (33) does not describe experimental curves exactly. Fig. 56 presents curves characterizing the breakdown of color centers with time after irradiation has been stopped. Typical of these is the tendency to saturation, which does not follow from equation (33a).

Evidently, at the initial concentration n_0 there are both thermal stable centers n_{st} as well as unstable thermal centers that break down with time. Then the differential equation characterizing the rate of isothermal de-excitation will be of the form

$$-\frac{dn}{dt} = (n - n_{ST})\, q_T.$$

Adopting as the boundary conditions $n = n_0$ when $t = 0$, let us find the solution of this equation:

$$n = n_{ST} + (n_0 - n_{ST})\, e^{-q_T t} = n_0 e^{-q_T t} + n_{ST}(1 - e^{-q_T t}). \qquad (34)$$

Hence

$$-\frac{dn}{dt} = (n_0 - n_{ST})\, q_T e^{-q_T t}. \qquad (35)$$

By comparing equations (33) and (35), we have

$$A = n_0 - n_{ST};\ b = q_T.$$

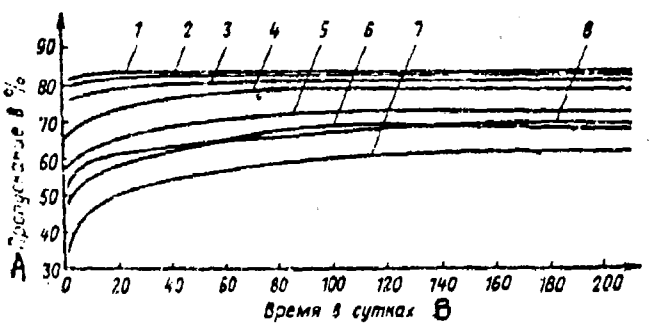

Fig. 56. Change in light transmission of irradiated glasses with time

1 -- $45SiO_2 \cdot Na_2O \cdot 0.5SnO_2$

2 -- $45SiO_2 \cdot Na_2O \cdot 0.25Sb_2O_3$

3 -- $45SiO_2 \cdot Na_2O \cdot 0.25As_2O_3$

4 -- $45SiO_2 \cdot Na_2O \cdot 0.25Nb_2O_5$

5 -- $45SiO_2 \cdot Na_2O \cdot 0.5CeO_2$

6 -- $45SiO_2 \cdot Na_2O \cdot 0.5CdO$

7 -- $45SiO_2 \cdot Na_2O \cdot 0.5ZnO$

8 -- $45SiO_2 \cdot Na_2O \cdot 0.25La_2O_3$

KEY: A -- Transmission in percent
B -- Time in days

Equations (34) and (35) describe the process of the isothermal breakdown of color centers in glasses when color that are stable and unstable at a given temperature are irradiated. Upon prolonged exposure following irradiation, the color center concentration drops off via zero, or to n_0.

The mean rate of isothermal de-excitation for several simple-composition glasses has been cited in the work [20] (Tables 24 and 25).

TABLE 24. MEAN RATE OF THERMAL DE-EXCITATION OF GLASSES OF THE SYSTEM Na_2O-Al_2O_3-SiO_2 AS A FUNCTION OF COMPOSITION

Состав стекла в мол. % A			Скорость термического обесцвечивания в мм$^{-1}$/мм при энергии в ев B				
Na_2O	Al_2O_3	SiO_2	5,6	5	4	2,8	2
25*	5	60	0,182	0,178	0,162	0,148	0,108
25*	10	55	0,222	0,254	0,178	0,15	0,108
25*	15	50	0,064	0,12	0,148	0,12	0,094
30**	—	70	—	—	0,174	0,224	0,162
30**	2,5	67,5	0,066	0,084	0,176	0,208	0,166
30**	7,5	62,5	0,138	0,162	0,148	0,134	0,114
30**	15	55	0,068	0,09	0,128	0,112	0,088

* de-excitation at 370° K

** de-excitation at 353° K

KEY: A -- Glass composition in mole percent

B -- Rate of thermal de-excitation in mm -- 1/mm at listed energy in ev

De-excitation of glasses 1-8 was conducted at 373° K, and at 353° K for glasses 9-17; here the rate of de-excitation of the 4.6 ev band of glasses 9-11 was too high to be measured.

Unfortunately, at present there are virtually no data on the q_m values for different glass compositions or for different temperatures. However, the value of q_m is necessary in determining the thermal stability of centers, which is vital in predicting induced absorption as a function of irradiation intensity.

CHAPTER NINE

EFFECT OF RADIATION ON ELECTRICAL PROPERTIES OF GLASSES AND CERAMICS

Electroconductivity, dielectric permeability, dielectric losses, and electrical strength of dielectrics are determined by physical processes associated with the liberation, displacement, mobility, and concentration of electrical charges in a dielectric. Irradiation increases the concentration of free electrons and changes the conditions of charge displacement. Some of these conditions act only during the irradiation time, while others persist even after irradiation. All this accounts for the complicated dependence of the enumerated characteristics on irradiation.

1. Accumulation of Charge and Breakdown of Dielectrics Caused by Irradiation

The ionization of atoms exposed to radiation and the initiation of free charge carriers causes a dielectric to be polarized, that is, induces an electric moment in it. Under some irradiation conditions polarization can be macroscopically manifested: after irradiation a charge with the opposite sign is detected on the opposing surfaces of the dielectric sample. Some glasses in this case are capable of retaining the induced charge for a long time, that is, they become electrets [1]. After irradiation, the dielectric can remain macroscopically neutral, but still induced charge and polarization can be manifested under certain conditions. It is sufficient, for example, to place the sample in an electrical cell, to short-circuit its opposite sides, and begin heating it as the discharge current is induced, whose value and direction can be recorded by connecting it to the external circuit of an ammeter.

The discharge of an irradiated dielectric when heated is associated with the fact that the distribution of charge carriers recorded at the irradiation temperature is disrupted, carriers begin moving toward the electrodes, and a current is induced in the external circuit. One of the typical features of discharge currents is the complicated dependence of their value and direction on temperature and time (Fig. 57) [1].

TABLE 25. RATE OF THERMAL DE-COLORIZING OF GLASSES IN THE SYSTEM Na_2O-ZnO-SiO_2

A Номер состава	B Состав стекла в мол. %			C Скорость термического обесцвечивания в мм⁻¹/мин при энергии полосы поглощения в эв	
	SiO_2	Na_2O	ZnO	4,6	2,8
1	77,5	20	2,5	0,546	0,274
2	75	20	5	0,474	0,172
3	72,5	20	7,5	0,418	0,132
4	65	20	15	0,238	0,092
5	62,5	20	17,5	0,338	0,092
6	60	20	20	0,142	0,05
7	58,5	20	22,5	0,086	0,044
8	45	20	35	0,11	0,02

A Номер состава	B Состав стекла в мол. %			C Скорость термического обесцвечивания в мм⁻¹/мин при энергии полосы поглощения в эв	
	SiO_2	Na_2O	ZnO	4,6	2,8
9	63,75	35	1,25	—	0,112
10	62,5	35	2,5	—	0,116
11	60	35	5	—	0,116
12	57,5	35	7,5	0,386	0,092
13	55	35	10	0,444	0,08
14	50	35	15	0,266	0,064
15	47,5	35	17,5	0,202	0,068
16	45	35	20	0,150	0,06
17	40	35	25	0,116	0,056

KEY: A — Composition number
B — Composition in glass in mole percent
C — Rate of thermal de-colorizing in mm/min, at an absorption band energy in ev

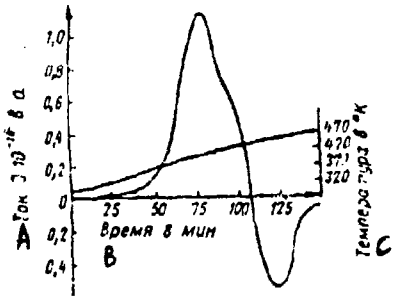

Fig. 57. Typical dependence of discharge current of glass irradiated with electrons on heating temperature and time (specimen thickness 17.5 mm)
KEY: A -- Current, I · 10^{-10}, in amperes
B -- Time in minutes
C -- Temperature in ^{o} K

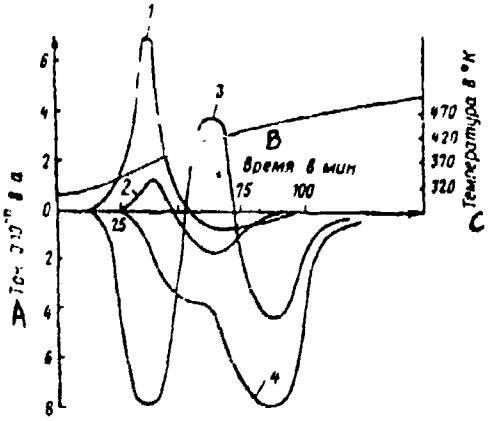

Fig. 58. Dependence of value and direction of discharge current on the site of measured section in irradiated sample
1 -- irradiated area of sample is 3 mm thick
2 -- as above, 10 mm
3 -- thickness of unirradiated sample area is 8.9 mm
4 -- as above, 5.5 mm
KEY: A -- Current, I · 10^{-10}, in a
B -- Time in min
C -- Temperature in ^{o} K

For the case of irradiation with electrons, polarization of the dielectric is easily accounted for by the introduction of excess negative charge, since sample thickness is greater than the electron path. However, the distribution of this charge across these sample thicknesses is of a complicated form. It is obtained from experiments measuring the discharge current at plates prepared by longitudinal cutting of the irradiated sample. The discharge current is produced both on irradiated or unirradiated, deeper-lying layers of the sample (cf. Fig. 58), which indicates the initiation of a compensating positive charge in the region of the sample that is not irradiated with electrons. The value and shape of the dependences of current on heating time and temperature enable us to plot the charge distribution and the distribution of the electrical field in the sample (Fig. 59) [1].

In Fig. 59 the point x_a is at the depth of maximum electron concentration (about 0.4 cm, which corresponds to the free path of 2 Mev electrons). The distribution curve of the electrostatic field in the sample is obtained by integrating the density of the space charge. Since the cell is short-circuited, the integral of the fields from one surface to another is zero, and x_a and x_b are the field inversion points.

The above-mentioned distribution curves correspond to the state immediately after irradiation at room temperature. When the temperature is increased negative charge carriers, initially captured by traps between the irradiated surface and point x_a, move toward electrode A. Positive charge carriers captured by traps between the unirradiated surface and point x_b move toward electrode B. Charge carriers between points x_a and x_b are subject to the reverse field, which shifts the negative charge in the reverse direction. The net external current recorded in the current is the sum of the positive and negative components. Since these components must be distinct time functions, the overall current can modify the direction.

In contrast to discharging electron-irradiated samples, samples irradiated with gamma-rays, according to [1-2], do not yield discharge currents when there is uniform heating in the electrolytic cell, which enables us to conclude that there is no polarization present upon gamma-radiation. However, heating a sample of Corning 707 glass uniformly irradiated with gamma-rays, in the presence of a temperature gradient, is accompanied by discharge currents [2]. Here the direction of the current observed corresponds to the movement of electrons toward the hotter electrode. The initiation of current is explained by the fact that in a nonuniform temperature field carriers begin to move opposite to the gradient, and the diffusion coefficients of the carriers of negative and positive charges differ from each other. This leads to the appearance of a net external current, whose polarity indicates the high mobility of the negative charge carriers, that is, electrons, which is wholly natural.

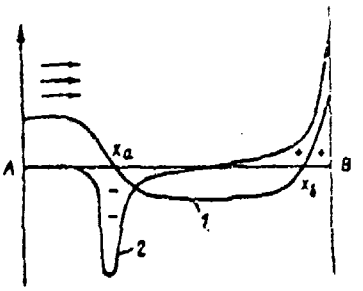

Fig. 59. Distribution of bulk charge and electrical field in dielectric irradiated with electrons (the arrow indicates the direction of the electron beam)
1 -- field
2 -- charge

Still, in more recent studies electrical polarization of various dielectrics after gamma-irradiation was detected [3]. Irradiated samples placed even in a uniform temperature field produce a discharge current, even though of a relatively low value. The initiation of a space charge in a sample subject to irradiation on one side is associated with the fact that the scattering of Compton electrons formed upon exposure to quanta occurs principally in the direction of the primary radiation, which then gives rise to the nonuniform distribution of electrons in the irradiated volume. The displacement of electrons in the direction of irradiation and their capture by traps at deeper layers lead to the buildup of negative charge near the unirradiated surface, which brings about a rise in the compensating positive charge on the side of the sample facing the irradiated surface (Fig. 60) [4, 5].

The value of the bulk charge depends on the absorbing ability of the glass, therefore polarization is manifested more strongly in lead glasses. This polarization was detected when lead silicate glass was irradiated with x-rays at doses from $2 \cdot 10^3$ to $2 \cdot 10^4$ r [6]. When a sample is heated in the 350-430° K range, a current was recorded that changed its direction at 390° K.

The polarization of lead-silicate glass caused by x-ray irradiation obeys several correlations, in particular, increasing the radiation temperature lowers the dose at which polarization saturation sets in (upwards of 10^6 r for 297° K; 10^5 r for 320° K; and $5 \cdot 10^4$ r for 343° K). Increasing the radiation dose intensity to 300-400 r/min causes more intense polarization; a further rise in dose intensity has no effect [7].

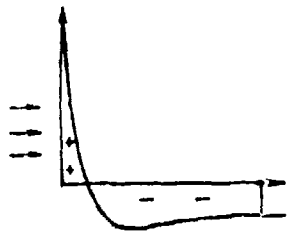

Fig. 60. Distribution of bulk charge in gamma-irradiated dielectric (the arrows denote the direction of irradiation)

When an irradiated sample with nonuniform distribution of charge carriers is placed in a uniform temperature field, the carriers freed under the effect of the internal field begin to migrate toward the sample surfaces, which induces a weak discharge current [8]. The need for nonuniform irradiation to cause polarization to rise has been confirmed by several experiments. For example, it is reported in the work [4] that samples of radiation-resistant flint, irradiated on one side with gamma-rays from a Co^{60} source, when placed in a uniform temperature field yielded two well-defined spikes of negative and positive current at temperatures of 410 and 450° K. After the samples were uniformly irradiated on all sides with the same gamma-ray dose, the discharge current curve recorded under the same conditions had two much weaker spikes, shifted toward the low-temperature side. Thus, to cause a discharge current to appear with heating, we need nonuniformity either of the radiation or of the temperature field in the sample.

When a nonuniformly irradiated sample is placed in a nonuniform temperature field, a current caused by the different diffusion coefficients of the carriers is superimposed on the current induced by the internal electrostatic fields. Therefore, depending on the direction of the fields, either strengthening or weakening of the external current can occur. Since both currents obey different temperature functions, a change in the position of the irradiated sample in the cell can alter the discharge current pattern [3].

The use of high temperature gradients causes an increase in the integral discharge current. Regardless of the gradient used, the integral current reaches saturation at doses of about $3 \cdot 10^6$ r [9, 10]. Even the application of a strong external electrical field to the discharge sample causes no marked change in the value and direction of the discharge current, which indicates an extremely high level of the pseudo-Thomsonian

coefficient (10-100 v/deg) for the discharge current caused by irradiation [3].

In addition to the discharge caused by heating and irradiated dielectric, a discharge photocurrent is induced when the same samples are irradiated with ultraviolet rays. In this case samples of quartz glass and Pyrex irradiated with beta-rays at a dose of $7 \cdot 10^5$ rad from a Sr^{90} source were placed in a cell and illuminated with a mercury lamp [11]. The charge accumulated upon irradiation was lowered by 50 percent in 3 minutes on quartz glass samples and in 90 minutes on Pyrex samples. The retarded discharge of Pyrex is associated by the authors with its lower ultraviolet transmission.

In many studies on the polarization and discharging of irradiated dielectrics, emphasis centers on the relationship of these phenomena with the formation and breakdown of color centers. In the literature it is noted that total discharge of a sample corresponds to its complete decolorizing, that is, the color centers are the charge carrier sources [1, 9]. Since the breakdown of color centers is accompanied by luminescence, naturally there is a specific relationship between thermal discharge and thermoluminescence. For example, in the work [12] attention is directed toward the relationship of the thermoluminescence spikes of glass (370 and 410° K) and the discharge current spikes (410° K).

The chemical composition of glasses, affecting the number and stability of color centers, also affects the polarization value. As indicated, polarization depends on the absorbed dose, therefore in the case of x-ray or gamma-ray irradiation these are more readily observed in heavy glasses with a large absorption coefficient. In the study [3], the investigation covered several commercial glasses, including quartz 7940 and borosilicate 7070 made by the Corning Glass Works, lead silicate protective glass from Pittsburg Glass, the quartz glass Suprasyl, and also two calcium aluminumborate glasses (Cabal-25: $CaO \cdot 4.5B_2O_3 \cdot Al_2O_3$ and Cabal-39: $CaO \cdot 2.5B_2O_3 \cdot Al_2O_3 \cdot 0.2CeO_2$). Here it was noted that the integral discharge current for quartz glass is much lower than for multicomponent technical glasses (Fig. 61). This fact is related by the author to the large number of traps in technical glasses, that is, to the large number of color centers. The presence of cerium in glass preventing the formation of color centers still does not reduce the accumulated charge and discharge current values [10]. In the study [4] it was found that the simultaneous presence in lead silicate glass of two transition elements causes the initiation of positive and negative maxima on the discharge current curve, while glasses containing a single transition element yield only one positive spike (Fig. 62).

On attainment of a sufficiently strong internal field in an irradiated dielectric, its breakdown may occur simultaneously. It is simple to observe a breakdown when mechanical damage is applied at the surface of an irradiated sample, for example, by puncturing it with a needle. In this case the breakdown voltage will be measured by connecting the needle to a voltmeter.

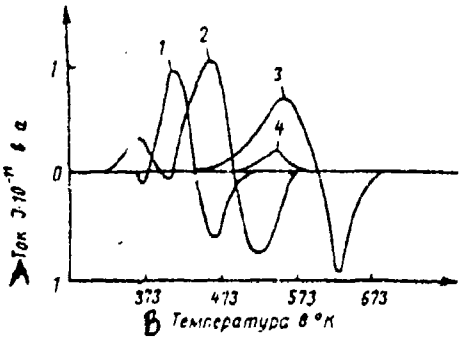

Fig. 61. Discharge current in glasses after gamma-irradiation with the dose $3.3 \cdot 10^4$ r at a temperature gradient of 31 deg/mm

1 -- Pittsburg Glass 6792
2 -- Corning 7070
3 -- Cabal-39
4 -- Suprasyl

KEY: A -- Current, $I \cdot 10^{-10}$ in a
B -- Temperature in ° K

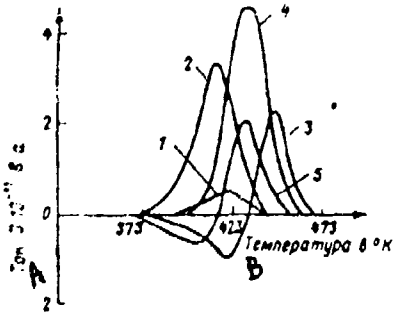

Fig. 62. Discharge current in the following glasses

1 -- glass with composition 60 % SiO_2 and 40 % PbO without additives
2 -- as above, with additive of 0.4 % CeO_2
3 -- as above, with additive of 0.1 % Fe_2O_3 + 0.5 % CeO_2
4 -- as above, with additive of 0.5 % Fe_2O_3
5 -- as above, with additive of 0.5 % TiO_2 + 0.1 % Fe_2O_3

KEY: A -- Current, $I \cdot 10^{-10}$, in amperes
B -- Temperature in ° K

Spontaneous breakdown of lead silicate glass (46 percent SiO_2; 0.5 percent Na_2O; 34.5 percent PbO; 13.6 percent K_2O; 2.4 percent CeO_2; and 0.9 percent Fe_2O_3) was noted for radiation doses of $(7-9) \cdot 10^7$ r [13]. The breakdown voltage measured in this fashion was $1.2 \cdot 10^6$ v/cm. This value is below the dielectric strength of a given glass ($5 \cdot 10^6$ v/cm), which accounts for the increase in the local concentration of the field immediately prior to breakdown. The reduction in the breakdown strength of radiation-resistant glass of the system K_2O-Na_2O-PbO-SiO_2 owing to irradiation has been reported in the paper [10]. The reduction is 25 percent of the initial value for alternating current and 9.5 percent for direct current.

Breakdown of an irradiated dielectric is usually accompanied by a flash of light, after which the characteristic discharge figure -- the so-called Lichtenberg figure -- becomes noticeable on the sample. In electronic irradiation, the depth at which the plane of the discharge figure lies corresponds to the depth of captured electrons. The area of the discharge figure is proportional to the integral discharge current [1, 14].

The overall discharge glow time of a radiation-resistant flint recorded by high-speed motion picture photography was 20-30 microseconds for a 10^6 r radiation dose. When the radiation dose was boosted to $3 \cdot 10^6$ r, the total discharge time was reduced to 17-18 microseconds.

Formation of Lichtenberg figures can also be produced and observed in different ways [14].

1. A dielectric with a notch on its surface made by impressing a needle, and then subsequently irradiated yields a discharge figure at the very first irradiation, where the onset of the discharge is at the damage site. The value and shape of the discharge figure depends on the integral dose of the first irradiation.

2. After irradiation a sample is placed on a grounded plate and a new indentation is made with a grounded needle. If the radiation dose or the accumulated charge are large enough, a flash takes place caused by the discharge occurring along the same path as in the first irradiation. For irradiation with low-energy electronic beams, the irradiated layer of the sample has a relatively shallow depth, and the electroconductivity of this layer is very high owing to the high concentration of the electrons, therefore the accumulated charge is released in a very short time. Characteristics of the materials and their properties are presented in Table 26 [14].

One more method of observing Lichtenberg figures and recording the discharge current is described in the work [10]. An irradiated glass sample is placed in a mechanical strength testing machine, and a load is

TABLE 26. EFFECT OF ELECTRONIC IRRADIATION ON ELECTRICAL PROPERTIES OF GLASS

A Стекло	B Сопротивление в ом·см	C Разрядный ток в мка	D Время облучения в сек	E Время до разрядки в ч
F Потемнеющее CN . . .	10^{17}—10^{18}	2,5	60	8
Свинцовое F-36-N G. . .	10^{16}—10^{18}	2,5	20	90
Свинцовое F-62-R H. . .	10^{17}—10^{18}	10	30	—
Натриевое I.	10^{4}	10	6—7	—

KEY: A -- Glass
B -- Resistance in ohms · cm
C -- Discharge current in microamperes
D -- Irradiation time in seconds
E -- Time to discharge in hours
F -- Nondarkening CN
G -- Lead F-36-N
H -- Lead F-62-R
I -- Sodium

applied in the center of the surface using a hard cone. At constant load (140 kg), the discharge current becomes maximum in 10 hours after irradiation with doses of 10^6 and 10^7 r.

When the study was made of discharging under the effect of variable load on samples of glasses with different chemical compositions irradiated with doses of 10^6 and 10^7 r (the measurement was taken 24 hours after irradiation), the following findings were made [10]:

a) as a rule the discharge current was stronger and the Lichtenberg figure had a distinctive central stem (dendritic form) in CeO_2-rich glasses;

b) the overall current is reduced and the damage area is also narrowed with decrease in the dimensions of radiated samples, that is, the current is nearly proportional to the irradiated surface area;

c) the discharge current is increased with decrease in applied load; and

d) the discharge current in the glasses is reduced when the potassium is partially replaced with sodium, when sodium and potassium are partly replaced with calcium, silicon -- with beryllium, potassium -- with zinc, silicon -- with aluminum, and silicon -- with phosphorus, and in the case of industrial radiation-resistant lead glass -- when slight amounts of WO_3 and Sb_2O_3 are introduced. However, adding a large amount of Sb_2O_3 (more than 8 percent) to sodium borosilicate glass, as shown by our investigations, leads to an increase in the region damaged by the discharge.

It is possible that the damage in borosilicate glasses intensively irradiated with ultraviolet rays is related to similar phenomenon [15], though the authors of this study attribute this effect to structural changes in the glass caused by the migration of alkali ions in the field of the charge induced by irradiation and caused by change in boron coordination. And naturally, the authors themselves note that when a sample of Terex glass that had received extended irradiation with ultraviolet rays was heated, a strong discharge current is induced in the electrolytic cell (up to 10^{-6} a), much higher than the current in glasses irradiated with x- or gamma-rays. In all probability here we have effects of different kinds induced upon irradiation being superimposed on each other: electronic effects -- the initiation of polarization owing to Compton electrons and structural effects -- change in the distribution of cations and the associated appearance of stresses in the irradiated layer.

2. Effect of Nuclear Radiation on the Electroconductivity of Glasses and Ceramics

Exposure of dielectrics to radiation causes two kinds of changes in the electroconductivity produced by the initiation of free charge carriers.

The first is radiation electroconductivity, observed directly on exposure to radiation and a rise in level because electrons carried into the conductivity zone travel in the dielectric under the effect of the applied field until they are captured by traps or else recombined with holes in the valency zone. Mobile ions of alkali metals can also serve as charge carriers in addition to electrons, since the applied electrical field hampers their recombination and stimulates their disunion [16].

An increase in the electroconductivity of a dielectric upon irradiation obeys the following relationship [17]

$$\sigma_r = en\mu,$$

where σ_r is the radiation electroconductivity; e is the elementary charge; n is the carrier concentration; and μ is their mobility.

This relationship applies to the electronic as well as the electronic component of electroconductivity, which are superimposed on each other. The value of σ_r as a function of radiation dose has the form of a saturation curve and its established value is proportional to the radiation intensity.

The second kind -- post-radiation electroconductivity -- is observed for some time after radiation has halted and is produced by carriers falling into potential wells that are not deep enough. The time dependence of current usually has a "declining" characteristic, which is associated with a decrease with time of the number of charges freed. The experimental

temperature strongly affects electroconductivity here, since on the temperature depends the stability of electronic and hole centers. As the measurement temperature is raised, we can observe heat-stimulated electroconductivity, which -- in contrast to the earlier-discussed discharge effect on exposure to an internal field induced by irradiation -- is manifested only when a voltage of high enough value is repeatedly applied to the irradiated dielectric.

Post-radiation conductivity also has the nature of a saturation curve, whose value is proportional to the measurement temperature. For example, it is $7 \cdot 10^{-10}$, $25 \cdot 10^{-10}$, and $90 \cdot 10^{-10}$ a, respectively, for MgO crystals irradiated with electrons at temperatures of 338, 356, and 376° K. The post-radiation conductivity is usually several orders of magnitude smaller than the radiation conductivity [18].

Changes in the electroconductivity induced by radiation and, in particular, the heat-stimulated conductivity are proportional to the intensity of the radiation dose, which has been noted in samples of lukalox irradiated with equal doses at rates of $5 \cdot 10^6$ and $5 \cdot 10^8$ r/hr [19]. It must be noted that during measurement of the heat-stimulated conductivity radiation damage undergoes annealing and in the area of 1000° K the curves of irradiated samples coincide with the curves of unirradiated samples [19].

In our experiments measuring heat-stimulated electroconductivity of quartz glasses of different grades (KI and KV) irradiated with x-rays, we simultaneously recorded the thermoluminescence of the samples. The radiation temperature was 100-105° K. After two-hour irradiation at the regime 50 kv and 10 ma, a voltage of 450 v was brought to the samples and they were simultaneously heated at the rate of 0.1 deg/sec. Experimental results (Fig. 63) allow us to note that the spikes of heat-stimulated luminescence (HSL) correspond to the spikes of heat-stimulated current (HSC). A rise in HSC in the temperature region near 300° K and above is associated with the intensified ionic conductivity of the glass, while the low-temperature section of the HSC curve is determined mainly by electronic processes. Thus, we can assume that the liberation of electrical charges captured by traps, induced by the temperature rise, and their passage into the conductivity zone account for the current in the sample.

Also capable of leading to higher electroconductivity following irradiation are processes which result in the formation of impurities that serve as charge carriers. For these processes to occur, enough of these impurities must form as the result of nuclear transformations. Thus, Budnikov et al. [20] maintains that the rise in the electroconductivity of clean polycrystalline corundum in alternating current at a frequency of 10^5 Hz induced by reactor irradiation is due to the initiation of donor levels at the sites of nuclear transformations Al^{27} (n, p) Si^{28}. This also gives rise to charges responsible for persistent changes in electroconductivity.

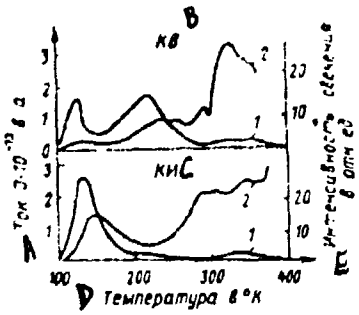

Fig. 63. Thermal luminescence 1 and heat-stimulated electric conductivity 2 of quartz glasses KI and KV irradiated at 100° K with x-rays

KEY: A -- Current, $I \cdot 10^{-13}$, in amperes
B -- KV
C -- KI
D -- Temperature in ° K
E -- Luminescence intensity in relative units

TABLE 27. SPECIFIC BULK RESISTANCE OF CERTAIN GLASSES IRRADIATED IN A REACTOR

A Состав стекла		B Удельное объемное сопротивление в ом·см при времени облучения в ч				
C окисел	D содержание в вес. %	0	1	5	10	100
Na_2O	21					
CaO	64	$2{,}22 \cdot 10^{10}$	$4{,}40 \cdot 10^{10}$	$4{,}13 \cdot 10^{10}$	$4{,}10 \cdot 10^{10}$	$4{,}30 \cdot 10^{10}$
SiO_2	72,2					
Li_2O	23,2					
Cu_2O	0,2					
BaO	7,5	$2{,}32 \cdot 10^{11}$	$2{,}07 \cdot 10^{11}$	$2{,}29 \cdot 10^{11}$	$2{,}00 \cdot 10^{11}$	$2{,}85 \cdot 10^{11}$
SiO_2	67,3					

KEY: A -- Glass composition
B -- Specific bulk resistance in ohms · cm for listed irradiation time, in hours
C -- oxides
D -- content in percent by weight

The effects of change in electroconductivity noted are small, and the current has the same order of magnitude as the discharge current caused by induction of the body charge. For example, borosilicate glass irradiated with gamma-rays, in the initial state yielding a current of $2.8 \cdot 10^{-12}$ a for a voltage of 22.5 v, after being irradiated with 10^5 r/hr yields a current $2.2 \cdot 10^{-11}$ a. Irradiation of sheet sodium calcium silicate glass shows virtually no change in its resistance [21]. At the same time samples of irradiated glasses become current sources in a circuit, resulting from polarization of the bulk charge, and the absence of external voltage. Thus, this irradiated borosilicate glass sample was de-excited in a circuit with a current of $3.4 \cdot 10^{-11}$ a [21].

When two multicomponent glasses were irradiated in a reactor at a beam strength of 10^{13} neutrons/cm^2 · sec, the following results were recorded [22] (Table 27).

It does not appear possible to arrive at any correlation between resistance change and dose.

Paymal in his work [23] on changes in the properties and structure of multicomponent glasses when exposed to the reactions (n,α) caused by thermal neutrons, associates the effect of changes in the electroconductivity and dielectric characteristics with specific damage under the effect of heavy charged particles. At small radiation reactor doses, changes in electrical properties are associated with the so-called "thermal effect" which results in changes in the depths of potential wells immobilizing the position of alkali cations in the tracks of charged particles formed in the nuclear reactions. As a result of this effect, the electrical resistance of Pyrex, lead, and borosilicate glasses is lowered by more than 50 percent for radiation doses of about $2 \cdot 10^{17}$ neutrons/cm^2.

This phenomenon is analogous to the moderate hardening of glasses. If prehardened glass whose initial resistance was below that of annealed glass undergoes irradiation in a reactor, some rise in resistance is observed. Thus, both hardened and annealed glasses acquire approximately identical electrical resistance values following irradiation. These effects are removed by annealing at relatively low temperatures (as low as 770° K).

In the studies by Ehrenberg et al. [24], it was shown that the current recorded for large number of glasses irradiated with cathode and gamma-rays does not exceed 10^{-11} a at voltages up to 500 v. At the same time Belyavskaya [25] reported that the emf induced in sodium silicate glass (20 percent Na_2O) by gamma-irradiation yields a current of $10^{-9} - 10^{-7}$ a, where the current is stabilized in the region of large applied stresses (approximately 1-2 kv). Samples of quartz glasses of different grades yield current values up to 10^{-7} as a function of radiation dose intensity for a voltage of 2000 v [26]. Current values for different grades of quartz glass differ by two orders of magnitude [26], and the presence of impurities of metal oxides lowers the induced conductivity [27]. This

relationship has also been noted by Belyavskaya [25]: pure grades of quartz glass change electroconductivity to a greater extent. But the presence of hydroxyl ions in quartz glass intensifies the effect of irradiation on the electroconductivity.

This dependence of radiation stability on chemical composition is caused by the phenomena of the initiation and breakdown of electron and hole capture centers. The presence of additives affecting radiation-optical stability alters not only the heat-stimulated current, but also its direction. For example, in glasses containing cerium oxide additive, when heat-stimulated electroconductivity was measured atfirst a current opposite to the applied voltage was present. When the temperature was raised it was increased and after passing through a maximum drop to zero, after which it took on the opposite direction. At 350-370° K the temperature dependence curves of the current approximate the curves recorded for unirradiated glasses. As the CeO_2 content was increased the reverse current spikes were stronger. At the same time, electroconductivity for irradiated glasses not containing CeO_2 varied according to the cubic parabola as a function of temperature [10]. The temperature at which the reverse current has a maximum and the area bounded by the reverse-current curve and the temperature axis depend on the total value of the discharge current.

Potakhova [27] indicates that gamma-irradiation leads only to an increase in the current established after glassy silica no longer is irradiated. At the same time the irradiation of monocrystalline quartz produces not only an increase in the absolute current, but also a rise in the time needed for it to reach its steady-state value.

The chemical composition of glass has a marked effect on changes in electroconductivity. Irradiating lead protective glass with a dose of $10^5 - 10^7$ r [28] is accompanied by an increase in its resistance, while it is reduced in moderate-density glasses.

Semiconductor glasses of the system U_2O_5-P_2O_5 are resistant to gamma-irradiation with a dose up to 10^8 r and to neutron irradiation -- with a dose up to $4 \cdot 10^{17}$ neutrons/cm^2. With increase in radiation dose specific conductivity begins to rise, producing a 10 percent increment [29].

3. Effect of Radiation on the Dielectric Properties of Materials

When an irradiated dielectric interacts with a variable electrical field, just as in processes of electroconductivity, we must differentiate phenomena occurring directly during the irradiation period from residual radiation effects. The extent of their interaction cannot be predicted in advance, therefore the absence of changes in the dielectric characteristics following irradiation still does not indicate that the parameters are stable and provides no grounds for recommending the use of the materials under irradiation conditions.

Dielectric losses and depolarization of charges depend on the packing density of structural elements, that is, on how compactly the minimum potential energy sites are filled and how deep the minima are. Structural distortions arising owing to irradiation can lead to some energy nonidentity of particular regions of a solid, thereby causing supplementary polarization of electrical charges. Conditions for the movement of weakly bound ions in restricted volumes are produced in a distorted lattice, which gives rise to dielectric losses. Since dielectric polarization and dielectric losses, depending on the frequency of the field and the temperature, proceed via a different mechanism, and naturally different radiation damage manifests itself in any particular temperature-frequency range.

The formation of electrons and holes leads to the appearance in an irradiated dielectric of new electrical transitions often with extremely low energies of activation, which produces some increase in dielectric losses. This phenomenon was noted by Stevels [30] who measured dielectric losses of monocrystalline quartz irradiated with electrons and x-rays, at a frequency of 32 kHz in the low temperature range. No increase in dielectric losses occurred in quartz glass and multicomponent glasses, in spite of the formation of color centers.

Comparison of radiation changes in dielectric properties of quartz and quartz glass enables us to trace the effect that the structure of a material has on its radiation resistance. Measurements made directly during x-ray irradiation showed that the rise in the dielectric loss angle for monocrystalline quartz is much greater than for the monocrystal or for quartz glass [31]. The increment becomes greater as the frequency is reduced (Table 28).

The frequency dependence of changes found enables us to relate them to the increase in the electroconductivity after irradiation. The dissimilar increase in conductivity for equal amounts of freed photoelectrons in fused and in monocrystalline quartz can be accounted for by the different conditions under which the current carriers move. The length of the free path of carriers becomes less as we go from monocrystalline to polycrystalline and amorphous states [32]. This function was observed also for gamma-irradiation [27]; here it was noted that change in the dielectric properties of natural quartz contaminated with impurities is much weaker than in pure synthetic quartz. Quartz glass at these frequencies remains virtually stable after irradiation.

The change in dielectric permeability of monocrystalline quartz that results in higher capacitance of a sample during its exposure to gamma-irradiation indicates the manifestation under these conditions of a supplementary polarization process, which may be, according to [27], the polarization of Compton or photoelectrons captured by traps. Chesney and Johnson [35] stated that changes in the dielectric properties of quartz glass subject to reactor irradiation are unrelated to the initiation of color centers. Otherwise saturation would be observed in the region of 10^{16} neutrons/cm^2, which corresponds to saturation of the optical absorption

TABLE 28. DIELECTRICAL LOSSES OF FUSED SILICA AND MONOCRYSTALLINE QUARTZ

A Частота в Гц	B Диэлектрические потери tgδ·10⁻⁴			
	C плавленого кремнезема		D монокристаллического кварца	
	E исходного	F облученного	E исходного	F облученного
30	5	7	42	2000
10^2	4	5,5	40	1100
10^3	3	4,5	35	360

KEY: A -- Frequency in Hz
B -- Dielectrical losses
C -- Of fused silica
D -- Of monocrystalline quartz
E -- Initial
F -- Irradiated

TABLE 29. CHANGES IN DIELECTRICAL PROPERTIES AND DENSITY OF QUARTZ GLASS AFTER REACTOR IRRADIATION [33]

A Доза в нейтрон/см²	ε	tgδ·10⁴	B Плотность в г/см³
0	3,8 ± 0,1	0,2 ± 0,1	2,196
$6\cdot10^{16}$	3,7 ± 0,1	0,2 ± 0,1	—
$2\cdot10^{17}$	—	0,4 ± 0,1	—
$6\cdot10^{17}$	—	6 ± 0,5	2,216
$2\cdot10^{19}$	3,6 ± 0,1	14 ± 1	2,238
$5\cdot10^{19}$	3,6 ± 0,1	18 ± 1	2,241

KEY: A -- Dose in neutrons/cm^2
B -- Density in g/cm^2

TABLE 30. CHANGE IN DIELECTRICAL PROPERTIES OF ALPHA-CORUNDUM RESULTING FROM REACTOR IRRADIATION

A Доза в нейтрон/см²	ε	tgδ·10⁴
0	9,2 ± 0,1	0,3 ± 0,1
$6\cdot10^{16}$	9,2 ± 0,1	0,3 ± 0,1
$2\cdot10^{17}$	9 ± 0,1	0,5 ± 0,1
$6\cdot10^{17}$	8,9 ± 0,1	4 ± 0,5
$2\cdot10^{19}$	8,4 ± 0,1	2 ± 0,25
$5\cdot10^{19}$	8,3 ± 0,1	1 ± 0,25

KEY: A -- Dose in neutrons/cm^2

band. The authors of the work [34] relate the rise in dielectric losses at a frequency of 1 MHz to the inception of oxygen and other vacancies. As follows from Table 29 [33], change in dielectric properties is not related to change in the density of quartz glass, which was mentioned earlier by Zubov and Grishin [34].

The above-noted frequency dependence of dielectric properties results in fused silica proving to be insensitive to neutron irradiation in the UHF range [35].

As for dielectric losses, corundum is less sensitive to irradiation compared with quartz. Still, its dielectric permeability at 10^6 Hz varies within the limits 10 percent (Table 30, [33]).

Very high integral beams of thermal neutrons (10^{21} neutrons/cm^2 and higher) have a very appreciable effect on the dielectric properties of corundum. These radiation defects are persistent and are not annealed at elevated temperatures [20].

Paymal [23], conducting an extensive study of several glasses subject to irradiation in a reactor, derived the dose function of changes in their dielectric properties. Here he noted an appreciable rise in losses in the UHF range for relatively small radiation doses (Fig. 64), while changes in dielectric permeability for the same doses do not exceed 1 percent for Pyrex and somewhat higher (up to 1.5 percent) for lead glass.

Restoration of certain properties takes place after heating to 770° K, that is, in the annealing temperature range. Here dielectric losses of irradiated glasses increase markedly at the beginning heat treatment, but then drop down to their initial values.

The reason for the changes in dielectric properties upon reactor irradiation is held by Paymal to be the inception of "hot zone", that is, regions with excited state in which potential wells containing alkali cations are modified. Still there are reports that dielectric properties of glass condensers subject to reactor irradiation at a dose of 10^{18} neutrons/cm^2 are stable [36].

Our investigation [37] of dielectric properties of reactor-irradiated pyroceramics, in particular, two lithium aluminum silicate, aluminum manganese, and aluminum borosilicate pyroceramics, conformed to the dependence found by Paymal: change in dielectric properties of the first three pyroceramics in the range 10^5 - 10^7 Hz is strongly manifested at weak radiation doses. The absence of any appreciable changes in the dielectric properties of aluminum borosilicate pyroceramic is explained by the absence of alkali cations in its composition. Changes caused by irradiation are reversible and are eliminated with annealing.

The stability of dielectric properties of ceramic materials depends on the chemical composition and the properties of the ceramic. There are

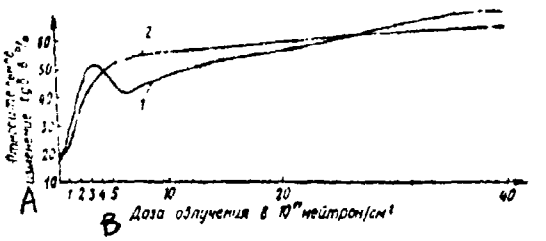

Fig. 64. Change in dielectrical losses of Pyrex 1 and lead 2 glasses at a frequency of 9000 MHz as a function of radiation dose

KEY: A -- Relative change, tg δ in %
B -- Radiation dose in 10^{17} neutrons/cm^2

reports that no changes in capacitance of ceramic condensers occur after irradiation with a dose of 10^8 neutrons/cm^2 [38]. At the same time, gamma-irradiation of B-1 ceramic with doses upwards of 10^6 r noticeably modifies its dielectric properties; relaxation losses become less, but conductivity losses mount [39]. After irradiation with decelerating gamma-rays from a betatron at a dose of $4.8 \cdot 10^4$ r, the dielectric properties of B-10 ceramic were unchanged [39]. Irradiation of ferroceramics in a reactor with doses up to $10^{17} - 10^{19}$ neutrons/cm^2 led to an appreciable change in the dielectric loss angle, and in some materials -- even to the appearance of a relaxation maximum on the frequency function curve [40].

Extended (three months' long) irradiation of barium titanate in a reactor caused the ferroelectrical properties to disappear; dielectric permeability was reduced by a factor of 2. The authors of this study [41] maintained that the noticeable change in the properties of the ceramic associated with structural disruption is possible only for neutron irradiation. For gamma-irradiation with doses upwards of 10^6 r, the change in the dielectric properties in a weak field is caused by the formation of color centers in the glass phase. This produces some reduction in relaxation losses and an increase in conductivity losses. In the range of strong fields (2 kv/cm), at the time of gamma-irradiation even a small dose -- approximately 10^4 r -- leads to an abrupt rise in dielectric permeability and losses owing to gas ionizing in the pores of the ceramic.

The relationship of changes in dielectric properties and the formation of color centers is emphasized in the work [42], where correspondence of the spikes of the temperature dependence of dielectric losses at 500 kHz and thermal luminescence of the titanates of magnesium and strontium irradiated with x-rays was discovered. On attaining the temperature of the thermal luminescence spike, the pattern of the temperature dependence of dielectric losses agrees with the pattern of this function for the unirradiated sample.

Change in the radiation dose intensity affects the results of measurements made of dielectric properties immediately during irradiation. Thus, a dose intensity of 400 r/min, when muscovite and phlogotite were irradiated in a betatron, caused no changes in the temperature dependence of dielectric losses. Raising the dose intensity to 1000 r/min for the same radiation doses ($5 \cdot 10^4$ r) leads to the shape of the curve being modified. These changes become greater as the frequency is lowered, and tg δ and ε of irradiated micas are lower in the low-temperature region than initial values, and vice versa -- in the high-temperature region [41].

CHAPTER TEN

EFFECT OF RADIATION ON THE STRUCTURE OF MATERIAL

1. Change in Phase Composition of Materials When Irradiated

Phase and structural changes in glasses, pyroceramic, and ceramic materials induced by nuclear radiation depend essentially on the kind of radiation exposure and the nature of the material irradiated. In spite of quite a large number of experimental data, thus far there is no clear answer to all problems of the relationship between the radiation stability of materials and their structure. Several experiments indicate that the radiation stability depends on the type of bonding, density of packing, and type of crystalline structure of the irradiated material [1]. In ionic structures, owing to the symmetric electrostatic bonds between particles, change in the mutual arrangement of the latter do not lead to bond rupture, but diffusion and annihilation of defects are facilitated. Confirmation of this kind of "crystallochemical" concept is the fact that as the ionicity of bonding is reduced, resistance to fast neutrons decreases in the series Be-O; Al-O; Zr-O; and Si-O [2]. It has been noted that more compact and symmetric structures have higher radiation stability.

In contrast to quartz, coecite, for example, with a density of 3.01 g/cm^3, does not change its structure at a radiation dose of $2 \cdot 10^{20}$ neutrons/cm^2 [3]. Irradiating anisotropic crystals is accompanied by anisotropic changes in their crystal lattice, which makes structural disruptions more extensive. A large number of displacements leading to the distortion mainly of one of the cell parameters caused the amorphization of beryllium, topaz, and zircon when irradiated with a beam of $6 \cdot 10^{20}$ neutrons/cm^2 [4]. One feature of phase transitions under the effect of nuclear radiation (mainly reactor) is the formation of more symmetric structures. Monoclinic zirconium dioxide, when subject to neutron irradiation at a dose of $3.6 \cdot 10^{20}$ neutrons/cm^2, changes into the cubic modification, whose temperature field of stability lies above 2170° K. In the presence of a small amount of impurities stabilizing the cubic phase (V, Cr, Ta, and so on), transformation occurs under conditions of moderate irradiation. The cubic structure parameter is noticeably

larger than in ordinary stabilized zircon. Tetragonal crystals of the titanates of beryllium and lead, and also potassium niobate undergo a transformation as the result of irradiation, initially leading to change in cell parameters, but then also to total transition to the high-temperature cubic structure [4].

According to the crystallochemical concept, phase transformation is possible only when it takes place via displacements of atoms under the effect of radiation and does not require the fundamental rearrangement of atoms [5]. Modification transitions occur through the accumulation of ordered displacements associated with the initial and terminal positions of atoms. Based on similar views, we can explain the phase transformations of quartz observed after neutron irradiation [6].

By comparing changes in the crystalline structure of several oxides, carbonates, and titanates after irradiation with a beam of fast neutrons, $2.8 \cdot 10^{19}$ neutrons/cm^2 at 353° K, with structural changes upon heat treatment, Hauser and Schenk [7] concluded that it is the displacements that have the determining role, and not the thermal effects of irradiation. At the same time it was noted that in the presence of even a small amount of impurities fissioning upon irradiation with the release of quite large quantity of energy, the crystalline structure of certain materials begin to undergo changes at lower radiation doses. The structure of tourmaline $NaMg_3B_3 \cdot Si_6O_{27}(OH)$ becomes amorphous at a dose of $7.8 \cdot 10^{19}$ neutrons/cm^2, owing to a nuclear reaction at the B^{10} isotope. The nuclear reaction products dissipate significant energy at short distances, which leads to phase transitions in the region of thermal spikes [4]. Possibly, the transition of monoclinic baddeleite into the cubic form is related to the presence of a small amount of uranium that is an accessory element to zirconium [4].

In contrast to the concepts emphasizing the role of the initial structure and the crystallographic ratio between it and the induced phase in the manifestation of radiation stability of a material, at present increasing confirmation is being found for views stating that the stability of a structure determined only by the presence in it of metastable high-temperature phases and by the possibility of the transition to their stability region under radiation conditions. This kind of "thermodynamic" concept was advanced by Prinak based on study of phase and structural changes in large number of crystalline materials (beryl, germanium dioxide, germanium, silicon, aluminum, rutile, fluorite, periclase, spinel, diamond, carborundum, chrysoberyl, phenacite, and quartz) [8-9]. The cause of phase transitions is to be found in thermal spikes, as a result of which a temperature and pressure essential for transformation into the modification corresponding to these conditions are provided in certain bounded volumes.

In contrast to experiments described in the study [5], Elston [10], based on a study of phase composition and structure of crystalline oxides of aluminum, magnesium, beryllium, silicon, and glassy silica irradiated

in a reactor at 353° K, showed that damage is quite limited if the structure of the oxide is stable throughout the temperature range all the way up to the melting point and the sites of localization of mixed ions have the same coordination as in normal ions. In contrast, the damage is greater if new types of crystalline structure of a given material exist at a high temperature. In this case neutron irradiation at 353° K causes the same effect as a temperature rise.

As far as we can see, both mechanisms of phase transformations upon irradiation can take place, however the predominance of a particular effect is determined by the phase composition of the material irradiated.

In all cases of phase transformation under the effect of thermal spikes, the high-temperature phase is characterized by high density (at least the density remains unchanged) [11]. The Clapeyron-Clasius equation will serve as a criterion for the possibility of a phase transformation in irradiated material:

$$dT/dp = (V_{HT} - V_{LT})/S,$$

where T is the temperature in ° K; p is the pressure in dynes/cm^2; V_{HT} is the molar volume of the high-temperature phase in cm^3/mole; V_{LT} is the molar volume of the low-temperature phase in cm^3/mole; and S is the entropy in cal/deg.

When the high-temperature phase is more dense, $V_{HT} < V_{LT}$ $(dT/dp) < 0$, that is, the phase transformation temperature decreases. Since the pressure within the thermal or structural spike is $2 \cdot 10^{10}$ neutrons/m^2 [12], the phase transformation temperature must be reduced by several hundreds of degrees.

The study [13] indicates that the transition of quartz into the high-temperature modification can occur at 473° K. Roy and Bushmer [13, 14] discovered a drop in the alpha-quartz → beta-quartz transformation temperature from 849 to 838° K after irradiation with a neutron beam of only $2.4 \cdot 10^9$ neutrons/cm^2. The transformation temperature of alpha-cristobalite to the beta-form after this irradiation regime was lowered from 533 to 415° K.

Irradiating calcium orthosilicate, gamma-Ca_2SiO_4, with a dose of 10^{17} neutrons/cm^2 increase the amount of the beta-form, which is denser, and this transformation took place at a temperature somewhat below the temperature in ordinary conditions [13]. A similar pattern is observed in the transition PbO (litharge) -- PbO (massicot) [13].

A dose of $6 \cdot 10^{19}$ neutrons/cm^2 causes the transformation of quartz into the high-temperature modification [3], though more recent studies showed that the structure resulting from irradiating quartz with doses of $(5\text{-}6) \cdot 10^{19}$ neutrons/cm^2 is not ordinary beta-quartz [15]. Transformations of quartz into cristobalite irradiated with a beam of $2.4 \cdot 10^{14}$

neutrons/cm^2 at temperatures of 1420-1800° K has not been observed, since at temperatures this high the radiation damage is annealed [14].

Results found by Roy and Buhsmer in the transformation of irradiated quartz to coecite and of irradiated coecite into quartz [13], and also in the crystallization of irradiated quartz glass in a field of quartz and coecite showed that due to the initiation of a special structural state upon irradiation, all phase transitions become facilitated, and the increase in the rates of transformations demonstrates the analogy between the effect of neutron bombardment and the effect of increasing the temperature. A dose of $2 \cdot 10^{20}$ neutrons/cm^2 causes devitrification of quartz glass, with the segregation of PbO_2 [16].

Phase transitions and structural changes induced by neutron irradiation of several silica modifications have been studied in close detail at the present time. Based on the work [12], three stages of radiation damage to the silica structure are differentiated:

1) the appearance of point defects leading to weakening and rupture of Si-O bonds and to change in the near order of tetrahedra;

2) conversion of alpha-quartz into the high-temperature (or a similar) modification; and

3) amorphization with the preservation of some symmetry of the host crystalline matrix.

Structural damage in the first stage of irradiation, in the view of some authors [17], amounts to a change in the Si-O-Si bonding angle. In the view of others [18], the change in the bonding angle between tetrahedra is impossible without change in the Si-O distance. Displaced silica atoms are mainly oxygen atoms, on advancing into a small volume, cause a cascade process -- a displacement spike or a thermal spike. This leads to the temperature in this region being raised to 2770° K during a period of about 10^{-12} sec [19]. Thus, even at early stages of irradiation thermal processes and related modification transformations in thermal spikes begin to come into play. Phase transitions at the second stage of irradiation (doses of 10^{19} - 10^{20} neutrons/cm^2) were discussed above.

At high doses (more than 10^{20} neutrons/cm^2), crystalline modifications of silica are observed to become amorphized. Initially small amorphous zones, about 2 nanometers in size, appear [20]. As the radiation dose is intensified, the number and dimensions of the amorphous zones rise (their diameters are 8, 12, and 21 nanometers and more and the volumes occupied by the zones are 0.8, 4, and 9.3 percent of the total irradiated volume at doses of 10^{19}, $6 \cdot 10^{19}$, and $8 \cdot 10^{19}$ neutrons/cm^2 [21]). When the doses are stronger than $8 \cdot 10^{19}$ neutrons/cm^2, these domains begin to interact, and stable hexagonal defects observed in an electron microscope are formed. The concentration and orientation of these defects, in the view of the author of [22] indicate the possibility of structural rearrangements taking place simultaneously according to the mechanism of displacements

and thermal spikes. A dose of $2 \cdot 10^{20}$ neutrons/cm^2 transforms crystalline quartz into the isotropic form with the symmetry of the high-temperature modification [23]. Irradiating rods of sintered quartz glass containing some cristobalite, with a dose of $4 \cdot 10^{20}$ neutrons/cm^2 causes cristobalite to become amorphized [24].

Thus, all known experimental facts showed that formation of submicroscopic amorphized domains accompanied by change in the surrounding crystal lattice is the dominant type of process causing phase changes in irradiated quartz and its modifications.

The source of thermal spikes in which mainly structural and phase changes are localized are the heavy particles, either bombarding the target from without or else formed through reactions of nuclei with neutrons. The thermal spike in this case is a particle track, that is, a section of the material lying along the particle's trajectory. The modified structure of the material in the tracks enables the tracks to be manifested after etching, and then to be observed in an electron and even in an optical microscope [25]. Track diameter and length depend on the kind of bombarding particles and the energy dissipated per unit path length. Light nuclei of hydrogen and helium do not produce tracks in minerals [26]. Lithium nuclei, when releasing energy of about 1000 ev/nanometer, produced detectable tracks in certain structures [27]. The most typical tracks are produced by bombardment with the fission fragments of uranium nuclei [27, 28]. In this case observation in the electron microscope of etched samples enables tracks with length from fractions to several tens of nanometers to be differentiated.

There is a well-defined relationship between the density of tracks in a volume and the degree of phase changes noted by x-ray diffraction patterns or in some other manner [21, 29]. At the same time, the possibility of recording tracks depends to a greater extent on the structure of the material (uniformity and grain size) and is uncorrelated with the extent of phase changes. Tracks are recorded more easily in glassy or fine-grained materials than in coarse-grained materials. This phenomenon, and also the fact that the diameter of track observed, regardless of the nature of the material (BeO, Al_2O_3, or ThO_2), usually corresponds to the size of the grain of the irradiated material is associated with the loss of thermal energy owing to its dissipation at intergrain or interphase boundaries [30, 31].

Naturally, phase transformation are observed also after bombardment with heavy particles. The difference between the results of this kind of irradiation lies in the thickness of the degenerate layer. These phase changes are observed when crystalline quartz is irradiated with 40 kev heavy xenon ions. A dose of $4 \cdot 10^{13}$ ions/cm^2 produces some amorphization in the surface of quartz, but a dose of $2 \cdot 10^{16}$ ions/cm^2 results in the inception of an amorphized layer, although differing in x-ray diffraction characteristics from glassy SiO_2 [32]. The author of [32] believes that anisotropy of expansion and low atomic packing density

are essential for phase transformations: irradiating anisotropic oxides TiO_2, Al_2O_3, and U_3O_8 transforms them into the quasi-amorphous state [33].

When the surface of glass and ceramic is bombarded with Xe, Kr, Ar, and Ne ions at different angles, it is possible to observe different cross-sections of ellipsoidal thermal spikes, whose major axis is oriented along the ion track. The central region of this spike proves to be depleted of mobile weakly bounded ions (Na, K, and Al), which are injected into the lattice at the periphery of the spike [34, 35]. A similar, though somewhat weaker effect is observed when glass is irradiated with alpha-particles emitted by radon, each of which releases about 10^5 cal/cm^3 within a track volume [36], corresponding to a temperature rise of the order of 10^4 deg during a period of about 10^{-11} sec. Naturally, chemical and thermal changes occurring in traps lead to different chemical stability of matrix and of sections that have been exposed, which reveal the nonuniformity of radiation damage to material caused by etching and the subsequent observation in the microscope [37].

Reactor irradiation of several refractory ceramic material (the ceramics 22KhS, M-7, MG-2, and uralite) at 470° K with doses from $2.2 \cdot 10^{19}$ to 10^{20} neutrons/cm^2 at a neutron beam intensity of $1.2 \cdot 10^{13}$ neutrons/cm^2 · sec and a gamma-background of $1.1 \cdot 10^4$ rad/sec enables us to conclude that these materials are resistant to this exposure. Changes noted in the parameter of the alpha-Al_2O_3 lattice (22KhS, M-7) and weakening of the diffraction maxima of anorthite and celsian (MG-2, uralite) were very weak [38].

In cordierite ceramic materials, the amount of crystalline phase determined roentgenographically, decreases as the result of reactor irradiation [39]. According to [15, 40], no changes were observed in the x-ray diffraction pattern of hot-pressed and monocrystalline aluminum oxide after being irradiated with integral beams of $2 \cdot 10^{20}$ neutrons/cm^2 at 305-310° K. However, in the study [41] an increase in diffusion scattering in the Laue diffraction pattern of corundum irradiated with the beam of $5.5 \cdot 10^{19}$ neutrons/cm^2 at 350° K was detected; this increase can be eliminated by annealing at 1470° K.

Our x-ray diffraction pattern study of polycrystalline aluminum quartz irradiated in a reactor with an integral beam up to $8 \cdot 10^{18}$ neutrons/cm^2 showed no changes in phase composition. Our x-ray diffraction pattern, petrographic, electron microscopic, and also dilatometric studies enable us to find changes in the phase composition of irradiated pyroceramics; if several phases differing in crystallization temperatures were present, low-temperature phases broke down and high-temperature phases became crystallized. Breakdown of low-temperature beta-eucryptite solid solutions occur, and to a greater extent if the solutions are in a mixture with high-temperature crystallization products, and if as the result of recrystallization high-temperature modifications and cristobalite are formed. In aluminum-magnesium pyroceramics where

cristobalite is the low-temperature phase, the cristobalite content becomes reduced after irradiation. There are no changes in phase composition in the borosilicate pyroceramic IV-23, whose crystalline phase is mullite, since higher temperature phases do not exist in the system [42-43].

As remarked, the radiation stability of crystalline phases depends on many factors; however in the case of pyroceramics which in themselves are metastable systems, evidently the stability of crystalline phases is determined primarily by their stability at temperatures building up in thermal spikes upon irradiation. Hence the determining role of thermodynamic stability of phases at the temperatures of radiation heating of domains of the material is confirmed. The authors of [34] reached these same conclusions based on a study of phase and structural changes in glasses and ceramics irradiated with ions of inert gases. Results of this investigation afford the conclusion that the predominant role in the changes occurring in the structure of crystalline bodies at low energy of bombarding particles is mainly that of the relatively uniformly distributed displacements, and the thermal spikes or displacement spikes begin to play a marked role as the particle energy is increased. But in amorphous glasses, nonuniformity of radiation exposure determined by the presence of spikes is observed at all energies.

All the above-described phase transitions in various materials are caused by strong radiation exposure to fast neutrons or nuclear fragments. However, we were able to observe phase changes, namely some increase in the quantity of crystalline phase in pyroceramics irradiated with gamma-radiation at doses of $10^5 - 10^6$ r [44, 45]. Evidently, this phenomenon is not merely accidentally noted in pyroceramics, since a heterogeneous metastable pyroceramic system is particularly sensitive, phasewise, to exposure of even relatively small amount of energy in any form — thermal or radiational. The possibility of a glass crystallizing when exposed to gamma-rays has been reported earlier [46] (the irradiation of a glass with the composition $BaO \cdot B_2O_3 \cdot PbO$, at a dose of 10^8 r, leads to devitrification).

2. Change in Density and Volume of Materials When Irradiated

Change in densit s one of the more important indicators of radiation damage suffere material (Table 31).

Naturally, density changes are related primarily with structural changes, in particular, with an increase in cell parameters; for example, a change in the density of sapphire (by 10 percent) is associated with a 0.3 percent increase in the cell parameter a, and a 0.45 percent increase in the cell parameter c [48], recorded by x-ray diffraction pattern. The density of alpha-corundum irradiated with an integral beam of 10^{19} fast neutrons/cm^2 at 310° K is reduced by 0.1-0.15 percent [49]. A decrease in the density of sapphire reaches saturation at 10^{2} neutrons/cm^2,

TABLE 51. EFFECT OF IRRADIATION ON THE DENSITY OF MATERIALS [44]

Материал A	Доза в нейтрон/см² B	Плотность материала в г/см³ C	
		исходного D	облученного E
Сапфир F	$6 \cdot 10^{20}$	3,98	3,94
BeO	$7 \cdot 10^{19}$	2,84	2,85
Шпинель G	$4 \cdot 10^{20}$	3,6	3,6
ZrO_2	$3 \cdot 10^{20}$	3,73	3,58
Стеатит H	$7 \cdot 10^{19}$	2,79	2,70
Кварцевое стекло I	$7 \cdot 10^{19}$	2,204	2,255
TiO_2	$3 \cdot 10^{20}$	4,01	3,98
Оконное стекло J	$3 \cdot 10^{19}$	2,509	2,53
Фарфор K	$4 \cdot 10^{20}$	3,41	3,39
Слюда L	$2 \cdot 10^{20}$	2,84	2,41
Форстерит M	$6 \cdot 10^{19}$	3,05	3,03

KEY: A -- Material
B -- Dose in neutrons/cm^2
C -- Density of material indicated below, in g/cm^3
D -- initial
E -- irradiated
F -- sapphire
G -- Spinel
H -- Steatite
I -- Quartz glass
J -- Window glass
K -- Porcelain
L -- Mica
M -- Forsterite

but after heating to 1670° K it is completely eliminated. The change in cell parameters takes place at constant c/a ratio up to $3 \cdot 10^{20}$ neutrons/cm^2, and then the c parameter begins to increase rapidly. In spite of the overall reduction in density, electron-microscopic study of irradiated sapphire reveals the presence of consolidated domains 0.15 nanometer in diameter, whose dimensions increase with dose [50].

Of particular interest are changes in the density of crystalline quartz and quartz glass. An integral beam of $7 \cdot 10^{19}$ neutrons/cm^2 causes the density of alpha-quartz to be reduced from 2.65 to 2.49 g/cm^2, that is, by 6 percent [12]. Increasing the integral beam up to $1.4 \cdot 10^{20}$ and $2 \cdot 10^{20}$ neutrons/cm^2 leads to a change in density of 13 and 14.7 percent, respectively [51, 52]. At the same time quartz glass becomes consolidated when irradiated. An integral beam of $7 \cdot 10^{18}$ fast neutrons/cm^2 yields a 0.3 percent consolidation [53], while a beam of $7 \cdot 10^{19}$ neutrons/cm^2 results in a 2.3 percent greater consolidation [48]. A 0.37 percent decrease in sampling and a 1.1 percent increase in density was achieved for pressed glassy silica after irradiation with a beam of $2 \cdot 10^{20}$ neutrons/cm^2 [54]. Saturation of density changes in quartz glass occurred at $4 \cdot 10^{20}$ neutrons/cm^2.

The increase in the density of quartz glass when irradiated does not lead to crystallization, evidenced by the x-ray diffraction pattern. According to the work [56], bulk changes occurring in quartz glass when irradiated in a reactor are due to three processes: nonuniform consolidation on exposure to fast neutrons (to $5 \cdot 10^{19}$ neutrons/cm^2), homogenization (up to $5 \cdot 10^{20}$ neutrons/cm^2), and expansion caused by ionization effects, which are noticeable at low doses, but then this expansion changes into compression.

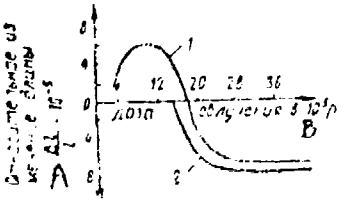

Fig. 65. Change in linear dimensions of quartz glass after gamma-irradiation. Dose intensity as below:
1 -- $6 \cdot 10^5$ r/hr
2 -- $2.7 \cdot 10^5$ r/hr
KEY: A -- Relative change in length
B -- Radiation dose in 10^5 r

Reactor irradiation of quartz glass previously compressed at high pressure, as well as x-ray irradiation, causes a decrease in existing consolidation. On this basis, ionization processes leading to electrostatic repulsion of ionized ions are resorted to in explaining the expansion [56], that is, change in interatomic distances and mutual arrangement of tetrahedra. However, exposure of quartz glass to ionizing radiation is also accompanied by consolidation, which is dose-dependent. An increase in the density of quartz glass of different grades after exposure to electrons, x-, and gamma-rays has been noted in the study [57]. A more complicated dose dependence of the density of quartz glass irradiated with gamma-radiation was obtained in the work [58] (Fig. 65).

Paymal et al. [59] investigated the change in the density of large number of glasses containing not less than 1 percent B_2O_3, as a function of their chemical composition and the neutron radiation dose. The principal role in the effects observed by the authors are attributed to the heavy particles initiated in the nuclear reaction $B^{10}(n, \alpha)Li^7$, where exposure to these particles leads to two competing processes: an increase in density in the external regions of the thermal spikes, and hardening, accompanied by disintegration in the internal domains of the thermal spikes. The saturation dose for the first process is five-ten times weaker than for the second. According to the model advanced, the thermal spike zone is similar to a walnut

with a loose kernel and a hard shell. Depending on how much volume is occupied by the kernel or the shell, either consolidation or reduction in the density of glass is observed after irradiation. The chemical composition of the glass has the same effect on the consolidation of glass that has been irradiated, as for glass exposed to high pressure, that is, the effect diminishes with increase in alkali constant [59, 60, 61]. If prestressed Pyrex is irradiated, this consolidation will be less.

Obviously, the density changes accompanied by a change in the volume of the sample. Shrinkage of a Pyrex glass sample 50 mm long when irradiated with a dose of $(7-8) \cdot 10^{18}$ neutrons/cm^2 and an intensity of $1 \cdot 10^{12}$ neutrons/cm^2 · sec is 2730 nanometers according to the study [62], but 1700 nanometers -- at an intensity of $1.9 \cdot 10^{13}$ neutrons/cm^2 · sec (this dependence on dose intensity is possibly related to the radiation heating of the sample). More appreciable consolidation (3.3 percent) is observed for Vycor glass at a dose of $5 \cdot 10^{18}$ neutrons/cm^2 [59].

According to our measurements of the density of pyroceramics of different compositions irradiated with doses of $10^{18} - 10^{19}$ neutrons/cm^2, the principal effect of irradiation is an increase in the density of boron-containing materials and a reduction in the density of nonboron-containing materials. However, at moderate doses (10^{16} neutrons/cm^2), a change of an opposite nature is observed. Gamma-irradiation with doses of $5 \cdot 10^8 - 10^9$ r do not cause detectable changes in density of the same pyroceramics and of the glasses K-8, LK-5, K-108, window glass, and glass 13 v.

At the same time, the report [63] notes that Terex glass used in mercury lamps (80 percent SiO_2, 13 percent B_2O_3, 4 percent Na_2O, 1 percent K_2O, and 2 percent Al_2O_3) is consolidated by $6 \cdot 10^{-3}$ g/cm^3 after extended ultraviolet irradiation.

Interferometric measurements of polished samples of polycrystalline materials expanded after irradiation showed that depending on the radiation dose, the irradiated section of the surface is observed to rise over the unirradiated surface. The height of the protrusion (in nanometers) at the surface of certain materials irradiated with 140 kev protons and 140 kev helium nuclei is as follows [64]:

sapphire	110
spinel	80
rutile	60
peridot	240

A quartz sample irradiated with 100 kev protons yield a protrusion 220 nanometers high. After glassy SiO_2 was irradiated, the sample was observed to be compressed by 0.9 percent in all directions [65].

The irradiation of mono- and polycrystals of carborundum, sapphire, stabilized and monoclinic zirconium oxide, beryllium oxide, quartz, copper,

and graphite with 95 Mev uranium decay products at integral beams up to $5 \cdot 10^{14}$ particles/cm^2 caused a bulge in the irradiated surface toward the radiation source side. An exception was monoclinic ZrO_2, whose surface bulged in the opposite direction [66]. The bulge increased in the series MgO-SiO-BeO-graphite-Al_2O_3-ZrO_2-carbon-SiC. Upon annealing, this effect disappeared more rapidly, the higher the temperature. X-ray diffraction measurement of lattice parameters shows that the difference in the relative expansion between the extreme members of the series exceeds one order of magnitude; still, there is no lattice breakdown even after the most intense increase in volume (SiC).

A bulge after neutron irradiation of Pyrex plates protected on one side with a cadmium shield was observed by Paymal [62], and the bulge maximum occurred at a dose of $2.5 \cdot 10^{17}$ neutrons/cm^2.

Table 32 gives the characteristics of the increase in samples of hard-pressed BeO (density 2.98 g/cm^3), and monocrystals of MgO and Al_2O_3 caused by reactor irradiation [67].

From Table 32 we see that BeO undergoes particularly intense volumetric changes. The causes of the BeO bulk expansion have been studied quite closely at the present time. At lower doses this amounts to anisotropic expansion of the crystal lattice producing, with increase in dose, cracking of the sample and separation of grains along the intergrain boundaries. Both factors dominate for low-temperature irradiation. As the radiation temperature is raised, processes of coalescence of point defects begin to be manifest and voids begin to deformed within grains, which are filled with gases formed in nuclear reactions in considerable amount at doses of approximately 10^{20} neutrons/cm^2. Then the gases are given off from the grains (even with an explosion) and cause the grains to split apart even further. Elston [68] maintains that the volumetric expansion of any material can be represented as the sum of the partial contributions of individual processes:

$$\left(\frac{\Delta V}{V}\right)_M + \left(\frac{\Delta V}{V}\right)_R + \left(\frac{\Delta V}{V}\right)_D + \left(\frac{\Delta V}{V}\right)_G + \left(\frac{\Delta V}{V}\right)_S,$$

where $(\Delta V/V)_M$ is the microscopic relative change in volume; $(\Delta V/V)_R$ is the relative change in volume due to the increase in the elementary cell parameters; $(\Delta V/V)_D$ is the same as above, owing to rupture of intergrain boundaries; $(\Delta V/V)_G$ is as above, due to the evolution of gases; and $(\Delta V/V)_S$ is as above, due to coalescence of defects and the initiation of voids and loops.

For BeO, $(\Delta V/V)_M = 2(\Delta a/a) + \Delta c/c$, and here $\Delta c/c \approx 4(\Delta a/a)$. At low temperatures and high radiation doses ($\sim 10^{21}$ neutrons/cm^2), the c/a ratio is as high as 10 [69], which leads to breakup of the material along the

grain boundaries [70]. For compact BeO, an integral beam of $(0.2\text{-}3) \cdot 10^{21}$ fast neutrons/cm^2 is the maximum allowable, after which the sample breaks down into a powder [71], and the powder grain size corresponds to the grain size in the initial material [72]. Raising the radiation temperature reduces the expansion of the material caused by an increase in the lattice parameters [73]; however, here gas evolution and coalescence of defects becomes stronger [70]. Still, the overall expansion of BeO at 370° K and an integral beam of $7 \cdot 10^{20}$ neutrons/cm^2 reaches a value of 6 percent, while that 870° and 1170-1270° K, the overall expansion is 6 and 1 percent, respectively [74], where 20 percent of the overall expansion is related to the evolution of gaseous helium. Defect cluster dimensions also increase with temperature. A dose of $6.5 \cdot 10^{19} - 1.5 \cdot 10^{21}$ neutrons/cm^2 at 348° K causes dark patches 3-7 nanometers in diameter to be formed, observable in an electron microscope; their size becomes 30 nanometers at 770-970°K [75].

High-temperature irradiation (1270-2270° K) of BeO with doses of $(3\text{-}5.3) \cdot 10^{20}$ neutrons/cm^2 makes it possible to observe clusters of defects in the form of 20-200 nanometer diameter of loops oriented in the basal plane or in the 1120 plane, in an electron microscope [76]. The same effect of clustering of defects oriented in specific crystallographic directions is observed after annealing at 1170-1770° K of BeO samples irradiated at low temperatures [77]. Coalescence of defects is observed also in filamentary BeO crystals after irradiation at a dose of 10^{20} neutrons/cm^2 at 1670° K [78]. Irradiation of monocrystalline BeO with 1.3 Mev electrons at doses of $(1.6\text{-}3) \cdot 10^{20}$ electrons/cm^2 causes a decrease in density by $(2.5\text{-}4) \cdot 10^{-4}$ g/cm^3, associated only with expansion of lattice parameters [79]. Macroscopic growth of polycrystalline BeO samples without transformation takes place upon x-ray irradiation and at elevated temperatures (870° K) [80]. Fig. 66 shows volumetric changes induced when various materials were irradiated in a reactor [68].

The causes of volumetric changes of quartz, quartz glass, and beryllium oxide were examined above. As for the expansion of oxides of magnesium and aluminum, they are determined mainly by lattice expansion [68]:

for hexagonal Al_2O_3 crystals

$$\left(\frac{\Delta V}{V}\right)_M \approx \left(\frac{\Delta V}{V}\right)_R = \frac{\Delta c}{c} + 2\frac{\Delta a}{a};$$

for cubic MgO crystals

$$\left(\frac{\Delta V}{V}\right)_M = \left(\frac{\Delta V}{V}\right)_R = 3\frac{\Delta a}{a}.$$

The increase in cell parameters in polycrystalline magnesium oxide reduces intercrystallite cohesion, which leads to a reduction in crystal strength.

With increase in radiation temperature or in annealing temperature of irradiated magnesium oxide, a deviation is observed between macroscopic expansion and the increase in the parameters of the elementary cell. This

TABLE 32. CHANGE IN LENGTH OF SAMPLES UPON IRRADIATION WITH NEUTRONS AT ENERGIES HIGHER THAN 1 MEV

Материал A	Относительное удлинение в % при дозе в нейтрон/см² B			
	4·10²⁰	11·10²⁰	4·10²¹	4·10²¹ при 1270°K C
BeO	0,06	0,72	—	0,68
MgO	0,091	0,295	0,349	0,003
Al_2O_3	0,072	0,287	0,406	0,05

KEY: A -- Material

B -- Relative elongation in % at dose in neutrons/cm^2 indicated below

C -- $4 \cdot 10^{20}$ at 1270° K

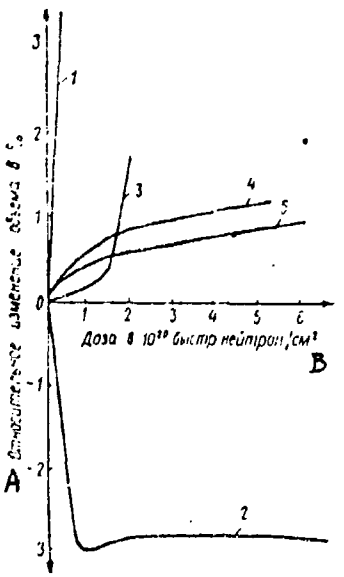

Fig. 66. Change in volume of certain materials after reactor irradiation

1 -- quartz
2 -- quartz glass
3 -- BeO
4 -- MgO
5 -- Al_2O_3

KEY: A -- Relative change in volume in percent

B -- Dose in 10^{20} fast neutrons/cm^2

is due to the mounting role of the coalescence of vacancies owing to diffusion. At low radiation temperatures and doses, these effects are weak in Al_2O_3 and MgO and are caused mainly by displacement spikes [81]. At elevated radiation temperatures, the concentration of defect clusters in MgO for doses higher than $3 \cdot 10^{19}$ neutrons/cm^2 reaches a value of $10^{15} - 10^{16}$ cm^3 for 10 nanometers diameter clusters, and the clusters are in the form of negative cubic crystals.

A further increase in radiation dose and temperature in the case of MgO leads to the evolution of inert gases formed in the reactions $Mg(n,\alpha)Ne$; $O^{16}(n,\alpha)C^{13}$, and their aggregation in pores formed, therefore gas bubbles have a regular crystalline form. The same result is attained by high-temperature annealing (1170-2070° K) of MgO crystals pre-irradiated at a dose of $4 \cdot 10^{20}$ neutrons/cm^2.

The evolution of gaseous products is a serious obstacle limiting the surface of materials under irradiation conditions. Radiation stability in this case is determined not only by the amount of gas given off, but to a large extent by the possibility of its diffusion and escaping to the surrounding space. In the case of a closed three-dimensional framework, gas diffusing through a lattice cannot escape freely, and this causes material to break up. But if the material has an open structure, for example, in the form of layers, the gas is able to collect between layers and to escape from these cavities [83]. Making porous materials with pores between grains can enhance their radiation stability [70].

Swelling of materials used in reactors due to gas evolution adversely affects their service qualities in reactors. At the same time, gas evolution upon irradiation must be reckoned with in designing electrovacuum instruments in which ceramics and especially glass have found extensive use.

In one of the first works [84] on gas evolution in this respect, various gases of commercial and specially prepared compositions coated with a film of metallic aluminum were irradiated with a beam of 20 kev electrons. After irradiation, the evolution of gas bubbles swelling the film was detected. Chemical analysis results showed that the gas was 95 percent oxygen, and its amount liberated under identical irradiation conditions was the smallest for quartz glass and increased as the test was made of alkali compositions in the series K-Na-Li (that is, with decrease in gas permeability and consolidation of the glass structure).

A detailed examination of this phenomenon made by Lineveawer [85] using electronic irradiation followed by heating to 470-620° K showed that the amount of gas given off obeys the following equation

$$Q = Q_E + Q_T = Q_\infty \left(1 - \exp \frac{t}{K}\right),$$

where Q is the total amount of gas given off in the time t; Q_E is the amount of gas given off upon irradiation; Q_T is the amount of gas given off with

subsequent heating; K is the measure of the time dependence of the degassing process; and Q_∞ is the maximum amount of gas capable of being evolved.

Table 33 gives the experimentally obtained Q_∞ values and calculated K values.

TABLE 33. CHARACTERISTICS OF THE GAS EVOLUTION OF VARIOUS GLASSES

Марка стекла A	Q_∞ при 300°K в мк·л* B	K в ч C	Марка стекла A	Q_∞ при 300°K в мк·л* B	K в ч C
0481	247	23,4	0120	72	7,7
8093	227	12,4	7740	66	5,5
9019	178	23,7	7070	51	12,5
9010	170	29,6	7800	49	3,2
0011	83	9,9	—		—

* microliter is the volume in liters at a pressure of 1 micron Hg

KEY: A -- Glass grade
B -- Q_∞ at 300° K, in microliters
C -- K in hours

The evolution of oxygen is associated with profound structural changes in irradiated glass sections, shown by a study of the cross-section of a sample [83]. In this examination the following was found:

1) the irradiated section of the surface is displaced in the direction of the electron beam; the displacement increases with increase in Q and reaches several nanometers for the amount of glass approximating Q_∞ ;

2) there is an abrupt change in the density of the sample at a depth of about 10 nanometers;

3) the depth at which the change in density occurs increases up to the free flight of electrons at a Q value approaching Q_∞ ;

4) coloring of samples begins at the boundary of layers with different density and extends depthwise by the amount of the free electron path;

5) in contrast to untreated glasses, the melting of irradiated glasses is not accompanied by the evolution of gas bubbles from the melt; and

6) when electronic bombardment was used, up to 10 percent of the oxygen contained in the glass was removed, that is, even oxygen incorporated into the structural network of the glass was removed.

The evolution of oxygen is intimately associated with processes of space charge accumulation (cf. Chapter Nine) and with the displacement of

mobile ions in the field of discharge. The displacement of alkali ions toward the glass surface liberates nonbridging oxygen ions previously associated with them, and the bonding of the oxygen ions in the lattice is disturbed, and they diffuse in the opposite direction. On approaching the grounded foil deposited on the glass surface, they become neutralized and form glass bubbles, aggregating under the foil.

Structural damage accompanied by degassing is so extensive that cases of breakdown of the following grades of glass samples are known: Corning 7720, 7052, 0080, 0120, and 1723 [86].

Irradiation with ionizing radiation (gamma-, x-, and ultraviolet rays) is also accompanied by the evolution of gases from the glass, intensified by subsequent calcining. However, here we must note that first of all the amount of gas evolved is much less than in electronic irradiation, and secondly the gas composition differs appreciably (Table 34). In this case the gas is mainly oxygen with impurities of carbon oxides. The evolution of hydrogen is more probably related to the radiolysis of water present in the glass and the dissociation of OH radicals [87]. Owing to the hindered diffusion in glasses with more compact structure, the amount of hydrogen given off is less. Oxides of carbon form near the glass surface via a reaction with the atmosphere [86].

TABLE 34. COMPOSITION AND AMOUNT OF EVOLVED GASES WHEN GLASS 7720 IS IRRADIATED

Количество газов в мкл, выделившихся из стекла A					
	после прокаливания в течение 3 ч при 588°K C				
без прокаливания B	H_2	CO	CO_2	H_2O	общее D
0	5,82	0,07	1,29	0,04	7,22
0,14	4,27	0,16	1,33	0,003	5,77

KEY: A -- Amount of gases in microliters evolved from the listed glasses
B -- without calcining
C -- after calcining for 3 hours at 588° K
D -- total

The hard-to-remove coloring of lead glasses caused by ionizing radiation is associated with the reduction of lead ions by hydrogen, in the view of the author of the study [86].

Alpha-particles have a weak effect on degassing owing to their weak penetrating ability. Irradiation with neutrons, especially of boron glasses, causes appreciable gas evolution, associated with nuclear reactions taking place at the B^{10} isotope. Alpha-particles and Li^7 nuclei forming due to the reaction alter the composition of the glass, cause helium to be given off, ionize atoms, and by breaking chemical bonds, lead to the initiation of thermal spikes promoting the degassing of the glass.

When boron-containing glasses undergo reaction irradiation, 94-99 percent of the evolved gas is helium. In addition, some of the gases associated with exposure to background gamma-radiation, whose chemical composition is the same as in pure gamma-irradiation, is given off. The evolution of helium is accompanied by the formation of some oxygen, evidently owing to the initiation of uncompensated oxygen ions after the fission of B^{10} nuclei into Li and He. This kind of structural damage led to the breakdown of several specimens at a dose of $4 \cdot 10^7$ neutrons/cm^2 [86].

CHAPTER ELEVEN

EFFECT OF IRRADIATION ON MECHANICAL AND THERMAL PROPERTIES OF MATERIALS

1. Initiation of Stresses and Change in the Strength of Materials when Irradiated

As the result of irradiation, in a material regions with altered characteristics, so-called failed regions, are produced in a material. In the failed regions bulk changes must be greater than those occurring usually with change in temperature. When a failed region is initiated, which can be represented as a core with radius a, the surrounding material will be impeded by the bulk changes.

According to [1], if in the "free" change in volume

$$\Delta V_a' = 4\pi a^3 \varepsilon',$$

where ε' is the "free" relative deformation, when the free "uninvolved" volume undergoes compression,

$$\Delta V_a = \frac{1}{3} \cdot \frac{1+\nu}{1-\nu} \Delta V_a' = \frac{4}{3} \pi a^3 \frac{1+\nu}{1-\nu},$$

where ν is Poisson's ratio.

With increase in the concentration of failed regions, each subsequent region will superimpose its stresses and strains on existing stresses and strains. When $\nu \approx 0.5$, total strain will be 5/9-th of the sum of free strains of all failed regions, and the nonhomogeneous macroscopic strain will be of the form [1]

$$\varepsilon = \frac{1}{3} \cdot \frac{\Delta V_a}{V} = \frac{1}{3} \cdot \frac{1+\nu}{1-\nu} p_v \Delta V,$$

where $\Delta\bar{V}$ is the mean bulk change per failed region and ρ_K is the concentration of the failed regions.

Let us consider the case when this failed region is caused by a single displacement. Elastic strains of the lattice caused by a vacancy can be calculated as for a cavity in a continuous medium. They are proportional to $1/r^3$ (where r is the distance to the vacancy). Observable displacements are experienced only by nearest-neighbor atoms. If the atoms and ions are considered as elastic spheres in contact, the mean displacements are very small and are directed in the metal toward the vacancy, and radially outwards -- in ionic crystals. In both cases the elastic proportion of the energy of defect formation as a rule does not exceed several tens of electron-volts.

An interstitial atom upon injection causes a stronger distortion of the lattice. The displacement of surrounding ions can extend to 20% of the lattice constant, and the corresponding strain energy can be much as several electron-volts.

Describing a point defect in a real crystal as a center of compression or expansion naturally represents a very crude approximation, since here we do not take account of the discrete atomic structure of the body. More precise calculations showed [2] that the resultant displacements, for example, in a cubic lattice are oriented outwardly along the axes of the cube, and inwardly -- in the remaining directions. Therefore, the displacement field is marked by significant anisotropy. This also is true of other lattice types. Displacement of the first layer around the interstitial atom in a face-centered cubic lattice is approximately six times greater than around the vacancy.

At present there are inadequate data for the calculation of the volumetric change $\Delta\bar{V}$ per single displacement in dielectrics. This quantity will depend upon numerous physical characteristics of the material as a whole, as well as of atoms or ions comprising it, and also on the structure of the material -- its crystal lattice, and the presence of cracks and other defects.

However, there are data [3] indicating that $\Delta\bar{V}$ in metals, for neutron irradiation, is of the order of 10^{-25} cm^3/defect for a number of defects equal to 10^4 per neutron. For the atomic volume $V_a = 10^{-24}$ cm^3, the volume change is 10 percent. At the same time, the volume change calculated for irradiation with uranium nuclei fusion fragments (95 Mev) is $1.2 \cdot 10^{-21}$ for MgO, and $16.4 \cdot 10^{-21}$ cm^3/defect for SiC [4]. The overall volume change for flux can be obtained by the formula [5]

$$\frac{\Delta V}{V} = 12\pi \frac{1+\nu}{1-\nu} \varphi \Delta\bar{V}.$$

If the failed region owes its origin to a nuclear reaction, for example, $B^{10}(n,)Li^7$, it will be much larger. The volume change calculated in the study [1], per nuclear reaction in glasses, is $3.6 \cdot 10^{-19}$ cm^3, and the mean volume of the failed region at the surface of the specimen where the density of reactions is the greatest and where these regions are in contact with each

other is $1.5 \cdot 10^{-16}$ cm^3. For these parameters, the relative strain of the surface layer ν is -0.08 percent. The strength of the material is determined by the strength of the surface layer in a state of tension.

Considering the thermal spike or the displacement spike as a center distorting the lattice, we can assume that since regardless of the nature of the spike the substance undergoes expansion within it, naturally around the spike a region of increased pressure will appear. The pressure p in the radial direction is

$$p = p_0 \left(\frac{a}{r}\right)^3,$$

where r is the distance to the center (or the axis of the spike); a is the radius of the zone undergoing melting; and p_0 is the pressure, which is a function of the shear modulus G, Poisson's ratio ν, and the relative allocation of the material in the spike zone $\Delta l/l$:

$$p_0 = \frac{4}{3} \cdot \frac{1+\nu}{1-\nu} G \frac{\Delta l}{l}.$$

According to the findings of Paymal [6], who maintains that the disintegration region within a spike must be surrounded by a compression zone around the core, the pressure in the shell must be in the range of 2000-200,000 atm.

Since the system has spherical symmetry and the tension is a radial stress, the tension related to compression by [illegible]ng function [1] will be a tangential stress

$$\sigma_t = -\frac{1}{2}\sigma_r \quad \text{or} \quad \sigma_t = -\frac{1}{2}(1+\nu)\frac{\sigma}{E}\left(\frac{a}{r}\right)^3.$$

In spite of the fact that tensile mi[illegible]sses exceed the ultimate strength, failure of the material cannot take [illegible]ce for the following reasons, owing to the small dimensions of the [illegible]d region, comparable with interatomic distances, the strength of the material must approach its theoretical value and, in addition, owing to local excitation of the lattice associated with ionization processes and displacement processes, the bonds between atoms are weakened and stress relaxation is facilitated.

If the mean density of failed regions fluctuates in the bulk material, internal macroscopic stresses appear as in an inhomogeneous cooled body. On the macroscopic scale even weak nonuniformity of irradiation produces large stresses.

Based on experiments on the annealing of neutron-irradiated quartz glass, Lungu [7] concluded that defects are unevenly distributed in specimens, in spite of the small coefficient of radiation absorption. In the case of materials strongly absorbing radiation, nonuniformity of the distribution of failed sections is very large. The plot of the distribution of macroscopic stresses in thermal-neutron-irradiated borosilicate glass Corning 7070 28 percent B_2O_3), given in report [1], indicates this (Fig. 67). The curvature of the branch of the curve is determined in this case by the concentration gradient of nuclear reactions, which are the dominant effect of irradiation. Our experiments on irradiating a series of glasses with variable B_2O_3 content with thermal neutrons showed that as the absorption coefficient is increased, stresses recorded by the polarization method increase, and for a high enough B_2O_3 content (up to 30 percent), the specimens fail when irradiated with a dose of $5 \cdot 10^{17}$ neutrons/cm^2, which is tolerated by glasses with a smaller B_2O_3 content without cracking.

When quartz is bombarded with 130 kev protons, the stresses in the irradiated surfaces are $(277-284) \cdot 10^4$ newtons/m^2, and when 100 kev ions are used, the stresses are $451 \cdot 10^6$ newtons/m^2 [8].

Growth of stresses is directly proportional to volume changes caused by irradiation. Radiation expansion, which depends on the structure and composition of the material, leads to the initiation of stress between layers of material experiencing different relative strains. In silicon carbide, these stresses are twice as great as the ultimate tensile strength, and in MgO tensile stress is 13 percent of the ultimate strength, and compressed stress is 8 percent of the ultimate strength [4].

In spite of the large value of irradiation-induced macroscopic stresses, occasionally exceeding ultimate strength values, material specimens nonetheless often are preserved without failure, for example, quartz, as described in the work [8]. This can be explained by the possibility of stress relaxation. Relaxation takes place in any case. For severely nonuniform irradiation this amounts to failure. For weak inhomogeneity in regions irradiated with not overly large doses, relaxation can occur via plastic flow, though the authors of the paper [9], in analyzing the results of the thermal relaxation of stresses in glasses subjected to ultraviolet irradiation, found that the energy of activation (1.3 ev) and the relaxation temperature (520° K) of these stresses is somewhat lower than the corresponding viscous-flow characteristics (4.3 ev, 818° K). Relaxation sets in either on attainment of a specific stress, that is, beginning with some dose, or occurs throughout the entire irradiation period. By the work [8], when the relative volume strain ℓ does not exceed 10^{-6} the material remains practically free of stresses.

Secondary effects associated with changes in phase composition, structure, and thermal prehistory of the material can be a source of stresses upon irradiation.

When several phases with different coefficients of thermal expansion are present in the material, abrupt cooling of heated sections, in particular, spikes, can lead to interphase stresses. According to the work [10], this stress is expressed as

$$\sigma_\alpha = \frac{E}{1-2\nu} 3(\alpha_a - \alpha_b)(t_1 - t_2),$$

where E is Young's modulus; ν is Poisson's ratio; α_a and α_b are the coefficients of thermal expansion of bounding phases; t_1 is the spike temperature; and t_2 is the temperature below which stress relaxation is impossible.

The irradiation of dense beryllium oxide with very high doses (to $2.6 \cdot 10^{21}$ neutrons/cm^2) leads to its breakdown to the powdered state, where the lower the irradiation temperature, the more pronounced this effect. Authors of the work [11] explained this phenomenon as, first of all, due to the anisotropic expansion of crystals and the initiation of stresses at their facets; secondly, by the forcing apart of grains under the pressure of diffusing helium.

When quartz and quartz glass are irradiated with heavy particles (protons and helium nuclei), the accumulation of gases at a depth of several millimeters produces lenticular voids, causing exfoliation of the surface layer and the flaking of specimens [8]. The bending strength of a material with 10-15 percent porosity after irradiation is reduced by 82 percent, and by 94 percent for a material with 4 percent porosity [12].

Initiation of the resultant surface tension is of interest for problems of the strength of glass and products. According to [13], glass with the following composition (mole percent) must be used to obtain uniform tensile stresses in the surface layer of a glass after its irradiation with thermal neutrons: SiO_2 -- 10 -- 70; Al_2O_3 -- 20; B_2O_3 -- 0 -- 50; R_2O -- 0 -- 30; RO -- 0 -- 30; and PbO -- 0 -- 85, given the condition that $SiO_2 + B_2O_3 + Al_2O_3 < 70$; $R_2O + RO + PbO > 15$; $B_2O_3 > 1$; $Li_2O > 10$. To achieve compressive stresses in the surface layer of the glass after it has been irradiated with thermal neutrons, the glass must have the following composition (in mole percent): SiO_2 -- 50 -- 90; Al_2O_3 -- 0 -- 20; B_2O_3 -- 0 -- 80; R_2O -- 0 -- 20; and RO -- 0 -- 30; PbO -- 0 -- 20, given the condition that $SiO_2 + B_2O_3$ 75; $R_2O + RO + PbO$ -- 0-25; $B_2O_3 > 1$; and $Li_2O > 10$.

[illegible] zones can be regulated by depth and along the surface of the glass by protecting given sections of the product with cadmium shields of appropriate thicknesses [14]. If as a result of the irradiation the glass increases in density, that is, it is compressed, the zones undergoing irradiation experience tension, while at the same time shielded sections in need of strengthening experience compression. If the composition of the glass is such that when irradiated experiences compression, the strengthened sections must be left exposed, and the shields must be used for the desirable distribution of stresses. In a prehardened glass subjected to irradiation, shields permit modifying the initially produced stresses, increasing them in some sections and reducing them in others.

It is noted in work [15] that the mechanical strength of quartz glass when irradiated with a dose of $2.4 \cdot 10^{18}$ neutrons/cm and at 373° K

is increased by 10 percent. However, Fleming [16], after irradiation with a dose of $4 \cdot 10^{20}$ neutrons/cm did not find flexural strength changes of fused quartz rods obtained by dross casting and sintering in spite of the fact that at this dose the cristobalite present in the glass underwent a transition to the amorphorus state.

Quartz glass specimens, depending on the method of production (molding or drawing), after irradiation with a dose of $2 \cdot 10^{20}$ neutrons/cm^2 revealed 5.5- 6.5 percent strength gains [17]. However, in our experiments no changes were found in the strength of KV and KI quartz glasses after irradiation in a reactor with fluxes of $7 \cdot 10^{18}$ thermal neutrons/cm^2. In a study of the mechanical properties of sintered alumina of various grain composition [18], no strength decreases were found, and there was even some gain in specimen strength (Table 35).

Fig. 67. Distribution of stresses in a sample of borosilicate glass Corning 7070 with thickness d, subjected to thermal neutron irradiation.
KEY: A -- Stress

TABLE 35. CHANGE IN STRENGTH OF ALUMINA UPON IRRADIATION

Диаметр зерна в мкм (A)	Доза в нейтрон/см²·10²⁰ (B)	$\sigma_{обл}/\sigma_{исх}$ (C)
4--6	1,3	0,8
	1,7	1,3
	2,1	1,5--1,7
	3,5	1--1,6
	5	1,6
40--200	2,1	1,1--1,2
	4,2	1,3
	5	1,2--1,3

KEY: A -- Grain diameter in microns
B -- Dose in neutrons/cm^2 $\cdot 10^{20}$
C -- σ_{ir}/σ_{in}

Irradiation with a dose of $3 \cdot 10^{18}$ neutrons/cm^2 does not cause changes in flexural strength of glass-crystalline materials of the system Na_2O-CaO-MgO-Al_2O_3-SiO_2 [19]. When plates of IV-23 sitall, 70 x12 x2 mm in size protected on one side with cadmium shields were irradiation with a dose of $5 \cdot 10^{18}$ neutrons/cm^2, deformation occurred. The specimens were bent in on the irradiation side, indicating compression and thickening of the surface layers and, therefore, the initiation of tensile stresses in them. Specimens uniformly irradiated with a dose of 10^{19} neutrons/cm^2 cracked [20], and the crack grew from one of the side faces and extended along the specimen axis, that is, along the zone of maximum tensile stresses. Measurement of strength with central bending of sitall IV-23 specimens and for transverse bending of sitall 224-18 specimens irradiated with a dose of 10^{18} neutrons/cm^2 showed no differences in its values from initial values. However, a dose of 10^{18} neutrons/cm^2 and lower causes stresses recorded by the polarization methods in the initial sitall glasses. [sitall(s) = pyroceramic(s) -- Tr.]

Birefraction of glasses becomes stronger with increase in irradiation dose, and at constant dose -- with increase in B_2O_3 content in a glass. Nonboron compositions produce weak birefraction only at a dose of 10^{18} neutrons/cm^2. Stresses induced in glasses at doses of $5 \cdot 10^{17} - 10^{18}$ neutrons/cm^2 in several cases lead to the cracking of samples. Sitalls formulated from these same glasses do not fail under the same irradiation conditions, which allows us to regard them as more resistant strength-wise than glasses.

Our study of the strength of certain industrial glasses (sheet, LK-5, K-8, and 13v) revealed the absence of strength changes after γ-irradiation with doses extending up to 10^9 r [roentgen].

2. Change in Elastic Constants of Materials when Irradiated

When the elastic constants of quartz and quartz glass were measured, it was found that after irradiation with a flux of up to $4 \cdot 10^{18}$ neutrons/cm^2, changes in the modulus of elasticity of quartz are as high as 3.2 - 16.5 percent, and 0.66 - 3.8 percent for quartz glass, that is the stability of the glass is higher [21]. Zhdanov et al. [22] noted only a slight increase in the constants C_{11} and C_{66} of the stress tensor of quartz when irradiated with fluxes up to $2 \cdot 10^{19}$ neutrons/cm^2. In an article by Zubov and Ivanov [23], it was stated that doses up to $2 \cdot 10^{20}$ fast neutrons/cm^2 produce different patterns in changes of the modulus of elasticity with respect to the different crystal axes, and the changes in the strain tensor constants do not at all tend, with increase in dose, to values of the corresponding end product of irradiation (cf. Chapter Ten). This same irradiation dose ($2 \cdot 10^{20}$ neutrons/cm^2) increases the modulus of elasticity of glassy silicon by 3 - 4 percent [16]. γ-Irradiation with a dose of up to 10^{19} r, x-ray irradiation, and neutron irradiation with a dose up to $8 \cdot 10^{16}$ neutrons/cm^2 do not affect the elastic constants of quartz [21, 22]. In our experiments irradiation of quartz glass with fluxes of $4 \cdot 10^{18}$ thermal neutrons/cm^2 do not produce noticeable changes in the modulus of elasticity measured by the ultrasonic method.

Large radiation doses ($5 \cdot 10^{19}$ fast neutrons/cm^2) caused an 85 percent drop in the rate of ultrasound propagation in quartz glass; here the shear

modulus rose by 2 percent, and compressibility was reduced by 20 percent [24]. The rise in the elasticity of glassy silica, based on data in [17], is extremely stable and is not eliminated completely after annealing at 1270° C for 75 hours.

Starodubtsev et al. [25] showed that the shear modulus of quartz glass increases with γ-radiation dose and the change is 0.22 ± 0.02 percent at a dose of $1.5 \cdot 10^9$ r. The authors assume that the increase in the elasticity of quartz glass, just as its reduced linear dimensions, occurs owing to the initiation of ordered regions in the structure, that is, partial long-range recovery.

A study by Vrekhovskikh et al. [26] showed that as the γ-radiation dose is intensified the modulus of elasticity and the shear modulus of sheet glass also rise. However, these changes reach saturation values at a dose of 10^6 r at a level of 1 percent. This effect is related by the authors to the healing of internal defects in glass structure, as well as with annealing.

The modulus of elasticity of boro-silicate glass irradiated with a flux of $5.2 \cdot 10^{17}$ thermal neutrons/cm^2 at 330-340° K, increases by 4%, which is associated, in the authors' view [27,28], with the formation of new bonds, resulting in intensified interaction between glass atoms. The elasticity modulus of the glass Vycor rises by 9 percent after irradiation with a flux of $5 \cdot 10^{18}$ neutrons/cm^2 [29].

Paymal and Le Clerk [30] investigated changes in the modulus of elasticity, on exposure to thermal neutrons of a large group of boro-silicate glasses with systematically varied composition in the systems $SiO_2 - B_2O_3 - K_2O$; $SiO_2 - B_2O_3 - Rb_2O$; $SiO_2 - B_2O_3 - Al_2O_3 - R_2O$, and $SiO_2 - B_2O_3 - Al_2O_3 - RO$. These experiments showed that since the modulus of elasticity depends more strongly on the specimen thermal prehistory than on its chemical composition, it is not possible to uniquely relate radiation changes in the modulus with chemical composition. Nonetheless, for small doses radiation changes of the modulus are governed by the same laws as its temperature dependence in the range 290 - 390° C. The difference is that radiation changes become frozen. At small radiation doses changes in Young's modulus (E) follow radiation changes in glass density ρ, where this change is greater than in rubidium glasses. In quartz glass this relationship is expressed as $\Delta E/E = 1.8 (\Delta\rho)/\rho)$; in alkali glasses the coefficient is between 2 and 3.

Large radiation doses lead to the radiation annealing of changes and to a reduction in the modulus [30]. This is also indicated by the results of irradiating sheet glass with a flux of $1.6 \cdot 10^{20}$ fast neutrons/cm^2, accompanied by some decrease in the modulus of elasticity (by less than $49 \cdot 10^6$ newtons/m^2) [31]. This is in fact also shown by our experiments on irradiating transparent semicrystalline aluminum oxide (luxor). After irradiating beryllium oxide with a flux of $7.3 \cdot 10^{19}$ fast neutrons/cm^2, its elasticity modulus changed very appreciably, but annealing at 1470 - 1670° K relieved these disruptions [33]. The elasticity modulus of TiO_2 changed only slightly after irradiation with fluxes up to $6 \cdot 10^{20}$ fast neutrons/cm^2 [31].

modulus rose by 2 percent, and compressibility was reduced by 20 percent [24]. The rise in the elasticity of glassy silica, based on data in [17], is extremely stable and is not eliminated completely after annealing at 1270° C for 75 hours.

Starodubtsev et al. [25] showed that the shear modulus of quartz glass increases with γ-radiation dose and the change is 0.22 ± 0.02 percent at a dose of $1.5 \cdot 10^9$ r. The authors assume that the increase in the elasticity of quartz glass, just as its reduced linear dimensions, occurs owing to the initiation of ordered regions in the structure, that is, partial long-range recovery.

A study by Vrekhovskikh et al. [26] showed that as the γ-radiation dose is intensified the modulus of elasticity and the shear modulus of sheet glass also rise. However, these changes reach saturation values at a dose of 10^6 r at a level of 1 percent. This effect is related by the authors to the healing of internal defects in glass structure, as well as with annealing.

The modulus of elasticity of boro-silicate glass irradiated with a flux of $5.2 \cdot 10^{17}$ thermal neutrons/cm^2 at 330-340° K, increases by 4%, which is associated, in the authors' view [27,28], with the formation of new bonds, resulting in intensified interaction between glass atoms. The elasticity modulus of the glass Vycor rises by 9 percent after irradiation with a flux of $5 \cdot 10^{18}$ neutrons/cm^2 [29].

Paymal and Le Clerk [30] investigated changes in the modulus of elasticity, on exposure to thermal neutrons of a large group of boro-silicate glasses with systematically varied composition in the systems $SiO_2 - B_2O_3 - K_2O$; $SiO_2 - B_2O_3 - Rb_2O$; $SiO_2 - B_2O_3 - Al_2O_3 - P_2O_5$ and $SiO_2 - B_2O_3 - Al_2O_3 - RO$. These experiments showed that since the modulus of elasticity depends more strongly on the specimen thermal prehistory than on its chemical composition, it is not possible to uniquely relate radiation changes in the modulus with chemical composition. Nonetheless, for small doses radiation changes of the modulus are governed by the same laws as its temperature dependence in the range 290 - 390° C. The difference is that radiation changes become frozen. At small radiation doses changes in Young's modulus (E) follow radiation changes in glass density ρ, where this change is greater than in rubidium glasses. In quartz glass this relationship is expressed as $\Delta E/E = 1.8 (\Delta\rho)/\rho)$; in alkali glasses the coefficient is between 2 and 3.

Large radiation doses lead to the radiation annealing of changes and to a reduction in the modulus [30]. This is also indicated by the results of irradiating sheet glass with a flux of $1.6 \cdot 10^{20}$ fast neutrons/cm^2, accompanied by some decrease in the modulus of elasticity (by less than $49 \cdot 10^6$ newtons/m^2) [31]. This is in fact also shown by our experiments on irradiating transparent semicrystalline aluminum oxide (Juxor). After irradiating beryllium oxide with a flux of $7.3 \cdot 10^{19}$ fast neutrons/cm^2, its elasticity modulus changed very appreciably, but annealing at 1470 - 1670° K relieved these disruptions [33]. The elasticity modulus of TiO_2 changed only slightly after irradiation with fluxes up to $6 \cdot 10^{20}$ fast neutrons/cm^2 [31].

3. Change in Hardness of Mater als when Irradiated

Hardness is a complex characteristic, dependent on a good many physical mechanical parameters of a material, moduli and limits of elasticity, plasticity, creep, atom-molecular rupture and shear strength, and the like. Hardness also depends on the actual structure of a solid, and the kind and density of lattice defects, which are significantly affected by nuclear radiation.

The most familiar effect of nuclear radiation on the hardness of materials is the increase in hardness for both crystalline and certain amorphous bodies. Thus, the hardness of neutron-irradiated BeO crystals is much higher than the initial value [11,34]. The microhardness of mica when irradiated in a nuclear reactor with a flux of $6 \cdot 10^{20}$ neutrons/cm^2 rises from $1110 \cdot 10^6$ to $4320 \cdot 10^6$ newtons/cm^2, and when sheet glass is irradiated with a flux of $3 \cdot 10^{19}$ and $6 \cdot 10^{20}$ neutrons/cm^2 -- from $1180 \cdot 10^6$ to $1420 \cdot 10^6$ and $4320 \cdot 10^6$ newtons/m^2, respectively [35]. But irradiation with x-rays at a voltage of 46 kv with a dose of $3 \cdot 10^7$ r increases the microhardness of quartz glass by an average of 3 - 4 percent [36]. At the same time it was noted that after certain materials had been irradiated, their hardness falls off. For example, the microhardness of quartz is reduced by half after irradiation with a flux of $6 \cdot 10^{20}$ neutrons/cm^2 [35].

In our experiments on irradiating a large series of glasses of commercial grades (sheet, 13 v, K-8, K-108, and LK-5) with γ-rays using a Co^{60} source with doses of 10^7, $2 \cdot 10^7$, and $5 \cdot 10^7$ r, no microhardness changes could be detected. Our irradiation of KV and KI grades of quartz glass in a nuclear reactor with fluxes of $4 \cdot 10^{18}$ and $7 \cdot 10^{18}$ neutrons/cm^2 also did not cause changes in microhardness.

Since with the increase in the absorbing power of materials and, therefore, in the absorbed dose radiation damage is intensified, we conducted a series of experiments on the irradiation of glasses and sitalls with regularly increasing boron content [37]. The starting compositions were glasses with the following molecular formulas: $Li_2O \cdot Al_2O_3 \cdot 4SiO_2 \cdot nB_2O_3$ (Series S) and $MgO \cdot Al_2O_3 \cdot 2.5SiO_2 \cdot nB_2O_3$ (Series M) in which n takes on the values 0, 0.25, 0.5, 1, and 2 (the indexes of the compositions are 0, 1, 2, 3, and 4, respectively).

Fig. 68 presents the dependence of changes in microhardness (PMT-3, instrument, 100 g load on indentor) of test materials on the reactor radiation dose. These curves show that an increase in the content of boric anhydride in glasses, therefore, the concentration of nuclear reactions and the absorbed dose, leads to a large drop in their microhardness when they are irradiated with the same exposure dose. In glasses not containing boron, no changes in microhardness occurred upon irradiation, which was confirmed by experiments also on commercial-composition sitalls. The microhardness decrease effect is less pronounced in sitalls than in glasses. Evidently, this is associated with the fact that radiation effects responsible for reducing microhardness take place only in the boron-containing glass phase. Since both crystals and glass are present in the zone of indentor action when sitalls were tested, the effective microhardness is more complexly dependent on dose than for the pure glass.

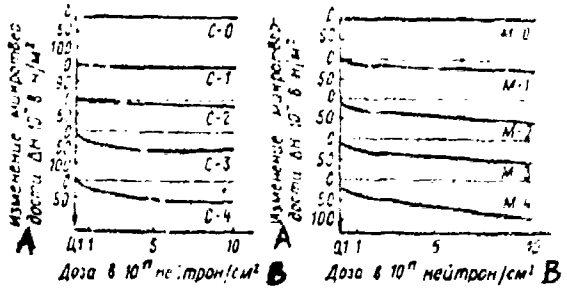

Fig. 68. Change in microhardness of glasses with the compositions $Li_2O \cdot Al_2)_3 \cdot 4\ SiO_2 \cdot nB_2O_3$ (series S) and $MgO \cdot Al_2O_3 \cdot 2.5\ SiO_2 \cdot nB_2O_3$ (series M) resulting from neutron irradiation

KEY: A – Change in microhardness, $H \cdot 10^{18}$ in newtons/m^2

B – Dose in 10^{17} neutrons/cm^2

In an interesting experiment measuring the microhardness of quartz glass when irradiation with α-particles using a Pu^{239} source [38], a reduction in microhardness with increase in dose was also achieved. The authors, in evaluating the increase in plasticity of the surface layer, believe that it is associated with the increased defect density of the glass. Evidently, here the effect of developing stresses of the surface hardness type is present.

4. Change in Thermal Properties of Materials when Irradiated

Thermal Conductivity

Change in the thermal conductivity of materials when irradiated in a reactor is vital in reactor engineering. Table 36 gives data for several materials finding application in reactor structures [35], which indicates quite large property changes.

Irradiation of quartz glass with a flux of $4.3 \cdot 10^{19}$ fast neutrons/cm^2 at low temperatures (3-14° K) increases its thermal conductivity from 16.7 to 29.3 w/m · deg [39]. At the same time, a flux of $2 \cdot 10^{20}$ fast neutrons/cm^2 does not cause changes in the thermal conductivity of quartz glass measured at 308 - 318° K [40]. The thermal conductivity of lead glass irradiated with the same dose, measured under the same conditions, is reduced by 40-45 percent. Data on the stability of the thermal conductivity of Al_2O_3, irradiated with a flux of $2 \cdot 10^{20}$ fast neutrons/cm^2, at 308 - 318° K, published in the work [39], contradict the data in Table 36. At odds with Table 36 are the results of a study [40] indicating the absence of changes

TABLE 36. CHANGE IN THERMAL CONDUCTIVITY OF CERTAIN MATERIALS UPON IRRADIATION

A Материал	B Доза в нейтрон/см²×10¹⁹	C Теплопроводность в вт/м·град	A Материал	B Доза в нейтрон/см²×10¹⁹	C Теплопроводность в вт/м·град
Al_2O_3	0	16,8 ± 4,2	Кордиерит G	0	30,6 ± 0,21
	3	9,65 ± 1,68		5	0,84 ± 0,08
	40	3,78 ± 0,21		30	0,84 ± 0,08
Шпинель D	0	10,5 ± 2,1	TiO_2	0	6,83 ± 0,84
	7	5,45 ± 0,42		6	4,63 ± 0,42
	40	5,45 ± 0,42		30	2,82 ± 0,21
Форстерит E	0	10,5 ± 2,1	Фарфор H	0	11,3 ± 2,1
		3,12 ± 0,42		6	5,01 ± 0,42
				40	3,57 ± 0,21
ZrO_2	0	5,05 ± 0,42	Сапфир I	0	25,2 ± 8,4
	5	0,96 ± 0,042		6	12,6
				60	8,4
Стеатит F	0	3,18 ± 0,21	BeO	0	25,2
		1,13 ± 0,042		7	16,8

KEY: A -- Material
B -- Dose in neutrons/$cm^2 \cdot 10^{19}$
C -- Thermal conductivity in w/m·deg
D -- Spinel
E -- Forsterite
F -- Steatite
G -- Cordierite
H -- Porcelain
I -- Sapphire

in the thermal conductivity of BeO irradiated with a flux of $2 \cdot 10^{20}$ fast neutrons/cm^2 at 308 - 318° K. However, according to [41], even a flux of $7.3 \cdot 10^{19}$ fast neutrons/cm^2 reduces the thermal conductivity of BeO by a factor of 6.

Coefficient of thermal expansion

Changes in the coefficient of thermal expansion (c.t.e) of irradiated materials are associated with disruption of phase composition, structure, or the initiation of stresses.

Structural damage in crystalline quartz caused by neutron irradiation leads to a reduction in the c.t.e. by 0.5 percent after irradiation with a flux of $2.2 \cdot 10^{18}$ neutrons/cm^2 [21]. After irradiation with a flux of $1.4 \cdot 10^{20}$ neutrons/cm^2, the c.t.e. of quartz reached a value of $5.4 \cdot 10^{-7}$ deg^{-1} [42], which is practically equal to the c.t.e. of quartz glass.

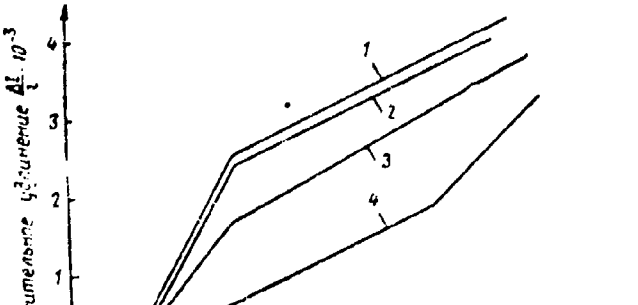

Fig. 69. Thermal expansion of Zh-3 sitall
1 -- Initial
2 -- - 4 - irradiated with doses of 10^{16}, 10^{18}, and 10^{19} neutrons/cm^2, respectively.
KEY: A -- Relative elongation
B — Temperature in °K

Paymal relates slight changes in the c.t.e. of borosilicate glasses irradiated with thermal neutrons to the effect of consolidation around thermal spikes. The extent of consolidation, in turn, is determined by the polarization of oxygen ions, that is, it depends on the chemical composition of the glass [29].

We did not observe differences in the dilatometric curves of initial borosilicate glass produced upon the crystallization of S-343 sitall, and the same borosilicate glass after irradiation with a flux of $4 \cdot 10^{17}$ neutrons/cm^2. At the same time, irradiating sitalls causes a change in their thermal expansion [20]. Figs. 69-72 present the dilatometric curves of several sitalls. The change in the thermal expansion of sitalls is associated with

the change in the phase composition, confirmed by x-ray phase, petrographic, and electron-microscopic analyses. In those cases when upon reactor irradiation the crystalline phase with a large c.t.e. breaks down, for example, crystobalite in Zh-3 sitall, the c.t.e. of sitall is reduced (Fig. 69). But in those cases when the content of crystalline phase is exhibiting a small c.t.e. is reduced, and the more stable phases have a higher c.t.e. an increase in the sitall (S-1214 and S-343) c.t.e. is the resultant effect. Change in the c.t.e. of sitall IV.23 (Fig. 72), with a stable crystalline phase observed in the temperature range to 770° K, is evidently associated with the appearance of stresses in its glass phase [33].

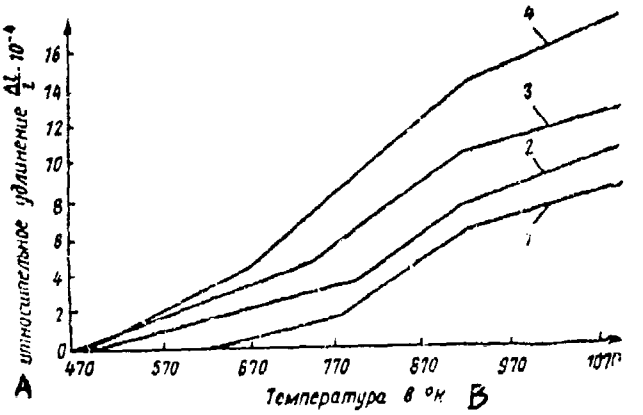

Fig. 70. Thermal expansion of S-1240 sitall
1 — Initial
2 - 4 -- irradiation with doses of 10^{18}, $5 \cdot 10^{18}$, and 10^{19} neutrons/cm^2, respectively
KEY: A — Relative elongation
B -- Temperature in ° K

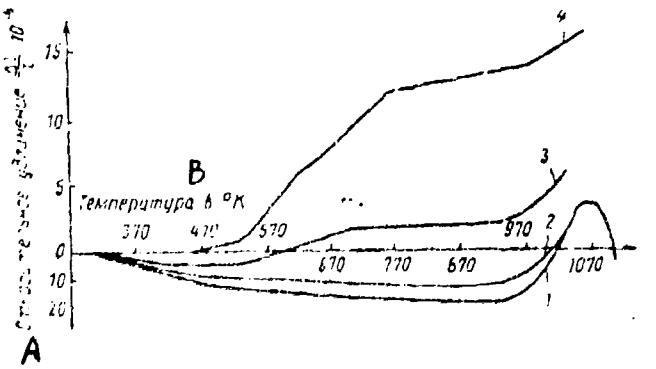

Fig. 71. Thermal expansion of S-343 sitall
1 -- Initial
2 - 4 - irradiated with doses of 10^{16}, 10^{18}, and 10^{19} neutrons/cm^2, respectively.
KEY: A — Relative elongation; B -- Temperature in ° K

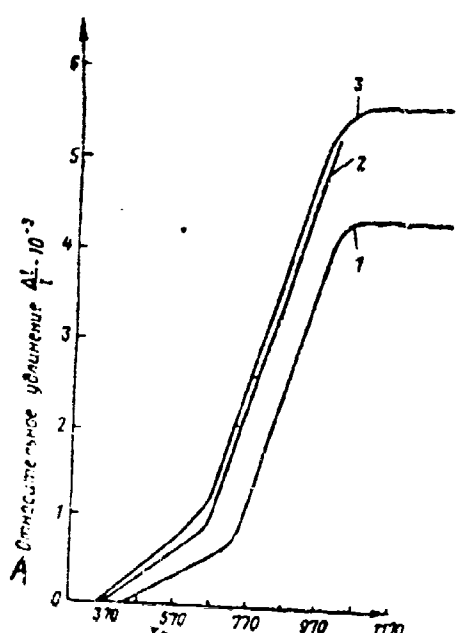

Fig. 72. Thermal expansion of IV-23 sitall
1 — Initial
2 - 3 — Irradiated with doses of $5 \cdot 10^{18}$ and 10^{19} neutrons/cm^2, respectively
KEY: A — Relative elongation
B — Temperature in ° K

CHAPTER TWELVE

RADIATION-RESISTANT MATERIALS

Materials capable of withstanding extended use in radiation fields without marked change in properties and structure are called radiation-resistant. The main condition determining radiation resistance is the slight interaction of the atoms of chemical elements incorporated in the material composition with radiation acting on the material. In most cases materials with low absorbability for a given type of radiation suffer less radiation damage. Besides this condition affording radiation stability of material is the low stability of the irradiation damage produced. For example, increasing the temperature or exposing to other kinds of radiation under surface conditions can promote recombination, annihilation and annealing of radiation defects.

At the present time no universal material with stability in all physical chemical properties and structure under conditions of exposure to any kinds of radiation exists.

The proposed classification of radiation-resistant materials provides for separating them into four groups by properties that are the main technical characteristics of the material and whose changes in which would render further use of the material impossible;

group 1 -- dielectrically radiation-resistant materials;
group 2 -- chemically radiation-resistant materials;
group 3 -- optically radiation-resistant materials; and
group 4 -- magnetically radiation-resistant materials.

Each of the groups is subdivided into several subgroups based on the fields of use of the materials (cf. scheme).

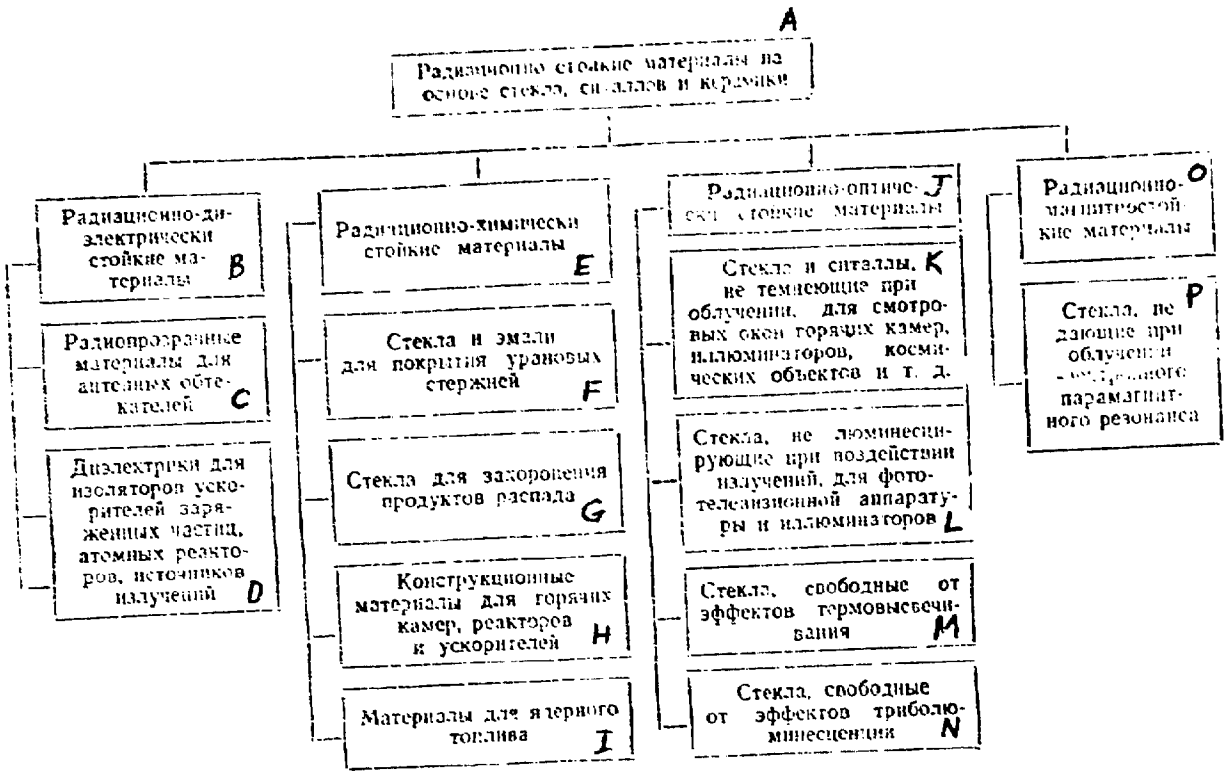

[KEY on following page]

[KEY for scheme]

A -- Radiation-resistant materials based on glass, pyroceramics, and ceramics
B -- Dielectrically radiation-resistant materials
C -- Radio transparent materials for antenna fairings
D -- Dielectrics for insulators of charged particle accelerators, atomic reactors, and radiation sources
E -- Chemically radiation-resistant materials
F -- Glasses and enamels for coating uranium rods
G -- Glasses for burying decay products
H -- Structural materials for hot chambers, reactors, and accelerators
I -- Materials for nuclear fuel
J -- Optically radiation-resistant materials
K -- Glasses and pyroceramics not darkening upon irradiation, for observation windows of hot cells, searchlights, spacecraft, and so on
L -- Glasses not luminescing when irradiated, for photo-television equipment and searchlights
M -- Glasses free of effects of thermal de-excitation
N -- Glasses free of triboluminescence defects
O -- Magnetically radiation-resistant materials
P -- Glasses not producing electron paramagnetic resonance when irradiated

1. Dielectrically Radiation-Resistant Materials

Materials for antenna fairings

One of the main requirements imposed on materials used in fabricating fairings of rockets is the stability of the dielectric characteristics under conditions of service and storage. The stability of the guidance system parameters is decisive in ensuring the precision of missile targeting.

Usually quartz glass, quartz glass-ceramic, ceramic based on alpha-corundum, and special-composition pyroceramics [1] are employed for antenna fairings functioning in the UHF radio wave range. All these materials, with their different dielectric permeabilities, differ by a small value of dielectric losses and by a weak temperature dependence of dielectric properties.

Change in dielectric properties of irradiated materials as the frequency of electrical field is increased becomes less noticeable (cf. text page 159 [p.148]). The results of our experiments on the irradiation of cordierite pyroceramic and glass-ceramics based on sintered quartz glass and silica made it possible to regard their dielectric properties as stable up to doses of $5 \cdot 10^{18}$ neutrons/cm^2.

Change in the dielectric permeability of materials is within the limits 0.5 percent, but changes in dielectric limits remained unrecorded in all cases ($tg\ \delta$ in all samples was less than $5 \cdot 10^{-3}$). The absence of changes in the UHF range is associated with the fact that dielectric polarization and losses at these frequencies are determined by resonance processes

caused by oscillations of ions and electrons and dependent on chemical bonds between lattice components at which radiation has a comparatively weak effect.

Dielectrics for insulators of charged particle accelerators, atomic reactors, and radiation sources

When glasses and ceramics are used as insulators for service with irradiation, several undesirable aftereffects of irradiation must be taken into account:

1) change in dielectric permeability and loss;
2) reduced the electrical resistance;
3) reduced dielectric strength
4) damage caused by discharge of electrical charge accumulated in the dielectric.

The causes of these defects, examined in detail in Chapter Nine, affords several conclusions about materials suitable for use in reactors, accelerators, hot cells, and so on.

In spite of the fact that the electrical resistance of radiation-resistant glasses containing CeO_2 decreases sharply on exposure to ionizing radiation, and even though this degrades their electrical characteristics as insulators, they have enhanced breakdown strength, do not produce discharge figures, and do not accumulate space charge, which in several cases can be decisive.

Quartz glass and materials based thereon have indisputable advantages over multi-component glasses. When quartz glasses are used, preference may be given to grades of glass containing the smallest amount of hydroxyl (KI grades). In examining dielectrics resistant to neutrons, one must consider the chemical composition of the material, since the presence of elements with large interaction cross-sections leads to intensified radiation damage. Still we found [2] that ε and tg δ of IV-23 pyroceramics with good dielectric properties, in spite of its large B_2O_3 content, show only slight changes at a frequency of 10^5-10^7 Hz even after irradiation with a beam of 10^{19} neutrons/cm^2. At the same time pyroceramics of the lithium aluminum-silicate system even with a small (up to three percent) B_2O_3 content produce an abrupt jump in ε and tg δ even at doses to 10^{17} neutrons/cm^2. This fact is related to the finding that relaxation processes associated with the transfer of labile ions, in particular alkali ions, represent the main source of polarization and losses in the region of 10^5 - 10^7 Hz; the absence of these ions in IV-23 pyroceramic gives it stability. We must note that changes in dielectric properties are nonpersistent and are readily annealed at fairly low temperatures.

The phase composition of the material is quite significant. Segregation of crystalline phases in lithium aluminum-silicate pyroceramic of the same chemical composition leads to changes in the initial dielectric characteristics and their resistance to irradiation. In our case crystalline phases of pyroceramics differ in the degree of bonding of alkali ions in the structure.

2. Chemically Radiation-Resistant Materials

Structural Materials

At present reactor construction makes wide use of beryllium oxide, with favorable nuclear and physicomechanical properties. However, a key drawback of BeO is its weak radiation resistance, stemming from the anistrophy of the crystal lattice and the accumulation of gaseous products of nuclear reactions. The latter factor is detrimental when BeO is used at elevated (above 850° K) temperatures, where it is especially valuable as a heat-resistant material. However, upon irradiation with doses up to 10^{19} neutrons/cm^2, changes in BeO properties are not observed.

Increasing the stability of beryllium ceramics necessitates obtaining fine-grain products or using plastic intergranular binder. For example, a ceramic made of 98 percent BeO with the addition of 2 percent bentonite withstands an integral beam of 10^{21} neutrons/cm^2 at 1270 - 2270° K [3].

Magnesium oxide, with a cubic lattice, has definite advantages over BeO, since the increase in its cell parameters upon irradiation occurs uniformly, without producing intergranular stresses, though at high radiation temperatures the evolution of gaseous products of nuclear reactions also poses a hazard at doses of about 10^{20} neutrons/cm^2, the high-temperature plasticity of MgO promotes relaxation of stresses induced here [4]. Nonetheless, there is a report that the brittleness of MgO monocrystals irradiated with a dose of $4 \cdot 10^{19}$ neutrons/cm^2 rises sharply at 470° K [5].

At the present much effort is directed toward using aluminum oxide as structural materials in reactor construction owing to its good high-temperature characteristics. In contrast to MgO and BeO, very weak damage to structure is observed in Al_2O_3 even at doses of $5 \cdot 10^{20}$ neutrons/cm^2, which indicates the intensity of radiation annealing processes occurring upon irradiation [6].

However, the view is held that the high-temperature strength of Al_2O_3 crystals is not realized at high radiation doses, since intergranular cohesion is disturbed owing to growth anisotropy (even though limited growth); therefore polycrystalline Al_2O_3 has no advantages over other materials at temperatures above 870° K and high doses [4]. Al_2O_3 monocrystals are free of this disadvantage, however obtaining monocrystals of the required dimensions thus far involved major technical difficulties, which results in articles made of Al_2O_3 monocrystals not yet finding wide application.

As remarked, some kinds of corundum and mullite ceramics prove to be stable at integral beams to 10^{20} neutrons/cm^2, which can serve as a basis for their use in reactors [7].

Glasses used in the design of reactors and accelerators must have high heat-resistance and high softening point, which is achieved by adding a minimum amount of alkalis (Table 37).

TABLE 37. HEAT-STABLE RADIATION-RESISTANT GLASSES

Composition in percent by weight A													Literature reference B
SiO_2	Al_2O_3	B_2O_3	Na_2O	K_2O	CaO	MgO	BaO	PbO	ZnO	TiO_2	Fe_2O_3	F	
54—65	15—22	>6	>3	—	7—30	7—30	10	10	3	—	—	—	[6]
54—65	15—22	0—6	0,3	0,3	0—30	0—30	0—10	10	0—3	0—3	—	—	[7]
45—48	20—22	4	—	—	11—14	[illegible]	5—9	—	—	—	0—10	4	[8]
45—50	—	2—4	—	—	11—13	—	—	37—45	—	—	—	—	[9]

KEY: A -- Composition in percent by weight; B -- Reference

Materials for Nuclear Fuel

The use of ceramic materials comprised of oxides of uranium or of thorium as nuclear fuels is well known and has been described in several articles and monographs [10-13]. Much less studied is the possible use of glasses for this purpose.

Of definite interest to nuclear technology is the use of glasses containing fissionable elements. The advantage of these glasses when used as fuel compared, for example, with ceramic uranium dioxide, is the reduced evolution of gaseous decay products. Ceramic fuels inevitably contain grains with interfaces facilitating the diffusion of gas through grains and its evolution from the fuel, which in turn leads to the breakdown of fuel elements. Naturally, in the absence of interfaces in glass, the only possible way that gases can be removed from glass is that they diffuse through the bulk of the material, a process which is much slower.

Besides containing as large as possible a quantity of fissionable element, any glass intended for use as a fuel must consist of substances that have a small thermal neutron capture cross-section. Since fission is attained by means of thermal neutrons, the fuel matrix must exercise also the functions of moderator, and, finally, a high softening point is one of the key requirements imposed on glasses of this kind.

Small additions of uranium oxides have long been used in coloring glasses. We know of attempts to formulate glasses containing a considerable larger amount of uranium (up to fifty percent by weight UO73) [14], but many of the resulting glasses have low heat resistance. Borosilicate glasses containing 50 percent by weight oxides of uranium, thorium, and plutonium [15], or boron aluminum-phosphate glasses containing these oxides up to 46 percent by weight have been described [16]. However, owing to the large capture cross-section of thermal neutrons by boron, these glasses are not of interest for this field of application.

Cashin [17] formulated two types of glasses containing uranium oxides. One type of glass was prepared by saturating the porous framework of Vycor glass with a solution of uranium nitrate salt, after which it was heated to decompose the salt down to U_3O_8 and for subsequent consolidation of the framework. The other type of glass is glass with the following composition (percent by weight) fabricated by the usual methods: 44.98 SiO_2; 8.48 Al_2O_3; 13.46 TiO_2; 4.49 $Zr)_2$; 17.96 Na_2O; 9.87 U_3O_8; and 0.26 Fe_2O_3. The amount of gases evolved in the fission of the uranium in these glasses is extremely small, and the temperature in the center of the glass sample, as shown by calculations, is as much as 1970° K, and gas bubbles are collected precisely in this region, which experiences viscous flow. To obtain infusible glasses, Heyns and Rawson [18] investigated several three-component systems: MgO -- ThO_2 -- ZrO_2; Al_2O_3 -- ThO_2 -- MgO; BeO -- Al_2O_3 -- SiO_2; MgO -- Al_2O_3 -- SiO_2; ZrO_2 -- Al_2O_3 -- SiO_2; MgO -- ZrO_2 -- SiO_2; ThO_2 -- Al_2O_3 -- SiO_2; ThO_2 - MgO -- SiO_2; ThO_2 -- ZrO_2 -- and SiO_2. By blending charges of silicate-system glasses with uranium dioxide,

it was possible to dissolve it up to 50 percent by weight. In addition, three-component glasses were obtained, which had UO_2 as one of their components. These compositions are found in the systems UO_2 -- Al_2O_3 -- SiO_2; UO_2 -- MgO -- SiO_2; UO_2 -- CaO -- SiO_2; UO_2 -- BaO -- SiO_2; UO_2 -- TiO_2 -- SiO_2; UO_2 -- Y_2O_3 and SiO_2.

However, all the experiments were conducted with a small (up to five mg) amount of glass. When it was increased even to 20 g, the regions of suitable compositions were markedly narrowed owing to weakening of glass forming ability and more intense volatility of the uranium.

Aluminum-magnesium silicate glasses are most promising as solvents of uranium oxides [19]. They have an annealing temperature of the same order as for quartz glass (about 1270° K), and a founding temperature of 1970 - 2070° K. Glasses containing up to 45 percent UO_2 can also be produced in alkaline systems [20], though these glasses soften at much lower temperatures.

To maintain the maximum amount of uranium dissolved in glass requires rapid cooling. Up to 20 percent by weight UO_2 can be maintained in several infusible aluminum silicate glasses. The amount of UO_2 can be boosted if the glass is produced in fiber form. Moreover, the use of glass fiber considerably reduces the demands on the heat-resistance of glass. By enclosing the fiber in a heat-conductive, for example, metal, matrix, one can avoid excessively high temperatures.

An infusible glass fiber with a U_3O_8 content of 35 percent by weight was proposed by Harteck and Dondes [21]. Compositions of glass fiber containing along with uranium another fissionable element - thorium -- are known [22]. Glass fiber 1 micron in diameter containing 10 percent U_3O_8 (enriched to 93 percent U^{235}) and 25 micron in diameter containing 35 percent U_3O_8 withstood 6 months in a beam of $2 \cdot 10^{12}$ neutrons/$cm^2 \cdot$ sec without visible damage [22]. Glass beads also possess this advantage. The following glass composition has been proposed for their manufacture (percent by weight): 25 - 35 SiO_2; 5 - 10 ZrO_2; 0 - 20 TiO_2; 2 - 5 MgO; 0 - 5 BeO; 0 - 15 ZnO; and 20 - 45 UO_2 (ThO_2) [23].

When homogenous glass containing uranium dioxide underwent heat treatment, UO_2 was liberated from the solution in a reducing or neutral medium. The resulting material contained UO_2 crystals, several microns in diameter and dispersed within the bulk of the crystallized glass [19]. Thus, heat treatment is a method of producing fuel in the form of a dispersed phase with particles not exceeding 5 microns in diameter.

Of interest in homogenous high-temperature reactors is the use of melts of oxides as a matrix for the distribution of nuclear fuel. The region in which this melt exists must be quite extensive. In the field of maximum operating temperatures (above 2270° K) processes such as

selective vaporization, chemical reactions with the atmosphere, liquation, dissociation, and so on must not exceed the allowable rates. At the same time the melt-initiation temperature must not be too high in order to ensure favorable operating conditions (homogenization and removal of gases) with low thermal productivity.

In spite of the high temperature in the core, the reactor walls through which heat is removed are protected against corrosion with a layer of hardened slag lining.

To use a melt for fuel distribution, the matrix must fulfill the functions of a moderator, just as in the case of glass. Table 38 gives the thermal and nuclear characteristics of several oxides [27].

From Table 38 data, BeO, ZrO_2, and Al_2O_3 are the most suitable for use. Oxides of magnesium and silicon cannot be used owing to the low temperature in which the melt exists. However, the high melting point of BeO, ZrO_2, and Al_2O_3 raised the threat of the melt crystallizing as the thermal capacity of the reactor is reduced. Best results are given by mixtures of nonvolatile oxides with a lower melting point than pure oxides. For example, BeO - ZrO_2 - MgO (the melting point of the eutectic is 1910° K).

TABLE 38. MODERATING AND THERMAL PROPERTIES OF OXIDES

A Окисел	B Плотность в г/см³	Замедляющая способность $\xi\Sigma_S^{n}$ в см⁻¹ C	D Замедляющее отношение $\xi\Sigma_S/\Sigma_a$	Температура в °K E: F плавления	G кипения	H Теплопроводность при 1870°K в вт/м·град
Al_2O_3	3,96	0,0367	3,4	2323	3773	6,3
BeO	3,01	0,123	160	2803	4530	29,9
MgO	3,58	0,04	12,4	3073	3110	6,7
SiO_2	2,2	0,235	8,1	1986	2500	6,7
UO_2	10,96	—	—	3078	4370	2,78
ZrO_2	6,14	0,059	11,6	2953	4570	2,3

Remark. ξ is the mean logarithm of the energy decrease; Σ_a is the absorption cross-section; and Σ_S is the scattering cross-section

KEY: A -- Oxide
B -- Density in g/cm^3
C -- Moderating ability $\xi\Sigma_S^{n}$, in cm^{-1}
D -- Moderating ratio
E -- Temperature in ° K
F -- melting point
G -- Boiling point
H -- Thermal conductivity at 1870° K in w/m · deg

Calculated determinations of the critical parameters of the homogenous reaction with a melt core showed that the UO_2 concentration needed to sustain the fission process is 0.5 - 3 percent by weight.

An application of glasses as a matrix for introducing measured amounts of radioactive additives (or additives subsequently activated by irradiation) is known. For this use compositions not producing radioactivity of themselves for yielding short-lived isotopes, for example the following compositions (in percent by weight) are used: 40 - 50 SiO_2; 10 - 25 Al_2O_3; 15 - 35 RO; 0 - 15 TiO_2; 0 - 15 Fe_2O_3; and 0 - 5 F'. Oxides of chromium, scandium, and zinc are the additives for this glass [25].

Materials for binding radioactive wastes

Glasses used as binders for radioactive wastes must meet specific requirements:

1) The wastes must be in the form of a solid, and not a powder;
2) The radioactive components must not be leachable; and
3) The solid must not disintegrate on undergoing internal irradiation and exposure to external corrosive agents when stored for 100 - 1000 years.

From the viewpoint of facilitating the assimilation of wastes, usually uranium or its alloy with aluminum, glass must be founded at the lowest possible temperature; in this case the service life of glass-making furnaces, remote-controlled, is prolonged; repairing them poses some difficulty. Grover and Chidley [26] propose compositions with a founding temperature of 1370 - 1520° K, for example, $CaO \cdot B_2O_3 \cdot Al_2O_3 \cdot 3.5\ SiO_2$. This composition has adequate chemical stability. It is necessary to increase the amount of Al_2O_3 without raising the founding temperature up to 10 percent Na_2O must be added.

These same authors recommended a glass with the following composition (in percent by weight) for binding degraded uranium: 15 - 20 U_3O_8; 14 - 22 Fe_2O_3; 9 - 23 Al_2O_3; 25 - 45 SiO_2; 3 - 9 Na_2O; and 7 - 25 B_2O_3. The first three-components are radioactive. The best chemical stability is observed for the following ratio of components: 40 - 55 percent SiO_2; 10 - 20 percent $Na_2B_4O_7$, 30 - 40 percent wastes. The chemical stability of these glasses, judging from the data of the authors [26], remains unchanged after irradiation with a dose of 10^9 rad.

One method of removing liquid radioactive wastes is absorbing liquids in dry clay. Subsequent drying and calcining produces a ceramic that has varying porosity, strength, and chemical stability depending on the conditions of clay production and composition [27].

Materials for fuel element shielding

Glasses and enamels can be shielding materials protecting fuel elements fabricated of metallic uranium and its oxides against corrosive exposure. These glasses must satisfy a number of requirements.

1) high chemical resistance to corrosive exposure by liquid and gaseous agents;
2) high radiation resistance;
3) coefficient of thermal expansion in accord with the material; and
4) minimum absorption of neutrons by the glass or enamel layer.

Phosphate glasses containing 1 - 9 percent alkali metals can be used for these purposes: 25 - 40 percent BaO; 1 - 4 percent Al_2O_3; and 55 - 65 percent P_2O_5. The coefficient of expansion of these glasses is close to that for uranium, $200 \cdot 10^{-7}$ deg^{-1} in the temperature range to 920° K [28].

The glass film prevents formation of easily removed flakes of uranium oxides.

3. Optically Radiation-Resistant Materials

The inception of atomic power engineering, expanded research in nuclear physics, space exploration, advances in radiochemistry and the development and introduction of new radiochemical and radiospectroscopic methods of investigating structure required specialized glasses with usually unknown combinations of physico-technical properties.

Depending on the purposes for which glasses are used, either the retention of these properties after irradiation or their predictable variation is essential. For example, for inspection windows and optical instruments exposed to radiation, invariability of the optical characteristics of glasses when irradiated is required. In contrast, requirements of variation in given optical characteristics upon irradiation are imposed on glasses used in radiation dosimetry.

We know that irradiating glass initiates processes leading to changes first of all of its spectral and optical characteristics. A result of the interaction of radiation with glass is the formation of color centers and paramagnetic centers, luminescence, thermal de-excitation, and triboluminescence. All these changes can render impossible further service of the glass for visual observations as well as for the performance of photo- and television equipment.

Glasses not darkening when irradiated

To prevent color centers in the visible spectral region from forming, usually to the glass composition are added elements with active donor-acceptor properties. Adding these elements leads to the formation of color centers not absorbing in the visible but in other spectral regions. Polyvalent elements -- antimony, bismuth, and cerium have these properties.

TABLE 39. COMPOSITIONS OF OPTICALLY RADIATION-RESISTANT GLASSES [28]

Стекло A	Состав в вес. % B											
	SiO_2	B_2O_3	Al_2O_3	PbO	BaO	ZnO	CaO	MgO	K_2O	Na_2O	CeO_2	As_2O_3
Листовое C	72,5	—	1,8	—	—	—	7,8	2,7	—	13,6	1,7	—
Легкий баритовый крон D	59	3,4	—	—	20	4,1	—	—	10,3	3,2	0,25–1,5	0,3
Крон E	62	2	—	1	11	3	—	—	15	5	0,25–1,5	—
Тяжелый баритовый крон F	46	6	3	—	42,3	8	—	—	—	—	0,25–1,5	—
Тяжелые флинты G	31,5	—	—	62,5	—	—	—	3	—	—	0,4–0,8	—
	35,4	—	0,05	5,9	—	—	—	4,1	—	—	1	0,2
	20,1	—	—	79,1	—	—	—	—	—	—	0,5	—

KEY A -- Glass
B -- Composition percent by weight
C -- Sheet
D -- Light barite crown
E -- Crown
F -- Heavy barite crown
G -- Heavy flints

Most effective from the standpoint of reduced color center formation upon irradiation are cerium ions. At the present time, in producing virtually all types of optical glasses on which requirements of constancy of light transmission in the visible spectral region when irradiated are imposed, cerium oxide is added to the glass compositions [29 - 35].

The mechanism of preventing coloration in glass on exposure to gamma-rays in the presence of small amounts of cerium oxide additives involves the ability of cerium to easily change its valency. Light transmission of glasses containing cerium dioxide in their composition remains practically unchanged after irradiation with gamma-ray doses up to 10^8 r.

Table 39 presents several glass compositions that are optically resistant to gamma-radiation.

Based on series-produced glasses of the optical catalog, the State Optical Insitute developed and industry has been manufacturing radiation-resistant glasses. The names of these glasses and their radiation resistance are given in Table 40.

Glasses containing more than one percent by weight CeO_2 are yellowish. Glasses containing, in addition to CeO_2 oxides of heavy metals (BaO or Sb_2O_3) have more intense color due to the higher proportion of Ce^{4+} [38]. The presence in glass compositions of antimony and arsenic ions weakens the stabilizing action of cerium ions.

Quartz glass has a noteworthy place in the class of optically radiation-resistant glasses. At present in all technically advanced countries there are organizations engaged in scientific research and technological development of quartz glass. As the result of the combined work by researchers and technologists, several kinds of transparent quartz glass have been formulated, and articles made of these glasses are being produced comercially.

There is a classification of transparent quartz glass, whose commercial grades are given in Table 41.

Type I glass is manufactured by melting the charge in vacuum or vacuum-compression electric furnaces. These glasses do not have absorption bands in the 2700 nm region owing to the absence of hydroxyl groups. However, glasses of this type are not radiation-resistant. Their light transmission is significantly decreased upon irradiation with doses of 10^3 - 10^4 r.

Type II glasses are prepared by fusing the charge in gas furnaces in a hydrogen-oxygen burner. Glasses of this type are virtually no change in light transmission when irradiated with doses up to 10^8 r.

Type III glasses are prepared by high-temperature hydrolysis of a volatile silicon compounds. They are characterized by high purity, a hydroxyl group content up to 0.12 percent, and high transmission in the ultraviolet spectral region.

TABLE 40. RADIATION-OPTICAL RESISTANCE OF CERTAIN GLASSES OF SERIES 100

1 Марка стекла	2 Приращение оптической плотности при облучении дозой 10^5 р в $см^{-1}$	1 Марка стекла	2 Приращение оптической плотности при облучении дозой 10^5 р в $см^{-1}$
3 ЛК-105	0,05	9 КФ-106	0,07
К-108	0,015	10 БФ-106	0,09
К-119	0,025	11 БФ-107	0,07
4 БК-104	0,015	12 БФ-108	0,04
5 БК-106	0,015	13 БФ-111	0,06
6 БК-108	0,02	14 БФ-112	0,045
7 БК-110	0,04	15 БФ-117	0,045
ТК-102	0,025	16 ЛФ-105	0,11
ТК-103	0,025	17 ЛФ-111	0,08
ТК-104	0,025	18 Ф-101	0,07
ТК-108	0,025	19 Ф-104	0,07
ТК-112	0,025	20 Ф-108	0,07
ТК-114	0,025	21 Ф-113	0,07
ТК-116	0,025	22 ТФ-101	0,08
ТК-120	0,02	23 ТФ-102	0,08
ТК-121	0,065	24 ТФ-108	0,08
8 КФ-104	0,06	25 ОФ-101	0,05

KEY: 1 -- Glass grade
2 -- Increment in optical density when irradiated with a dose of 10^5 r, in cm^{-1}
3 -- LK-105
4 -- LK-104
5 -- BK-106
6 -- BK-108
7 -- BK-110
8 -- KF-104
9 -- KF-106
10 -- BF-106
11 -- BF-107
12 -- BF-108
13 -- BF-111
14 -- BF-112
15 -- BF-117
16 -- LF-105
17 -- LF-111
18 -- F-101
19 -- F-104
20 -- F-108
21 -- F-113
22 -- TF-101
23 -- TF-102
24 -- TF-108
25 -- OF-101

TABLE 41. GRADES OF QUARTZ GLASS

A Страна	Тип стекла B			
	I	II	III	IV
C Англия	JR-Vitreosil	GV-Vitreosil, OH-Vitreosil	Spectrosil	Spectrosil WF
D Франция	Pursil 453	Pursil Pursil ultra Pursil optique	Tetrasil	—
E ФРГ	—	--	Suprasil	—
США	201,204	---	7940	7943
F				

KEY: A -- Country
B -- Type of glass
C -- United Kingdom
D -- France
E -- FRG
F -- United States

Type IV glass is prepared by direct oxidation of silicon tetrachloride. Glasses of this type are not yet produced commercially.

The light transmission of type II and IV glasses undergoes virtually no change upon irradiation with doses up to 10^{10} r. For example, the light transmission of the quartz glass Suprasil remains unchanged when irradiated with a dose corresponding to the dose acting on an artificial satellite in earth orbit for a year [39].

The radiation-optical resistance of quartz glasses depends evidently on the hydrogen present in the hydroxyl groups as well as in the free state. Heat treatment of KI quartz glass conducted in a hydrogen atmosphere enabled us to boost its radiation-optical resistance. Results of comparative studies of the irradiation-optical resistance of initial KI quartz glass and in the same glass when treated with hydrogen are given in Table 42.

TABLE 42. EFFECTIVE TREATMENT IN HYDROGEN ON RADIATION-OPTICAL RESISTANCE OF QUARTZ GLASS

Вид облучения A	B Светопропускание в % стекла	
	C исходного	D обработанного
γ-лучи E	80	92
Рентгеновы лучи F	48	80

KEY: A -- Kind of irradiation
B -- Light transmission in percent of glass as listed
C -- initial
D -- treated
E -- gamma-rays
F -- x-rays

By selecting the temperature regime for the processing of KI quartz glass, one can provide conditions under which no hydroxyl groups are formed in the glass and the light transmission in the infrared region is not degraded.

Radiation-resistant glasses with low luminescence level

Series-produced optically radiation-resistant glasses of grades K-108 and K-208, by withstanding large radiation doses without noticeable change in optical density, exhibit very intense photoluminescence. The luminescence of these glasses is determined by cerium ions present in the glass and serving as an activator.

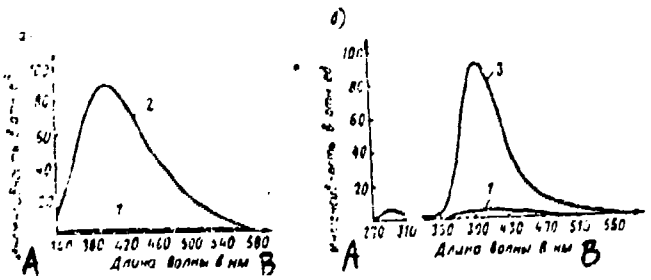

Fig. 73. Luminescence of glasses when excited with light at the wavelength indicated:
A -- 310 nm
B -- 250 nm
1 -- SK glass
2 -- K-108 glass
3 -- KRL glass
KEY: A -- Intensity in relative units
B -- Wavelength in nm

The requirements of enhanced radiation-optical resistance and slow luminescence are most fully satisfied by a grade KRL optical quartz glass. However, even this glass manifests quite intense luminescence when irradiated with protons and electrons and also when excited with light at a wavelength of 250 nm.

Our systematic studies of the effect polyvalent ions have on radiation-optical resistance and luminescence of cerium-containing glasses enable us to develop a glass with the following complex of properties:

1) resistant to gamma-ray doses up to 10^7 r;
2) photoluminescence that is two orders smaller than the photoluminescence of commercial K-108 radiation-resistant glass, nearly 30 times less than for KRL quartz glass;

3) glasses free of the thermal de-excitation effect; and
4) luminescence of glass when excited with protons and electrons is 50 times less than the radioluminescence of quartz glasses.

Radiation-optical and luminescence properties of this glass are given in Table 43 and Figs. 73-74.

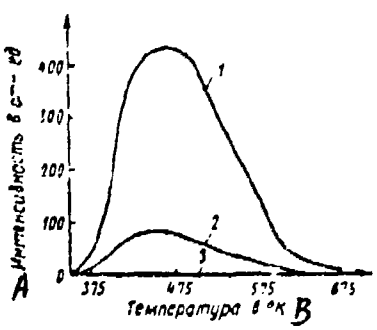

Fig. 74 - Thermal de-excitation of the following glasses
1 -- a and b
2 -- K-108 glass when irradiated with doses of 10^7 and $1.5 \cdot 10^6$ r, respectively
3 -- SK glass when irradiated with doses of 10^7 r
KEY: A -- Intensity in relative units
B -- Temperature in ° K

Glasses with low thermal de-excitation level

As stated above, requirements that thermal de-excitation be absent can be imposed on certain glasses, in addition to enhanced radiation-optical resistance, since when radiation interacts with glass, some of the absorbed energy stored in the glass at metastable energy levels of structure defects and impurity ions in the form of color centers can be emitted as light quanta when they are exposed to external stimulating factors.

At present radiation-resistant glasses free of thermal de-excitation are available. Light transmission of these glasses remains unchanged after gamma-irradiation with doses up to 10^7 r, and they are free of the thermal de-excitation effect. This group of glasses must also embrace glasses of the SK class, which also retain light transmission when gamma-irradiated with doses of up to 10^7 r and which do not produce thermal de-excitation when exposed to high and low temperatures.

TABLE 43. RADIATION-OPTICAL RESISTANCE AND RADIOLUMINESCENCE

A Марка стекла	B Интегральное светопропускание в %				E Интенсивность свечения в условных единицах при возбуждении	
	C до облучения	после облучения дозами в р D			F протонами	G электронами
		10^4	10^6	10^7		
H СК	90	90	89	87	J Не обнаружена	
К-108	91	91	88	82	K Не определялась	
I КРЛ	92	92	92	92	5	5,5

KEY: A -- Glass grade
B -- Integral light transmission in percent
C -- before irradiation
D -- after gamma-irradiation with listed doses, in r
E -- Intensity of luminescence in relative units after excitation by listed particles
F -- protons
G -- electrons
H -- SK
I -- KRL
J -- N not detected
K -- N not determined

4. Magnetically Radiation-Resistant Materials

To conduct structural studies of liquid and powered organic and inorganic materials by radiospectroscopy, glass ampules are needed meeting the following requirements: their light transmission when the ampules are exposed to penetrating radiation remains unchanged and the ampules do not produce an electron paramagnetic resonance (EPR) signal at $g \approx 2$.

Resonance-free glasses

The glasses Luch-I and Luch-II meet the above requirements [40]; these glasses suffer no change in light transmission and do not produce an electron paramagnetic resonance signal after exposure to penetrating radiation. Compositions of these glasses are given in Table 40, and their optical and radiation-magnetic properties are given Table 45.

TABLE 44. COMPOSITION OF RESONANCE-FREE GLASSES

Марка стекла A	Состав в вес. % B								
	SiO_2	Al_2O_3	CaO	MgO	Fe_2O_3	F	BaO	B_2O_3	CeO_2
«Луч-I» C	47,63	8,08	0,11	—	—	—	30,38	13,8	0,8
«Луч-II» D	64,09	18,11	14,93	2,87	0,4	4	—	—	0,4

KEY: A -- Glass grade
B -- Composition in percent by weight
C -- Luch-I
D -- Luch-II

TABLE 45. CHARACTERISTICS OF RADIATION-FREE GLASSES

A Марка стекла	Спектры ЭПР стекла при дозе 10^7 р и температуре в °К B				Интегральное светопропускание в % E	
	300		77			
	C ширина спектра ЭПР в э	D число парамагнитных центров *ПМЦ/г*	ширина спектра ЭПР в э	то же парамагнитных центров *ПМЦ/г*	F до облучения	G после облучения дозой 10^7 р
H «Луч-I»	J Сигнала ЭПР не обнаружено		50	$4 \cdot 10^{16}$	89	89
I «Луч-II»	То же K		60	$1 \cdot 10^{16}$	86	86

KEY: A -- Grade of glass
B -- EPR spectra of glasses at a dose of 10^7 r and indicated temperatures in °K
C -- Width of EPR spectra in oersteds
D -- number of paramagnetic centers, PMC/g
E -- Integral light transmission in %
F -- prior to irradiation
G -- after irradiation with a dose of 10^7 r
H -- Luch-I I -- Luch-II
J -- EPR signal not detected K -- As above

The EPR signal is virtually absent also in the SK-4B glass we formulated. This glass does not yield an electron paramagnetic signal at radiation doses to 10^{10} r in the 77-300° K range.

CHAPTER THIRTEEN

MATERIALS SENSITIVE TO RADIATION

Dosimetry is based on the laws of the passage of charged particles, x- or gamma-rays, and neutrons through matter. All these processes are accompanied by the absorption of radiation energy and ionization of the medium.

Materials used for dosimetry must have regular variation in given properties as a function of absorbed dose. Crystals, liquids, and glasses are employed as materials for dosimetry.

The proposed classification of glasses for dosimetry (cf. scheme) provides for their segregation into four groups by physical processes on which the determination of the absorbed dose is based:

group I -- glasses for dosimetry in the optical range and radio range;
group II -- scintillating glasses;
group III -- glasses for activated dosimeters; and
group IV -- glasses for luminescent dosimeters.

1. Glasses for Dosimetry in the Optical Range

Glasses for dosimetry in the optical range -- absorption dosimeters -- are based on the effect of glass darkening when exposed to radiation. Glasses used in absorption dosimeters must insure the linear dependence of absorption on the radiation dose. The Bausch-Lomb Company (United States) produces F-0621 glass, capable of determining radiation doses from several hundreds of roentgens to 10^6 r [1]. This glass has the following composition (percent by weight): 62.6 SiO_2; 10.6 MaO; 20.7 B_2O_3; 6 Al_2O_3; 0.1 Co_2O_3.

The absorption coefficient of this glass as a function of radiation dose all the way up to 10^6 r varies linearly, and with a further rise in radiation dose the sensitivity of the glass is diminished.

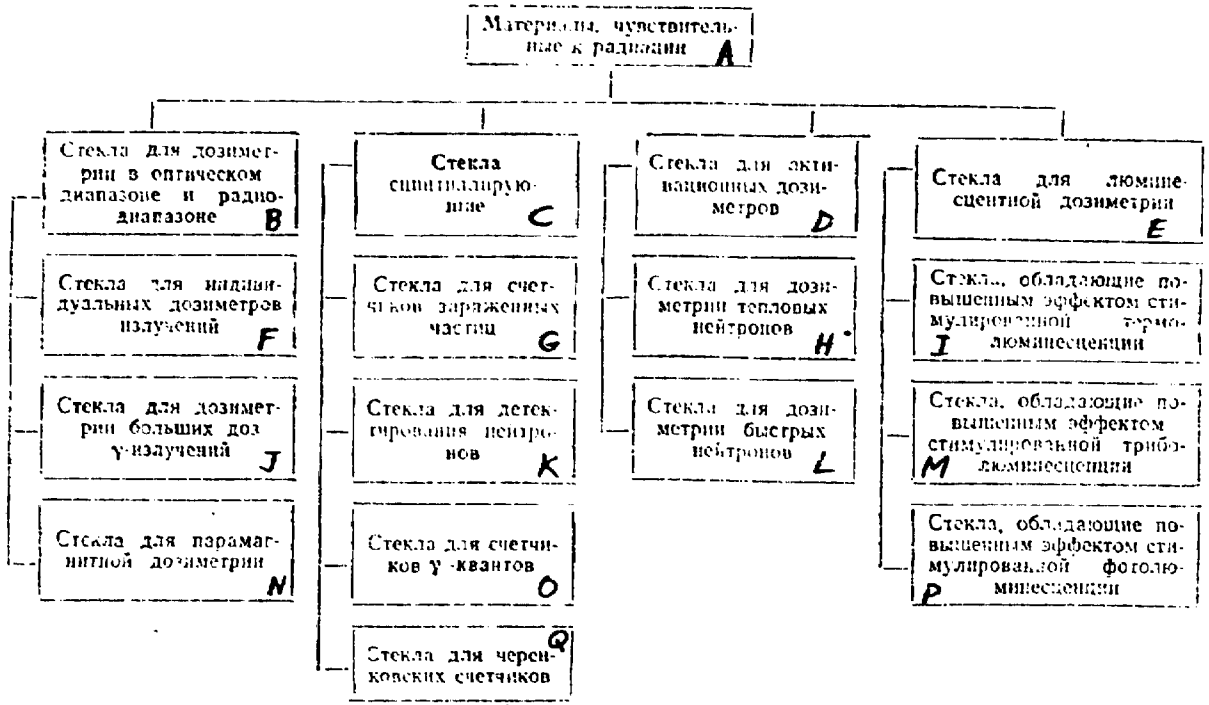

[KEY on following page]

[KEY to scheme presented on preceding page]

A -- Materials sensitive to radiation
B -- Glasses for dosimetry in the optical range and radio range
C -- Scintillating glasses
D -- Glasses for activated dosimeters
E -- Glasses for luminescent dosimetry
F -- Glasses for personal radiation dosimeters
G -- Glasses for charged-particle counters
H -- Glasses for thermal neutron dosimetry
I -- Glasses exhibiting increased effect of stimulated thermal luminescence
J -- Glasses for dosimetry of high doses of gamma-radiation
K -- Glasses for detecting neutrons
L -- Glasses for dosimetry of fast neutrons
M -- Glasses exhibiting enhanced property of stimulated triboluminescence
N -- Glasses for paramagnetic dosimetry
O -- Glasses for gamma-quanta counters
P -- Glasses exhibiting increased effect of stimulated photoluminescence
Q -- Glasses for Cerenkov counters

Adding a coloring alkali to silicate glass yielded a dosimetric glass with stable induced absorption spectra [2-6]. For example, glass containing the following (percent by weight) has a stable induced spectrum: 70 SiO_2, 18 Na_2O, 10 CaO, 1 MgO, 1 B_2O_3 with the addition of about 0.5 percent Co_2O_3 [7].

Combined addition of several variable-valency ions, for example MnO_2, Fe_2O_3, SnO_2, yields on exposure to radiation stable coloring and enhanced sensitivity to low radiation doses. Adding V_2O_5 and Cr_2O_3 to glasses containing MnO_2 also increases sensitivity to weak radiation doses. These oxides slow down the decolorizing of a glass after irradiation, but to a lesser extent than Fe_2O_3 and SnO_2. The amount of oxides added is as follows (in percent by weight): 0.3 MnO; 0.05 -- 0.3 Fe_2O_3; 0.5 -- 4 SnO_2 or 0.3 -- 2 MnO; 0.2 - 2 V_2O_5; and 0.02 - 0.2 Cr_2O_3. Manganese is added to the glass composition as the chlorides; iron -- as Fe_2O_3, tin -- as SnO_2 and anadium -- as V_2O_5 [4-6]. Glasses containing a large amount of antimony are promising in dosimetry [8]. Adding oxides of cobalt, arsenic, and manganese to a glass containing antimony enables it to be used in dosimetry for exposure to high radiation doses (10^6 - 10^9 r) [9].

2. Glasses for Luminescent Dosimetry

Luminescent dosimeters are used for personal dosimetry of gamma- and x-ray irradiation in the dose range from several biological equivalent-roentgens to 600-800 ber.

Photoluminescent dosimeters

Glasses used in luminescent dosimeters must ensure the linear dependence of the luminescent intensity on the radiation dose. Phosphate Corning glass 9761 activated with silver and with the following composition (in parts by weight) is used for these purposes: 50 $Al(PO_3)_3$, 25 $Ba(PO_3)_2$, 25 KPO_3, and 8 $AgPO_3$. This glass exhibits orange luminescence when excited with ultraviolet light at a wavelength of about 340 nm. However, it reduces its sensitivity as the energy of x- and gamma-radiation is intensified. To ensure sensitivity uniform over the energy spectrum, a glass with the following composition (in parts by weight) is used: 50 $Al(PO_3)_3$, 25 $Mg(PO_3)_2$, 25 $LiPO_3$, 8 $AgPO_3$ [1].

In Japan [10] a phosphate glass activated with silver and containing a large amount of lithium and some boron has been produced. Seven glasses have been synthesized, of which the most interesting is a glass with the composition (in parts by weight) as follows: 50 $LiPO_3$, 50 $AL(PO_3)_3$ with additives of $AgPO_3$ and B_2O_3. This glass is highly sensitive to thermal neutrons and gamma-rays. A composition of the charge for a similar Austrian glass (in parts by weight) is as follows: 6 $AL(OH)_3$, 7 LiOH, 3 H_3BO_3, 63 - 75 H_3PO_4, 4 - 5 $AgNO_3$; it is presented in a patent [11]. The studies [12-18] deal with the formulation of radio photoluminescent dosimetric systems based on phosphate glasses containing silver.

Dosimeters based on glasses with heat-stimulated luminescence

In making personal radiation dosimeters, especially in the low-dose range, much interest lies in glasses exhibiting the property to store energy on exposure to various kinds of radiation, and then upon external stimulation to emit it in the form of light. Ordinarily temperature is used as the external stimulus, which gives rise to the phenomenon of thermal deexcitation. The thermal de-excitation effect permits the attainment of high sensitivity and the measurement of doses over a wide range.

The overall light yield for glass dosimeters evidently will always be smaller than for crystal phosphors. However, glass dosimeters can have their own advantages. They can be made in practically any size and are marked by high uniformity, high chemical resistance, enhanced mechanical strength, and low cost in mass production.

Dosimeters based on glass with the thermal-excitation effect have found practical application as personal dosimeters with a wide period of working exposure. The following composition of glasses [19] activated with manganese (in mole percent) are recommended:

1) $50Al_2O_3 \cdot 3P_2O_5$, $50Li_2O \cdot P_2O_5$;
2) $50Al_2O_3 \cdot 3P_2O_5$, $50MgO \cdot P_2O_5$;
3) $50Al_2O_3 \cdot 3P_2O_5$, $50SrO \cdot P_2O_5$.

Glasses containing several alkaline-earth elements have been proposed [20] (in percent by weight): 82 - 90 P_2O_5, 3 - 8 MgO, 3 - 12 SrO, 3 - 8 Al_2O_3, 0 - 2 PbO, 0 - 2 Na_2O, 0 - 3 Li_2O, and activated with 0.5 - 0.15 MnO.

3. Scintillating Glasses

Scintillation is a short-term weak flash of light produced by individuals and photons when absorbed in a medium capable of luminescing. Both crystalline and glassy materials can be used as an appropriate medium.

Scintillating glasses for gamma-spectrometers

The well known solid inorganic scintillators are crystalline in structure. NaI(Tl) and KI(Tl) monocrystals are successfully used in recording gamma-radiation. Also, certain inorganic compounds not classified as monocrystal or crystalline powders exhibit appreciable light yield.

Several photoluminescent glasses prove to be quite effective scintillators. In producing glasses scintillating on exposure to gamma-radiation, cerium is used as an activator. It produces a luminescence in silicate glasses lying in the range of maximum sensitivity of the most common photomultipliers with antimony-cesium photocathodes.

A glass with a composition 3.5 BaO · B_2O_3 · 3.5 SiO_2 · 0.4 Al_2O_3 exhibits bright blue photoluminescence. S3-56 and 3-56-8 glasses are quite good in their luminescent properties and suitable for protecting gamma-radiation (Table 46). The scintillation efficiency of these glasses when excited with scattered gamma-rays from a Co^{60} source is 2 - 3 percent compared to a NaI(Fe) crystal.

Table 46. COMPOSITION OF SCINTILLATING GLASSES [19].

A Марка стекла	B Состав в вес. %					
	SiO_2	BaO	Li_2O	B_2O_3	CeO_2*	NH_4F*
C С3-56	77,14	16,42	6,43	3	0,08	2
3-56-8	64,81	18,21	9,68	7,29	0,08	2

*Above 100 percent.

KEY: A -- Glass grade
B -- Composition in percent by weight
C -- S3-56

The scintillation efficiency of these glasses can be enhanced by using ultrapure materials. A glass with a high silica content activated with cerium is most efficient. The amplitude of pulses received

when this glass is used is 10 percent of the pulses fed into the crystal. Glasses with the following most effective composition are recommended: $Na_2O \cdot 0.3\ CeO_2 \cdot 3 - 4\ (B_2O_3;\ SiO_2) \cdot 1 - 1.3\ Al_2O_3$.

Glasses for detecting neutrons

Glass for detecting slow neutrons must contain enough lithium or boron. We can anticipate that the ratio of light yield for excitation with electrons to the light yield for excitation with heavy particles will, for this glass, be close to the ratio typical of other inorganic scintillators. To reduce sensitivity to gamma-radiation it is desirable that the glass base not contain elements with a high atomic number.

The composition of the scintillation glass must be selected so that the radiation spectrum will lie within the region of maximum sensitivity of the photoelectric multiplier, but not be superimposed on the absorption spectrum. Maximum sensitivity of the FEU-S and FEU-29 spectrophotometric photomultipliers is the region 380-420 nm.

Silicate glasses activated with cerium [21-22] have bright blue luminescence. The absorption spectrum of these glasses is in the ultraviolet region. Lithium can be added to the glasses as an alkali component. From these considerations, lithium silicate glass activated with cerium was selected to record slow neutrons.

A glass with composition $Li_2O \cdot 2\ SiO_2(Ce)$ can be used in detecting slow neutrons [23]. The scintillation efficiency of the glass compared to NaI(Tl) or electronic excitation is 1.4 percent; the ratio between scintillation yields for irradiation with electrons and with alpha-particles is 3.8 - 4; the de-excitation time constant is 0.15 microseconds. The efficiency of glass 0.1 cm thick containing lithium with the concentration of the Li^6 isotope at 90.5 percent is 82 percent for thermal neutrons. The efficiency of a glass 0.5 cm thick is 40 percent for 10 ev neutrons.

A glass with the composition $Li_2O \cdot SiO_2 \cdot 0.8\ Al_2O_3(Ce)$ is also recommended. CeO_2 is added in the amount of 1 mole percent in the form of $CeCl_3$ [24]. Lithium silicate glasses activated with cerium are also recommended for neutron detection by other authors [25].

Glasses for Cerenkov counters

Scintillation counters, whose operating principle involves measuring the effect of Cerenkov luminescence, are used in measuring the energies of gamma-rays, electrons and protons. Lead glass containing 55 percent oxide is used for late-model Cerenkov spectrometers [26].

A spectroscope for gamma-rays has been built in the United Kingdom [27], where the scintillation material consists of a cylinder of F65335 lead glass. The glass is made from pure quartz and specially purified lead oxide. A lead glass with high light transmission is used in the

United States for Cerenkov counters [28]. The density of the glass is 4.6 g/cm^3 and its index of refraction is 1.724.

CHAPTER FOURTEEN

MATERIALS FOR ABSORBING RADIATION

The ability of a material to most strongly influence a radiation beam passing through it is achieved by adding to its composition chemical elements with high cross-sections of interaction with given kinds of radiation.

Intense interaction of absorbing materials with radiation results in the dose they absorb proving to be the optimum compared with other materials placed under the same conditions. Therefore to ensure the requisite service life of absorbing materials, requirements of high radiation stability are imposed on them.

Since the interaction cross-section and thus, the absorbability of a material depend on the kind of radiation and its energy, the material of a specific chemical composition proves to be effective only for a specific kind of radiation, often in a quite narrow energy range.

In particular, this is true of neutron absorption, since as one proceeds from thermal neutrons to fast neutrons, the pattern of their interaction with nuclei changes. Nuclear reactions with fast neutrons are threshold in nature, and their cross-sections are not large compared with the enormous cross-sections of certain elements or their isotopes have in the thermal range. Nonetheless, as the atomic number of an element is increased, the cross-sections of its nuclear reactions with rapid neutrons become greater, which enables us to regard materials containing heavy elements as been more suitable for this purpose.

As for the absorption of charged particles, by virture of their weak penetrating ability practically any material with a sufficiently thick layer can serve as an absorber.

Depending on the kind and energy of radiation they are intended to absorb, materials under consideration can be divided into the following groups (cf. scheme).

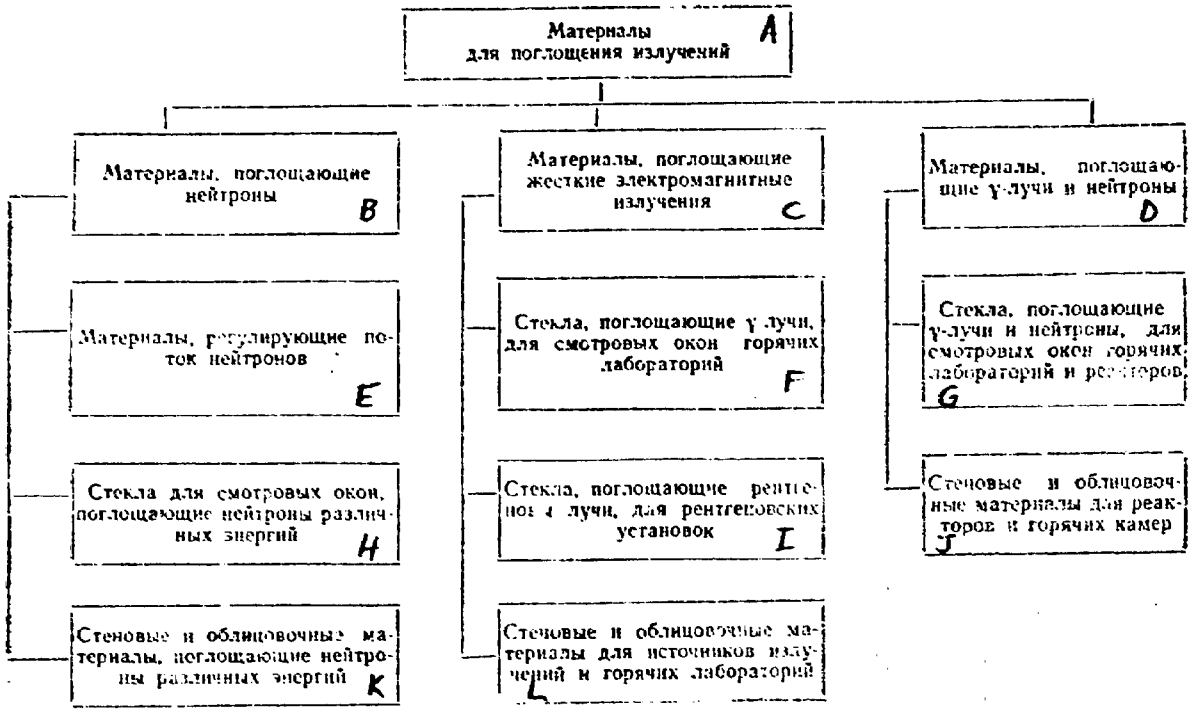

[KEY on following page]

[KEY to scheme presented on preceding page]

A -- Materials for absorbing radiation
B -- Materials absorbing neutrons
C -- Materials absorbing hard electromagnetic radiation
D -- Materials absorbing gamma-rays and neutrons
E -- Materials regulating neutron beam
F -- Glasses absorbing gamma-rays for the inspection windows of hot laboratories
G -- Glasses absorbing gamma-rays and neutrons, for the inspection windows of hot laboratories and reactors
H -- Glasses for inspection windows, absorbing neutrons at various energies
I -- Glasses absorbing x-rays, for x-ray installations
J -- Wall and lining materials for reactors and hot cells
K -- Wall and lining materials absorbing neutrons at different energies
L -- Wall and lining materials for radiation sources and hot laboratories

1. Materials Absorbing Hard Electromagnetic Radiation

Beginning with the initial use of x-rays, and then of nuclear radiation, efforts were made to find the materials for building protective inspection windows absorbing x-rays and gamma-rays. The main requirements imposed on glasses protecting against ionizing radiation is high density, which is achieved by introducing oxides of heavy elements. This requirement is met by heavy optical glasses, for example, crowns and flints that contain oxides of lead, bismuth, and barium [1]. A second important requirement imposed on protective glasses is their ability to preserve adequate transparency throughout the entire service period. Since lead glasses are marked by reduced radiation-optical stability, it is preferable to use glasses with additives of 0.5-3 percent cerium [2-3].

Silicate, borate, and phosphate glasses used as protection containing up to 85 percent by weight PbO or up to 60 percent Bi_2O_3 and their density is as high as 7.8 g/cm^3. Some compositions of foreign protective glasses are given in the handbook [4].

Domestic glasses used for absorbing gamma-rays, classified as superheavy flints contain up to 86 percent by weight PbO and have a density up to 6.5 g/cm^3. Besides these grades of glasses, there are also superheavy crowns that have, in addition to high absorbability, also high (up to 10^6 r) radiation-optical stability.

As we know, when irradiated, glasses accumulate electrical charge, which can produce breakdown and disintegration of the article. At the present time there are protective phosphate glasses that yield a weak effect of charge accumulation. The composition of a charge for this kind of glass, proposed in [5] is as follows (in percent): 26-51 P_2O_5, 33-56

H_2O, 12-26 PbO ($HgCl$, Tl_2O), and 0-5 Al_2O_3, with additives of BaO, ThO, Cs_2O, Bi_2O_3, K_2O, SnO, and ZnO. There are also several compositions of nonsilicate protective glasses intended for absorbing x- and gamma-radiation (in percent by weight): 50-90 PbO, 2-20 TeO_2, 0-25 Bi_2O_3, 0-10 B_2O_3, and 0-10 GeO_2 [6].

Ceramic materials serving as protection against ionizing radiation have a chemical composition that is similar to protective glasses, that is, they contain oxides of heavy elements usually serving as fillers, for example, monazite sand or PbO [7]. Additionally, an increase in absorbability occurs when a compact material with minimum porosity is produced.

2. Materials Absorbing Thermal Neutrons and Gamma-Neutron Radiation

The interaction of a material with neutrons depends on the properties of atomic nuclei in its composition. Fast neutrons are very weakly absorbed by materials without preliminary moderation, which takes place mainly via multiple scattering. The stopping power increases with decrease in the element's atomic weight [8]. Isotopes of hydrogen have, as we know, the highest stopping power. Of solid moderators, beryllium oxide is of interest, which can be added to glassy or ceramic materials. Below is given a characterization of certain moderators [9].

Замедлитель A	H_2O	D_2O	Be	BeO	C
Коэффициент замедления B	67	6520	160	180	169

KEY: A -- Moderator
B -- Moderation ratio

Thermal neutrons produced after moderation of fast neutrons can be absorbed via a nuclear reaction with certain elements. In making glasses capable of absorbing thermal neutrons, of particular interest are oxides of cadmium and boron, since with a large capture cross-section they can be added to a glass in the required amount. Oxides of certain rare-earth elements, in spite of extremely large capture cross-sections, are used less often mainly due to economic considerations.

For practical purposes cadmium borate is the optimum material from the standpoint of ability to absorb neutrons, however it has not found use as a glass owing to its slight chemical stability [10]. To enhance the chemical stability of cadmium borate glasses, oxides of beryllium or aluminum are added to them [11], or else they are converted to the borosilicate compositions [12-13]. The chemical stability is quite appreciably enhanced by adding calcium fluoride or the oxides of titanium and zirconium (Table 47).

TABLE 47. COMPOSITION OF CERTAIN GLASSES ABSORBING THERMAL NEUTRONS

Состав в вес. % A								B
CdO	B_2O_3	$BaCO_3$	Al_2O_3	SiO_2	CaF_2	TiO_2	ZrO_2	Литературный источник
50—80	20—50	5—0	—	—	—	—	—	[11]
50—80	20—50	—	2,5—10	—	—	—	—	[11]
28—65	2—35	—	0,9—1,5	16—30	8—22	—	—	[12]
63—67	26—32	—	—	—	—	2,6	—	[15]
60—61	31—35	—	—	—	—	—	3,5	[14]
1—67	0—40	—	1—1,5	6—28	0—5	—	—	[13]

KEY: A -- Composition in percent by weight
B -- Reference

Glasses containing, in addition to cadmium and boron, oxides of heavy elements (for example, lead or barium), have an added advantage. Glasses in the system $CdO-PbO-B_2O_3$ are capable of absorbing x- and gamma-rays, but their chemical stability remains only moderate. More resistant are glasses in the system $CdO-BaO-B_2O_3$. They have good optical properties (colorless or slightly yellowish) and are capable of trapping gamma-rays in addition to thermal neutrons. However, it is difficult to produce these glasses under industrial conditions, since they strongly attack the refractory owing to their corrosiveness.

Glass compositions in the systems $Bi_2O_3-CdO-B_2O_3$ and $Bi_2O_3-CdO-SiO_2$ [16-17] are known, which can be used to absorb radiation. SPN-1 glass with a linear coefficient of absorption 32 cm^{-1} is recommended for absorbing neutrons with energies up to 0.5 ev. SPN-2 glass is suitable for absorbing neutrons at energies above 0.5 ev. This glass, due to its CeO_2 content, is marked by enhanced radiation-optical stability, Glasses in the system $Li_2O-PbO-B_2O_3$, absorbing thermal neutrons and bremsstrahlung gamma-radiation are good material for protection against radiation [18].

Tomas and Lukas [19] present several glass compositions for the manufacture of glass fiber absorbing thermal neutrons (Table 48).

TABLE 48. COMPOSITIONS OF GLASSES FOR MANUFACTURE OF GLASS FIBER ABSORBING THERMAL NEUTRONS [19]

Состав в вес. % A							
SiO_2	P_2O_5	CaO	MgO	Li_2O	B_2O_3	Na_2O	CdO
8,6	2	9,0	4,8	5,4	80,1	—	—
52,5	13,5	1,3	—	—	12,1	4	20
50,7	13,2	1,1	—	—	9,9	3	24,6
47,2	12,3	1	—	—	9,2	3	30

KEY: A -- Composition in percent by weight

In several cases, indium oxide is added to cadmium borate glasses to expand the energy range of neutrons absorbed, for example, a glass with the composition (in percent by weight): 55 CdO, 33 B_2O_3, and 12 In_2O_3, has $\mu = 26$ cm^{-1} for 1.4 ev neutrons [20].

To produce chemically stable glasses capable of absorbing thermal neutrons, Bishop and Pinotti [21] employed a method of adding oxides of rare-elements to a matrix corresponding to the composition of chemically resistant commercial borosilicate glasses (Table 49). From 2 to 5 percent Gd_2O_3 or Sm_2O_3 about 100 percent were added to each of these glasses.

TABLE 49. CHEMICALLY RESISTANT GLASSES ABSORBING NEUTRONS [21]

Состав в вес. % A									
SiO_2	B_2O	Al_2O_3	K_2O	Na_2O	CaO	MgO	Fe_2O_3	Cl	BaO
80,6	13	2,2	—	—	—	—	0,05	0,1	—
74,7	11,2	5	0,4	5,8	—	—	—	—	2,8
61,5	—	18,8	—	—	11,4	8,2	—	—	—

KEY: A -- Composition in percent by weight

The absorption coefficient is particularly high for glasses containing, in addition to oxides of boron and cadmium, gadolinium oxide. For example, a glass with the following composition (in percent by weight): 35 CdO, 33 B_2O_3, and 32 Gd_2O_3, has $\mu = 413$ cm^{-1} [20].

All the glass compositions listed, whose development aimed mainly at making transparent protective shields, have relatively low softening points, which does not permit their use as reactor parts functioning at elevated temperatures. Ceramic materials are more suitable for service under severe reactor conditions. Ceramics for these purposes can be produced by sintering oxides as well as nonoxygen compounds, for example, B_4C (boron carbide).

Ceramic materials containing oxides of rare-earth elements and cadmium exhibit high absorbing ability [22-23]. Owing to the melting points of these oxides, these ceramics can be used as control rods and shielding for high-temperature reactors [23]. An unseparated mixture of the isotopes Eu, Sm, and Gd fully ensures a high absorption coefficient and can be used as fillers (up to 3 percent by weight) in ordinary heat-resistant ceramic [24]. Of special interest is the use of ceramics as a matrix with enhanced density, for example, in the system $BaO-R_2O_3-SiO_2$, where R_2O_3 is the rare-earth oxide [25]. This material has good shielding also against gamma-rays, with an adequate coefficient of absorption for thermal neutrons, for example, for the composition (in mole percent): 20 BaO, 50 SiO_2, and 30 Gd_2O_3 -- W is 98 cm^2/g [25].

Ceramic materials prepared on the basis of absorbing oxides have adequate heat resistance, however they do not exhibit requisite gas-tightness owing to the porosity inherent in any ceramic. This disadvantage, and also the impossibility of producing ceramics by sintering the oxides CdO and B_2O_3 most widely used in absorbing neutrons (owing to their high volatility) has compelled efforts to find a way of producing a material free of these drawbacks.

One way of obtaining heat-resistant, gas-tight materials based on CdO and B_2O_3 is to produce pyroceramics. Compositions of glass-crystalline materials based on silicate and borate glasses with high content of oxides of cadmium and indium are known [26-27]. These materials are gas-impermeable and have a high coefficient of neutron absorption, high mechanical strength, and satisfactory refractoriness. Besides these properties, pyroceramics can meet the requirements on compatibility with the materials of the supporting structure.

Use of pyroceramics in control rods is somewhat more advantageous compared to the use of boron steel both in terms of efficiency of neutron absorption, as well as economy of structural weight, which is of no small importance for nuclear engines.

Somewhat more promising compared with borate pyroceramics are silicate glass-crystalline materials (Table 50), owing to their higher softening point. The radiation stability of these materials must also be higher, due to their absence of B_2O_3, which reduces their resistance to neutron irradiation.

TABLE 50. CERTAIN COMPOSITIONS OF CADMIUM SILICATE PYROCERAMICS [26]

Состав в вес. % A									
CdO	In_2O_3	SiO_2	K_2O	TiO_2	Al_2O_3	Na_2O	CaF_2	BaF_2	CdF_2
60	5	20	—	10	5	—	—	—	—
60	5	15	5	15	—	—	—	—	—
60	5	15	5	10	5	—	—	—	—
60	5	15	10	5	5	—	—	—	—
60	5	15	10	—	—	—	—	—	—
60	5	20	—	5	—	—	—	—	—
60	5	25	—	—	—	10	—	—	—
60	5	25	—	5	—	5	—	—	—
60	5	25	—	—	—	5	5	—	—
60	5	20	—	5	—	5	5	—	—
60	5	20	—	—	—	10	5	—	—
60	5	25	—	—	—	5	—	5	—
60	5	25	—	5	—	5	—	—	10

KEY: A -- Composition in percent by weight

We have been able to produce glass-crystalline silicate materials with high CdO content and with a softening point of about 1270° K (Table 51). The satisfactory body crystallization of the glass was attained by adding an oxide catalyst, in contrast to the report [27] where metallic gold was used to induce the glass to crystallize.

TABLE 51. PROPERTIES OF SYNTHESIZED PYROCERAMICS

Материал A	Коэффициент B		Плотность в г/см³ E	Температура размягчения в °К F
	поглощения в $см^{-1}$ C	термического расширения в интервале 300 - 1000°К $\alpha \cdot 10^{-7}$ в $град^{-1}$ D		
E-10	32	68,5	4,72	1230
E-11	36	85	4,88	1220
E-12	38	76,8	5,03	1140
E-13	40	81,8	5,18	1270
E-14	42	86,4	5,43	1270

KEY: A -- Material
B -- Coefficient
C -- of absorption, in cm^{-1}
D -- of thermal expansion in the 300-1000° K range, $\alpha \cdot 10^{-7}$ in deg^{-1}
E -- Density in g/cm^3
F -- Softening point in ° K

REFERENCES TO CHAPTER ONE

1. Аглинцев К. К. и др. Прикладная дозиметрия. «Атомиздат», 1962.

2. Защита ядерных реакторов. ИЛ., 1958.

3. Будылин Б. В., Воробьев А. А. Действие излучения на ионные структуры. Госатомиздат, 1962.

4. Report of the International Comission on Radiological Units nd Measurements NBS Hand-book, 62, 1957.

5. Верещинский И. В., Пикаев А. К. Введение в радиационную химию. Изд. АН СССР, 1963.

6. Голубев Б. П. Дозиметрия и защита от ионизирующих излучений. Госэнергоиздат, 1963.

7. Справочник по производству стекла. Под ред. И. И. Китайгородского и С. И. Сильвестровича. Т. 1, Госстройиздат, 1963.

8. Стародубцев С. В., Романов А. М. Прохождение заряженных частиц через вещество. Изд. АН УзССР. Ташкент, 1962

9. Экспериментальная ядерная физика. Под ред. Э. Сегрэ, т. I ИЛ., 1955.

10. Bethe H. A. Ann d. Phys, v. 5, 325, 1930.

11. Fluharty R. G. Nucleonics, v. 3, № 5, 28, 1948.

12. Воробьев А. А., Кононов Б. А. Прохождение электронов через вещество. Изд. Томского университета, Томск, 1966.

REFERENCES TO CHAPTER TWO

1. Глесстон Дж. Атомы, атомное ядро, атомная энергия. ИЛ., 1958.

2. Seitz E. G., Koeler G. Solid State Physics, v. 2, N.—Y., 1956.

3. Динс Дж., Виньярд Дж. Радиационные эффекты в твердых телах. ИЛ., 1960.

4. Хэрвуд Дж. Действие ядерных излучений на материалы. Судпромгиз, 1959.

5. Действие ядерных излучений на материалы. Под ред. С. Т. Конобеевского. Изд. АН СССР, 1963.

6. Моррей Н., Тейлор Н. Действие ядерных излучений на свойства металлов и сплавов. ИЛ., 1957.

7. Варли Х. Материалы Международной конференции по мирному использованию атомной энергии, т. 7, Госхимиздат, 1958.

REFERENCES TO CHAPTER THREE

1. Будянин Б. В., Воробьев А. А. Действие излучения на ионные структуры. Госатомиздат, 1962.
2. Seitz F. Rev. Mod. Phys, v. 26, № 7, 1954.
3. Varley J. J. Nucl. Energy, v. 1, № 8, 130, 1954.
4. Seitz F. Rev Mod. Phys, v. 18, 384, 1946.
5. Парфианович И. А., Шуралева Е. И. Изв. АН СССР. Серия физическая, 29, 1, 1965.
6. Центры окраски в щелочно-галоидных кристаллах. Сб. статей, ИЛ., 1958.
7. Kats A. Proceedings of the Fourth International Congress on Glass, Paris, 1956.
8. Kats A., Stevels M. Verres et refractaires, 10, 135, 1956.
9. Данилов В. П., Вербан И. В., «Оптико-механическая промышленность», 1962, № 4.
10. Yokota R. Phys. Rev. v. 93, № 4, 896, 1954.
11. Bayntun P., Moore H. J. Soc. Glass Technol, v. 40, № 191, 187, 1956.
12. Barker R. S., Richardson D. A. Nature, v. 188, № 4757, 1960.
13. Barker R. S., Richardson D. A. Nature, v. 187, № 4732, 1960.
14. Schmidt R. Glasstechn. Ber., v. 10, 150, 1932.
15. Варгин В. В., Степанов С. А. ДАН СССР, т. 147, 609, 1962.
16. Bishay A. J. Amer. Ceram. Soc., v. 43, 417, 1960.
17. Yokota R. Phys. Rev. v. 101, № 2, 522, 1956.
18. Bishay A. Phys. and Chem. Glasses, v. 2, № 32, 1961.
19. Bishay A. Phys. and Chem. Glasses, v. 2, № 33, 1961.
20. Cohen A. J. Glastechn. Ber., v. 32, № 6, 1959.
21. Cohen A. J., Smith H. L. Bull. Am. Phys. Soc., v. 2, № 2, 1957.
22. Cohen A. J. J. Phys. Chem. Solids, v. 7, № 3, 287, 1958.
23. Kreidl N. J., Hensler J. R. Proceedings of the Fourth International Congress on Glass, Paris, 1956.
24. Yokota R. Phys. Rev., v. 95, № 6, 1145, 1954.
25. Kreidl N., Hensler J. J. Amer. Ceram. Soc., v. 38, № 12, 423, 1955.
26. Schulman J., Klick C., Rabin H. Nucleonics, v. 13, № 2, 30, 1955.
27. Weyl W. A. Coloured Glasses. Sheffield, 1951.
28. Cambrissio J., Vebersfeld J. Compt. Rend., v. 238, 572, 1954.
29. Yasaitis E., Smaller B. Phys. Rev., v. 92, 1068, 1953.
30. Bishay A. J., J. Am. Ceram. Soc., v. 44, № 1, 515, 1961.
31. Kugler J. Atomkernenergie, v. 4, № 67, 1959.

REFERENCES TO CHAPTER FOUR

1. Mitchell E. W., Paige E. G. Proc. Roy. Soc. v. 67, 264, 1954.

2. Кроуфорд Дж., Миттелс М. Обзор исследований влияния облучения на ковалентные и ионные кристаллы. В кн.: «Материалы международной конференции по мирному использованию атомной энергии», Женева,1955, т. 7. Госхимиздат, 1958.

3. Donnay G., Wyart J., Sabatier G. Zeitschrift Kristall, v. 112, 1955.

4. Smith G. S. Acta Crystal, v. 10, № 6, 1966.

5. Бреховских С. М. «Стекло и керамика», 1964, № 12.

6. Бюргановская Г. В., Орлов П. Ф. «Оптика и спектроскопия», 1962, № 12.

7. Levi M., Varley J. Proc. Phys. Soc., v. 68, 223, 1955.

8. Lautout-Magat M., Kieffer F. J. Chim. phys. et phys.-chim. biol., v. 61, 3, 1964.

9. Орлов П. Ф. Роль примесей и кристалличности сетки в окраске кварцевых стекол. Труды III совещания по стеклообразному состоянию. Изд. АН СССР, 1960.

10. Levy P. W. J. Chem. Phys., v. 23, 764, 1955.

11. Mitchell E., Paige E. Phil. Mag., v. 1, 1085, 1956.

12. Yokota R. J. Phys. Soc. Japan, v. 7, 316, 1952.

13. Ditchburn R. W. et at. Report of Bristol Conference on Defects in Crystalline Solids, London, 1955.

14. Lell E. J. Am. Cer. Soc., v. 43, № 8, 422, 1960.

15. O'Brien M. C. Proc. Roy. Soc. A., v. 231, 404, 1955.

16. Stevels J., Kats A. Phil. Res. Rep. № 11, 103, 1956.

17. Kats A. IV Congress international du verre. Paris, 1956.

18. Lee S., Bray P. Phys. Chem. Glass, 3, 37, 1962.

19. Lell E. Phys. Chem. Glass 3, 81, 1962.

20. Yokota R. J. Phys. Rev., v. 91, 1031, 1953.

21. George W., Arnold J. J. Chem. Phys. v. 22, 1959, 1954.

22. Бреховских С. М., Ланда Л. М. Журнал прикладной спектроскопии, т. 2, № 4, 1965.

23. Бреховских С. М. «Атомная энергия», т. 8, вып. 1, 1960.

24. Справочник по производству стекла. Под ред. П. И. Китайгородского и С. И. Сильвестровича, Т. I. Госстройиздат, 1963.

25. Бреховских С. М. «Стекло и керамика», 1958, № 1.

26. Бюргановская Г. В., Варгин В. В. и др. Действие излучений на неорганические стекла. Атомиздат, 1968.

27. Echert F., Schmidt K. Glasstechn. Ber., v. 10, 80, 1932.

28. Smith H., Cohen A. Amer. Ceram. Soc., v. 47, 564, 1964

29 Stroud J., Schreurs J., Tucker K. VI Congress International du Verre, Brussels, 1965

[illegible]

32 Cohen A. J. VII Congress International du Verre, Bruxelles, 1965

REFERENCES TO CHAPTER FOUR (CONCLUDED)

33. Ботвинкин Д. К., Запорожский А. Н. Кварцевое стекло. Стройиздат, 1966.

34. Бреховских С. М., Ланда Л. М., Окулович В. С. Тезисы доклада на II Всесоюзном симпозиуме по кварцевому стеклу, Л., 1968.

35. Патент США 1003974.

36. Faile S. P. et al. Science, v. 156, № 3782, 1967.

REFERENCES TO CHAPTER FIVE

1. Ferguson K. IV Congress International du Verres, Paris, 1956.

2. Levy P. I. J. Amer. Ceram. Soc., v. 43, № 8, 389, 1960.

3. Cropper W. J. Amer. Ceram. Soc., v. 45, № 6, 1962.

4. Бюргановская Г. В., Варгин В. В., Леко Н.-А., Орлов Н. Ф. Действие излучения на неорганические стекла. Атомиздат, 1968.

5. Мелик-Гайказян И. Я. В сб.: «Радиационная физика неметаллических кристаллов». «Наукова думка», Киев, 1967.

6. Бреховских С. М. и др. Тезисы доклада на II Всесоюзном симпозиуме по кварцевому стеклу, Л., 1968.

7. Kreidl N., Hensler I. J. Amer. Ceram. Soc., v. 38, № 12, 433, 1955.

8. Stroud I., Schreurs I., Tucker R. VI Congress International du Verres, Bruxelles, 1964.

REFERENCES TO CHAPTER SIX

1. Вавилов С. И. Изв. АН СССР. Серия физическая, т. 9 278, 1945.

2. Вавилов С. И. О «теплом» и «холодном» свете (Тепловое излучение и люминесценция). Изд. АН СССР, 1949.

3. Левшин В. Л. Изв. АН СССР. Серия физическая, т. 9, 355, 1945.

4. Vavilov S. I., Levshin V. L. J. Phys., v. 48, 397, 1928.

5. Толстой Н. А., Феофилов П. П. ДАН СССР, т. 60, 235, 1948.

6. Левшин В. Л., Винокуров Л. А. ЖФХ, 8, 181, 1936.

7. Вавилов С. И., Шишловский А. В. «Советская физика», № 5, 379, 1934.

8. Stokes G. Phil. Trans., v. 143, 2, 1852.

9. Einstein A. Ann. d. Phys., v. 17, 132, 1905.

10. Lommel E. Ann. d. Phys., v. 3, 133, 1878.

11. Nichols E., Merritt E. Studies in luminescence, № 1921.

12. Lommel R. Ann. d. Phys., v. 8, 244, 1879.

13. Vavilov S. I. Phil. Mag., v. 43, 307, 1922.

REFERENCES TO CHAPTER SIX (CONTINUED)

14. Вавилов С. И. Изв. АН СССР. Серия физическая, т. № 3, 1943.

15. Vavilov S. I. J. Phys., v. 9, 68, 1945.

16. Вавилов С. И. Собрание академиков АН СССР, посв щенное Великой Октябрьской социалистической революции. Из АН СССР, 1948.

17. Фок М. В. Введение в кинетику люминесценции крист лофосфоров. «Наука», 1964.

18. Блохинцев Д. И. ДАН СССР, т. 2, № 76, 1934.

19. Адирович Э. И. Некоторые вопросы теории люминесце ции кристаллов. Гостехиздат, 1956.

20. Möglich F., Rompe F. Zs. f. Phys., v. 115, 707, 1940.

21. Галанин М. Д. ЖЭТФ, т. 28, 485, 1955.

22. Антонов-Романовский В. В., Галанин М. Д. «Оптика и спектроскопия», т. 3, № 3, 389, 1957.

23. Свешников Б. Я. ДАН СССР, III, 78, 1958.

24. Розман И. М. «Оптика и спектроскопия», т. 4, № 4, 536, 1958.

25. Forster T. Zs. Naturforsch, v.49, 321, 1949.

26. Курский Ю. А., Селиванеико Л. С. «Оптика и спектроскопия», т. 8, № 5, 643, 1960.

27. Бюргановская Г. В., Варгин В. В. и др. Действие излучений на неорганические стекла. Атомиздат, 1968.

28. Брехов ских С. М., Ланда Л. М., Викторова Ю. П. ДАН СССР, т. 163, № 1, 1965.

29. Каранетян Г. О., Шерстюк А. И., Юдин Д. М. «Оптика и спектроскопия», т. 22, № 3, 443, 1967.

30. Arnold G. W. Phys. Rev., v. 139, № 4A, 1965.

31. Lell E. Phys. Chem. Glass, v. 3, № 3, 1962.

32. Лущик Ч. Б. Труды ИФА АН ЭССР, т. 31, 19, 1966.

33. Schulman J. H., Compton W. D. Color Centers in Solid Pergamon Press, N.—Y., 1962.

34. Garino-Canina V. Verres et refract, v. 10, № 2, 63, 1956

35. Garino-Canina V. Compt. rend., v. 238, 1577, 1954.

36. Garino-Canina V. Compt. rend., v. 239, 875, 1954.

37. Garino-Canina V. Compt. rend., v. 240, № 12, 1331, 1955.

38. Turner W., Lell H. J. Chem. Phys., v. 43, № 4, 1428, 1965.

39. Garino-Canina V. Compt. rend., v. 342, 198, 1956.

40. Cohen A. J. Phys. Rev., v. 105, 1131, 1957.

41. Hetherington G., Jack K., Ramsay M. Phys. Chem Glass, v. 6, № 1, 6, 1965

42. Трухин А. Н., Силинь А. Н., Ланда Л. М., Виго л Н. К., Зальис Ю. Р., Зирлов В. Э. Изв. АН СССР. Серия физическая, т. 31, № 5, 911, 1969

43. Брехов ских С. М., Виго л Н. К. и др. Тезисы доклады на II Всесоюзном симпозиуме по халькогенидному стеклу, Л., 1968.

44. Орлов Н. Ф. «Оптико-механическая промышленность», 1966, № 7.

REFERENCES TO CHAPTER SIX (CONTINUED)

45. Ланда Л. М. Тезисы докладов межвузовской конференции по радиационной физике. Изд. Томского университета, 1967.

46. Веркин Б. И., Маркус Л. М. и др. Сборник «Радиационная физика неорганических кристаллов». «Наукова думка», Киев, 1967.

47. Weyl W. Ind. Eng. Chem., v. 34, 1942.

48. Kikuchi T. J. Phys. Soc. Japan, v. 13, № 5, 1958.

49. Gibbs R. Phys. Rev. v. 28, 361, 1909.

50. Брехновских С. М. и др. Журнал прикладной спектроскопии, т. 4, № 4, 1967.

51. Брехновских С. М. «Стекло и керамика», 1964, № 12.

52. Феофилов П. П. «Оптика и спектроскопия», т. 8, № 6, 824, 1960.

53. Nickols E. L., Slattery M. K. J. Opt. Soc. Am. 12, 1926.

54. Вейнберг Т. Н. ДАН СССР 46, 8, 1945.

55. Варгин В. В. Производство цветного стекла. Гизлегпром. 1940.

56. Вейнберг Т. Н. Труды сессии памяти акад. С. И. Вавилова, ГОИ, Л., 1953.

57. Карапетян Г. О., Рейнахрит А. Л. Изв. АН СССР, Серия «Неорганические материалы», 3, 2, 1967.

58. Bruninghaus L. J. de Phys. et de Rad., 2, 1931.

59. Варгин В. В., Вейнберг Т. Н. Изв. АН СССР. Серия физическая, т. 9, 563, 1945.

60. Жиров Н. Ф. Люминофоры. Оборонгиз, 1940.

61. Прингсгейм П. Флюоресценция и фосфоресценция. ИЛ., 1951.

62. Левшин В. Л. Фотолюминесценция твердых и жидких тел. Гостехиздат, 1951.

63. Claffu E. W., Schulman J. H. J. Electrochem. Soc., v. 98, 403, 1951.

64. Rodrigner A. R., Parmelee C. V. J. Am. Ceram. Soc., v. 26, 137, 1947.

65. Кац М. Л. ДАН СССР, т. 85, 757, 1952.

66. Rexer E. Glastechn. Ber., v. 16, 90, 1938.

67. Егорова В. Ф., Зубкова В. С. и др. «Оптика и спектроскопия», т. 23, № 2, 1967.

68. Феофилов П. П. и др. Изв. АН СССР. Серия физическая, 27, 467, 1963.

69. Варгин В. В., Карапетян Г. О. «Оптико-механическая промышленность», 1964, № 1.

70. Карапетян Г. О. и др. «Журнал прикладной спектроскопии, № 1, 193, 1964.

71. Данилов В. П. ДАН СССР, т. 58, 1365, 1947.

72. Ванюков М. П., Исаенко В. В. и др. ЖЭТФ, т. 44, 1151, 1963.

REFERENCES TO CHAPTER SIX (CONCLUDED)

73. Бонч-Бруевич А. М., Карпее Я. Э. и Феофилов П. П. «Оптика и спектроскопия», т. 14, № 6, 821, 1963.

74. Китайгородский и др. ДАН СССР, т. 161, 118, 1965.

75. Weyi W. A. J. Opt. Soc. Am., v. 37, 519, 1947.

76. Snitzer E. Phys. Rev. Lett, 7, 444, 1961.

77. Hirayama C. H. Phys. Chem. Glasses, v. 5, 44, 1964.

78. Harper D. W. Phys. Chem. Glasses, v. 5, 11, 1964.

79. De Sharer L. G. J. Opt. Soc. America, v. 8, 55, 1965.

80. Hirayama C. Phys. Chem. Glasses, v. 6, 104, 1965.

81. Maurer R. D. Appl. Optics, v. 2, 87, 1963.

82. Maurer R. D. Proc. Symp. on Optical Masers, Brooklyn 1963.

83. Maurer P. B. Appl. Optics, v. 3, 433, 1964.

84. Mauer P. B. Appl. Optics, v. 3, 153, 1964.

85. Young C. G. Appl. Phys. Lett, v. 2, 151, 1963.

86. Snitzer E. Technical Papers, VI Intern. Congr. on Glass, Washington, 1962.

87. McAvoy T. C. SCP and Solids State Technology, № 8, 23, 1965

88. Snitzer E. Materials of III Intern. Symp. on Quantum Electr. Paris, p. 1, 1964.

89. Hauptmanova K. Czechosl. J. Phys., v. 14, 698, 1964.

90. Hauptmanova K. et al. Proc. Phys. Inst. Prague, 1965.

91. Namba U. et al. Oyo buturi, v. 32, 474, 1963.

92. Kanai E. et al. Oyo buturi, v. 33, 264, 1964.

93. Tohyama et al Oyo buturi, v. 33, 390, 1964.

94. Гань Фу-си и др. Кэсюе тунбао, № 1, 54, 1964.

95. Гань Фу-си и др. Кэсюе тунбао, № 1, 54, 1964.

96. Гань Фу-си и др. Кэсюе тунбао, № 11, 1012, 1965; Гань Фу-си. Сб. «Стеклообразное состояние», т. 4. «Наука», 1965.

97. Карапетян Г. О. Изв. АН СССР. Серия физическая, т. 27, 799, 1963.

98. Макеева Г. А. и др. Журнал прикладной спектроскопии, № 4, 245, 1966.

99. Jaekel G. Z. Techn. Phys., v. 7, 301, 1926.

100. Вайнберг Т. И. Изв. АН СССР. Серия физическая, т. 13, 203, 1949.

101. Карапетян Г. О. Изв. АН СССР. Серия физическая, т. 23, 1382, 1959.

102. Карапетян Г. О. «Оптика и спектроскопия», т. 3. № 4, 511, 1957.

103. Феофилов П. П. «Оптика и спектроскопия», т. 5, № 2, 1958

104. Tomaschek R. et al. Phys. Z. v. 34, 373, 1933.

105. Gandy H. W. et al. Appl. Phys. Lett, v. 1, 25, 1962.

106. Tomaschek R. et al. Glastechn. Rev., v. 16, № 5, 155, 1938

107. Tomaschek R. et al. Ergebn. exakt. Naturwiss, v. 20, 268, 1963

108. Kurkijan et al. Phys. Chem. Glasses, v. 4, 239, 1963.

REFERENCES TO CHAPTER SEVEN

1. Nelson S., Wiks R., A. J. Americ. Cer. Soc., v. 4, № 8, 1960.
2. Weeks R. A. J. Appl. Phys., v. 27, 1376, 1956.
3. Silsbee R. H. J. Appl. Phys, v. 32, 1459, 1961.
4. Griffits L. et al. Report on the Conference of Defects in Crystalline Solids, London, p. 81, 1955.
5. O'Brien. Proc. Proc Roy. Soc. A. 231, 404, 1955.
6. Сидоров Т. А., Тюлькин В. А. Изв. АН СССР. Серия «Неорганические материалы», т. 2, № 11, 1966
7. Weeks R A. Phys. Rev. v. 130, 570, 1963.
8. Кайтмазов С. Д., Прохоров А. М. ФТТ, т. 5, № 1, 347, 1963.
9. Scholmaher D., Boesman G. Compt. Rend, v. 252, № 14, 2099, 1961.
10. Van Wieringen J. S., Kats A. Phyl. Res. Rep., v. 12, 432, 1957.
11. Карапетян Г. О., Юдин Д. М. ФТТ, т. 4, 2647, 1962.
12. Lee S., Bray P. J. Phys. Chem. Glass., v. 3, 37, 1962.
13. Сидоров Т. А., Тюлькин В. А. Журнал структурной химии, № 3, 8, 1967.
14. Бреховаских С. М. и др. Изв. АН СССР. Серия «Неорганические материалы», т. 3, № 12. 1967.
15. Jasuo N. J. Japan Pure Chem. Soc., v. 82, 1629, 1961.
16. Карапетян Г. А., Юдин Д. М. ФТТ, т. 3, 2827, 1961.
17. Obersfeld J. Ann. Phys., v. 1, 395, 1956
18. Гарифьянов Н. С., Токарева Л. В. ФТТ. т. 6, № 5, 1453, 1964.

REFERENCES TO CHAPTER EIGHT

1. Arnold G. W., Compton W. D. Phys. Rev. 116, 802, 1959.
2. Ferguson K. R. IV Congres Internationale du Verre, VII—2, Paris, 1956.
3. Kats A. IV Congres Internationale du Verre, VII—7, Paris, 1956.
4. Орлов Н. Ф., Леко Н. А. Журнал прикладной спектроскопии, т. 4, 323, 1967.
5. Compton W. D., Arnold G. W. Discuss Faraday Society № 31, 1961.
6. Lell E. Phys. and Chem. Glass, 3, 84—94, 1962.
7. М. А. Элангго. Труды ИФ АН ЭССР, № 21, 215, 1962.
8. Grawford J. H., Nelson C. M. Phys. Rev., v. 101, 177, 1956.
9. Gordon R. B., Nowich A. S. Phys. Rev., v. 116, 314, 1959.
10. Levy P. W. Brookhaven national Laboratory, № 5, 1963.
11. Kikuchi T. Phys. Soc. Japan, v. 13, 5, 1958.
12. Yokota R. Phys. Rev., v. 91, 1013, 1953.
13. Kukuchi T. J. Phys. Soc. Japan, v. 10, 826, 1955.

REFERENCES TO CHAPTER EIGHT (CONCLUDED)

14. Fröhlich S. Proc. Roy. Soc., v. 188, 521, 1947.

15. Сародубцев С. В., Спирина Г. С., Юнусов М. Сб. «Радиационные эффекты в твердых телах». АН УзССР, Ташкент, 1963.

16. Fröman P., Peterson R., Vänngard T. Arkiv Ins., v. 15, 6, 559, 1959.

17. Yokota R. Ceram. Assoc. Japan, v. 62, 694, 1954.

18. Чернова Л. Г. и др. «Оптика и спектроскопия», т. 6, № 3, 619, 1957.

19. Garino-Canina M. V. C. r. Acc. Sci, v. 40, № 12, 1331, 1955.

20. Степанов С. А. Автореферат диссертации. ГОИ, Л., 1964.

21. Антонов-Романовский В. В. Кинетика люминесценции кристаллофосфоров. «Наука», 1966.

22. Лущик Н. Б. Труды ИФА АН ЭССР, № 3, 1955.

23. Riehl N., Bam J., Knoblock I. Prep. Internat. Conf. on Luminescence, Budapest, v. 6, № 1, 122, 1966.

24. Gobrecht H., Hoffman D. J. Phys. Chem. Sol. 27, 3, 503, 1966.

25. Брехковских С. М., Витол Н. К. и др. Тезисы доклада на II симпозиуме по кварцевому стеклу, Л., 1968.

26. Kondo S. J. Phys. Soc. Japan, v. 13, № 2, 224, 1958.

27. Barker K. et al. Phys. Chem. Glasses, 6, 124, 1965.

28. Бюргановская Г. В. и др. Действие излучений на неорганические стекла. Атомиздат, 1968.

29. Levy N., Varley J. Proc. Phys. Soc., v. 68, № 424 B, 223, 1955.

REFERENCES TO CHAPTER NINE

1. Gross B. Phil. Res. Rep., v. 107, № 2, 3, 1957.

2. Gross B. Phys. Rev., v. 110, № 2, 337, 1958.

3. Hardtke F. C. J. Chem. Phys., v. 42, № 9, 3000, 1965.

4. Asada T. et al. Intern. Simp. Def. Glass. Tokio, 1966.

5. Murphy P., Gross B. J. Appl. Phys., v. 35, № 1, 171, 1964.

6. Knechtel G., Scharmann A. Z. Angew. Phys., v. 19, № 5, 389, 1965.

7. Proctor T. M. Phys. Rev. v. 116, № 6, 1436, 1959.

8. Gross B., de Moraes R. J. Phys. Rev., v. 125, № 3, 930, 1962.

9. Hardtke F. C. Phys. Rev. Lett., v. 9, № 8, 339, 1962.

10. Moriya T. Int. Simp. Defects Glass. Tokio, 1966.

11. Murphy P., Ribeiro S. C. J. Appl. Phys., v. 34, № 2061, 1963.

12. Asada T. et. al. Mem. Inst. Sci. Ind. Res. Osaka Univ., v. 22, 85, 1965.

13. Gross B. J. Appl. Phys., v. 36, № 5, 1635, 1965.

14. Furuta J. et al. J. Appl. Phys., v. 37, № 4, 1873, 1966.

15. Kishii T., Ooka K. J. Phys. Soc. Japan., v. 22, 657, 1967

REFERENCES TO CHAPTER NINE (CONCLUDED)

16. Сирак А. М. Изв. МВО. Серия «Физика», № 4, 31, 1 66.

17. Вул Б. М. ДАН. т. 139, 1939, 1961.

18. Pollard J. et. al. J. Phys. Chem. Sol., v. 26, № 8, 1325, 1965.

19. Dau G., Davis M. Nucl. Sci. Eng., v. 25, № 3, 223, 1966.

20. Будников П. П. и др. Изв. АН СССР. Серия «Неорганические материалы», т. 3, № 1, 94, 1967.

21. Cutler V. E. Insulation, v. 6, № 12, 98, 1960.

22. Schvalbe K. Lüdenbach. Chem. Techn., v. 1, 42, 1965.

23. Payral J. Ver. et refr., v. 16, № 2, 100, 1962.

24. Ehrenberg W. et al. Brit. J. Appl. Phys., v. 17, № 1, 63, 1966.

25. Беляевская Л. М. Изв. МВО. Серия «Физика», № 1, 164, 1963

26. Bagge E., Janssen U. Atomkernenergie, v. 10, № 5—6, 19., 1965.

27. Потахова Г. И. Изв. МВО, Серия «Физика», № 4, 110, 1966.

28. Yamamoto K., Tsuchija M. J. Appl. Phys., v. 33, № 10, 3016, 1962.

29. Hench L. L., Daughenbaugh G. J. Nucl. Mat., v. 25, № 1, 58, 1968.

30. Stevels J. Phil. Res. Rep., v. 11, 103, 1956.

31. Потахова Г. И. Изв. МВО. Серия «Физика», № 3, 71, 1963.

32. Губанов П. Г. ЖТФ, т. 27, 11, 1957.

33. Chesney J., Johnson G. E. J. Appl. Phys., v. 35, № 9, 2784, 1964.

34. Зубов В. Г., Гришина А. П., «Кристаллография», т. 7, № 2, 238, 1962.

35. «Электротехника». Экспресс-информация № 42, реф. 241, 1959.

36. Davis J. K. Electr. Manufact., v. 151, 1962.

37. Бреховских С. М., Гринштейн Ю. Л. «Стекло и керамика», 1965, № 8.

38. Thompson C. Nucleonics, v. 14, № 9, 53, 1956.

39. Ворожцов Б. И., Филатов И. С. Изв. МВО. Серия «Физика», № 3, 7, 1964.

40. Водопьянов Л. К., Скапави Г. И. Изв. АН СССР. Серия физическая, т. 24, № 2, 253, 1960.

41. Водопьянов К. А., Воронцова Н. Г. Изв. МВО. Серия «Физика», № 1, 18, 1962.

42. Rao V. J. Sci. Research. Engin., v. 7, № 1, 5, 1963.

REFERENCES TO CHAPTER TEN

1. Биллингтон М. Материалы Международной конференции по мирному использованию атомной энергии, Женева, 1955. Госхимиздат, 1958.

2. Кроуфорд Дж. Х., Уителс М. Г. Металлургия ядерной энергетики и действие облучения на материалы, Металлургиздат, 1956.

3. Wittels M. G. Phil. Mag. v. 2, № 24, 1445, 1957.

4. Wittels M. G., Sherrill F. Advances in X-ray analysis, v. 3, 269, 1960.

5. Hauser O., Schenk M. Phys. Stat Sol., v. 6, 83, 1964.

6. Колонцова Е. В., Телегина И. В. ФТТ, т. 8, № 11, 3412, 1966.

7. Hauser O., Schenk M. Wiss. Humboldt. Univ. Berlin Ges. Sprachwiss Reishe., v. 13, № 6, 59, 1964.

8. Primak W. Phys. Rev., v. 95, 837, 1954.

9. Primak W. Phys. Rev., v. 98, 1854, 1955.

10. Elston J. Rev. hautes temp. et refr., v. 2, № 4, 323, 1965.

11. Пеньковский В. В. Действие облучения на металлы и некоторые тугоплавкие материалы. Изд. АН УССР, 1962.

12. Roy R., Buhsmer C. P. Amer. Mineralogist, v. 50, № 9, 1473, 1965.

13. Жданов Г. С. и др. «Кристаллография», т. 8, № 2, 207, 1963.

14. Roy R., Buhsmer C. P. J. Appl. Phys., v. 36, № 1, 331, 1965.

15. Колонцова Е. В., Телегина И. В. ФТТ, т. 7, № 9, 2730, 1965.

16. Warde J. M., Johnson J. R. J. Amer. Franklin Inst., v. 260, 455, 1965.

17. Simon I. Phys. Rev. v. 90, 350, 1953.

18. Primak W. S. Phys. Rev., v. 103, № 6, 1691, 1956.

19. Lukesh J. S. Phys. Rev., v. 97, № 2, 345, 1955.

20. Baierlein K. Phys. Stat. Sol., v. 7, № 2, 415, 1964.

21. Weissmann S., Nakajima J. J. Appl. Phys., v. 34, № 10, 3152, 1963.

22. Зубов В. Г., Иванов А. Г. «Кристаллография», т. 11, № 3, 423, 1966.

23. Mayer G, Lecomte M. J. Phys. Rad., v. 21, № 12, 846, 1960.

24. Fleming J. D. Ceram. Bull., v. 41, № 7, 472, 1962.

25. Price R. B., Walker R. H. Nature, v. 196, № 4856, 1962.

26. Кашкаров Л. Л., Гонаева Л. Н. Изв. АН СССР, Серия физическая, т. 30, № 11, 1799, 1966

27. Noggle T. S., Hlegler J. O. J. Appl. Phys., v. 31, № 12, 2199, 1960.

28. Caspar P. E. J. Appl. Phys., v. 37, № 1, 427, 1966

29. Romien M., Bloch J. C. r. Ac. Sci., v. 260, № 15, 4194, 1965.

30. Whapham A. D., Makin M. J. Phil. Mag, v. 7, № 81, 1441, 1962.

31. Chute J. H. J. Nucl. Mater., v. 21, № 1, 77, 1967.
32. Matzke H. Phys. Stat. Sol., v. 18, № 1, 285, 1966.
33. Matzke H., Whitton J. Canad. J. Phys., v. 44, 995, 1966.
34. Carter G., Grant W. A. Phys. Chem. Glas., v. 7, № 3, 94, 1966.
35. Naves H., Sella C., Chaperot D. C. r. Ac. Sci., v. 254, 240, 1962.
36. Tuck et al. Intern. J. Appl. Rad. Isotop, v. 15, № 4, 49, 1964.
37. Tuck D. G. Nature, v. 177, № 4505, 434, 1956.
38. Костюков Н. С. Изв. АН СССР. (сиб. отд.), № 9 (129), вып. 4, 43, 1967.
39. Воробьев А. А. Действие излучений на материалы. Межвузовский сборник трудов, № 62, Новосибирск, 1963.
40. Berman R. M. et al. J. Nucl. Mater., v. 2, 129, 1960.
41. Комобеевский С. Т., Бутра Ф. П. «Атомная энергия», № 5, 572, 1958.
42. Брековских С. М., Гринштейн Ю. Л. Изв. АН СССР. Серия «Неорганические материалы», 1, 6, 947, 1965.
43. Брековских С. М. и др. Изв. АН СССР. Серия «Неорганические материалы», 3, 8, 1474, 1967.
44. Брековских С. М. и др. Стеклообразное состояние. «Наука», 1962.
45. Брековских С. М. и др. ДАН СССР, 157, 938, 1964.
46. Брековских С. М. Стеклообразное состояние. «Наука», 355, 1960
47. Crawford J. H. Amer. Ceram. Soc. Bull., v. 44, № 12, 963, 1965.
48. Crawford J. H. Progress Nucl. Energy, ser. V, v. 3, 371, 1961.
49. Antal J. J., Goland A. N. Phys. Rev, v. 112, 103, 1958.
50. Hickman B. S., Walker D. G. J. Nucl. Mater., v. 18, № 2, 197, 1966.
51. Simon J. J. Amer. Ceram. Soc., v. 40, № 4, 150, 1957.
52. Griffits J. et al. Nature, v 173, 439, 1954.
53. Primak W. Phys. Rev., v. 110, № 6, 1240, 1958.
54. Elston J., Gewiss C. New Nucl. Mater., v. 2, 201, Vienna, 1963.
55. Primak W., Edwards E. Phys. Rev., v. 128, № 6, 2560, 1962.
56. Primak W. et al. Phys. Rev., v. 133, № 2a, 531, 1964.
57. Primak W., Campwirs R. Bull. Amer. Phys. Soc., v. 10, № 8, ser. II, 1095, 1965.
58. Стародубцев С. В., Аюпов С. Труды Ташкентской конференции по мирному использованию атомной энергии, т. 1, стр. 283. Изд. АН СССР, 1961.
59. Paymal J., Bonnaud M. Silic. Ind., v. 27, № 1, 17, 1962.
60. Bridgman P. W., Simon J. J. Appl. Phys., v. 24, 405, 1954.
61. Paymal J. Verr. et refr., v. 16, № 2, 100, 1962.
62. Paymal J. Verr. et refr., v. 16, № 6, 341, 1961.
63. Kishii T., Ooka N. Intern, Simp. defects of Glass. Tokio, 1966.

REFERENCES TO CHAPTER TEN (CONCLUDED)

64. Primak W. J. Appl. Phys., v. 34, № 12, 3630, 1963.

65. Primak W. J. Appl. Phys. v. 35, № 4, 1342, 1964.

66. Eleman J. S., Price R. B., Sunderman D. D. J. Nucl. Mat., v. 15, № 3, 165, 1965.

67. Desport J. A., Smith J. A. J. Nucl. Mat., v. 14, № 11, 155, 1964.

68. Elston J. E. Bull. Soc. Franc. Ceram., v. 70, 29, 1966.

69. Конобеевский С. Т. и др. ДАН СССР, т. 165, 524, 1965.

70. Rau R. C. J. Nucl. Mat., v. 14, № 11, 320, 1964.

71. Hickman B. S., Walker D. G. J. Nucl. Mat., v. 14, № 11, 167, 1964.

72. Худяков А. В. и др. «Атомная энергия», т. 23, № 3, 226, 1967.

73. Austerman S. P. J. Amer. Cer. Soc., v. 50, № 4, 124, 1967.

74. Collins C. F. J. Nucl. Mat., v. 14, № 11, 69, 1964.

75. Chute J. H., Walker D. G. J. Nucl. Mat., v. 14, № 11, 187, 1964.

76. Rau R. C. Nature, v. 211, № 5044, 71, 1966.

77. Bisson A. J Nucl. Mat., v. 10, № 4, 321, 1963.

78. Wilks R. C., Clarke F. J. J. Nucl. Mat., v. 14, № 11, 179, 1964.

79. Walker D. C. J. Nucl. Mat., v. 11, № 11, 195, 1964.

80. Hickman B. S., Pryor A. W. J. Nucl. Mat., v. 14, № 11, 96, 1964.

81. Clarke F. J. et al. Trans. Brit. Cer. Soc., v. 62, № 2, 83, 1963.

82. Morgan C. S., Bowen D. H. Phil. Mag., v. 16, № 139, 165, 1967.

83. Самсонов Г. В. «Атомная энергия», т. 6, 588, 1963.

84. Todd B. et al. J. Appl. Phys., v. 31, № 1, 51, 1960.

85. Lineveawer J. J. Appl. Phys., v. 34, № 6, 1786, 1966.

86. Aitemose V. O. J. Amer. Cer. Soc., v. 49, № 8, 446, 1966.

87. Rawson H. Glass Techn., v. 7, № 4, 115, 1966.

REFERENCES TO CHAPTER ELEVEN

1. Milorus C., Trueli R. J. Appl. Phys., v. 29, № 8, 1252, 1958.

2. Hall G. L. J. Phys. Chem. Solids, v. 6, № 3, 210, 1954.

3. Ремнев Ю. Н. Научные доклады высшей школы, № 3, 145, 1959.

4. Eleman J. S., Price R. B. J. Nucl. Mater., v. 15, № 3, 164, 1961

5. Eshelby J. D. J. Appl. Phys., v. 25, 255, 1954.

6. Paymal J. Verres et refract., v. 16, № 1, 20, 1962.

7. Lungu S. Rev. Roumaine Phys., v. 10, № 6, 603, 1965.

8. Primak W. J. Appl. Phys., v. 35, № 4, 1342, 1964.

9. Kishii T., Ooka N. Intern. Simp. Defect Glas, Tokio, 1966.

10. Kumar S., Nag B. Trans. Indian Cer. Soc., v. 22, № 1, 30, 1963.

REFERENCES TO CHAPTER ELEVEN (CONCLUDED)

11. Rau R. C. et al. J. Amer. Cer. Soc., v. 48, № 5, 233, 1965.
12. Elston J. E. et al. C. r. Ac. Sci., v. 249, 1655, 1959.
13. Патент Франции 1253955.
14. Патент Франция 1253956.
15. Кроуфорд Дж. Х., Уиттелс М. Г. Металлургия ядерной энергетики и действие облучения на материалы. Металлургиздат, 1956, стр. 487.
16. Fleming G. D., Ceram. Bull., v. 41, № 7, 472, 1962.
17. Elston J. E., Gewiss C. New Nucl. Mater., v. 2, 201, Wienna, 1963.
18. Hickman B. S., Walker D. G. J. Nucl. Mater., v. 18, № 2, 197, 1966.
19. Lungu S. Studii si cercetari fiz. ac. RPR, v. 14, № 6, 815, 1963.
20. Бреховских С. М., Гриштейн Ю. Л. Изв. АН СССР. Серия «Неорганические материалы», т. 1, № 6, 947, 1965.
21. Mayer A. C., Gigon J. J. Phys. Rad., v. 18, № 2, 109, 1957.
22. Жданов Г. С. и др. «Кристаллография», т. 3, 720, 1958.
23. Зубов В. Г., Иванов А. Т. «Кристаллография», т. 12, № 12, 365, 1967.
24. Straka R. et al. J. Appl. Phys., v. 34, № 5, 1439, 1963.
25. Стародубцев С. В. и др. Сб. «Действие ядерных излучений на материалы». Изд. АН СССР, стр. 342, 1962.
26. Бреховских С. М. и др. Стеклообразное состояние, т. 3, в. 2, 1963.
27. Paumal J., Susse C. C. r. Ac. Sci., v. 253, № 11, 1196, 1961
28. Paumal J. et al. C. r. Ac. Sci., v. 247, № 25, 2335, 1958.
29. Paumal J. Bonnaud Silic. Ind., v. 27, № 1, 17, 1962.
30. Paumal J., Le Clerk P. J. Amer. Cer. Soc., v. 47, № 11, 548, 1964.
31. Кроуфорд Дж., Уиттелс М. Труды II Женевской конференции по мирному использованию атомной энергии, т. 6, 435. Атомиздат, 1959.
32. Пеньковский В. В. Действие ядерных излучений на металлы и некоторые тугоплавкие материалы. Изд. АН УССР, 1962.
33. Johnson R. J. Metals, v. 8, 660, 1956.
34. Bisson A. J. Nucl. Mater., v. 10, № 4, 231, 1963.
35. Crawford J. Progr. Nucl. Energy. s. V, № 3, 371, 1961.
36. Gorski W. Glastechn. Ber., v. 34, № 4, 215, 1961.
37. Бреховских С. М., Гриштейн Ю. Л. Симпозиум тепловые и механические свойства и строение неорганических стекол. Тезисы докладов. Гос. комитет при Совете Министров СССР по науке и технике. М., 1967.
38. Троицкий А. О., Терехова Н. Б. Изв. АН СССР. Серия «Неорганические материалы», т. 3, № 1, 200, 1967.
39. Cohen A. F. J. Appl. Phys., v. 29, 591, 1958.
40. Warde J. M., Johnson J. R. J. Amer. Franklin Inst., v. 260, 455, 1955.
41. Киттел Ч., Пейн У. Труды II Женевской конференции по мирному использованию атомной энергии, т. 6, 310. Атомиздат, 1959.
42. Simon I. J. Amer. Ceram. Soc., v. 41, № 3, 1958.
43. Гриштейн Ю. Л. Тезисы докладов межвузовской конференции по вопросам радиационной физики. Томский политехнический институт, 1967.

REFERENCES TO CHAPTER TWELVE

1. Research Engineering, 15, 1, 16, 1960.
2. Брехонских С. М., Гринштейн Ю. Л. «Стекло и керамика», 1965, № 8.
3. Патент США 3137657.
4. Clarke F., Bowen D., Wilks R. S. Trans. Brit. Cer. Soc., v. 62, № 2, 83, 1963.
5. Growes G. W., Kully A. Phil. Mag., v. 8, 1437, 1963.
6. Hickman B. S., Walker D. G., J. Nucl. Mater., v. 18, № 2. 197, 1966.
7. Костюков Н. С. Изв. АН СССР (Сиб. отд.), № 9, 1967.
8. Патент Франции 1152230.
9. Патент США 3138567.
10. Самойлов А. Г. и др. Дисперсионные тепловыделяющие элементы ядерных реакторов. Атомиздат, 1965.
11. Industrial Heating, v. 31, № 1, 132, 1964.
12. Lang J. E. et al. Ceram. Age, v. 11, 43, 1966.
13. Murray P. Trans. Brit. Ceram. Soc., v. 62, № 2, 71, 1963
14. Bayntun P. L., Rawson H., Stanworth J. E. Nature., v. 178, 910, 1956.
15. Jochman F. Glas-Email-Keram-Techn. № 5, 166, 1958.
16. Патент Англии 1050818.
17. Cashin V. M. J. Amer. Ceram. Soc., v. 42, № 7, 328, 1959
18. Heyns M. S., Rawson H. Phys. Chem. Glas., v. 2, № 1 1, 1961.
19. Tuite G., Rawson H., Heyns M. S. Trans. Brit. Cer Soc., v. 62, № 3, 299, 1963.
20. Патент Англии 900080.
21. Harteck P., Dondes S. Nucleo En., v. 6, № 6, 332, 1961.
22. Патент США 3132033.
23. Патент Франции 1193211.
24. Klaus J. Interceram, v. 7, 219, 1965.
25. Патент США 3218262.
26. Grover J. R., Chidley B. E. J. Nucl. Energ., v. 16, № 8, 405, 1962
27. Wisnyi L. G. Ceram. Ind., v. 74, № 2, 69, 1960.
28. Справочник по производству стекла. Под ред. Н. Н. Китайгородского и С. Н. Сильвестровича. Т. I, Госстройиздат, 1963.
29. Schmidt R. Glastechn. Ber., № 10, 150, 1932.
30. Hoffmann J. Glastechn. Ber., № 3, 482, 1932.
31. Патент США 1545509.
32. Kugler G. Atomkernenergie, v. 11, № 2, 67, 1959.
33. Sun K., Kreidl N. Glass Ind., v. 33, № 10, 511, 1959.
34. Barker K., Richardson D. J. Amer. Cer. Soc., v. 44, № 11, 28, 1961
35. Jahn W. Glastechn. Ber., v. 35, № 11, 472. 1962.
36. Eckert E. Zeitschr. Techn. Phys., v. 7, 300, 1962.
37. Landerlik M., Dvorak J. Veda a vyskum v prymyslu sklarskem, № 4, 81, 1958.
38. Бюрановская Г. В. и др. Действие излучений на неорганические стекла. Атомиздат, 1968.
39. Sprech. Keram Glas. Em. Silik, № 5, 194, 1968.
40. Авторские свидетельства 154006, 149194.

REFERENCES TO CHAPTER THIRTEEN

1. Blair G. J. Amer. Ceram. Soc., v. 43, № 8, 426, 1960.

2. Kreidl N., Blair G. Nucleonics, v. 11, № 3, 82, 1956.

3. Taimuty S., Glass R., Deaver B. Proc. Second International. Conference on Peaceful Uses Atomic Energy, Geneva, 1958.

4. Paymal J. et. al. Glass Ind., v. 40, № 12, 771, 1959.

5. Kügler G. Atomkernenergie, v. 4, № 2, 67, 1959.

6. Paymal J., Bonnaud M., Le Clerc P. J. Amer. Ceram Soc., v. 43, № 8, 430, 1960.

7. Патент Франции 1200104.

8. Hedden W. A., Kercher J. E., Kind B. W. J. Amer. Ceram. Soc., v. 43, № 8, 1960.

9. Bishay A. Phys. and Chem. Glasses, v. 22, 33, 1961.

10. Yokota R., Nakajima S. Health phys., v. 5, № 3—4, 1961.

11. Патент Австрии 257858.

12. Kügler G. Atomkernenergie, № 1, 105, 1959.

13. Becker K. Zivil Luftschutz, № 2, 56, 1966.

14. Yokota R. J. Phys. Soc. Japan, v. 20, № 8, 1537, 1965.

15. Патент Японии 5021, 21A29.

16. Патент Франции 1327699.

17. Патент Франции 1207967.

18. Кеприм-Маркус Н. Б., Якубик В. В. «Атомная энергия», 1963, № 6.

19. Бреховских С. М., Шаповалова Н. Ф. Изв. АН СССР. Серия физическая, т. 25, № 4, 1961.

20. Патент ЧССР 123817.

21. Gunter R. J., Schulman J. H. Nuclear Science, № 5, 1958.

22. Gunter R. J., Schulman J. H. Phys. and Chem. of Glass, № 2, 1960.

23. Войтовецкий В. К., Толмачева Н. С., Арсаев М. И. «Атомная энергия», 1959, № 3.

24. Войтовецкий В. К., Толмачева Н. С. «Атомная энергия», 1959, № 4.

25. Egelstaff P. Nuclear Instrum, v. 1, № 4, 1957.

26. Грушин В. Ф., Залевалов З. А., Лейкин Е. М. «Приборы и техника эксперимента», № 2, 1960.

27. Bastick R. E. J. Soc. Glass Technol, 205, 1958.

28. Simpson N. Glass Ind., 13—23, 1959.

REFERENCES TO CHAPTER FOURTEEN

1. Шено П. Защита от радиоактивных элементов. ИЛ., 1954.
2. Патент США 3046148.
3. Патент ФРГ 951391.
4. Справочник по производству стекла. Под ред. Н. Н. Китайгородского и С. Н. Сильвестровича. Т. I. Госстройиздат, 1963.
5. Патент Англии 903450.
6. Патент Англии 770784.
7. Патент США 3145184.
8. Мухин К. Н. Введение в ядерную физику. Атомиздат, 1965.
9. Справочник по ядерной физике. Физматгиз, 1963.
10. Kordes E. Zeitsch. f. Anorgan. Chem., № 1, 44, 1939.
11. Патент США 2298746.
12. Melnick J. M. et al. J. Amer. Ceram. Soc., v. 34, № 3, 82, 1951.
13. Патент США 2660532.
14. Патент США 2582081.
15. Brewster G., Kreidl N. J. Amer. Cer. Soc., v. 35, № 10, 259, 1952.
16. Brechovskich S. M. Glastech. Ber., v. 32, № 11, 437, 1959.
17. Rao J. J. Amer. Ceram. Soc., v. 45, № 11, 555, 1962.
18. Sigiura T. et al. Ceram. Assoc. Japan, v. 72, № 822, 71, 1964.
19. Tomas D., Lukas L. Glass Ind., v. 35, № 10, 1954.
20. Sun K., Sun L. Glasse Ind., v. 3, № 10, 507, 1950.
21. Патент США 3216808.
22. Патент США 3219593.
23. Патент США 3250729.
24. Патент США 3185652.
25. Lemann H., Muller K. Keram. Rundschau, № 9, 195, 1962.
26. McMillan P. W., Hodson B. P. Glass Technol., v. 5, № 4, 142, 1964.
27. Патент Англии 958790.